INSTITUTO DE TECNOLOGÍA QUÍMICA
(UPV-CSIC)

UNIVERSITAT POLITÈCNICA DE VALÈNCIA

Catalytic transformations of glycerol via hydroxyacetone into nitrogen heterocycles of industrial interest

PhD in Sustainable Chemistry

Doctoral candidate:
Jaime Mazarío Santa-Pau

Director:
Dr. Marcelo E. Domine

Valencia, November 2021

Agradecimientos

A lo largo de la lectura de la presente tesis, se le hará evidente al lector el hecho de que este trabajo se sustenta en el esfuerzo, dedicación y apoyo que otras muchas personas le han brindado al autor del mismo para que pudiera llevarlo a cabo de forma exitosa. Por ello, en estas líneas, me gustaría agradecer a todos aquellos que, de una u otra manera me han brindado a mí o a la presente tesis doctoral cualquier tipo de ayuda, personal o profesional, que haya quedado reflejada en mayor o menor medida en cualquiera de las líneas expuestas en el documento que se presenta a continuación. Pido disculpas de antemano por los muchos nombres que se me olvidarán, pero a todos, sabed que os estoy infinitamente agradecido.

En primer lugar, debo dar las gracias a mi director de Tesis el Dr. Marcelo E. Domine por su apoyo y confianza desde nuestra primera reunión en septiembre de 2015, por haber visto en mí alguien en que merecía la pena apostar, y por seguir considerándolo así hasta el día de hoy. Por sus consejos, enseñanzas y, en especial, su paciencia conmigo durante todos estos años.

En segundo lugar, a la Profesora Patricia Concepción y al doctor Yannick Mathieu. Gracias por toda vuestra ayuda y por todo el conocimiento que habéis volcado en mí. Siempre os voy a considerar referentes y espero teneros siempre cerca, para seguir aprendiendo y, lo más importante, disfrutando de vuestras opiniones, de vuestros consejos y de nuestras discusiones.

A los doctores Pascual Oña-Burgos, Daniel Delgado y Luis Miguel Martínez-Prieto (aquí también debo incluir a Yannick). A lo largo de estos años son incontables los momentos que hemos compartido. Vuestro entusiasmo, vuestra pasión a la hora de entender esta profesión han sido, en muchos momentos, la verdadera fuerza motriz de esta Tesis Doctoral. Cada ratito con vosotros ha alimentado mi motivación, gracias además por vuestro cariño y apoyo. He tenido mucha suerte de encontrarme unos amigos tan buenos.

A Silvia, una amiga excepcional, siempre dispuesta a escucharme, a apoyarme y a ayudarme. Uno de los grandes tesoros producidos, mejor dicho, descubiertos, en estos años. Ferrán, Agustín, Jorditan, Xisco, Alfonso, Jorge, Andrés, Laurent, Jose, Rocío,

Agradecimientos

Cristina, Sebas, Marcos, Nuria, Ximo, Cris, Prof. José M. López-Nieto, Prof. Agustín Martínez, gracias por todos los momentos compartidos. Trabajar con gente así al lado hace todo inmensamente más sencillo.

A mis compañeros de grupo, por todo el apoyo y paciencia que han tenido conmigo a largo de estos años. Alberto, Carles, Chelo, Paola, Madalina, Fran, Cristina, Carlos, Zoel, Marisa,… Mención especial para Míriam, que siempre ha sido un apoyo y la persona junto a la que di mis primeros pasos en el laboratorio. También para Marvin y María, dos fantásticos amigos, gracias por el apoyo y cariño que seguís mostrándome en la distancia.

Cómo no a mi "*labmate*", el ya Dr. Zaher Raad. Cuánto hemos compartido, cuantísimo, amigo mío. Gracias por todos los momentos vividos amigo mío y, ojalá, mis próximos compañeros de despacho o laboratorio sean la mitad de buenas personas que tú. Sólo con eso ya tendría muchísima suerte. Un abrazo.

Agradecer a todos los técnicos y personal de taller, que facilitan enormemente el trabajo de investigación en el ITQ, y cuyo esfuerzo diario es directamente responsable de la calidad de cualquiera de las Tesis, artículos científicos, o patentes que este centro lleva produciendo semana tras semana durante los últimos 30 años. Por nombrar algunos de los mismos, en representación de todos: gracias, Javier Z., Álvaro, Maribel, Amparo, Carmen, Rosa, M.ª Jesús, Fanny, José Miguel, Adelina. Mención especial merece José Gaona. Sencillamente, eres un talento impresionante, como profesional y como persona. Gracias por toda tu ayuda. Por supuesto, al director Prof. Fernando Rey, por mantener ensamblado todo este engranaje que hace del ITQ un fantástico sitio donde venir cada día a investigar.

En último lugar, seré muy breve con los agradecimientos para mi familia y amigos. Realmente, unas pocas líneas más o menos no os van a hacer justicia, de ninguna de las maneras. Sólo con mi actitud para con vosotros el resto de mi vida podré llegar alguna vez a demostraros lo mucho que os quiero.

A mis amigos de siempre, los que siempre han estado, están y estarán. Gracias por intentar entender lo inentendible y por quererme como soy. A mi familia, entre la que, por supuesto te incluyo a ti Karen, gracias por vuestro apoyo y cariño, absolutamente incondicional. Esto sin vosotros, no sé si sería posible, pero, desde luego, no valdría en absoluto la pena. Os quiero con todo mi corazón.

Abstract

Based around the idea of searching for sustainable alternatives to fossil sources for manufacturing fuels and chemical products, this doctoral thesis addresses the development of new catalytic processes centered on glycerol valorization, which is the main by-product of biodiesel synthesis. In this sense, the main aim focused on using it as a carbon source to generate nitrogen heterocycles of industrial interest, specifically, to produce 2-methylpiperazine and 2-methylpyrazine.

However, due to the low reactivity of glycerol and the severe reaction conditions necessary to carry out the transformations towards these N-heterocycles, previous detailed research to optimize and understand the selective dehydration process of glycerol to hydroxyacetone (or acetol) was undertaken. Through obtaining this intermediate compound, it has been possible to develop efficient and selective nitrogen heterocycles production processes under reasonably moderate reaction conditions.

In this regard, Cu-Mg-Al hydrotalcite precursors give rise to a family of materials based on Cu-Mg-Al mixed oxides capable, if their composition is adequately optimized, of carrying out the selective dehydration of glycerol to acetol continuously with yields of ≈40%. In addition, these catalysts are stable for more than 8 hours under operational conditions, showing excellent regeneration capacity and reusability.

In the same way, through the combination of catalytic and characterization studies, the interesting mix of acid-base and redox centers exhibited by these materials has allowed for advancing significantly in the state of the art regarding understanding this glycerol catalytic dehydration reaction. Hence, it has been possible to verify the fundamental role of Cu species and, specifically, Cu(I) species present in the catalysts, in the generation of glyceraldehyde as a critical reaction intermediate for acetol production. Similarly, the acid centers of the catalyst facilitate the first adsorption of glycerol, thus accelerating the reaction.

However, the need to achieve higher acetol productivities from glycerol to stand a chance to succeed in the overall strategy motivated the development and study of a second family of catalysts based on copper oxide supported on different metal oxides (SiO_2, Al_2O_3 and ZrO_2) combining Lewis acid centers and high Cu exposure. The proper selection and optimization of these materials lead to reaching, with several of them, yields of 60% to acetol with much higher glycerol concentrations in the starting feed.

Abstract

On the one hand, the CuO/SiO_2 series of materials present a catalytic behavior highly dependent on the CuO dispersion degree. The high dispersion brings with it an upsurge in the Cu active area, higher acidity and, consequently, a superior catalytic activity, being able to pass, with the same compositions, from practically inert materials to catalysts with increased activity. However, an excess of CuO nanoparticles dispersion generates too much acidity, decreasing the acetol yield. On the other hand, the CuO/Al_2O_3 catalysts show a high dependence on the acid-base properties of the alumina chosen as support. Specifically, the CuO/Al_2O_3-*npw* material appears to expose the proper acidity necessary to enable glycerol adsorption without forming excessive by-products or impairing liquid product yield.

In the study of CuO/ZrO_2 materials, again, the different acid-base properties exhibited by the catalyst as a function of the zirconia phase employed as support determine the catalytic activity. In this sense, CuO/*m*-ZrO_2 has a lower acid density than CuO/*t*-ZrO_2, which entails carrying out the reaction more selectively. Specifically, the former catalyst is the one that, under the chosen reaction conditions, presents the best performance and productivity to the desired product, being able to carry out the process for a longer time and being possible to reuse it. Furthermore, incorporating the CuO nanoparticles by a deposition-precipitation method through the formation of reversed-phase micelles permits generating more active nanoparticles. Therefore, this catalyst can carry out the reaction even with lower Cu contents.

Once several catalytic systems had been established to produce acetol, the generation of the nitrogen heterocycles of interest from the combination of this molecule with ethylenediamine was investigated. First, the materials based on Pd-nanoparticles supported on simple and mixed metal oxides achieved good yields in synthesizing 2-methylpiperazine from acetol and ethylenediamine. Specifically, the Pd/TiO_2-Al_2O_3 catalyst presents high specific activity when forming 2-methylpiperazine (80% yield). These excellent results could be attributed to the enhanced exposure of unsaturated Pd centers observed in this material, critical for activating the C=N double bond and thus proceeding to the hydrogenation of the intermediate imines, which apparently constitutes the limiting reaction step. Secondly, it has been found that, in the presence of a mainly acid catalyst containing Cu, it is possible to dehydrocyclize acetol with ethylenediamine to 2-methylpyrazine and other alkyl-pyrazines. In this sense, supports such as ZrO_2 and

Abstract

Al_2O_3 turned out to be the most suitable and stable to carry out the reaction. Specifically, the CuO/Al_2O_3-*npw* catalyst yields 50% to 2-methylpyrazine, reaching values close to 60% when, as happened for the CuO/*m*-ZrO_2 catalyst, the precipitation-deposition method by micelles in reverse phase is used to incorporate the CuO nanoparticles. Finally, a proof of concept of 2-methylpyrazine synthesis starting from glycerol by using a specially designed multi-bed catalytic reactor to perform the two-steps process in one-pot with the same CuO-supported catalyst was assayed, with promising results.

In summary, two new catalytic routes have been established to produce nitrogen heterocycles with glycerol as the main carbon source through its derivative hydroxyacetone. Moreover, as demonstrated in this work, it is even possible to design catalytic processes for N-heterocycles production in which the glycerol is fed directly as starting reagent, opening in this way new perspectives in the field of sustainable valorization of biomass-derived platform chemicals.

Resumen

En el contexto de la búsqueda de alternativas sostenibles a la utilización de fuentes fósiles para la producción de combustibles y productos químicos, la presente tesis doctoral aborda el desarrollo de nuevos procesos catalíticos centrados en la valorización del glicerol, subproducto principal en la síntesis de biodiesel. El objetivo principal del trabajo consiste en utilizarlo como fuente de carbono para la producción de heterociclos nitrogenados de interés industrial, en concreto, para la producción de 2-metilpiperazina y 2-metilpirazina.

No obstante, debido a la baja reactividad del glicerol y las drásticas condiciones de reacción que serían necesarias para llevar a cabo las transformaciones a estos heterociclos, se ha planteado como paso previo un estudio detallado acometiendo la optimización y el entendimiento del proceso de deshidratación selectiva de esta molécula a hidroxiacetona (o acetol). A través de la obtención de este compuesto intermedio, se han podido desarrollar procesos de producción de los heterociclos nitrogenados eficientes y selectivos, llevados a cabo en condiciones de reacción razonablemente moderadas.

A este respecto, los precursores de hidrotalcitas del tipo Cu-Mg-Al dan lugar a una familia de materiales basados en óxidos mixtos Cu-Mg-Al capaces, una vez optimizada su composición, de llevar a cabo la deshidratación selectiva de glicerol a acetol en continuo con rendimientos del ≈40%. Además, estos catalizadores son estables durante más de 8 horas bajo condiciones de operación, mostrando también una excelente capacidad de regeneración y reusabilidad.

Del mismo modo, la interesante combinación de centros ácido-base y redox exhibida por estos materiales ha permitido, a través de la combinación de estudios catalíticos y de caracterización, avanzar significativamente en el estado del arte en lo que respecta a la comprensión de esta reacción de deshidratación catalítica de glicerol. De esta forma, se ha podido comprobar el papel fundamental de las especies de Cu y, en concreto de las especies Cu(I) presentes en los catalizadores, en la generación de gliceraldehido como intermedio clave para la producción de acetol. Del mismo modo, los centros ácidos del catalizador facilitan la primera adsorción del glicerol, acelerando así la reacción.

No obstante, la necesidad de alcanzar productividades de acetol más elevadas para asegurar el éxito de la estrategia global motivó el desarrollo y estudio, en este proceso de

deshidratación selectiva de glicerol en continuo, de una segunda familia de catalizadores basados en óxido de cobre soportado sobre diferentes óxidos metálicos (SiO_2, Al_2O_3 y ZrO_2), combinando centros ácidos de Lewis y una alta exposición del Cu. La adecuada selección y optimización de estos materiales lleva a lograr, con varios de ellos, rendimientos del 60% a acetol con concentraciones de glicerol en la alimentación mucho más elevadas.

Por un lado, la serie de materiales CuO/SiO_2 presenta un comportamiento catalítico altamente dependiente del grado de dispersión del CuO. La alta dispersión trae consigo un aumento del área activa de Cu, una mayor acidez y, en consecuencia, una mayor actividad catalítica, pudiendo pasar, con las mismas composiciones, de materiales prácticamente inactivos a catalizadores con una alta actividad. No obstante, un exceso en la dispersión de las nanopartículas de CuO genera demasiada acidez, disminuyendo el rendimiento a acetol. Por otro lado, los catalizadores CuO/Al_2O_3 presentan una alta dependencia de las propiedades ácido-base de la alúmina escogida como soporte. Concretamente, el material CuO/Al_2O_3-*npw* parece exponer la acidez apropiada para permitir la adsorción de glicerol, sin formar excesivos subproductos ni perjudicar el rendimiento a productos líquidos.

En el estudio de los materiales CuO/ZrO_2, nuevamente, las diferentes propiedades ácido-base exhibidas por el catalizador en función de la fase de zirconia usada como soporte son fundamentales para determinar la actividad catalítica. En este sentido, CuO/*m*-ZrO_2 tiene menor densidad ácida que CuO/*t*-ZrO_2, lo que conlleva realizar la reacción de manera más selectiva. En concreto, el primer catalizador es el que, en las condiciones de reacción escogidas, presenta el mejor rendimiento y productividad al producto deseado, pudiendo realizar el proceso por más tiempo, y siendo posible su reutilización. Además, la incorporación de las nanopartículas de CuO por un método de deposición-precipitación mediante formación de micelas en fase reversa, permite generar nanopartículas más activas, capaces de llevar a cabo la reacción incluso con contenidos más bajos de Cu.

Una vez establecidos varios sistemas catalíticos para la producción de acetol, se abordó la producción de los heterociclos nitrogenados de interés a partir de la combinación de esta molécula con etilendiamina. En primer lugar, la serie de materiales basados en nanopartículas de Pd soportadas sobre óxidos metálicos simples y mixtos logró buenos

rendimientos en la síntesis 2-metilpiperazina a partir de acetol y etilendiamina. En concreto, el catalizador Pd/TiO_2-Al_2O_3 tiene alta actividad específica hacia la formación de 2-metilpiperazina (80% de rendimiento), gracias a su elevada exposición de centros de Pd insaturados, crítica para activar el doble enlace C=N y así proceder a la hidrogenación de las iminas intermedias, que constituye, aparentemente, la etapa limitante de la reacción. En segundo lugar, se ha podido comprobar que, en presencia de un catalizador principalmente ácido conteniendo Cu, es posible realizar la dehidrociclación de acetol con etilendiamina para dar lugar a 2-metilpirazina y otras alquil-pirazinas. En este sentido, soportes como ZrO_2 y Al_2O_3 resultaron ser los más adecuados y estables para llevar a cabo la reacción. Concretamente, el catalizador CuO/Al_2O_3-*npw*, muestra rendimientos del 50% a la 2-metilpirazina, siendo posible alcanzar valores cercanos al 60% cuando, al igual que pasaba para el catalizador CuO/*m*-ZrO_2, se usa el método de precipitación-deposición por micelas en fase reversa para incorporar las nanopartículas de CuO. Finalmente, se llevó a cabo una prueba de concepto para la síntesis de 2-metilpirazina a partir de glicerol en un reactor multi-lecho especialmente diseñado para realizar las dos etapas del proceso en "one-pot" con el mismo catalizador basado en CuO-soportado, obteniéndose resultados prometedores.

En definitiva, se han establecido dos nuevas rutas catalíticas para la producción de heterociclos nitrogenados con glicerol como la principal fuente de carbono a través de su derivado hidroxiacetona, siendo posible incluso, tal y como se ha demostrado en el trabajo, diseñar procesos catalíticos en los que el glicerol se alimente directamente como reactivo de partida; lo cual abre nuevas perspectivas en el campo de la valorización sostenible de moléculas plataforma derivadas de biomasa.

Resum

En el context de la cerca d'alternatives sostenibles a la utilització de fonts fòssils per a la producció de combustibles i productes químics, la present tesi doctoral aborda el desenvolupament de nous processos catalítics centrats en la valorització del glicerol, subproducte principal en la síntesi de biodièsel, utilitzant-lo com a font de carboni per a la producció d'heterocicles nitrogenats d'interès industrial. En concret, per a la producció de 2-metilpiperazina i 2-metilpirazina.

No obstant això, a causa de la baixa reactivitat del glicerol i les dràstiques condicions de reacció que serien necessàries per a dur a terme les transformacions a aquests heterocicles, s'ha plantejat com a pas previ un estudi detallat escometent l'optimització i l'enteniment del procés de deshidratació selectiva d'aquesta molècula a hidroxiacetona (o acetol). A través de l'obtenció d'aquest compost intermedi, s'han pogut desenvolupar processos de producció dels heterocicles nitrogenats eficients, selectius i en condicions de reacció raonablement moderades.

Referent a això, els precursors hidrotalcítics Cu-Mg-Al donen com a resultat una família de materials basats en òxids mixtos Cu-Mg-Al capaços, una vegada optimitzada la seua composició, de dur a terme la deshidratació selectiva de glicerol a acetol en continu amb rendiments del 40%. Així mateix, aquests catalitzadors són estables durant més de 8 hores d'operació, mostrant a més una excel·lent regenerabilitat i reusabilitat.

De la mateixa manera, la interessant combinació de centres àcid-base i redox exhibida per aquests materials ha permès, a través de la combinació d'estudis catalítics i de caracterització, avançar significativament en l'estat de l'art pel que fa a la comprensió d'aquesta reacció catalítica. D'aquesta manera, s'ha pogut comprovar el paper fonamental del Cu i, en concret del Cu(I), en la generació de gliceraldehid com a intermedi de reacció clau. De la mateixa manera, els centres àcids del catalitzador faciliten la primera adsorció del reactiu, accelerant així la reacció.

No obstant això, la necessitat d'aconseguir productivitats de acetol més elevades per a assegurar l'èxit de l'estratègia global va motivar l'ús, en aquest procés de deshidratació selectiva de glicerol en continu, d'una segona família de catalitzadors basats en òxid de coure suportat sobre diferents òxids inorgànics d'alta àrea (SiO_2, Al_2O_3 i ZrO_2), combinant centres àcids de Lewis i una alta exposició del Cu. L'adequada selecció i optimització

d'aquests materials aconsegueix, amb alguns d'ells, rendiments del 60% a acetol amb concentracions de glicerol en l'alimentació molt més elevades.

Per una banda, la sèrie de materials CuO/SiO_2 presenta un comportament catalític altament dependent del grau de dispersió del CuO. L'alta dispersió porta amb si un augment de l'àrea activa de Cu, una major acidesa i, en conseqüència, una major activitat catalítica, podent passar, amb les mateixes composicions, de materials pràcticament inactius a catalitzadors amb una alta activitat. No obstant això, un excés en la dispersió de les nanopartícules de coure genera massa acidesa, disminuint el rendiment a acetol. D'altra banda, els catalitzadors CuO/Al_2O_3 presenten una alta dependència de les propietats àcid-base de l'alúmina triada com a suport. Concretament, el material CuO/Al_2O_3-*npw* sembla exposar l'acidesa apropiada per a permetre l'adsorció de glicerol, sense formar excessius subproductes ni perjudicar el rendiment a productes líquids.

En l'estudi dels materials CuO/ZrO_2, novament, les diferents propietats àcid-base exhibides pel catalitzador en funció de la fase de zircònia emprada com a suport són fonamentals per a determinar l'activitat catalítica. En aquest sentit, CuO/*m*-ZrO_2 té menor densitat àcida que CuO/*t*-ZrO_2, la qual cosa implica realitzar la reacció de manera més selectiva. En concret, el primer catalitzador és el que, en les condicions de reacció triades, presenta el millor rendiment i productivitat al producte desitjat, podent realitzar el procés per més temps, i sent possible la seua reutilització. A més, la incorporació de les nanopartícules de CuO per un mètode de deposició-precipitació mitjançant formació de micel·les en fase revessa, permet generar nanopartícules més actives, capaces de dur a terme la reacció fins i tot amb continguts més baixos de Cu.

Una vegada establits diversos sistemes catalítics per a la producció d'acetol, es va abordar la producció dels heterocicles nitrogenats d'interès a partir de la combinació d'aquesta molècula amb etilendiamina. En primer lloc, la sèrie de materials basats en nanopartícules de Pd suportades sobre òxids metàl·lics simples i mixtos va aconseguir bons rendiments en la síntesi 2-metilpiperazina a partir d'acetol i etilendiamina. En concret, el catalitzador Pd/TiO_2-Al_2O_3 té una alta activitat específica cap a la formació de 2-metilpiperazina (80% de rendiment), gràcies a la seua elevada exposició de centres de Pd insaturats, crítica per a activar el doble enllaç C=N i així procedir a la hidrogenació de les imines intermèdies, que constitueix, aparentment, l'etapa limitant de la reacció. En

Resum

segon lloc, s'ha pogut comprovar que, en presència d'un catalitzador principalment àcid contenint Cu, és possible realitzar la dehidrociclació d'acetol amb etilendiamina per a obtindre 2-metilpirazina i altres alquilpirazinas. En aquest sentit, suports com ZrO_2 i Al_2O_3 van resultar ser els més adequats i estables per a dur a terme la reacció. Concretament, el catalitzador CuO/A_2O_3-*npw*, mostra rendiments del 50% a la 2-metilpirazina, sent possible aconseguir valors pròxims al 60% quan, igualment que com passava per al catalitzador CuO/*m*-ZrO_2, s'utilitza el mètode de precipitació-deposició per micel·les en fase revessa per a incorporar les nanopartícules de CuO. Finalment, es vadur a terme una prova de concepte per a la síntesi de 2-metilpirazina a partir de glicerol en un reactor multi-llit especialment dissenyat per realitzar les dues etapes del procés en "one-pot" amb el mateix catalitzador basat en CuO-suportat, obtenint resultats prometedors.

D'aquesta manera, s'han establit dues noves rutes catalítiques per a la producció d'heterocicles nitrogenats amb glicerol com a la principal font de carboni, a través del seu derivat hidroxiacetona, sent possible fins i tot, tal com s'ha demostrat en el treball, dissenyar processos en els quals el glicerol s'alimenta directament com a reactiu de partida; obrint així noves perspectives en el camp de la valorització sostenible de molècules plataforma derivades de la biomassa.

Index

Chapter 1
Introduction

1.1 Biomass as an Alternative Source of Carbon

Nowadays, fossil fuels such as coal, oil, and natural gas still account for more than 75% of the planet's global primary energy[1]. Furthermore, oil and natural gas are also the primary source of raw materials for the chemical industry[2]. Nonetheless, over the last decades, the decreasing fossil reserves to production ratio[1], their uneven distribution around the world[1] and an increment in the levels of GHG in the atmosphere[3] have led the scientific community to the lookout for the conversion of alternative, clean and renewable raw materials into energy, fuels and chemicals. As a result of this academic and industrial effort, renewable power capacity (i.e., solar PV, onshore and offshore wind, hydropower, and bioenergy) already represents an 11% share of primary energy in the EU. Furthermore, it is set to internationally increase by 50% between 2019 and 2024[4]. Nevertheless, and despite there is also a worldwide trend towards green and natural products, renewable chemicals just include about 1.0% of the current global chemical market[5]. Thus, finding alternative ways to produce valuable fuels and chemicals is currently considered a critical scientific target.

In this sense, biomass outstands as an up-and-coming alternative to produce both fuels and organic chemicals. Notably, among all the available sustainable options under development to either replace or partially substitute fossil resources, biomass is the only one that can be can be used as a supply of carbon to make both renewable fuels and chemicals[6–10]. CO_2 hydrogenation has recently been considered, under specific scenarios, another possibility[11,12]. Nevertheless, its dependence on a variety of hydrogen issues such as cost-effective availability, storage, and transportation has left biomass alone as the only renewable resource chemically comparable, up to a point, and, therefore, with similar potential usages.

Biomass can be defined as the biodegradable fraction of products, waste, and residues from agronomy (including substances of plant and animal origin), forestry and related industries, as well as the biodegradable fraction of industrial and municipal waste. In the case of lignocellulosic biomass, it denotes any biological or organic matter that has been ultimately generated through photosynthesis, thereby posing solar energy storage in their most fundamental structural components' chemical bonds[13]. Consequently, biomass production is believed to generate lower CO_2 emissions since this CO_2 of biological origin

can be consumed during the subsequent growth of said biomass[14]. Despite this would only be true as long as certain requirements were fulfilled, such as the preferential use of either woody wastes from annual crops or intensive crops, there is currently no doubt that lignocellulosic biomass offers encouraging results in reducing CO_2 emissions[15].

Multiple ways to classify biomass have been proposed; according to the supply sector: forestry, agricultural, energy crops, livestock waste, industrial waste, urban waste…[16]; the way it is produced: dedicated energy crops and residues and wastes[17]; or its degree of overlap with edible resources: first-generation biomass, second-generation, and third-generation[18]. This latter classification is likely to be, these days, the one which is receiving a more significant deal of attention due to increasing reluctance to the use of agriculturally suitable land for biomass production.

For a more detailed explanation, first-generation biomass is essentially related to commonly edible biomass or even crops grown on arable land. Second-generation biomass is supplied from various feedstock, ranging from woody biomass to agricultural residues and industrial/urban wastes. Third-generation biofuels are, at this time, related to algal biomass produced in ponds or tanks on land and out at sea but could, to a certain extent, be also associated with the utilization of CO_2 as a raw material.

1.1.1 Second-generation biomass

After decades of spotlighting a biomass that could interfere in food production, scientific and industrial communities have resolved to focus on second-generation resources. As previously explained, and in contrast to first-generation biomass, these second-generation technologies convert non-edible biomass and agricultural and urban waste into clean and reasonably priced high-value fuels or chemicals. Essential types of non-food biomass include woody crops, agricultural residues such as leafy materials, stems, stalks, and other wastes such as animal fats or cooking oils.

Most of these second-generation supplies can be chemically classified as lignocellulosic biomass, which is, by far, the most abundant biomass on earth. Lignocellulosic biomass is generated from CO_2 and H_2O, using sunlight as an energy source, and producing O_2 as a by-product. C5 and C6 sugars are the primary products, which form the hemicellulose and cellulose polymers, respectively. *Cellulose* is a linear

crystalline polysaccharide based on chains of several hundred to thousands of β (1-4) linked D-glucose molecules[19]. In contrast, *hemicellulose* is a branched hetero-polymer shorter than cellulose. This polysaccharide includes five different sugar monomers: glucose, xylose, mannose, galactose, and arabinose. Hemicellulose is present as an amorphous matrix that surrounds the crystalline cellulose skeleton[20]. There is a third component, lignin, which, together with cellulose and hemicellulose, gives plants strength. *Lignin* is a highly crosslinked polymer made up of phenylpropane monomers, methoxylated to various degrees: p-coumaroyl alcohol, coniferyl alcohol, and sinapyl alcohol[21]. For instance, a common wood mainly comprises 38-50% of cellulose, 23-32% of hemicellulose, and 15-25% of lignin. In addition to these major components, lignocellulosic biomass also presents other compounds that serve as an energy store, such as lipids, carbohydrates, starch, and other products rich in carbon and hydrogen, such as terpenes, which are components of resins, steroids, and rubbers[9].

Other second-generation biomass becoming more and more important are the oils and fats used for cooking or frying in the food industry, restaurants, and households. The growing world population has brought an upsurge in food consumption and, consequently, an increment in many waste cooking oils/fats (WCO)[22]. The conversion of this amount of WCO unseals opportunities for fuel and chemical products and offers the possibility of minimizing the environmental impacts caused by these waste oils' disposal[23].

Apart from the WCO, other second-generation biomass that cannot be included in the lignocellulosic fraction comes from urban wastes. This leaves aside the previously mentioned WCO and the urban wood wastes, which belongs to the lignocellulosic category. On the one hand, this would entail municipal sewage, divided into industrial liquid waste and sanitary sewage. On the other hand, municipal solid wastes, commonly known as garbage or rubbish; the discarded solid waste produced in households, commercial establishments, and businesses in urban areas. Currently, the main feasible application of this biomass is thought to be related to self-sufficiency energy purposes[24], either after its combustion or through the production of biogas (CH_4 + CO_2) by its anaerobic digestion by microorganisms under anaerobic conditions[25]. Additionally, some of its fractions can be composting and used as a soil conditioner[26].

Figure 1.1. Different types of second-generation biomass raw materials.

1.1.2 Fuels and chemicals from biomass: The biorefinery

Due to its richness in organic carbon, biomass can serve both as a renewable energy source and a renewable source of chemicals. On the other hand, this dual functionality also allows synergies between both applications, thus giving rise to the concept of biorefinery. The biorefinery would cover a wide range of technologies capable of separating the biomass resources (wood, oils, fats, food wastes) into their basic units (carbohydrates, triglycerides, proteins), and converting them into high added value chemical products. The biorefinery would be a facility (or network of facilities) that could

integrate the processes and technical equipment necessary to produce transportation fuels, energy, and chemicals from biomass. The concept is analogous to the current oil refinery, which produces many fuels and products from crude oil[27,28]. By establishing this synergy and prioritizing higher-value chemicals and products or coupling their production with that of the advanced biofuels, the latter is expected to follow. Furthermore, this turn toward renewable chemicals and bio-based products is highly motivated by the need to fill the gap mentioned at the beginning of this introduction, concerning organic chemical manufacture. So far, most of the research has been directed to developing catalytic processes for the conversion of biomass into biofuels[29–32], despite the many other available alternatives for energy production. In contrast, the chemical industry does not have that many options and will always need a carbon-based feedstock[33].

The biorefinery concept has been widely discussed, and many alternatives are proposed regarding its model and biomass feedstock[34]. Following the discussion up to now, the most attractive fraction to be used as raw material would be that coming from secondary biomass resources. Moreover, establishing synergies between conventional refinery units and biorefineries seems essential for the short-term success of the latter[10]. Figure 1.2 illustrates what would be an example of an ideal scheme for the biorefinery herein described.

Figure 1.2. Simplified second-generation biorefinery proposal. Based on references [35–41].

1.1.3 Heterogeneous catalysis in biomass valorization

The use of catalysts increases the reaction rate and allows it to be carried out with a lower energy contribution. Moreover, the catalyst enhances selectivity to the desired product, diminishing by-product generation, following environmental and economic

benefits. Although molecular and enzymatic catalysts can achieve very high selectivity levels[42], the use of solid catalysts presents a series of specific advantages, such as easy separation, recovery, reuse, and less waste production[43]. Heterogeneous catalysis, therefore, constitutes a way to fulfill several of the Green Chemistry principles[44]. Also, heterogeneous catalysts are ideal candidates to carry out multistage processes[45–47], mainly when a process requires the participation of different active centers. Thus, bi, or multifunctional heterogeneous catalysts can be designed with isolated and well-defined active centers to act cooperatively (for example, acid-base along with redox centers) or in different reaction stages, generating a cascade-type process.

In the same way that heterogeneous catalysis has played a crucial role in improving and optimizing the petrochemical industry, several authors have claimed the likelihood of heterogeneous catalysis to become a powerful tool to convert renewable biomass resources to fuels and chemicals[48–51]. In fact, there are already multiple well-established catalytic processes for biomass valorization. Some of the most important examples include zeolites for fast catalytic pyrolysis[52,53], transition metal-based catalysts for biomass gasification[54] and upgrading of biomass-derived oxygenates[55] *via* aqueous-phase reforming[56] and condensation reactions[57,58].

However, many of the current approaches focus on developing industrial processes, while there is a lack of fundamental studies. Although the high level of functionality of those molecules obtained from biomass can somehow help their transformation into higher value-added products with few synthetic steps[9,59–61], they will also generally impose processing restrictions. Overcoming these limitations requires a more comprehensive insight into how these reactions work at a molecular level. In this sense, there is a great need to have fundamental studies for biomass conversion. This necessity has motivated the in-depth understanding of the reaction mechanisms described throughout the present thesis, together with the effort made in establishing solid structure-activity relationships for the different materials herein used.

1.2 Novel biodiesel production and the glycerol surplus

As far as the so-called biofuels are concerned, the core problem has been the broadly criticized usage of crops and feedstocks that the food industry could otherwise use. Using these first-generation biomass resources fosters land clearing and the rise in their prices, along with the consequent risk of putting some marginal populations on the edge of starvation[62]. Thus, various advances recently appeared to obtain the traditional bio-based fuels, such as bioethanol[63,64], biobutanol[65], or biodiesel[66], avoiding the use of edible biomass. Instead, the aim is to use resources derived from second-generation biomass. Among the preferred feedstocks, there are several alternatives, such as non-edible vegetable oil (i.e., jatropha, karanja, mahua, linseed, cottonseed, neem, camelina, and beauty leaf tree/polanga), waste or recycled oil (i.e., cooking oil, frying oil, vegetable oil soap stocks, and pomace oil) and animal fats (i.e., beef tallow, pork lard, yellow grease, chicken fat and by-products from fish oil)[67].

Apart from skipping the disadvantages already described, some studies claim that CO_2 emissions would be considerably reduced by replacing first-generation biomass. The explanation for this reduced CO_2 footprint relies on the much higher potential for CO_2 sequestration that low-input, high-diversity grassland perennials show compared to monocultures[68]. Additionally, the cultivation of this biomass for fuel production is believed to improve the standard of living of some rural regions and developing countries[69].

Regarding biodiesel, in the last years, after the restrictions imposed on the use of agriculturally suitable land for the fuel industry, the production has started to focus on transforming and upgrading second-generation sources; non-edible vegetable oils, waste cooking oils as well as waste animal fats. All of them pose promising substitutes for traditional edible food crops as they neither compete with food crops nor lead to deforestation. Moreover, the price of waste cooking oils (WCO) is far cheaper than virgin vegetable oils. As a result, the total manufacturing cost of biodiesel can be significantly reduced[23], while keeping a similar quality if working under optimum operating conditions[70]. Even though there is still a long way to go as regards the evaluation of second-generation biodiesels in internal combustion engines, they already constitute a reality in academic studies for plausible industrial scenarios[66].

Independently of the non-conventional raw materials used, transesterification is common in most new production cases, and it is considered the preferred chemical process to produce biodiesel. The reaction implies the replacement of glycerol in triglycerides by three methanol (or other alcohol) molecules to give the corresponding methyl fatty esters (FAMEs, see Scheme 1.1) in the presence of a basic catalyst. Hence, glycerol is still present as a by-product at three equivalents at the end of the reaction, representing around the 10% weight of the final product. Consequently, it needs to be valorised if the biorefinery wants the overall process to be profitable[71].

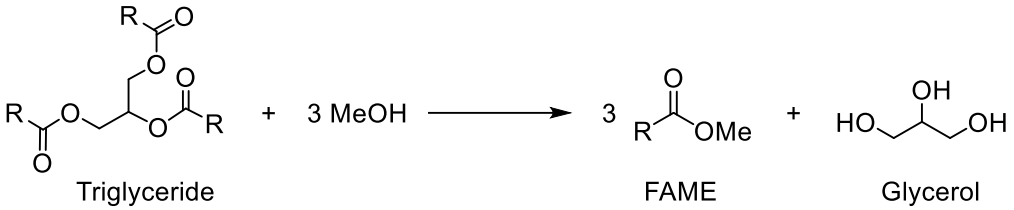

Scheme 1.1. Transesterification reaction of triglycerides with methanol to produce FAMEs (or biodiesel).

1.2.1 Glycerol valorisation

Traditionally, glycerol has been obtained as a by-product in four processes that use biomass as a raw material: soap making, fatty acid production, fatty ester production, and microbial fermentation. However, it was not until relatively recently that transesterification of triglycerides, using rapeseed and sunflower oils, has gained significant importance due to the boom in the manufacture of high-quality biodiesel[72].

After the biodiesel production, the finished product is an impure mixture comprising a glycerol-phase and an ester-phase containing the biodiesel. Crude glycerol, with the highest density, represents the lowest phase[73]. Because of this distribution, the glycerol-phase can be easily separated from the biodiesel-phase. After this first separation, crude glycerol and crude biodiesel are obtained. Nevertheless, purification of these phases is essential for further use of both glycerol and biodiesel[74]. In that regard, crude biodiesel can be purified by distillation, adsorption, membrane separation, reactive separation, etc. These methods are used in addition to the traditional washing methods with water, supercritical carbon dioxide, or ionic liquids. The success of the purification represents a

critical stage, since the final biodiesel must have a minimal amount of glycerol, water, fatty acids, and soaps to meet the standards required for its commercialization[74].

Over the last decade of the 20th century, the new surge in biodiesel production was the cause of glycerol overwhelming the demand of the industries which, traditionally, had been using glycerol as a humectant, excipient, or sweetener (i.e., cosmetic, pharmaceutical, and food industries). This new reality led to low prices and the total abandonment of the traditional petrochemical synthesis, based on propylene transformation through the epichlorohydrin process[75]. As a result, the scientific community attempted to find new ways to convert and add value to this chemical, whose disposal became one of the main problems faced by the biodiesel production plants. All this effort gave rise to the inclusion of glycerol in the list of the so-called platform molecules[76]. Because of their abundance, these bio-derived molecules were considered pivotal in the new development of chemicals coming from biomass, acting as the fundamental building blocks.

The role of glycerol as an emerging building block has resulted in many academic works involving homogeneous and heterogeneous catalysis, primarily aimed at producing higher value-added oxygenated chemicals (see Figure 1.3). Some important and widely studied processes are the synthesis of glycerol carbonate with basic catalysts, used as a polar solvent as well as a chemical intermediate in the synthesis of polycarbonates[77]; the acrolein synthesis over catalysts with acidic Brønsted sites[78], for the manufacture of other chemicals, such as allyl alcohol and acrylic acid; the steam reforming to produce H_2, usually by employing a Ni-based catalyst[79], glycerol hydrogenolysis into propanediols for polyester resins, food additives, solvents or antifreeze agents, with either transition metals or noble metals supported on acid or basic supports[80]; and acetalization, etherification or esterification reactions to diminish the O/C ratio, thereby generating compounds which can act as fuel additives[81].

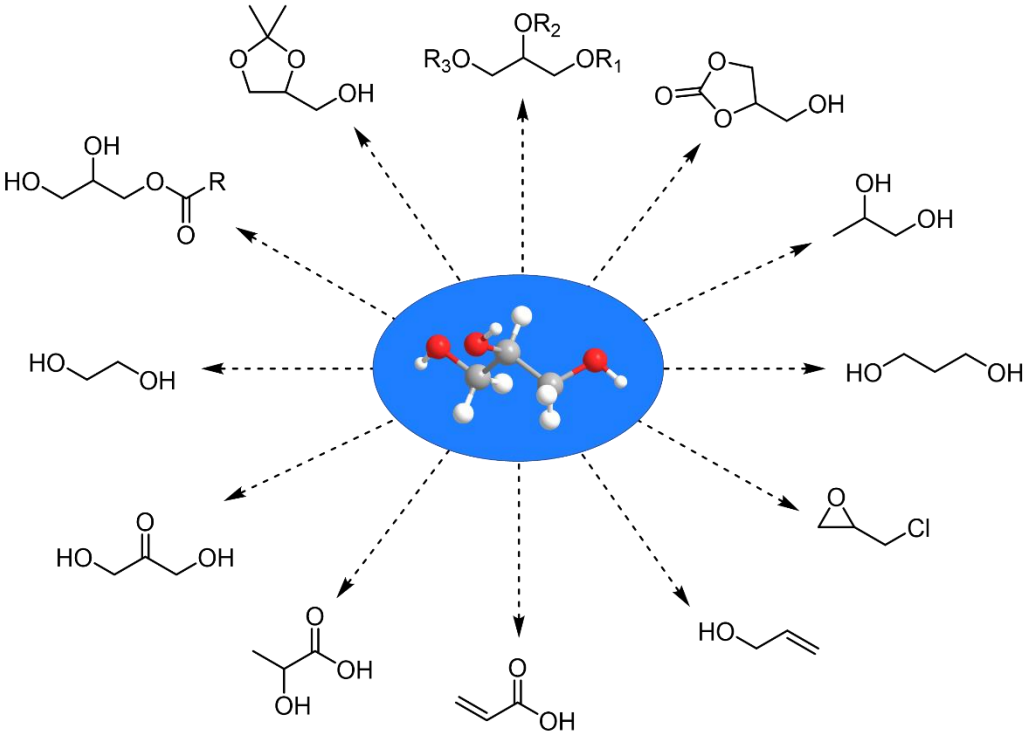

Figure 1.3. Examples of oxygenated glycerol derivatives obtained *via* heterogeneous catalysis.

Nevertheless, over the past decades, factors such as the trend towards using non-edible lignocellulosic biomass or the decrease in the price of fossil resources compromised the affordability of first-generation biodiesel technologies[82]. Despite this recent trend downwards, the introduction of the second-generation resources, already discussed in the previous section, has recently boosted biodiesel production prospects, thereby envisaging a future production up to 50 Mt/year[83]. This latest perspective has recently provoked a renewed scientific interest in glycerol valorisation. In fact, this significant attention as a promising feedstock for chemical manufacturing is clearly stated by recent studies on glycerol supply optimizations[84], continuous glycerol valorisation processes[85,86], and reviews by Pérez-Ramírez and co-workers, exploring the possibilities posed by establishing a glycerol biorefinery through environmental and economic analyses[71,75]. These latest studies are just examples of how glycerol technologies are regaining attention and, therefore, recovered, compiled, and reassessed.

1.3 Glycerol dehydration to acetol: a way to enhance reactivity

Among all the catalytic routes through which glycerol can be valorised, the selective glycerol dehydration to acetol (hydroxyacetone) will be a key reaction throughout this thesis. Acetol is a non-toxic compound, usually produced in the ketonic fraction of biomass pyrolysis liquids (bio-oil)[87]. Acetol can be used as a flavour in the food industry, as an additive in dyes and cosmetics, and as a skin tanning agent[88,89]. But notably, this molecule is of interest in this work due to its higher reactivity compared to that exhibited by glycerol, given by having a terminal hydroxyl group and a carbonyl group in the second carbon. These functional features enable acetol to participate in different organic reactions, such as the Mannich reaction[90] or some aldolic condensations[91]. Besides that, acetol can be applied to produce other chemicals such as olefins, acetone and furan derivatives[92], acetic acid[93], lactic acid[94,95], and, especially, it is a crucial intermediate when producing propylene glycol[96]. Newly, acetol has been proposed as a platform molecule for the electrocatalytic synthesis of acetone, 1,2-propanediol, and 2-propanol[97] and even a recent study describe acetol as a high-performance fuel for electrochemical oxidation in a direct alkaline liquid fuel cell[98]. Hence, a better knowledge of this glycerol dehydration could likewise increase the yield of these chemicals and any products obtained from them.

As far as acetol production is concerned, most academic works focus on its obtention from glycerol. Apart from its more traditional synthesis *via* a substitution reaction on bromoacetone[99], the palladium catalysed dehydrogenation of aqueous propylene glycol in the presence of hydrogen peroxide[100], and some biosynthetic routes requiring metabolically engineered micro-organisms and consuming several substrates[101–103], only a handful of studies are recounted off the glycerol catalytic path. In this sense, G.J. Suppes and co-workers described a catalytic screening for the selective dehydration of glycerol to acetol with different heterogeneous catalysts ($2CuO{\cdot}Cr_2O_3$, Ru/C, Ru/Al_2O_3, Pd/C, Raney Nickel, among others) in a reactive distillation system at 240 ºC and a reduced pressure of 98 kPa. They reported the highest acetol yield from pure glycerol up to date, achieved when using copper chromite as catalyst (≈85% yield)[104]. Although other examples working with other catalysts in similar systems have since then been described, any of these discoveries is nowhere near reaching the same acetol yield and production rates[105–107]. However, the process with copper chromite is not totally

satisfactory because of several shortcomings, such as the catalyst toxicity and, from an industrial viewpoint, the difficulty of scaling-up the reactive distillation process. In this direction, current academic efforts straddle between developing continuous and sustainable catalytic processes by using efficient heterogeneous catalysts and progressing on fundamental studies to fully understand the reaction mechanism involved in this catalytic transformation.

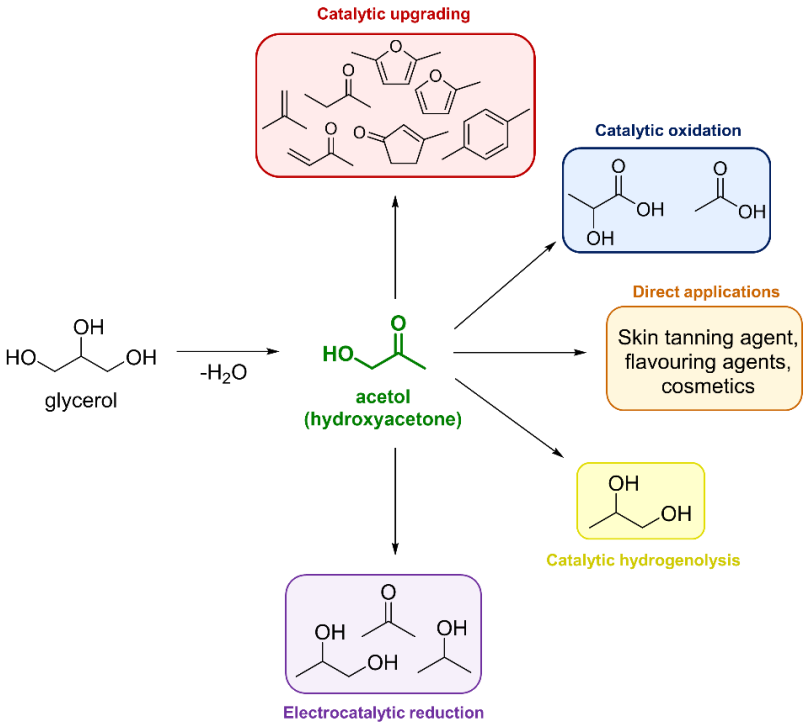

Figure 1.4. Synthesis and current acetol (hydroxyacetone) usages.

1.3.1 Continuous catalytic processes for glycerol dehydration to acetol

Concerning the advances on heterogeneous catalysts with the capability to work under continuous operation conditions, although not so many articles appear in the literature compared to the widely studied acrolein, which is the other possible dehydration product, some studies have been reported. These works can be divided into two main categories depending on the preferred catalyst: monofunctional acid and/or basic catalysts and copper-based materials. Several monofunctional acid catalysts based on promoted zirconia such as ZrS, ZrW, ZrWSi, ZrWAl, or SiO_2-Al_2O_3 could transform glycerol to

acetol with yields ≥ 70%, as long as temperatures above 300 ºC were reached[108,109]. However, on acidic catalysts, acetol tends to be unstable from 280 ºC onwards[110], which indeed constitutes a significant challenge for acetol production. In the same way, catalysts with a certain basic character were also reported to catalyse glycerol dehydration to acetol in high yield at a reaction temperature of 350 ºC. In this sense, a continuous process to convert glycerol into acetol using a sodium-doped metal oxide that combines acid and basic centres in the same catalyst has been reported. However, the main drawback of the process is the rapid catalyst deactivation[111].

Unlike the harsh conditions needed for acid-basic materials, copper-based catalysts have been described to dehydrate glycerol into acetol under milder conditions, usually between 220-280 ºC, at atmospheric pressure. Consequently, the Cu-based catalysts undoubtedly pose a far more advisable alternative from an energetic, economic, and environmental standpoint. In most cases, the metallic copper function is combined with acid-basic supports so that in these catalysts, the former acid and/or basic contribution is presented together with the specific role of Cu, which will be later discussed. Some of these bifunctional catalytic systems are efficient under N_2, while others need a H_2 atmosphere to work efficiently.

Probably, the first example of a catalyst involving the use of hydrogen in a continuous system that was described is, again, the copper chromite[112], which has earlier been identified as the most active catalyst for converting glycerol to acetol when combined with a reactive distillation technology[104]. In this case, the glycerol is loaded into an evaporator operated at a temperature of 230 ºC to promote glycerol evaporation and form a vapor reactor influent. The packed bed reactor is heated by immersing it in a constant temperature oil batch (230 ºC). Nevertheless, yields to acetol from pure glycerol are considerably lower in this system (≈60%), and the need to vaporize glycerol to work in a vapor-phase packed bed system should count as a disadvantage. This necessity to establish a vapor phase reaction leans on lessening the residence time and the density of the reaction mixture. The decrease in these two parameters reduces polymerization reactions, one of the primary sources of by-product formation and catalytic deactivation. Regarding the use of H_2 as a gas feed (and not only for catalyst activation), authors emphasized that higher acetol yields were noticed under an H_2 atmosphere than N_2[112]. The beneficial effect of

this operational choice relies not only on H_2 acting as a gas diluent promoting glycerol evaporation, but also on the fact that H_2 can minimize hydrogen scavenging from acetol. This second-order process can yield a more considerable number of by-products. Nonetheless, the work advices towards a careful optimization of the hydrogen feed depending on the glycerol dilution degree, since copper chromite is also said to be an active system to produce 1,2-propanediol under a H_2 atmosphere. As for the catalyst life, the material worked satisfactorily for 15 reaction cycles of 4-h duration, according to authors.

Later, T.P. Braga *et al.* reported a γ-Al_2O_3 phase containing a non-crystalline copper oxide with a high surface area, achieving an acetol yield of 80 %[113], and also mixed Cu-Al and Cu-Si oxides synthesized from polymeric precursors, which can reach acetol yields close to 90 %[114]. Reactions were carried out at 250 ºC, by working with a 10 wt.% glycerol aqueous solution, previously vaporized, and under a H_2 atmosphere. Additionally, the influence of the support in this type of reaction was further proved, showing that solids composed of Cu/Zn/Al and Cu/Fe/Al, with a copper-modified structure, attained notably higher catalytic stability compared to other samples only comprising isolated copper oxide (such as W and Sb-solids), mainly due to less sintering of Cu and lower coke formation[115]. In the same line, synthesized M_xO_y–Al_2O_3 (M = Ba, Mg, K or La) combined with copper species were tested in the conversion of glycerol to acetol yielding ≈70 % of the desired product in the first 2 h of reaction. However, for all these studies, catalyst deactivation at TOS ≤ 5-6 h and the use of H_2 remain as essential disadvantages to be overcome. Besides that, other minor drawbacks are usually the need to preheat the glycerol or even vaporize it before its introduction in the catalytic reactor along with the requirement of carrying out a catalyst activation under H_2[116].

In the absence of hydrogen, S. Sato *et al.* reported that Cu/Al_2O_3, Raney Cu, and Cu/SiO_2 showed selectivities higher than 80 % to acetol in N_2 flow when the catalyst was preheated under a H_2 flow. Additionally, they managed to achieve yields close to 90%, by working at 250 ºC and using a 30 wt.% glycerol aqueous solution, over a Cu-Al_2O_3 (Cu:Al = 3:2 mol.) catalyst prepared by coprecipitation[117]. Another Cu:Al (1:1 mol) mixed oxide was claimed as an efficient catalyst in the continuous dehydration of 20 wt.% aqueous glycerol carried out at 220 ºC and 20 bar of N_2 pressure, the catalyst being pre-

activated under a H_2 flow. The liquid analysis after every 5 h showed that glycerol conversion was ≤95% with ≈50% selectivity to acetol, with a catalyst stability lasting up to 400 h for this continuous dehydration of glycerol[118,119]. Additionally, La_2CuO_4 is another catalyst capable of effectively carrying out the reaction by using pure glycerol in the gas phase without any previous catalyst activation with H_2 (280 ºC, yield to acetol ≈76 mol.%)[120]. Nevertheless, in the case of Cu:Al mixed oxide, deactivation by coke deposition and copper sintering is still a problem, while for the La_2CuO_4 catalyst, the main drawbacks are its incompatibility with water as well as the need of vaporizing glycerol at ≥280 ºC before introducing it into the reactor along with N_2. Moreover, all these catalysts contain high copper loadings (> 15 wt.%), making them more expensive and metal demanding than usual. More recently, C. Batiot-Dupeyrat and co-workers also claimed that by using 80 wt.% aqueous glycerol, the $CuMgF_2$ catalyst (≈40% yield to acetol at 260 ºC, 5 wt.% Cu) showed to be more active than La_2CuO_4 (≈30% yield to acetol at 260 ºC, 16 wt.% Cu)[121].

Despite these recent findings, the narrow array of emerging technologies capable of continuously transforming glycerol to acetol indicates that the catalytic route is still in the early stages. In this regard, several key points, such as catalyst stability, catalyst reusability, attainment of high yields to acetol from glycerol in the liquid phase and working in the total absence of hydrogen and with low copper loadings, must be addressed and taken into account, before designing any novel catalytic process. Thus, realizing the physicochemical phenomena lying behind either the success or the failure of the process is a challenge that must be met. This leads us to the other noteworthy side of the literature on the selective glycerol dehydration to acetol, which is the understanding of the mechanism and those active sites involved in this chemical reaction.

1.3.2 Mechanistic insights into glycerol dehydration to acetol

Owing to the vast number of academic works devoted to gaining insight and enhancing acrolein production, the other plausible dehydration product, by using acid materials, a broad consensus has been reached to establish a relationship between selectivity and type of acidity. On this subject, acrolein selectivity is said to be dependent on the Brønsted acid site concentration, which are also more active centres, whereas Lewis acid sites are thought to be more selective to acetol production[122–126]. Separate pathways explain

this different behaviour for glycerol activation in every centre (*Scheme 1.2*). On a Brønsted acid site, the reaction would be initiated by protonating the secondary hydroxyl group of the glycerol molecule[124,127,128]. The reason for this preferential protonation has a lot to do with the fact that the intermediate between the protonated molecule and the corresponding enol is likely to be a carbocation[129]. Therefore, on the absence of critical steric constraints, which is the most common situation with Brønsted sites, the reaction will move on through the most stable intermediate, the secondary carbocation[130]. The resulting enol can easily tautomerize to the unstable 3-hydroxypropenal, which suffers the last dehydration to yield acrolein[131]. On the contrary, on a more sterically constrained Lewis acid site, it would begin with a concerted transfer of a terminal hydroxyl group on a Lewis acid site and the secondary proton migration to the adjacent oxygen[78,124]. The suggested intermediate formation of an enol, which can quickly tautomerize to hydroxyacetone[131], would justify the higher selectivity towards the latter compound on a Lewis acid site. It is worth mentioning that the water produced can hydrate a Lewis site that might further function as a pseudo-Brønsted site. These new Brønsted centres can either catalyse glycerol dehydration to acrolein, as outlined previously, or be dehydrated; for instance, thermal activation can regenerate the original Lewis acid site[132].

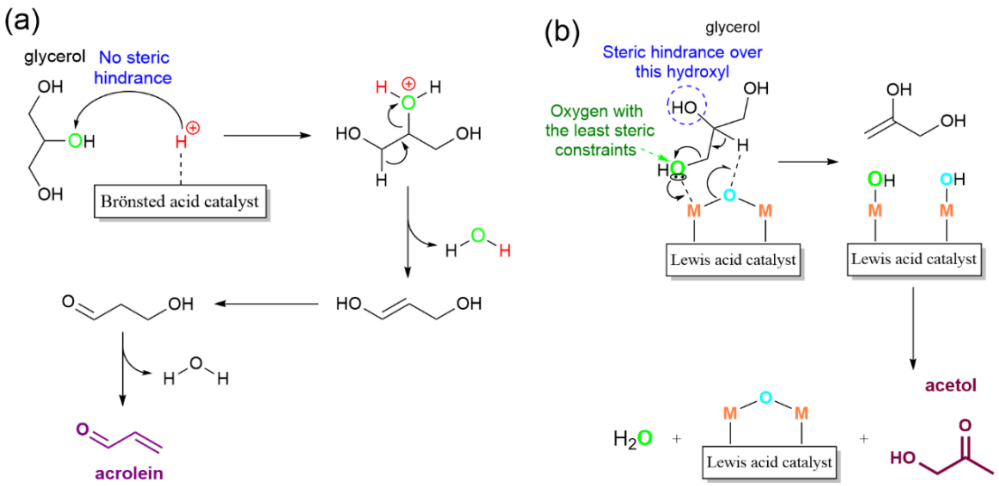

Scheme 1.2. Commonly accepted pathways for glycerol dehydration on acid catalysts[78,124,127,128].

Nonetheless, although *Scheme 1.2* can be considered representative of the current scientific mainstream in literature, several contradictory opinions can be found. Some authors still argue that Brønsted acid sites may operate in glycerol dehydration through two parallel reaction pathways depending on whether Lewis acid sites are located in their surroundings. Each of these mechanisms would give rise to a different dehydration product (i.e., acrolein or acetol). This proposal relies on the formation of acrolein and acetol being initiated by dehydration involving protonation of either secondary or primary −OH groups, respectively[110,133]. The most recent and convincing work on this mechanistic alternative provides proof, based on FTIR spectroscopy supported by DFT calculations, in order to claim that, in the presence of Lewis acidity, there should be a first step where glycerol can be adsorbed on a Lewis acid site by the primary hydroxyl group. When this happens, the primary C−O bonds would be polarized and, in the presence of an acidic proton, it is more likely that one of the primary hydroxyl groups, whose protonation is usually disfavoured with respect to that on the secondary one, is dehydrated to form 2-propene-1,2-diol[134]. This would lead, again, to the formation of the enol intermediate already described (*Scheme 1.2b*), which can undergo a rapid rearrangement to acetol[131].

By and large, and despite differing voices, it is broadly accepted that Lewis acidity would be the principal function on those catalysts providing more selectivity towards acetol. However, several catalysts showing acceptable acetol yields also contain a non-negligible number of basic sites[135–137]. Accordingly, the role and plausible mechanisms for glycerol dehydration on basic catalytic sites have also been investigated.

In contrast to the mechanism proposed over Lewis acid sites, the reaction over basic ones would not start with dehydration directly, but with a dehydrogenation step, which would produce 2,3-dihydroxypropanal (glyceraldehyde), a molecule whose dehydration and subsequent (re)hydrogenation yields the desired acetol (*Scheme 1.3*). Nonetheless, the intermediate glyceraldehyde can also undergo a retro-aldol reaction, thereby generating formaldehyde and hydroxyacetaldehyde, which can be afterwards hydrogenated to ethylene glycol[111]. These by-products would decrease the selectivity of this pathway, partially explaining why not so many reports with purely basic materials can be found in the literature about acetol production. Additionally, other authors reported that in the glycerol hydrogenolysis to 1,2-propanediol (in the presence of hydrogen), basic media

could first drive to the already mentioned glycerol dehydrogenation to glyceraldehyde, followed by dehydration to 2-hydroxyacrolein and then, this molecule can be hydrogenated with two H_2 molecules instead of one, thus yielding 1,2-propanediol and not acetol. As glycerol can serve as a hydrogen donor and the intermediates mentioned above as hydrogen scavengers, this could also constitute a disadvantage in terms of acetol selectivity[138–140].

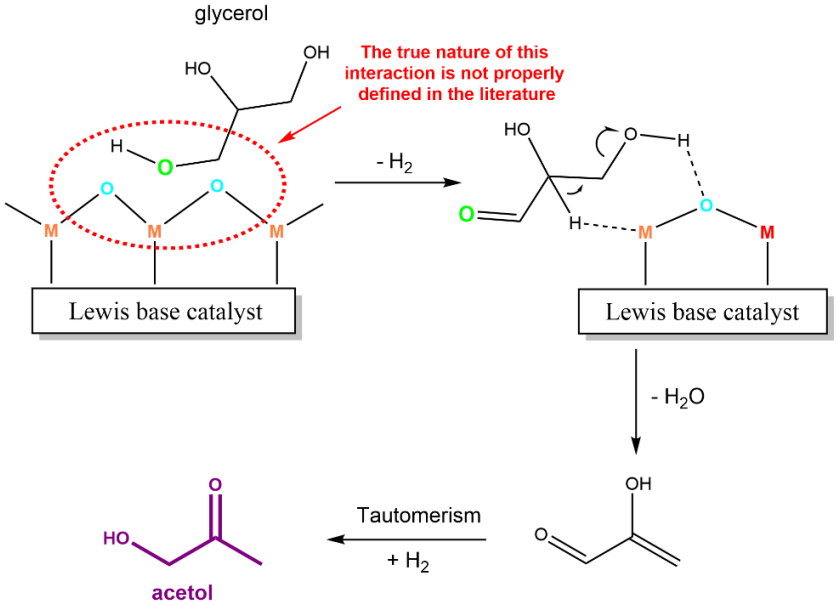

Scheme 1.3. Commonly accepted pathway for glycerol dehydration on a basic catalyst[111].

A different possibility is that reaction over basic sites progresses through dehydration starting from a terminal hydroxyl group. This would again generate the enol intermediate, which can experience a rapid rearrangement towards acetol[122]. The pathway would be very similar to the one described in Scheme 1.2b, but O-H and M-O's strength order would be swapped with respect to the one showed in a Lewis acid material. As in this latter case, steric factors would control the dehydration.

As stated by the different mechanisms over acid-base catalysts mentioned up to now, glycerol transformation to acetol might advance in parallel through different and

competitive pathways. Taking that into consideration, noticing direct correlations between activity and selectivity with surface acid/base properties is an arduous task and, therefore, the discussion about the reaction mechanism is still at stake. Some authors even argue that acetol formation could be favoured by a certain ratio between acid and basic Lewis centres[111,137].

So far, the dissertation on the reaction mechanism has been focused on those materials working at reaction temperatures equal to or above 280 ºC, and only possessing acid-base functionalities. However, as discussed in the last section, the presence of certain specific elements was proved beneficial for acetol production, enabling working at lower temperatures while achieving higher yields to the desired products. The conflicting discussion about the plausible reaction pathways over acid-base materials becomes even more complicated when introducing these other functionalities susceptible to participate in the reaction, such as certain noble metals (i.e., Ru, Pd, Pt), first-row transition metals (i.e., Cu, Ni, Co, Cr) and some lanthanides (i.e., Ce). In this direction, several authors have suggested that diverse mechanisms could arise in polyol dehydration in the presence of Cr, Cu, and Ce oxides with a change in the oxidation state of the transition metal and the assistance of neighbouring acid-base sites. The redox cycle of the transition metal is believed to affect product distribution[117,141–143].

As earlier stated in the previous section, among all these approaches based on introducing a new metallic functionality inside the catalyst, copper has been proved to be the most promising alternative in terms of catalytic results[104,117,120]. In their catalytic screening using the reactive distillation system, Suppes and co-workers found that Ru-based catalysts presented low-selectivities and high by-product formation, greater than 30%, due to the condensation reactions of hydrocarbon free radicals, which contribute to catalyst deactivation. As for nickel and palladium-based catalysts, low-selectivities and low-residue to initial glycerol ratios were detected due to their high catalytic activity, leading to an excess of degradation reactions of glycerol and giving rise to lower-molecular weight alcohols and gases[104]. On the contrary, copper is well-known for its limited capability to cleave the C-C bonds of a glycerol molecule compared with Co and Ni, thereby avoiding unwanted degradation products[144]. Besides that, plausible

condensation reactions catalysed by acid sites are more likely to occur over Ni[145] or acid sites[146] of the support rather than on the moderately acid copper sites.

The nature of the interaction Cu–glycerol has been the subject of debate in the literature from the moment Cu was found to be a key functionality to carry out the glycerol dehydration reaction to acetol. Given that the introduction of Cu boosts the catalytic activity and shifts selectivity towards acetol production, thinking about Cu either providing the reaction with a new pathway or enhancing one of the already existing seems reasonable. This insight seems essential to understand why the marked increase in activity and acetol selectivity at temperatures where, otherwise, the same catalyst but without Cu would be practically inactive. Nonetheless, an agreement on the glycerol dehydration pathway followed in the presence of Cu is nowhere near to be reached. Although several options have been proposed, precise experimental shreds of evidence for the selected mechanism are conspicuously absent. Likewise, authors have not come to a common decision about the oxidation state of Cu required to carry out the reaction. In this case, the identification of the active species is especially difficult as Cu can easily change its oxidation state under a reductive or oxidative environment.

As one of the first to approach this mechanistic issue, Scheme 1.4 illustrates the two routes proposed by Sato *et al.*[117]. Scheme 1.4a is based on the reaction of polyols such as glycerol and propanediols over a copper catalyst surface[147,148]. In this sense, for the gas-phase glycerol dehydration, the authors suppose that the reaction might occur *via* Cu-alkoxide species formed at the secondary carbon together with another hydrogen radical. This alkoxide allows for the release of an OH radical from a primary –OH group, so that water comes off the molecule. The other mechanistic approach (Scheme 1.4b), based on establishing an analogy to the dehydration of 1,3-propanediol[149], supposes that the alkoxide would be formed at the primary carbon so that glycerol is converted into 2-hydroxypropanal, which is readily tautomerized to hydroxyacetone. However, to discriminate between these mechanisms, the authors remark that determining which OH group of glycerol generates the alkoxide over the Cu metal surface to release hydrogen must be done. It should be mentioned that, although Schemes 1.4a and 1.4b represent processes that proceed *via* homolytic ruptures, the authors explain that the elimination of OH radical in the second step of these pathways may involve the release of an OH anion

attacked by an acid site. Then, an electron is transferred from the hydrogen radical to the surface alkoxide[117]. This hypothesis is in good agreement with different works using Cu-based catalysts on the fact that an acidic support promotes hydroxyacetone formation. Nevertheless, much more in-depth research should be conducted with the aim of distinguishing between a radical and an ionic mediated mechanism as well as between the presence of radicals and carbocations as reaction intermediates. Additionally, Sato *et al.* do not close the door on the possibility of a mechanism over Cu sites involving a dehydrogenation-dehydration-(re)hydrogenation sequence, which would be similar to the one over basic sites (see Scheme 1.3). Other authors have also supported this mechanism as an alternative that could be occurring on Cu[150,151].

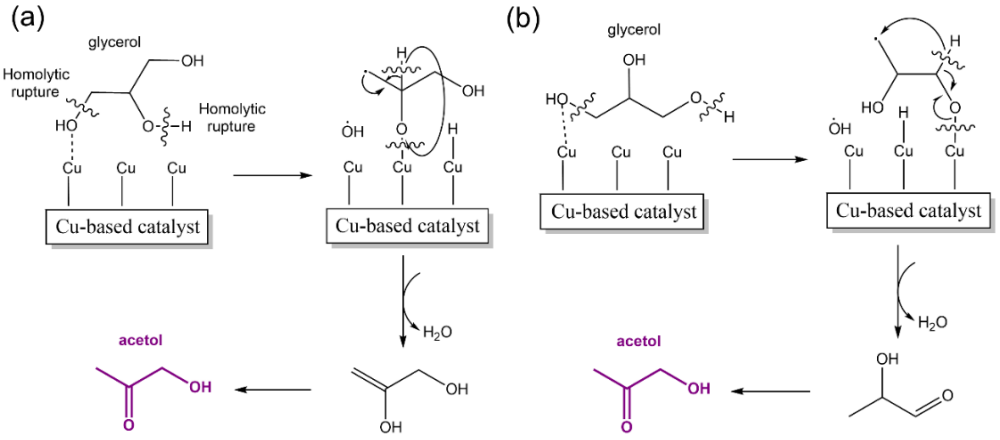

Scheme 1.4. Glycerol dehydration routes on Cu-based catalysts proposed by Sato *et al.*[117].

Regarding the nature of the active Cu species, Sato *et al.* directly assume that metallic Cu should account for the dehydration activity since the catalyst displays the best behaviour after treatment under a H_2 flow. Additionally, the validity of the proposed mechanisms relies upon other studies applied to the hydrogenation/dehydrogenation properties of metallic Cu surfaces[147,148]. Hence, at this point, the lack of characterization techniques helping to determine which is the Cu oxidation state throughout the reaction makes it wise to be cautious when considering these mechanisms.

Instead of proposing mechanistic alternatives, C.V. Rode and co-workers suggest that metallic copper could act along with Brønsted and Lewis acidity[152], thereby enhancing the mechanisms leading to acetol over these sites, which have been explained during the first two paragraphs of this section. As above-mentioned, the mechanism on Lewis acid sites would include the abstraction of a terminal hydroxyl group and simultaneous migration of the proton of the adjacent C to the O atom of the metal oxide. However, if the polarization of the metal accompanying Cu in the catalyst is higher than that exhibited by the latter, Cu would not be involved in the –OH abstraction and would take part only in the enol tautomerization to give acetol. The authors propose that metallic Cu or CuO would participate through an abstraction of a proton and simultaneous protonation of the secondary carbon[152]. However, the strong effect of Cu in the catalytic behaviour seems unlikely to rely just on facilitating this tautomerization process, which is known to occur fast independently of the presence of a catalyst[131].

As for the reaction occurring by combining Cu and Brønsted acid sites, although the protonation of the secondary –OH by Brønsted acids is favoured because the intermediate secondary carbocation is more stable[130], this pathway would lead to acrolein. Hence, the authors claim that in the presence of Cu, the reaction should proceed through protonation of the primary –OH of glycerol. In this case, the Cu is suggested to be involved, not only in the tautomerization but also in the proton abstraction during dehydration. As authors found by XRD and EXAFS that most of the Cu was in metallic form, they propose that metallic copper rather than the metal oxide acted as the true catalyst[152]. Again, probably an *in-situ* study and/or a study of the used catalyst should be included to support this hypothesis further.

Despite being reasonable alternatives, not all the proposed mechanisms offer convincing explanations about the Cu oxidation states involved in the glycerol dehydration reaction. Thus, lately, researchers on the lookout for new catalytic systems to carry out either glycerol hydrogenolysis or glycerol dehydration have started emphasising the critical role of the copper oxidation state.

In good agreement with what had been observed in the dehydration of 4-hydroxy-2-butanone, several authors discarded the weak acid sites; Cu^{2+}[153]. Pinheiro *et al.* observed that all the catalysts displayed inferior activities when treated under a N_2

atmosphere. They further investigated by XPS, H_2-TPR, and calorimetry the active species for glycerol dehydration to acetol, finding that they were likely to be reduced Cu species (Cu^I and/or Cu^0)[116]. Similarly, Liang and co-workers attributed the good catalytic behaviour of Cu-Cr catalyst in glycerol hydrogenolysis to a synergetic effect between Cu^I and Cu^0. In this sense, and supported by XPS measurements, they propose a first dehydration step, without additionally specifying any mechanistic details, that would be carried out by reduced $CuCr_2O_4$ spinel particles containing Cu^{1+} species, which might act as stronger acid sites than Cu^{2+}. The second step would consist of the hydrogenation of acetol on the Cu^0 sites[154]. However, as both reduced species might be present throughout the reaction, these statements about the Cu oxidation state remain as attractive suggestions.

In their work with La_2CuO_4 as the catalyst, C. Batiot-Dupeyrat, and co-workers determined by XRD and XPS that both Cu^{2+} and Cu^{1+} are present at the catalyst surface. Besides, they begin to tackle the oxidation state changes taking place during the reaction. Thus, they noticed that Cu^{2+} is partially reduced into Cu^{1+} during the time on stream. Interestingly, after reducing La_2CuO_4 into Cu^0/La_2O_3, a low catalytic activity was observed, these results pointing that metallic copper might not be the essential species to carry out the glycerol dehydration to hydroxyacetone[120].

The last results are awe-inspiring because they leave aside Cu^0 as the active site. We must consider that those mechanisms assuming that metallic copper is an active site for dehydration of glycerol to acetol through the alkoxide formation (Scheme 1.4) fit really well with what has been reported during alcohol dehydrogenation at the surface of Cu^0 [147,148]. In the same line, and more recently, C. Batiot-Dupeyrat and co-workers have tried to establish a reaction mechanism over Cu^{1+}[121]. They claim this active species selection is supported, not only with the results they achieved in their works, but also by DFT calculations which show that the hydrogen-bonded to carbon is more labile on Cu^+ than on Cu^0, thus propositioning a C-H bond rupture at the surface of Cu^{1+} similar to that postulated on cyclohexanol dehydrogenation to cyclohexanone[155]. Nevertheless, C. Batiot-Dupeyrat and co-workers highlight the difficulties involved in differentiating if Cu^{1+} is an active site "per se" or due to the Lewis acid properties of Cu^{1+}, which casts doubts on the selection of latter schemes. They suggest two new alternatives, although

closely related to some of the mechanisms already seen in this section. A first hypothesis, which was also proposed in their earlier work with La_2CuO_4[120], where Cu^{1+} is supposed to act as a Lewis acid site, is an analogy to the mechanism described in *Scheme* 1.2b[78,124]. However, Cu^{1+} would be the active site for the transfer of a terminal hydroxyl group. In the second mechanism, a homolytic C-H bond dissociation like the one proposed on metallic copper (Scheme 1.4) is suggested[117]. Although theoretical calculations support the formation of the proposed reaction intermediates in both cases[121,131] under the common experimental conditions, there are simulation limitations such as not considering the "Transition State" theory or the catalyst surface. In fact, authors recommend further discussion to clarify the reaction mechanism totally[121].

To the best of our knowledge, the most recent work approaching the identification of active sites for the dehydration of glycerol to acetol is that from W. Fan and co-workers. Their study of glycerol hydrogenolysis to 1,2-propanediol over Cu/SiO_2 catalysts points that the Lewis site Cu-O-Si-O- (with Cu^{2+}) would be crucial for achieving excellent hydrogenolysis performance. Based on FTIR and DFT studies, the authors claim that those moieties should be the active sites during glycerol dehydration[156]. Nonetheless, although it is clear from their findings that those fresh materials having a higher presence of those sites can attain better results for the overall process, the prevalence of those structures under the hydrogen atmosphere needed for the hydrogenolysis seems unlikely to happen. In contrast, from our perspective, the possibility of these moieties being involved in the subsequent formation of the actual active sites after their reduction seems a more plausible alternative.

On balance, there is no broad agreement regarding the active copper species and the reaction intermediates, nor about which are the interactions established between them and the reactant, the intermediates, and the product. Even so, it seems that the mainstream and the most convincing proofs point to the presence of reduced copper species in the working catalysts. Likewise, the scarce theoretical studies so far provided give slight preference to Cu^{1+} as the plausible active centre. Nonetheless, *in-situ* and/or *operando* studies would be necessary to unequivocally determine the true nature of the active copper species. That effort seems essential to complete the understanding of the process and pave the way towards selecting an efficient catalyst. In this sense, the present thesis tried to deal with

this need, which has been understood as crucial to overcoming all the shortcomings displayed by the catalysts reported up to date.

1.4 New alternatives for glycerol valorisation: towards organonitrogen chemicals

In this context, once glycerol could be transformed into a more reactive molecule such as acetol, it would be easier to associate this product formation to the manufacture of higher added value chemicals using highly selective processes and reducing synthesis steps. However, a critical problem with much of the literature on biomass transformation is that it has been usually dedicated to producing carbon, hydrogen, and oxygen-based chemicals. In view of this, the lack of works towards other heterorganic compounds suggests alternative directions for future research. In particular, the opportunities offered by the oxygenated functionalities of biomass-derived molecules, such as glycerol or acetol, for their catalytic conversion into organonitrogen chemicals by solid catalysts are currently attracting a new surge of interest[157–159]. As formerly stated, to achieve this objective, it is essential to develop new multi-functional catalysts capable of carrying out several cascade-type reactions in a single stage[10,14,160], solid catalysts being promising candidates to carry out this type of processes[47,50].

Notably, organonitrogen chemicals play a central role in many areas of modern life. Key examples include alkanolamines[161] and nitrogen functionalized porous materials for carbon dioxide absorption[162–165], surfactants[166–168], large polymer manufacturing (i.e., nylon), fertilisers[169] and pesticides[170] for the agricultural industry, as well as various amino acids presenting broad applications as nutrients for the food industry[171]. In the same way, amino acids serve as the building blocks for proteins with critical biological functions. On top of that, it must be mentioned the importance of organonitrogen chemicals for the medical industry given the fact that all top 15 pharmaceutical products by sales in 2017 were organonitrogen chemicals, with an annual market value of over 110 billion USD[172]. Other examples include chiral catalysts[173], synthetic precursors[174], solvents[174], or epoxy resins curing agents[175], among others.

Nowadays, most commercial precursors for organonitrogen chemicals are still synthesized within the petroleum refinery scheme, contributing to the carbon and hydrogen supply. On the other hand, nitrogen gas is the source of all synthetic organonitrogen substances at the end of the day. However, it needs to be activated and transformed into ammonia either chemically or biologically before being combined with organic compounds[176]. In industries, the nitrogen source is regularly ammonia (NH_3) or an NH_3-containing or derived starting material. Currently, the Haber-Bosch process produces this feedstock under high temperatures and high pressure, yielding ammonia at a scale of 140 million tonnes annually[177]. Unfortunately, the prevailing pathways to make N-containing chemicals from NH_3 are often indirect or under harsh reaction conditions.

For example, in the case of aliphatic amines, they are commonly produced by alkene hydroamination[178] or by ammonia alkylation with alcohols[179]. In the first case, a major drawback is the dependence on the traditional fossil-based refinery, while in the second case, to produce long aliphatic amines, usually, fatty acids are employed, and the process involves multiple steps. In that case, fatty acids react with ammonia under high temperatures to form fatty acid ammonium salts in the first step. Subsequently, the corresponding amides are produced after a dehydration step, followed by a second dehydration step to generate nitriles. Finally, further reduction of nitriles under high-pressure hydrogen affords primary fatty amines mixed with secondary and tertiary amines as side products[179].

The reaction pathway is also complex for industrial aromatic amine synthesis. First, benzene is nitrated with concentrated nitric and sulfuric acid mixture at around 50 ºC to generate nitrobenzene. Relevantly, benzene comes from the distillation of crude oil followed by catalytic reforming, while NH_3 oxidation is needed to yield nitric acid. The nitrobenzene is then hydrogenated (typically at 200–300 ºC) in the presence of metal catalysts, based on nickel or copper, to aniline[180,181]. By the same token, aniline derivatives are frequently prepared by nitration of the substituted aromatic compounds followed by reduction[182]. Alternatively, benzene can be transformed into halogen benzene in the Friedel−Crafts halogenation using Lewis acids as catalysts[183]. Afterwards, transition metal-catalysed amination of aryl halides with ammonia results in

aniline as the product[184]. Similarly, several similar multistep syntheses can be found in available manufacturing methods to produce nitriles[185] or amides[186].

Other examples include alkanolamines and ethyleneamines. The former family of compounds is usually generated by the reaction of amines with epoxides, which are, in turn, synthesized through different oxidation methods from alkenes coming from the petrochemical route[174]. Concerning ethyleneamines, there are two main routes for producing these chemicals; the reaction between ethylene dichloride and ammonia and the reductive amination of monoethanolamine. Historically, much of the production comprised the ethylene dichloride route. In this route, first, ethylenediamine is produced by treating 1,2-dichloroethane with ammonia under pressure at 180 ºC in an aqueous medium. Therefore, the starting product of this reaction is ethylenediamine. In the presence of an excess of 1,2-dichloroethane, the initial ethylenediamine is extended by one ethylene unit. The terminal alkyl chloride reacts with ammonia to deliver the amine, and the polyamine chain can be lengthened this way. The addition of a polyamine to the initial reaction mixture can give a boost to the concentration of higher-order polyamines. A stoichiometric base is required to transform the amine hydrochloride to free amines[187].

The manufacture of nitrogen heterocycles constitutes another vital issue on account of the tremendous importance of these compounds, containing at least one nitrogen atom in the ring. Nitrogen heterocycles can be aromatic, saturated, or unsaturated. Examples of saturated nitrogen heterocycles are azetidines, pyrrolidines, piperidines, and piperazines, while some of the aromatic simplest nitrogen heterocycles are pyrroles, pyridines, imidazoles, pyrazines, pyrimidines, pyridazines, triazoles, triazines and tetrazoles. Since the production of N-heterocycles deserves special mention because of their importance during the present thesis, *Section 1.5* delivers a more careful examination of their applications, current syntheses, and bio-based opportunities and perspectives.

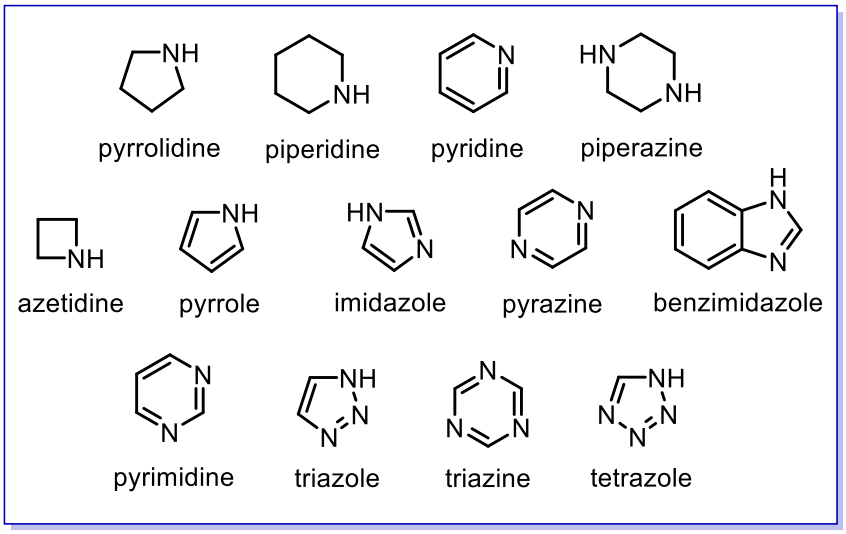

Figure 1.5. Chemical structures for some of the most important nitrogen heterocycles.

Overall, the multiple steps involved in the manufacturing processes of these chemicals are known to suffer from several problems, comprising dependence on non-renewable feedstock, low overall carbon yields, and the employment of harsh reaction conditions. Consequently, the lookout for alternative ways to produce organonitrogen chemicals from renewable sources efficiently and cost-effectively focuses on employing greener substrates and less-toxic ingredients, creating less waste, and working under milder conditions, which are critical targets in synthetic chemistry.

1.4.1 Bio-based organonitrogen chemicals

Within this framework, and in the same way that various biomass components continue to be extensively studied as raw materials for catalytic fuel and chemical production in the last decade[188–191], biomass may be used as the feedstock to produce organonitrogen chemicals. This usage can alleviate the carbon footprint, and simplified synthesis routes may arise if exploiting the specific functional groups and heteroatoms (e.g., N, S, P) present in biomass resources, which already proved to be able to provide a wide array of possibilities for the insertion of nitrogen atoms in organic structures[192–195]. In this way, complex organonitrogen compounds become accessible *via* innovative chemical transformations using biomass as the source of C or as the source of both C and

N. Moreover, incorporating biomass into the organonitrogen chemical supply chain would go beyond the boundaries of the current biorefinery, thus increasing product diversity and enhancing the economic competitiveness of the sector[157,158,196,197]. In this context of organonitrogen chemical synthesis, a wealth of clean alternatives are opening up to yield the desired products.

The first approach would consist of coupling oxygen-containing bio-based derived molecules with several organonitrogen chemicals (mainly amines) coming from the conventional refinery scheme. Among the processes following this methodology, the direct coupling of bio-alcohols with amines *via* the borrowing hydrogen approach[198] has been broadly believed to be a clean and efficient method for synthesizing N-alkylamines and amides[196]. This method is usually chosen because a vast assortment of alcohols is accessible from biomass, it can occur without consuming a reductive agent, and water is generated as the sole by-product[199]. Although alcohols are more readily available substrates than aldehydes/ketones, the amination of alcohols to produce amines requires one additional dehydrogenation step to generate the carbonyl group. Furthermore, this alcohol activation generally requires high temperatures (between 180 and 250 ºC)[157]. Therefore, an analogous strategy gaining much attention in recent years is the amination of aldehydes (or even ketones) *via* reductive amination with amines and molecular hydrogen[200] or the utilization of CO_2 and CO, coming from the processing of biomass wastes, as the carbon source in N-alkylamines and amides synthesis[201]. Due to its importance for the present thesis, a more detailed discussion on reductive amination can be found in later sections. Advantageously, the reductive amination of carbonyl compounds with amines can be carried out under milder reaction conditions (even at room temperature), is not burdened with inherent toxicity and corrosion issues, and does not generate waste salts. In addition, it is generally low-priced due to inexpensive and broadly accessible substrates. However, major drawbacks are the H_2 consumption and the need to choose a catalytic system with a preference towards imine or enamine hydrogenation rather than direct hydrogenation of the carbonyl substrate into the corresponding alcohol[196].

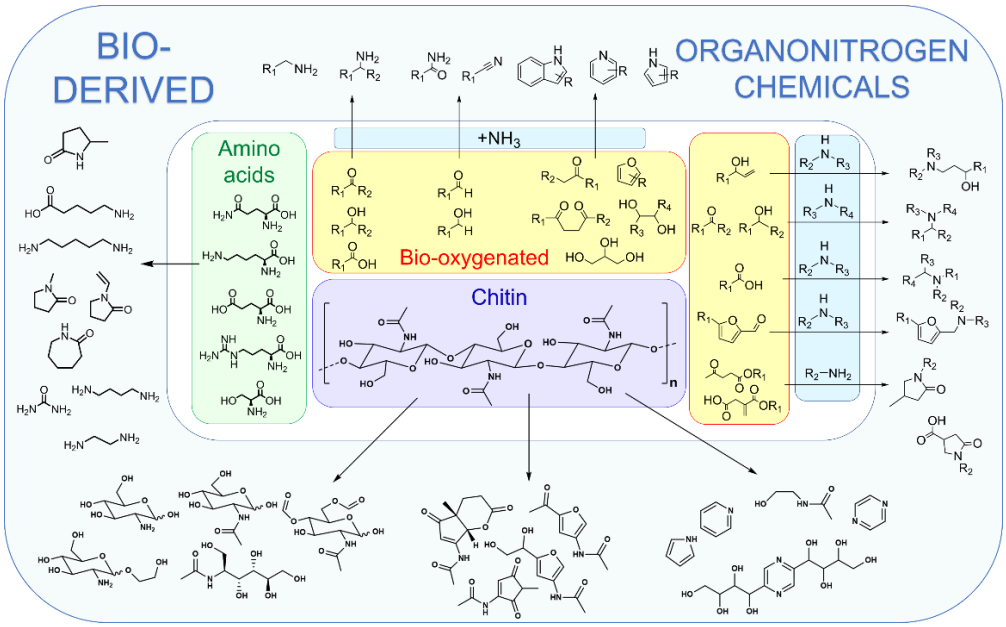

Figure 1.6. Overview of the different strategies to produce organonitrogen chemicals from biomass and bio-derivatives[157,158,198,200,202,203].

On the other hand, in recent years, there has been a growing interest in the single-step conversion from abundant bio-derived alcohols or aldehydes into various N-containing functional groups using NH_3 as the nitrogen source[157]. Again, the process can start from an alcohol *via* dehydrogenation-condensation-hydrogenation[204] or from a carbonylic compound *via* reductive amination[196]. Regarding the amination of alcohols, the production of alkylamines from bio-derived alcohols (i.e., bioethanol, biobutanol) is an area of active research[205–207]. Conversely, *via* reductive amination, important bio-derived carbonyl compounds such as furfural and other furan derivatives, cyclopentanone, glycolaldehyde and widely available organic acids (i.e., levulinic acid, succinic acid, itaconic acid, among others) can be used to make amines, nitriles, amides, and amino acids[202].

Another thrilling option consists in using amino acids as a source of both organic N and organic C to produce organonitrogen chemicals. Since biomass is derived from living matter, it also contains a small amount of protein that could be separated before processing. Concretely, focusing on second-generation biomass, let us remember that it

contains a significant fraction of waste, which might be very rich in protein. Examples coming from food and beverage wastes include stillage (from sugar beet or sugar cane), soluble distillers' grains (from wheat or corn), pressed cakes (from oilseeds such as palm and rapeseed and jatropha), fish silage, bird feathers, among others[208]. Other amino acid sources from second-generation biomass can be plant leaves, waste oils or biodiesel by-products, and slaughterhouse waste[209]. A great deal of this waste protein is now processed as animal feed or employed in nutrition, medicine, or drug formulations impacting physiological function[203,210]. However, it could also be a cost-effectively and environmentally attractive raw material for basic chemicals. In an ideal biorefinery, essential amino acids would be used for animal feed, while non-essential amino acids could be a source of bulk chemicals[203,210].

Although it has indeed been suggested that basic nitrogen-containing chemicals could be produced more economically and with a smaller environmental footprint from biomass-derived amino acids, to be competitive with petrochemical pathways, amino acid production and conversions should accomplish specific requirements. Efficient technologies for the isolation of the different amino acids will have to be implemented[209], their conversion should involve as few functional group modifications as possible[203], and new routes to manufacture amino acids from other biomass components should be developed[211].

Last, besides proteins, chitin is the other important natural reservoir of biologically fixed nitrogen that would establish processes not dependent on the fuel refinery or the Haber process[212]. Chitin is a biopolymer that accounts for about 15–40% of the weight of crustacean shells[213]. It can also be found in insects and fungi' skeletons, thereby being the world's second most abundant biopolymer next to cellulose[214]. The fundamental molecule is a polymer of repeating amino sugar units. In fact, the structure of chitin closely resembles that of cellulose apart from the substitution of the –OH group with $–NH_2$ or an acetamido group at the C_2 position[214,215]. That repetitive structure raises the possibility to produce well-defined product mixtures after the deconstruction of the biopolymer[216–222], instead of the complex hydrolysates resulting from protein hydrolysis[223,224]. As a result, several different N-containing chemicals have been effectively obtained in the laboratory, including amino sugars, amino alcohols, amino

acids, and heterocyclic compounds showing potential medicine, food, beverages, and cosmetics applications, and others[215]. Indeed, a novel concept of *shell biorefinery* has been proposed owing to the huge potentials of chitin valorisation[214,215]. However, new improvements need to be implemented for shell fractionation and novel pre-treatment of chitin to fully exploit these technologies. In addition, a deeper insight into reaction mechanisms about chitin biomass conversion is required to develop efficient and reusable solid-acid catalysts for chitin hydrolysis and conversion, eliminating toxic solvents and non-environmentally friendly separation procedures[214,215,225].

1.5 N-heterocycles

Bearing in mind the tremendous importance of organonitrogen chemicals and that two-thirds of the N-containing chemicals, comprising approximately 80% of the top medicines by sales, incorporate N-heterocyclic skeletons[226], an extraordinary research effort should be conducted to develop green and practical approaches to synthesize these heterocycles. Indeed, this has been one of the main driving forces of the present thesis. Again, the synthesis methodologies need a transition from fossil resources to renewable biomass feedstocks *via* sustainable chemistry.

For instance, the pyrrole-containing N-heterocycles, structural units broadly applied in pharmaceuticals, pesticides, and functional materials[227,228], are industrially obtained from the naphtha acquired by crude oil distillation. This naphtha is steam cracked into 1,3-butadiene at ≥750 ºC. Subsequently, catalytic oxidation is carried out, followed by a reaction with NH_3 in the presence of a solid acid (i.e., Al_2O_3) to form the pyrrole[229]. In opposition, as bio-based alternatives, from 1,4-dicarbonyl compounds, N-substituted pyrroles can be synthesized by Paal–Knorr condensation with primary amines over acid catalysts[230–232]. Biomass-derived alcohols are also a green feedstock for pyrrole synthesis. Examples are the catalytic acceptorless dehydrogenative coupling with amines of 1,4-butanediols[233,234] and unsaturated diols[235,236] over base-metal complexes and, on the other hand, the metal-catalysed hydrogen borrowing strategy converting alcohols to carbonyl compounds, followed by condensation to give imines, and reduction to amines by the H_2 liberated[237]. Although the reported homogeneous catalysts carry out the reaction with remarkable performances, recovery problems bring around

additional costs and damaging environmental effects. A recent and comprehensive assessment of these alcohol reactions stresses heterogeneous catalysis to overcome these difficulties, certainly leaving room for improvement on issues such as catalyst recycling or the prevalence of noble metals[238]. Other methods are catalytic amination of bio-furans with primary amines and acid catalysts (e.g., TiO_2, zeolites)[239,240] or reaction of hexose sugars with amines[241], having the potential to produce pyrrole alkaloid natural products.

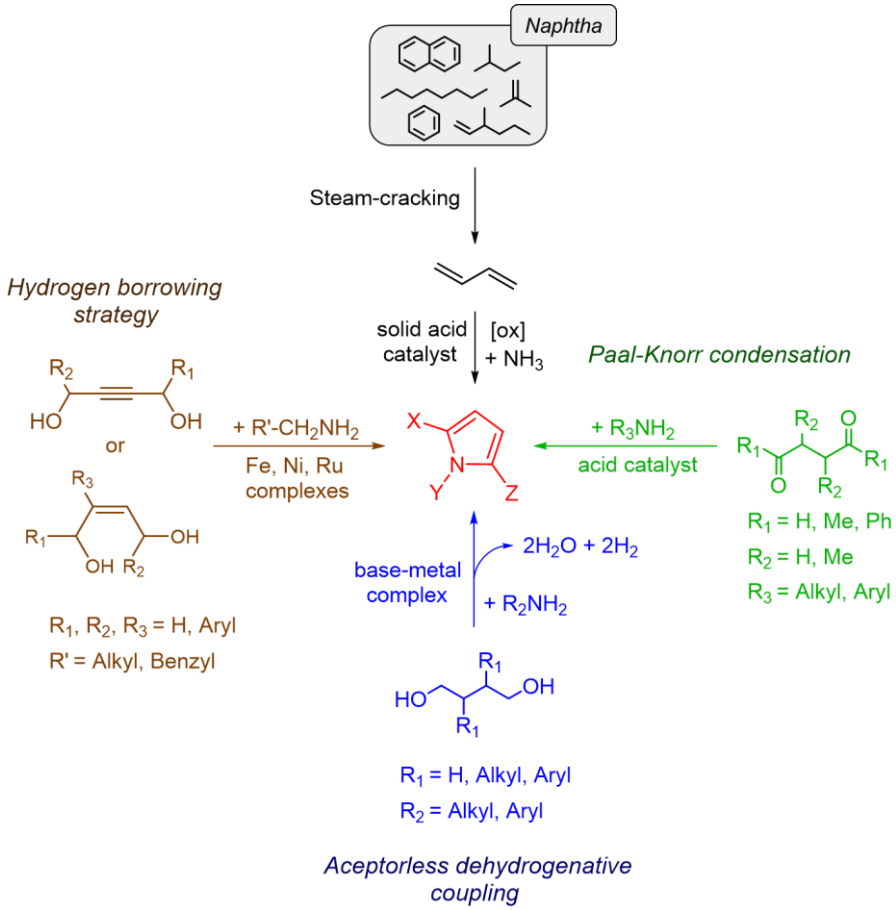

Figure 1.7. Classical and bio-based routes to produce pyrrole and pyrrole derivatives.

Pyridines, compounds with high biological activity and found in numerous agrochemicals, pharmaceuticals, catalysts, and solvents[242], stand out among 6-membered heterocycles. Some traditional pyridine synthesis include the Chichibabin

condensation of aldehydes with ammonia in fixed-bed reactors, using CdF_2 or MnF_2, or the Bönnemann cyclization with a nitrile molecule and two parts of an acetylene derivative[242,243]. A more promising approach for producing pyridines consists of reacting acrolein, coming from glycerol dehydration, with NH_3 to yield pyridine. The latter reaction combines C–N condensation, Michael addition, hydrogenation, and dehydrogenation steps. In this sense, zeolite-based catalysts (e.g., HZSM-5) have unique shape selectivity, high surface area, and remarkable thermal stability. They are highly active to produce pyridines by promoting C–N condensation and Michael addition when their pore size and acidity are accurately tailored[244–248]. Interestingly, a neater approach starts directly from glycerol by carrying out *in-situ* dehydration, which is possible to accomplish with the same catalysts[249–252]. Other bio-derived compounds such as isomaltulose, fructose[253], or furan derivatives[254] have also been successfully employed to reach pyridine-based molecules through synthetical routes involving a higher degree of complexity.

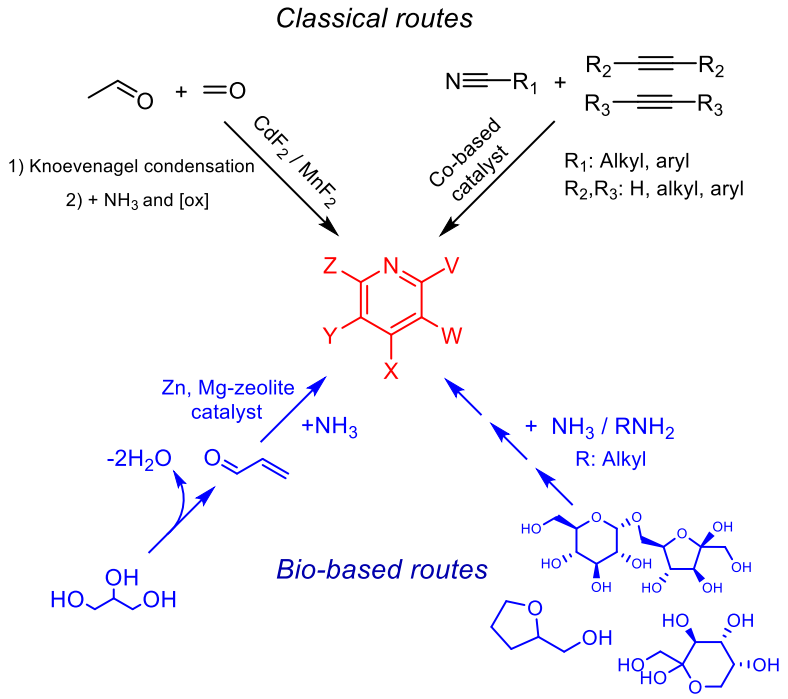

Figure 1.8. Classical and bio-based routes to produce pyridine and pyridine derivatives.

Another representative case is pyrrolidone. Pyrrolidones are applied in pharmaceuticals, printing inks, fiber dyes, surfactants, and solvents[255]. 2-Pyrrolidone is produced industrially by treating gamma-butyrolactone with ammonia at 250–290 ºC and pressures ranging from 0.4–1.4 MPa over solid magnesium silicate catalysts[255]. However, γ-Butyrolactone has been traditionally prepared by dehydrogenation of 1,4-butanediol[256] which, in turn, comes from butane oxidation[257]. Alternatively, over the last decades, there has been a surge of heterogeneous metal catalysts to produce pyrrolidones from biomass-derived levulinic acid[258–261] and derivatives by catalytic reductive amination with primary amines *via* amination–reduction–cyclization or amidation–cyclization–dehydration–reduction[262,263].

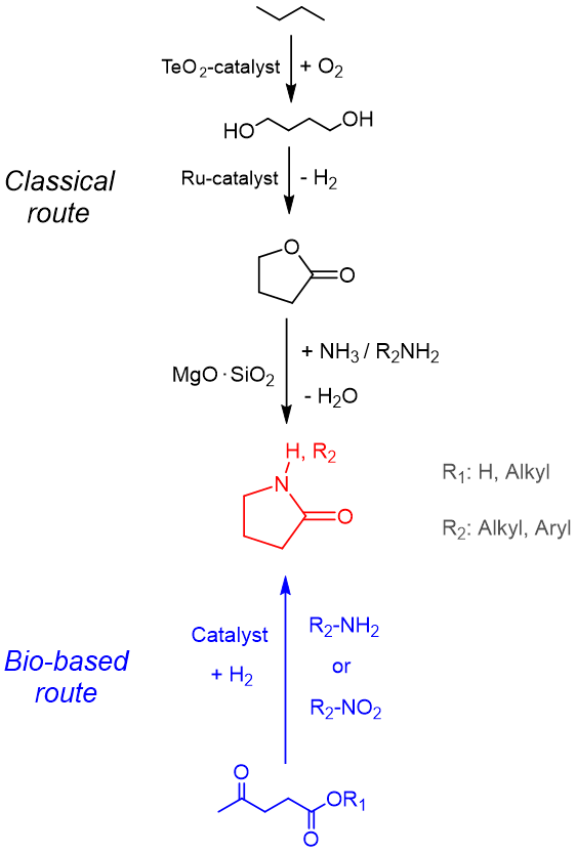

Figure 1.9. Classical and bio-based routes to produce pyrrolidone and pyrrolidone derivatives.

Recent literature teems with other examples of simple N-heterocycles whose synthesis are shifting from fossil-based resources towards biomass-derived feedstocks. For example, pyrazoles, traditionally synthesized by the reaction of hydrazines with α,β-unsaturated aldehydes or diketones[264,265], ultimately coming from olefins, are also being prepared from sugars[266,267], β-ketoesters and aromatic aldehydes from lignin[268], and 1,3-diols[269], reacting with hydrazine derivatives to yield a diversity of pyrazole derivatives. Industrially, imidazoles are synthesized from the condensation of 1,2-dicarbonyls with ammonia and aldehydes *via* the Radziszewski reaction[270]. Alternatively, several synthetic approaches are being developed to produce substituted imidazoles from sugars such as fructose, glucose, isomaltulose, melibiose, leucrose, maltose, cellobiose, lactose, and arabinose[271–273].

In this context, the transformation of glycerol into nitrogenated compounds and, specifically, into N-heterocycles, is a path that is already offering some exciting options to produce amines and hydroxyl amines. For instance, BASF claimed a hydrogen borrowing one-step process to generate amines from glycerol and NH_3 in H_2O, under elevated H_2 pressure and 200 ºC in the presence of a metal catalyst (e.g., Ni-RANEY® or Co-RANEY®). Here, glycerol undergoes sequential dehydrogenation, amination, and hydrogenation[274]. Another alternative, particularly considered in this thesis, consists of combining dehydration to acetol and reductive amination in the presence of H_2. Glycerol was first converted into hydroxyacetone (acetol) using a $2CuO{\cdot}Cr_2O_3$ catalyst at 230 ºC. Next, acetol was converted into 2-amino-1-propanol *via* reductive amination using a solid Ni catalyst in the presence of 76 bar H_2 and aqueous ammonia, at 85 ºC[275]. More recently, Katryniok and co-workers described another two-step strategy for aqueous glycerol amination into dimethylamino-2-propanone at 250 ºC based on first dehydration and a subsequent hydroamination. Accordingly, mesoporous SiO_2 supported phosphomolybdic acid ($H_3PMo_{12}O_{40}$) was used as catalyst[276]. A similar scheme but based on dehydration followed by amination can be used to obtain dimethylamino-3-propanal with heteropolyacid/Zr-MCM-41 as catalysts at 300 ºC[277]. BASF also claimed another unusual process involving a C–C cleavage with NH_3 in H_2O over Pd/C at 230 ºC and 250 H_2 bar to convert sugar alcohols into ethylene and propylene diamines and their heterocyclic adducts (piperazines and heteroaromatics)[278].

In the same way, a growing body of literature has recently started to examine the use of glycerol and glycerol derivatives as a carbon source to produce N-heterocycles. Some reports on pyridine synthesis that have been already mentioned[249–252], the oxazoline[279] and 3-methylindole[280] syntheses, processes to produce pyrazinyl compounds[281–287] or, more specifically, the work carried out by Venugopal's group on 2-methylpyrazine production[288–292], which will be more deeply discussed later, are among recent examples of this novel glycerol usage. Nonetheless, in most cases, processes and catalysts are either highly specific and expensive or not environmentally friendly, and the yields to N-heterocycles obtained are moderate.

Against a backdrop of examples where glycerol requires severe reaction conditions that ultimately lead to decreased product selectivity, several other cases can be found of attempts made with other glycerol intermediates to enhance the reactivity of the initial substrate, thus allowing for working under milder conditions. As examples, glyceraldehyde can be used for the synthesis of 3-amino-1,2-propanediol over Ru/ZrO_2 at 65 ºC and 20 H_2 bar[293], and the glycerol derivative solketal can be aminated with a homogeneous Ru-based catalyst[294]. Although in the former case, a reactive intermediate such as glyceraldehyde is challenging to be produced with high selectivity, and in the latter, the development of highly efficient heterogeneous catalysts has not yet been achieved, this previous transformation of glycerol into a suitable intermediate is an appealing strategy. Therefore, this thesis intends to propose alternative strategies using glycerol through its derivative acetol as starting compounds to synthesize chemicals of the N-heterocycle-type among different nitrogenated chemical products with high added value and industrial interest. As previously said in this introduction, glycerol dehydration to acetol still requires a higher degree of optimization and understanding. But, having said that, we have also seen several examples where acetol can act as intermediate in synthesising organonitrogen chemicals from glycerol[275,276].

To be specific, prior to the beginning of this thesis, a lack of works with heterogeneous catalysts to produce piperazines and pyrazines was noticed. Therefore, the possibility of valorising glycerol by using it as a carbon source to produce these N-heterocycles was considered. However, these new alternatives will be based on a series of cascade-type reactions involving a sequence of elementary reaction steps that will require different

catalytic sites. Therefore, it will be highly desirable to develop catalytic systems and multi-functional heterogeneous catalysts capable of efficiently and selectively carrying out several consecutive reaction steps.

1.5.1 Piperazines: applications and synthesis

The piperazine ring itself is an anthelmintic[295], and a large number of piperazine derivatives such as piperazine hydrate, piperazine adipate, and piperazine citrate also have anthelmintic action[296]. In addition, the piperazine ring can also be found as a building block for many high added value drugs, from antihistamines to antidepressants, thus being highly valued synthesis intermediate chemicals in organic chemistry[297]. Importantly, a 2014 analysis reported that piperazine is the third most commonly used N-heterocycle in small-molecule pharmaceuticals, with several piperazine-containing drugs being within the top 100 best-selling pharmaceutical products[298,299].

On the other hand, CO_2 capture systems based on amine scrubbing using concentrated piperazine recently were shot into the spotlight due to the high energy and adsorption performances of such technology. Indeed, these systems have demonstrated excellent regeneration ability by thermal swing regeneration, without significant degradation of the scrubbing solvent, good resistance to oxidative degradation, lower volatility compared to other typical amine-based solvents, and a corrosion-resistant behaviour to stainless steel[300–302]. Additionally, piperazine is often used in relatively small amounts to supplement specific amine blends, taking advantage of how piperazine protects from significant thermal and oxidative degradation at typical coal flue gas conditions. At the same time, the CO_2 absorption rate, the heat of absorption, and the solvent capacity are increased through the addition of the piperazine[303,304].

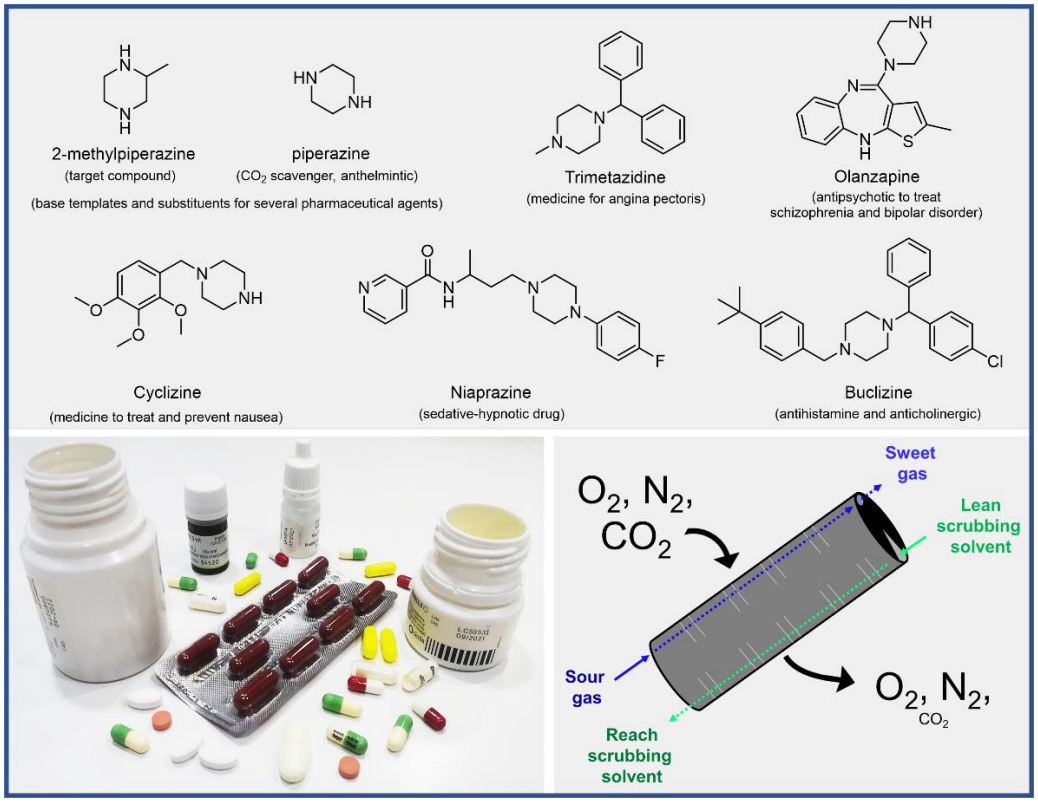

Figure 1.10. Piperazine related compounds examples and applications.

Today, the favourite commercial method to obtain piperazine derivatives entails the ammonization of either 1,2-dichloroethane or ethanolamine over a Ni-RANEY® catalyst at 195 ºC and very high H_2 pressures (>130 bar). In any case, the piperazine got as a by-product needs to be separated from ethylenediamine, triethylenediamine, and other related cyclic and linear nitrogenated compounds[305]. But, again, it is necessary to note that 1,2-dichloroethane and ethanolamine are primarily obtained from fossil resources and, in particular, from ethylene[306,307]. As regards the synthesis of 2-methylpiperazine, old synthetic procedures to yield this chemical also involved the use of Ni-RANEY® catalysts in batch reactors by using N-β-hydroxypropyl-ethylenediamine and hydrogen (at 13 bar and 200 ºC), with moderate yields (≈50%) and no existing data about catalyst recyclability[308]. Recently, the use of heterogeneous catalysts in continuous processes for another type of syntheses has been reported, such as the intra-cyclization of N-β-hydroxypropyl-ethylenediamine over Cu–Cr–Fe/γ-Al_2O_3 (at 205 ºC and high H_2

pressure)[309], or H-ZSM-5 (at 260 ºC)[310], and the intermolecular cyclization of diethanolamine and methylamine to N,N′-dimethylpiperazines and N-methylpiperazines at 300 ºC and high H_2 pressures (80–100 bar) with H-ZSM-5 as a catalyst[311,312]. The attainment of the piperazine ring by condensation–cyclization reactions of diethanolamine with NH_3 and a catalyst containing Al, Co, Ni, Cu, and Sn-oxides working at 200 ºC and a H_2 pressure of 200 bar is remarkable as well[313]. However, and mainly because of severe reaction conditions, the commercial use of these processes becomes difficult, and the synthesis methodologies must be improved yet. Hence, in this thesis, the reductive cyclo-amination of acetol (obtained *via* glycerol dehydration in a first step) with a diamine and a heterogeneous catalyst is considered an encouraging option to produce 2-methylpiperazine (Scheme 1.5).

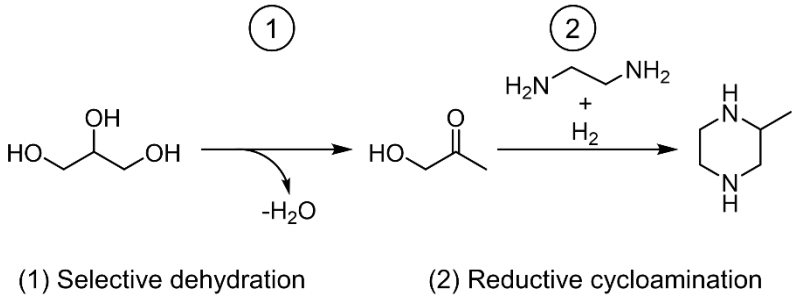

Scheme 1.5. Intended route to synthesize 2-methylpiperazine.

1.5.2 Pyrazines: applications and synthesis

It should be mentioned that 2-methylpyrazine, one of the main targets of this thesis research, is an intermediate compound for the synthesis of pyrazinamide[314], shown in Figure 1.8a, a well-known bacteriostatic drug used against tuberculosis[315].

Other alkyl pyrazines are naturally occurring highly aromatic substances which are often associated with the taste and aroma of numerous foods (Figure 1.11b), including roasted peanuts, cooked potatoes, coffee beans, cocoa, baked goods, and wines[316]. Some of these alkyl pyrazines are also formed by heating some foods *via* Maillard reactions, a reaction between reducing sugars and amino acids[317].

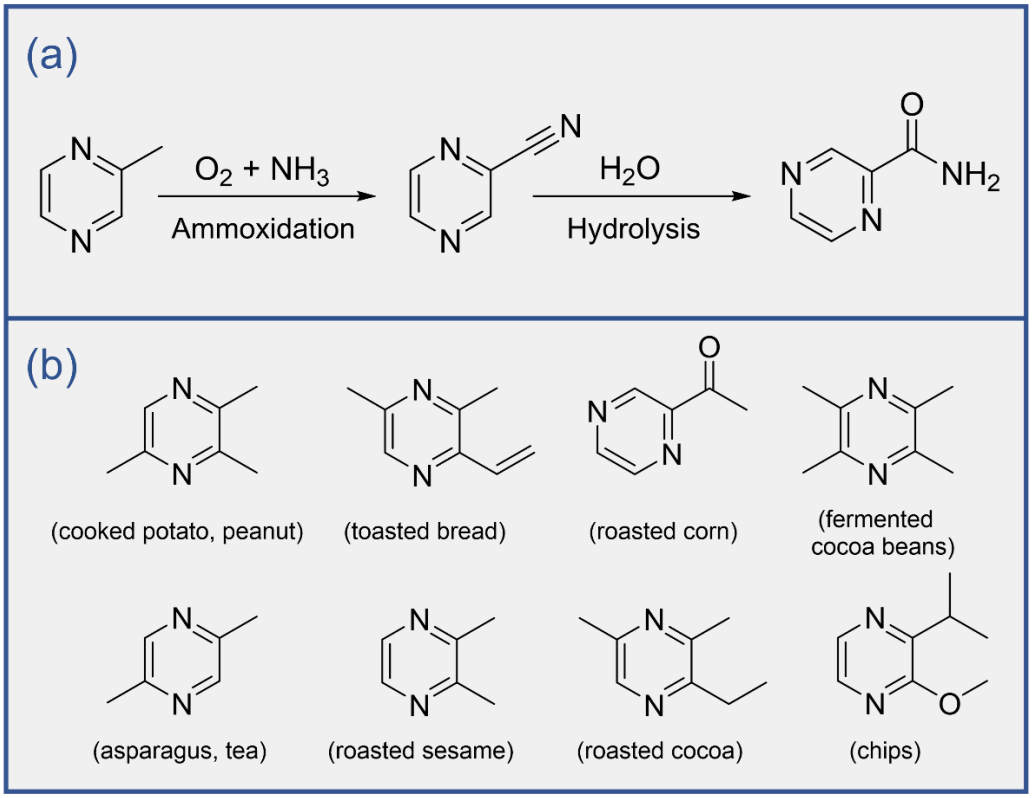

Figure 1.11. (a) Synthesis of pyrazinamide from 2-methylpyrazine. (b) Pyrazine derivatives contributing to the flavour of a variety of foods.

Other pyrazine derivatives can be used in drugs against glaucoma. Glaucoma is an eye disease characterised by excessive intraocular pressure, which may cause an irreversible loss of visual functions and even blindness. The intraocular pressure can be lowered using specific alkyl pyrazine structures[318,319].

A number of old organic methodologies for synthesising pyrazine and its derivatives were reported more than two centuries ago. The self-condensation of α-ketoamines or the combination of α-diketones with vicinal diamines followed by dehydrogenation are among the oldest synthesis reactions to produce pyrazines that continue to be exploited[320].

Importantly, pyrazine can also be synthesized through heterogeneous catalysis, usually comprising metals or metal oxides. To the best of our knowledge, Anderson *et al.* claimed

the first heterogeneous catalyst for this process, exploring the deamination of diethylenetriamine using a catalyst mixture Al_2O_3:MoO_3:P_2O_5 in the ratio of 94:5:1. The study achieved a 27.5% of pyrazine, with a maximum selectivity to the desired product, and without the presence of other by-products[321].

Another possibility for pyrazine synthesis consists of using ethylenediamine in the presence of a copper oxide-copper chromite catalyst. Two moles of ethylenediamine undergo cyclization to eliminate an ammonia molecule to give piperazine, followed by dehydrogenation to yield pyrazine. The mixture of copper oxide/copper chromite with a Cu/Cr ratio 2:1 showed ≥80% conversion with more than 95% pyrazine selectivity over the temperature range of 380-420 ºC[322].

In another alternative approach, J. Okada produced the first example of pyrazine compounds synthesis by reacting diamines with diols in a vapor-phase system in the presence of granular alumina [323]. Another important example applying a similar strategy is the Ag-La-Zn/Al_2O_3 catalyst, claimed to achieve a conversion rate of 100% and a yield of 2-methylpyrazine of 88% at 360 ºC, starting from propylene glycol and ethylene diamine[324]. The pyrazine synthesis was successfully afforded (55-78% yield) from a diamine and a diol over zinc oxide or a mixture of 10% zinc with other metals such as cobalt, nickel, iron, aluminium, and chromium as catalyst through a gas-phase reaction at 300-600 ºC, and by using silica, alumina, or silica-alumina as the catalyst carrier[325]. Moreover, Park et al. concluded that the cyclization of propylene glycol and ethylenediamine to give 2-methylpyrazine using CuO-ZnO-SiO_2 catalyst showed outstanding results (84% of 2-metylpyrazine yield at ≈99% conversion) attributed to the combined effect of the dehydrogenation properties of CuO-SiO_2 and the cyclization properties of ZnO-SiO_2[326]. Other catalytic systems with limited data in reference patents are based on copper-chromium, copper-zinc-chromium, or zinc phosphates with manganese[320]. In the same line, R. Anand *et al.* reported the reaction of ethylenediamine and propylene glycol over ZnO-modified FER[327] and ZnO-modified ZSM-5[328] catalysts, achieving yields close to 65% when working with an excess of ethylenediamine at 450 ºC.

Similarly, over the last two decades, several scientific reports are marshalling their efforts towards substituting propyleneglycol with glycerol as the source of the oxygenated

carbon moiety for continuous pyrazine synthesis. In this regard, Venugopal and co-workers used glycerol and ethylenediamine in the presence of a pre-reduced mixture of ZnO and $Zn_2Cr_2O_4$ to produce 2-methylpyrazine, reporting yields around 65% at 400 ºC after careful optimization of both synthetic and operational parameters[288–292]. Also, Venugopal's team worked with several M_xO_y–MCr_2O_4 systems to synthesize 2,6-dimethylpyrazine from 1,2-propanediamine and glycerol, concluding that the system CuO-$CuCr_2O_4$ (Cu:Cr molar ratio equal to 2) was able to yield 68% of 2,6-dimethylpyrazine at 350 ºC[283–285]. In addition, M-ZnO/Al_2O_3 (M: Zr, Ce, Ca, Mn, Mo)[282] and Cu-TiO_2/Al_2O_3[287] have been reported to achieve good yields of a mixture of pyrazine-type compounds at 380 ºC.

Despite all these examples to attain pyrazine by working with glycols and diamines as reactants over heterogeneous catalysts, the developed processes have several common shortcomings, such as harsh reaction conditions, hydrogen activation procedures, chromium-based catalysts, and complicated work-up procedures. Alternatively, there is a new surge in works aiming at using more reactive starting chemicals, thus allowing for working under milder reaction conditions. In this sense, Richard *et al.* reported the catalytic formation of pyrazine *via* reaction between α-hydroxyketones and 1,2-diamines performed in the presence of an excess of manganese dioxide. The addition of KOH in methanol to the reaction mixture proved decisive and could give 10-66% of pyrazine[329]. Likewise, γ-maghemite-silica showed an outstanding performance in yielding a broad variety of pyrazine derivatives at 55 ºC for 6 h when starting from diketones and α-hydroxyketones, although an incipient catalyst deactivation was noticed[330]. Even though in these cases reactions made use of discontinuous reactors, these innovative solutions led us to think of hydroxyacetone (or acetol) as a key intermediate to achieve the synthesis of 2-methylpyrazine (see Scheme 1.6), thus allowing for using milder reaction conditions than what is usually reported when starting from glycerol.

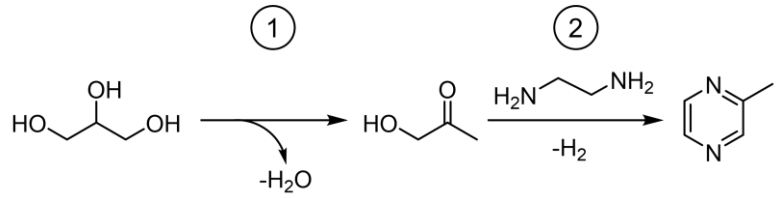

Scheme 1.6. Intended route to synthesize 2-methylpyrazine.

1.6 References

[1] B. Dudley, BP Statistical Review of World Energy 2019, no.68, Br. Pet. (2017). https://doi.org/bp.com/statisticalreview.

[2] P.G. Levi, J.M. Cullen, Mapping Global Flows of Chemicals: From Fossil Fuel Feedstocks to Chemical Products, Environ. Sci. Technol. 52 (2018) 1725-1734. https://doi.org/10.1021/acs.est.7b04573.

[3] EPA, U.S. Greenhouse Gas Emissions and Sinks, 1990-2016, Epa 430-R-18-003. (2018). https://doi.org/EPA 430-R-12-001.

[4] IEA, Renewables 2019, Market analysis and forecast from 2019 to 2024, ISBN 978-92-64-30684-4. (2019).

[5] L.A. Pfaltzgraff, J.H. Clark, Green chemistry, biorefineries and second generation strategies for re-use of waste: An overview, in: Adv. Biorefineries Biomass Waste Supply Chain Exploit., 2014. https://doi.org/10.1533/9780857097385.1.3.

[6] D. Jullesson, F. David, B. Pfleger, J. Nielsen, Impact of synthetic biology and metabolic engineering on industrial production of fine chemicals, Biotechnol. Adv. 33 (2015) 1395-1402. https://doi.org/10.1016/j.biotechadv.2015.02.011.

[7] J. Becker, C. Wittmann, Advanced biotechnology: Metabolically engineered cells for the bio-based production of chemicals and fuels, materials, and health-care products, Angew. Chemie - Int. Ed. 54 (2015) 3328-3350. https://doi.org/10.1002/anie.201409033.

[8] U.T. Bornscheuer, A.T. Nielsen, Editorial overview: Chemical biotechnology: Interdisciplinary concepts for modern biotechnological production of biochemicals and biofuels, Curr. Opin. Biotechnol. (2015). https://doi.org/10.1016/j.copbio.2015.07.002.

[9] A. Corma Canos, S. Iborra, A. Velty, Chemical routes for the transformation of biomass into chemicals, Chem. Rev. 107 (2007) 2411-2502. https://doi.org/10.1021/cr050989d.

[10] G.W. Huber, A. Corma, Synergies between bio- and oil refineries for the production of fuels from biomass, Angew. Chemie - Int. Ed. 46 (2007) 7184-7201. https://doi.org/10.1002/anie.200604504.

[11] J. Artz, T.E. Müller, K. Thenert, J. Kleinekorte, R. Meys, A. Sternberg, A. Bardow, W. Leitner, Sustainable Conversion of Carbon Dioxide: An Integrated Review of Catalysis and Life Cycle Assessment, Chem. Rev. 118 (2018) 434-504.

https://doi.org/10.1021/acs.chemrev.7b00435.

[12] S. Saeidi, N.A.S. Amin, M.R. Rahimpour, Hydrogenation of CO2 to value-added products - A review and potential future developments, J. CO2 Util. 5 (2014) 66-81. https://doi.org/10.1016/j.jcou.2013.12.005.

[13] X.G. Zhu, S.P. Long, D.R. Ort, What is the maximum efficiency with which photosynthesis can convert solar energy into biomass?, Curr. Opin. Biotechnol. 19 (2008) 153-159. https://doi.org/10.1016/j.copbio.2008.02.004.

[14] J.N. Chheda, G.W. Huber, J.A. Dumesic, Liquid-phase catalytic processing of biomass-derived oxygenated hydrocarbons to fuels and chemicals, Angew. Chemie - Int. Ed. 46 (2007) 7164-7183. https://doi.org/10.1002/anie.200604274.

[15] S. Jones, C. Valkenburg, C. Walton, Production of gasoline and diesel from biomass via fast pyrolysis, hydrotreating and hydrocracking: a design case, Energy. (2009). https://doi.org/PNNL-22684.pdf.

[16] F. Agrela, M. Cabrera, M.M. Morales, M. Zamorano, M. Alshaaer, Biomass fly ash and biomass bottom ash, in: New Trends Eco-Efficient Recycl. Concr., 2018, 23-58. https://doi.org/10.1016/B978-0-08-102480-5.00002-6.

[17] S. Gent, M. Twedt, C. Gerometta, E. Almberg, Introduction to Feedstocks, in: Theor. Appl. Asp. Biomass Torrefaction, 2017, 17-39. https://doi.org/10.1016/b978-0-12-809483-9.00002-6.

[18] S.K. Bardhan, S. Gupta, M.E. Gorman, M.A. Haider, Biorenewable chemicals: Feedstocks, technologies and the conflict with food production, Renew. Sustain. Energy Rev. 51 (2015) 506-520. https://doi.org/10.1016/j.rser.2015.06.013.

[19] D. Klemm, B. Heublein, H.P. Fink, A. Bohn, Cellulose: Fascinating biopolymer and sustainable raw material, Angew. Chemie - Int. Ed. 44 (2005) 3358-3393. https://doi.org/10.1002/anie.200460587.

[20] X. Zhou, W. Li, R. Mabon, L.J. Broadbelt, A critical review on hemicellulose pyrolysis, Energy Technol. 5 (2017) 52-79. https://doi.org/10.1002/ente.201600327.

[21] P. Azadi, O.R. Inderwildi, R. Farnood, D.A. King, Liquid fuels, hydrogen and chemicals from lignin: A critical review, Renew. Sustain. Energy Rev. 21 (2013) 506-523. https://doi.org/10.1016/j.rser.2012.12.022.

[22] M. Pugazhvadivu, K. Jeyachandran, Investigations on the performance and exhaust emissions of a diesel engine using preheated waste frying oil as fuel, Renew. Energy. 30 (2005) 2189-2202. https://doi.org/10.1016/j.renene.2005.02.001.

[23] Z. Utlu, Evaluation of biodiesel fuel obtained from waste cooking oil, Energy Sources, Part A Recover. Util. Environ. Eff. 29 (2007) 1295-1304. https://doi.org/10.1080/00908310500434564.

[24] Y. Li, L.W. Zhou, R.Z. Wang, Urban biomass and methods of estimating municipal biomass resources, Renew. Sustain. Energy Rev. 80 (2017) 1017-1030. https://doi.org/10.1016/j.rser.2017.05.214.

[25] N. Scarlat, J.F. Dallemand, F. Fahl, Biogas: Developments and perspectives in Europe, Renew. Energy. 129 (2018) 457-472. https://doi.org/10.1016/j.renene.2018.03.006.

[26] M. Himanen, K. Hänninen, Composting of bio-waste, aerobic and anaerobic sludges - Effect of feedstock on the process and quality of compost, Bioresour. Technol. 102 (2011) 2842-2852. https://doi.org/10.1016/j.biortech.2010.10.059.

[27] F. Cherubini, The biorefinery concept: Using biomass instead of oil for producing

energy and chemicals, Energy Convers. Manag. 51 (2010) 1412-1421. https://doi.org/10.1016/j.enconman.2010.01.015.

[28] J.H. Clark, R. Luque, A.S. Matharu, Green Chemistry, Biofuels, and Biorefinery, Annu. Rev. Chem. Biomol. Eng. 3 (2012) 183-207. https://doi.org/10.1146/annurev-chembioeng-062011-081014.

[29] G.W. Huber, J.N. Chheda, C.J. Barrett, J.A. Dumesic, Chemistry: Production of liquid alkanes by aqueous-phase processing of biomass-derived carbohydrates, Science 308 (2005) 1446-1450. https://doi.org/10.1126/science.1111166.

[30] J.P. Lange, R. Price, P.M. Ayoub, J. Louis, L. Petrus, L. Clarke, H. Gosselink, Valeric biofuels: A platform of cellulosic transportation fuels, Angew. Chemie - Int. Ed. 49 (2010) 4479-4483. https://doi.org/10.1002/anie.201000655.

[31] J.Q. Bond, D.M. Alonso, D. Wang, R.M. West, J.A. Dumesic, Integrated catalytic conversion of γ-valerolactone to liquid alkenes for transportation fuels, Science 327 (2010) 1110-1114. https://doi.org/10.1126/science.1184362.

[32] D.A. Simonetti, J. Dumesic, Catalytic production of liquid fuels from biomass-derived oxygenated hydrocarbons: Catalytic coupling at multiple length scales, Catal. Rev. - Sci. Eng. 51 (2009) 441-484. https://doi.org/10.1080/01614940903050626.

[33] A. Deneyer, T. Ennaert, B.F. Sels, Straightforward sustainability assessment of sugar-derived molecules from first-generation biomass, Curr. Opin. Green Sustain. Chem. 10 (2018) 11-20. https://doi.org/10.1016/j.cogsc.2018.02.003.

[34] B. Kamm, M. Kamm, Biorefinery - systems, Chem. Biochem. Eng. Q. 18 (2004) 1-6.

[35] J.R.H. Ross, Catalysis in Biomass Conversion, in: Contemp. Catal., 2019, 343-364. https://doi.org/10.1016/b978-0-444-63474-0.00015-1.

[36] M. Hingsamer, G. Jungmeier, Chapter Five - Biorefineries, in: Role Bioenergy Emerg. Bioeconomy Resour. Technol. Sustain. Policy, 2019, 179-222.

[37] A. Patel, K. Hrůzová, U. Rova, P. Christakopoulos, L. Matsakas, Sustainable biorefinery concept for biofuel production through holistic volarization of food waste, Bioresour. Technol. 294 (2019) 122247. https://doi.org/10.1016/j.biortech.2019.122247.

[38] B.H.H. Goh, C.T. Chong, Y. Ge, H.C. Ong, J.H. Ng, B. Tian, V. Ashokkumar, S. Lim, T. Seljak, V. Józsa, Progress in utilisation of waste cooking oil for sustainable biodiesel and biojet fuel production, Energy Convers. Manag. 223 (2020) 113296. https://doi.org/10.1016/j.enconman.2020.113296.

[39] G. Moretto, I. Russo, D. Bolzonella, P. Pavan, M. Majone, F. Valentino, An urban biorefinery for food waste and biological sludge conversion into polyhydroxyalkanoates and biogas, Water Res. 170 (2020) 115371. https://doi.org/10.1016/j.watres.2019.115371.

[40] H.T.N. Hao, O.P. Karthikeyan, K. Heimann, Bio-refining of carbohydrate-rich food waste for biofuels, Energies. 8 (2015) 6350-6364. https://doi.org/10.3390/en8076350.

[41] W.A. Qazi, M.F.M. Abushammala, M.H. Azam, Multi-criteria decision analysis of waste-to-energy technologies for municipal solid waste management in Sultanate of Oman, Waste Manag. Res. 36 (2018) 594-605. https://doi.org/10.1177/0734242X18777800.

[42] D.J. Cole-Hamilton, Homogeneous catalysis - New approaches to catalyst separation,

recovery, and recycling, Science 299 (2003) 1702-1706. https://doi.org/10.1126/science.1081881.

[43] I.T. Horváth, P.T. Anastas, Innovations and green chemistry, Chem. Rev. 107 (2007) 2169-2173. https://doi.org/10.1021/cr078380v.

[44] P. Anastas, N. Eghbali, Green Chemistry: Principles and Practice, Chem. Soc. Rev. 39 (2010) 301-312. https://doi.org/10.1039/b918763b.

[45] F.X. Felpin, E. Fouquet, Heterogeneous multifunctional catalysts for tandem processes: An approach toward sustainability, ChemSusChem, 1 (2008) 718-724. https://doi.org/10.1002/cssc.200800110.

[46] M.J. Climent, A. Corma, S. Iborra, Mono-and multisite solid catalysts in cascade reactions for chemical process intensification, ChemSusChem. 2 (2009) 500-506. https://doi.org/10.1002/cssc.200800259.

[47] M.J. Climent, A. Corma, S. Iborra, Heterogeneous catalysts for the one-pot synthesis of chemicals and fine chemicals, Chem. Rev. 111 (2011) 1072-1133. https://doi.org/10.1021/cr1002084.

[48] Y.C. Lin, G.W. Huber, The critical role of heterogeneous catalysis in lignocellulosic biomass conversion, Energy Environ. Sci. 2 (2009) 68-80. https://doi.org/10.1039/b814955k.

[49] R. Rinaldi, F. Schüth, Design of solid catalysts for the conversion of biomass, Energy Environ. Sci. 2 (2009) 610-626. https://doi.org/10.1039/b902668a.

[50] P. Sudarsanam, R. Zhong, S. Van Den Bosch, S.M. Coman, V.I. Parvulescu, B.F. Sels, Functionalised heterogeneous catalysts for sustainable biomass valorisation, Chem. Soc. Rev. 47 (2018) 8349-8402. https://doi.org/10.1039/c8cs00410b.

[51] M. Ventura, A. Marinas, M.E. Domine, Catalytic Processes for Biomass-Derived Platform Molecules Valorisation, Top. Catal. 63 (2020) 846–865. https://doi.org/10.1007/S11244-020-01309-9.

[52] D.J. Mihalcik, C.A. Mullen, A.A. Boateng, Screening acidic zeolites for catalytic fast pyrolysis of biomass and its components, J. Anal. Appl. Pyrolysis. 92 (2011) 224-232. https://doi.org/10.1016/j.jaap.2011.06.001.

[53] M.M. Rahman, R. Liu, J. Cai, Catalytic fast pyrolysis of biomass over zeolites for high quality bio-oil – A review, Fuel Process. Technol. 180 (2018) 32-46. https://doi.org/10.1016/j.fuproc.2018.08.002.

[54] F.L. Chan, A. Tanksale, Review of recent developments in Ni-based catalysts for biomass gasification, Renew. Sustain. Energy Rev. 38 (2014) 428-438. https://doi.org/10.1016/j.rser.2014.06.011.

[55] A.M. Robinson, J.E. Hensley, J. Will Medlin, Bifunctional Catalysts for Upgrading of Biomass-Derived Oxygenates: A Review, ACS Catal. 6 (2016) 5026-5043. https://doi.org/10.1021/acscatal.6b00923.

[56] G.W. Huber, R.D. Cortright, J.A. Dumesic, Renewable alkanes by aqueous-phase reforming of biomass-derived oxygenates, Angew. Chemie - Int. Ed. 116 (2004) 1575-1577. https://doi.org/10.1002/anie.200353050.

[57] D. Gabriëls, W.Y. Hernández, B.F. Sels, P. Van Der Voort, A. Verberckmoes, Review of catalytic systems and thermodynamics for the Guerbet condensation reaction and challenges for biomass valorization, Catal. Sci. Technol. 5 (2015) 3876-3902. https://doi.org/10.1039/c5cy00359h.

[58] L. Wu, T. Moteki, A.A. Gokhale, D.W. Flaherty, F.D. Toste, Production of Fuels and Chemicals from Biomass: Condensation Reactions and Beyond, Chem. 1 (2016) 32-58. https://doi.org/10.1016/j.chempr.2016.05.002.

[59] P. Gallezot, Conversion of biomass to selected chemical products, Chem. Soc. Rev. 41 (2012) 1538-1558. https://doi.org/10.1039/c1cs15147a.

[60] M.J. Climent, A. Corma, S. Iborra, Converting carbohydrates to bulk chemicals and fine chemicals over heterogeneous catalysts, Green Chem. 13 (2011) 520-540. https://doi.org/10.1039/c0gc00639d.

[61] J.C. Serrano-Ruiz, R. Luque, A. Sepúlveda-Escribano, Transformations of biomass-derived platform molecules: From high added-value chemicals to fuels via aqueous-phase processing, Chem. Soc. Rev. 40 (2011) 5266-5281. https://doi.org/10.1039/c1cs15131b.

[62] I.B. Banković-Ilić, O.S. Stamenković, V.B. Veljković, Biodiesel production from non-edible plant oils, Renew. Sustain. Energy Rev. 16 (2012) 3621-3647. https://doi.org/10.1016/j.rser.2012.03.002.

[63] H.B. Aditiya, T.M.I. Mahlia, W.T. Chong, H. Nur, A.H. Sebayang, Second generation bioethanol production: A critical review, Renew. Sustain. Energy Rev. 66 (2016) 631-653. https://doi.org/10.1016/j.rser.2016.07.015.

[64] M. Rastogi, S. Shrivastava, Recent advances in second generation bioethanol production: An insight to pretreatment, saccharification and fermentation processes, Renew. Sustain. Energy Rev. 80 (2017) 330-340. https://doi.org/10.1016/j.rser.2017.05.225.

[65] D. Kushwaha, N. Srivastava, I. Mishra, S.N. Upadhyay, P.K. Mishra, Recent trends in biobutanol production, Rev. Chem. Eng. 35 (2019) 475-504. https://doi.org/10.1515/revce-2017-0041.

[66] M.M.K. Bhuiya, M.G. Rasul, M.M.K. Khan, N. Ashwath, A.K. Azad, M.A. Hazrat, Second generation biodiesel: Potential alternative to-edible oil-derived biodiesel, in: Energy Procedia. 61 (2014) 1969-1972. https://doi.org/10.1016/j.egypro.2014.12.054.

[67] N. Kumar, Varun, S.R. Chauhan, Performance and emission characteristics of biodiesel from different origins: A review, Renew. Sustain. Energy Rev. 21 (2013) 633-658. https://doi.org/10.1016/j.rser.2013.01.006.

[68] D. Tilman, J. Hill, C. Lehman, Carbon-negative biofuels from low-input high-diversity grassland biomass, Science. 314 (2006) 1598-1600. https://doi.org/10.1126/science.1133306.

[69] O.R. Inderwildi, D.A. King, Quo vadis biofuels?, Energy Environ. Sci. 2 (2009) 343-346. https://doi.org/10.1039/b822951c.

[70] M. Çetinkaya, F. Karaosmanoğlu, Optimization of base-catalyzed transesterification reaction of used cooking oil, Energy and Fuels. 18 (2004) 1888-1895. https://doi.org/10.1021/ef049891c.

[71] S.C. D'Angelo, A. Dall'Ara, C. Mondelli, J. Pérez-Ramírez, S. Papadokonstantakis, Techno-Economic Analysis of a Glycerol Biorefinery, ACS Sustain. Chem. Eng. 6 (2018) 16563-16572. https://doi.org/10.1021/acssuschemeng.8b03770.

[72] C.H. Zhou, J.N. Beltramini, G.Q. Lu, Chemoselective catalytic conversion of glycerol as a biorenewable source to valuable commodity chemicals, Chem. Soc. Rev. 37 (2008) 527-549. https://doi.org/10.1039/b707343g.

[73] M. Hájek, F. Skopal, Treatment of glycerol phase formed by biodiesel production, Bioresour. Technol. 101 (2010) 3242-3245. https://doi.org/10.1016/j.biortech.2009.12.094.

[74] H. Bateni, A. Saraeian, C. Able, A comprehensive review on biodiesel purification and upgrading, Biofuel Res. J. 4 (2017) 668-690. https://doi.org/10.18331/BRJ2017.4.3.5.

[75] G.M. Lari, G. Pastore, M. Haus, Y. Ding, S. Papadokonstantakis, C. Mondelli, J. Pérez-Ramírez, Environmental and economical perspectives of a glycerol biorefinery, Energy Environ. Sci. 11 (2018) 1012-1029. https://doi.org/10.1039/c7ee03116e.

[76] T. Werpy, G. Petersen, Top Value Added Chemicals from Biomass, U.S. Dep. Energy. (2004). https://doi.org/10.2172/926125.

[77] M.O. Sonnati, S. Amigoni, E.P. Taffin De Givenchy, T. Darmanin, O. Choulet, F. Guittard, Glycerol carbonate as a versatile building block for tomorrow: Synthesis, reactivity, properties and applications, Green Chem. 15 (2013) 283-306. https://doi.org/10.1039/c2gc36525a.

[78] B. Katryniok, S. Paul, V. Bellière-Baca, P. Rey, F. Dumeignil, Glycerol dehydration to acrolein in the context of new uses of glycerol, Green Chem. 12 (2010) 2079-2098. https://doi.org/10.1039/c0gc00307g.

[79] B. Dou, Y. Song, C. Wang, H. Chen, Y. Xu, Hydrogen production from catalytic steam reforming of biodiesel byproduct glycerol: Issues and challenges, Renew. Sustain. Energy Rev. 30 (2014) 950-960. https://doi.org/10.1016/j.rser.2013.11.029.

[80] Y. Wang, J. Zhou, X. Guo, Catalytic hydrogenolysis of glycerol to propanediols: A review, RSC Adv. 5 (2015) 74611-74628. https://doi.org/10.1039/c5ra11957j.

[81] N. Rahmat, A.Z. Abdullah, A.R. Mohamed, Recent progress on innovative and potential technologies for glycerol transformation into fuel additives: A critical review, Renew. Sustain. Energy Rev. 14 (2010) 987-1000. https://doi.org/10.1016/j.rser.2009.11.010.

[82] OECD/FAO, Agricultural Outlook 2016-2025, in: OECD Publ. (2016). https://doi.org/https://doi.org/10.1787/agr_outlook-2016-10-en.

[83] B. Kayode, A. Hart, An overview of transesterification methods for producing biodiesel from waste vegetable oils, Biofuels. 10 (2019) 419-437. https://doi.org/10.1080/17597269.2017.1306683.

[84] C.L. Gargalo, P. Cheali, J.A. Posada, K. V. Gernaey, G. Sin, Economic Risk Assessment of Early Stage Designs for Glycerol Valorization in Biorefinery Concepts, Ind. Eng. Chem. Res. 55 (2016) 6801-6814. https://doi.org/10.1021/acs.iecr.5b04593.

[85] C. Len, F. Delbecq, C. Cara Corpas, E. Ruiz Ramos, Continuous Flow Conversion of Glycerol into Chemicals: An Overview, Synth. 50 (2018) 723-741. https://doi.org/10.1055/s-0036-1591857.

[86] R.S. Varma, C. Len, Glycerol valorization under continuous flow conditions-recent advances, Curr. Opin. Green Sustain. Chem. 15 (2019) 83-90. https://doi.org/10.1016/j.cogsc.2018.11.003.

[87] A. Oasmaa, D. Meier, Norms and standards for fast pyrolysis liquids: 1. Round robin test, J. Anal. Appl. Pyrolysis. 73 (2005) 323-334. https://doi.org/10.1016/j.jaap.2005.03.003.

[88] M. Mohamad, R. Awang, W. Yunus, A review of acetol: application and production,

Am. J. Appl. Sci. 8 (2011) 1135–1139. https://doi.org/10.3844/ajassp.2011.1135.1139.

[89] K. Lacasse, W. Baumann, Textile Chemicals: Environmental Data and Facts. Springer Science & Business Media, Germany, 2012.

[90] B. List, The direct catalytic asymmetric three-component Mannich reaction, J. Am. Chem. Soc. 122 (2000) 9336-9337. https://doi.org/10.1021/ja001923x.

[91] W. Notz, B. List, Catalytic asymmetric synthesis of anti-1,2-diols, J. Am. Chem. Soc. 122 (2000) 7386-7387. https://doi.org/10.1021/ja001460v.

[92] A. Eschenbacher, J. Andersen, A. Jensen, Catalytic conversion of acetol over HZSM-5 catalysts–influence of Si/Al ratio and introduction of mesoporosity, Catal. Today. 365 (2021) 301-309. https://doi.org/10.1016/j.cattod.2020.03.041.

[93] M.L. de Araújo, D. Mandelli, Y.N. Kozlov, W.A. Carvalho, G.B. Shul'pin, Oxidation of hydroxyacetone (acetol) with hydrogen peroxide in acetonitrile solution catalyzed by iron(III) chloride, J. Mol. Catal. A Chem. 422 (2016) 103-114. https://doi.org/10.1016/j.molcata.2016.02.011.

[94] E.M. Albuquerque, L.E.P. Borges, M.A. Fraga, Lactic acid production from aqueous-phase selective oxidation of hydroxyacetone, J. Mol. Catal. A Chem. 400 (2015) 64-70. https://doi.org/10.1016/j.molcata.2015.02.005.

[95] Y. Wan, M. Zhuang, S. Chen, W. Hu, J. Sun, J. Lin, S. Wan, Y. Wang, One-Pot Production of Lactic Acid from Acetol over Dealuminated Sn-Beta Supported Gold Catalyst, ACS Catal. 7 (2017) 6038-6047. https://doi.org/10.1021/acscatal.7b01499.

[96] M.A. Dasari, P.P. Kiatsimkul, W.R. Sutterlin, G.J. Suppes, Low-pressure hydrogenolysis of glycerol to propylene glycol, Appl. Catal. A Gen. 281 (2005) 225-231. https://doi.org/10.1016/j.apcata.2004.11.033.

[97] W. Sauter, O.L. Bergmann, U. Schröder, Hydroxyacetone: A Glycerol-Based Platform for Electrocatalytic Hydrogenation and Hydrodeoxygenation Processes, ChemSusChem. 10 (2017) 3105-3110. https://doi.org/10.1002/cssc.201700996.

[98] T.C. Gentil, V.S. Pinheiro, F.M. Souza, M.L. de Araújo, D. Mandelli, B.L. Batista, M.C. dos Santos, Acetol as a high-performance molecule for oxidation in alkaline direct liquid fuel cell, Renew. Energy. 165 (2021) 37–42. https://doi.org/10.1016/J.RENENE.2020.10.150.

[99] P.A. Levene, A. Walti, Acetol: 2-Propanone, 1-hydroxy-. Org. Synth., 10 (2003) 1-1. https://doi.org/10.1002/0471264180.os010.01.

[100] R. Disselkamp, B. Harris, T. Hart, Hydroxy acetone and lactic acid synthesis from aqueous propylene glycol/hydrogen peroxide catalysis on Pd-black, Catal. Commun. 9 (2008) 2250–2252. https://doi.org/10.1016/j.catcom.2008.05.005.

[101] J. Ko, I. Kim, S. Yoo, B. Min, K. Kim, C. Park, Conversion of methylglyoxal to acetol by Escherichia coli aldo-keto reductases, J. Bacteriol. 187 (2005) 5782-5789. https://doi.org/10.1128/JB.187.16.5782-5789.2005.

[102] P. Soucaille, F. Voelker, R. Figge, Metabolically engineered microorganism useful for the production of acetol, US20100279369A1 (2010).

[103] H. Zhu, X. Yi, Y. Liu, H. Hu, T.K. Wood, X. Zhang, Production of acetol from glycerol using engineered Escherichia coli, Bioresour. Technol. 149 (2013) 238-243. https://doi.org/10.1016/j.biortech.2013.09.062.

[104] C.W. Chiu, M.A. Dasari, G.J. Suppes, W.R. Sutterlin, Dehydration of glycerol to acetol via catalytic Reactive distillation, AIChE J. 52 (2006) 3543-3548. https://doi.org/10.1002/aic.10951.

[105] S. Mészáros, J. Halász, Z. Kónya, P. Sipos, I. Pálinkó, Reconstruction of calcined MgAl- and NiMgAl-layered double hydroxides during glycerol dehydration and their recycling characteristics, Appl. Clay Sci. 80 (2013) 245-248. https://doi.org/10.1016/j.clay.2013.04.010.

[106] S. Basu, A.K. Sen, M. Mukherjee, Synthesis and performance evaluation of silica-supported copper chromite catalyst for glycerol dehydration to acetol, J. Chem. Sci. 131 (2019) 1-15. https://doi.org/10.1007/s12039-019-1662-1.

[107] S. Basu, A.K. Sen, Dehydration of glycerol with silica–phosphate-supported copper catalyst, Res. Chem. Intermed. 46 (2020) 3545–3568. https://doi.org/10.1007/s11164-020-04161-4.

[108] G. Raju, P.S. Reddy, B.M. Reddy, Selective gas-phase conversion of glycerol to acetol over promoted zirconia solid acid catalysts, Open Catal. J. 4 (2011) 83-87. https://doi.org/10.2174/1876214x01104010083.

[109] Y.T. Kim, K.D. Jung, E.D. Park, Gas-phase dehydration of glycerol over silica-alumina catalysts, Appl. Catal. B Environ. 107 (2011) 177-187. https://doi.org/10.1016/j.apcatb.2011.07.011.

[110] W. Suprun, M. Lutecki, T. Haber, H. Papp, Acidic catalysts for the dehydration of glycerol: Activity and deactivation, J. Mol. Catal. A Chem. 309 (2009) 71-78. https://doi.org/10.1016/j.molcata.2009.04.017.

[111] A.K. Kinage, P.P. Upare, P. Kasinathan, Y.K. Hwang, J.S. Chang, Selective conversion of glycerol to acetol over sodium-doped metal oxide catalysts, Catal. Commun. 11 (2010) 620-623. https://doi.org/10.1016/j.catcom.2010.01.008.

[112] C.W. Chiu, A. Tekeei, W.R. Sutterlin, J.M. Ronco, G.J. Suppes, Low-pressure packed-bed gas phase conversion of glycerol to acetol, AIChE J. 54 (2008) 2456-2463. https://doi.org/10.1002/aic.11567.

[113] T.P. Braga, N. Essayem, A. Valentini, Non-crystalline copper oxide highly dispersed on mesoporous alumina: Synthesis, characterization and catalytic activity in glycerol conversion to acetol, Quim. Nova. 39 (2016) 691-696. https://doi.org/10.5935/0100-4042.20160074.

[114] T.P. Braga, N. Essayem, S. Prakash, A. Valentini, Gas-Phase conversion of glycerol to acetol: Influence of support acidity on the catalytic stability and copper surface properties on the activity, J. Braz. Chem. Soc. 27 (2016) 2361-2371. https://doi.org/10.5935/0103-5053.20160134.

[115] T.P. Braga, N. Essayem, A. Valentini, Synthesis of Cu-MxOy/Al2O3 (M = Fe, Zn, W or Sb) catalysts for the conversion of glycerol to acetol: Effect of texture and acidity of the supports, RSC Adv. 5 (2015) 93394-93402. https://doi.org/10.1039/c5ra16166e.

[116] T.P. Braga, N. Essayem, A. Valentini, Correlation between the basicity of Cu–MxOy–Al2O3 (M = Ba, Mg, K or La) oxide and the catalytic performance in the glycerol conversion from adsorption microcalorimetry characterization, J. Therm. Anal. Calorim. 129 (2017) 65-74. https://doi.org/10.1007/s10973-017-6145-3.

[117] S. Sato, M. Akiyama, R. Takahashi, T. Hara, K. Inui, M. Yokota, Vapor-phase reaction of polyols over copper catalysts, Appl. Catal. A Gen. 347 (2008) 186-191.

https://doi.org/10.1016/j.apcata.2008.06.013.

[118] C.V. Rode, M.A. Hengne, A.A. Ghalwadkar, R.B. Mane, P.H. Mohite, H.S. Potdar, Process for preparation of hydroxyacetone or propylene glycol, WO2011/138643 (2014).

[119] R.B. Mane, C. V. Rode, Continuous dehydration and hydrogenolysis of glycerol over non-chromium copper catalyst: Laboratory-scale process studies, Org. Process Res. Dev. 16 (2012) 1043-1052. https://doi.org/10.1021/op200383r.

[120] M. Velasquez, A. Santamaria, C. Batiot-Dupeyrat, Selective conversion of glycerol to hydroxyacetone in gas phase over La2CuO4 catalyst, Appl. Catal. B Environ. 160 (2014) 606-613. https://doi.org/10.1016/j.apcatb.2014.06.006.

[121] S. Célerier, S. Morisset, I. Batonneau-Gener, T. Belin, K. Younes, C. Batiot-Dupeyrat, Glycerol dehydration to hydroxyacetone in gas phase over copper supported on magnesium oxide (hydroxide) fluoride catalysts, Appl. Catal. A Gen. 557 (2018) 135-144. https://doi.org/10.1016/j.apcata.2018.03.022.

[122] S.H. Chai, H.P. Wang, Y. Liang, B.Q. Xu, Sustainable production of acrolein: Investigation of solid acid–base catalysts for gas-phase dehydration of glycerol, Green Chem. 9 (2007) 1130-1136. https://doi.org/10.1039/b702200j.

[123] Q. Liu, Z. Zhang, Y. Du, J. Li, X. Yang, Rare earth pyrophosphates: Effective catalysts for the production of acrolein from vapor-phase dehydration of glycerol, Catal. Letters. 127 (2009) 419-428. https://doi.org/10.1007/s10562-008-9723-y.

[124] A. Alhanash, E.F. Kozhevnikova, I. V. Kozhevnikov, Gas-phase dehydration of glycerol to acrolein catalysed by caesium heteropoly salt, Appl. Catal. A Gen. 378 (2010) 11-18. https://doi.org/10.1016/j.apcata.2010.01.043.

[125] F. Cavani, S. Guidetti, L. Marinelli, M. Piccinini, E. Ghedini, M. Signoretto, The control of selectivity in gas-phase glycerol dehydration to acrolein catalysed by sulfated zirconia, Appl. Catal. B Environ. 100 (2010) 197-204. https://doi.org/10.1016/j.apcatb.2010.07.031.

[126] A. Talebian-Kiakalaieh, N.A.S. Amin, H. Hezaveh, Glycerol for renewable acrolein production by catalytic dehydration, Renew. Sustain. Energy Rev. 40 (2014) 28-59. https://doi.org/10.1016/j.rser.2014.07.168.

[127] B. Katryniok, S. Paul, M. Capron, F. Dumeignil, Towards the sustainable production of acrolein by glycerol dehydration, ChemSusChem. 2 (2009) 719-730. https://doi.org/10.1002/cssc.200900134.

[128] E. Tsukuda, S. Sato, R. Takahashi, T. Sodesawa, Production of acrolein from glycerol over silica-supported heteropoly acids, Catal. Commun. 8 (2007) 1349-1353. https://doi.org/10.1016/j.catcom.2006.12.006.

[129] J. Ten Dam, U. Hanefeld, Renewable chemicals: Dehydroxylation of glycerol and polyols, ChemSusChem. 4 (2011) 1017–1034. https://doi.org/10.1002/cssc.201100162.

[130] D. Coll, F. Delbecq, Y. Aray, P. Sautet, Stability of intermediates in the glycerol hydrogenolysis on transition metal catalysts from first principles, Phys. Chem. Chem. Phys. 13 (2011) 1448-1456. https://doi.org/10.1039/c0cp00858c.

[131] M.R. Nimlos, S.J. Blanksby, X. Qian, M.E. Himmel, D.K. Johnson, Mechanisms of glycerol dehydration, J. Phys. Chem. A. 110 (2006) 6145-6156. https://doi.org/10.1021/jp060597q.

[132] T.J. Bandosz, J. Jagiełło, K.A.G. Amankwah, J.A. Schwarz, Chemical and structural properties of clay minerals modified by inorganic and organic material, Clay Miner. 27 (1992) 435-444. https://doi.org/10.1180/claymin.1992.027.4.04.

[133] B. Katryniok, S. Paul, F. Dumeignil, Recent developments in the field of catalytic dehydration of glycerol to acrolein, ACS Catal. 3 (2013) 1819-1834. https://doi.org/10.1021/cs400354p.

[134] G.S. Foo, D. Wei, D.S. Sholl, C. Sievers, Role of Lewis and brønsted acid sites in the dehydration of glycerol over niobia, ACS Catal. 4 (2014) 3180-3192. https://doi.org/10.1021/cs5006376.

[135] P. Lauriol-Garbey, G. Postole, S. Loridant, A. Auroux, V. Belliere-Baca, P. Rey, J.M.M. Millet, Acid-base properties of niobium-zirconium mixed oxide catalysts for glycerol dehydration by calorimetric and catalytic investigation, Appl. Catal. B Environ. 106 (2011) 94-102. https://doi.org/10.1016/j.apcatb.2011.05.011.

[136] D. Stošić, S. Bennici, J.L. Couturier, J.L. Dubois, A. Auroux, Influence of surface acid-base properties of zirconia and titania based catalysts on the product selectivity in gas phase dehydration of glycerol, Catal. Commun. 17 (2012) 23-28. https://doi.org/10.1016/j.catcom.2011.10.004.

[137] D. Stošić, S. Bennici, S. Sirotin, C. Calais, J.L. Couturier, J.L. Dubois, A. Travert, A. Auroux, Glycerol dehydration over calcium phosphate catalysts: Effect of acidic-basic features on catalytic performance, Appl. Catal. A Gen. 447 (2012) 124-134. https://doi.org/10.1016/j.apcata.2012.09.029.

[138] J. Feng, J. Wang, Y. Zhou, H. Fu, H. Chen, X. Li, Effect of base additives on the selective hydrogenolysis of glycerol over Ru/TiO2 catalyst, Chem. Lett. 36 (2007) 1274-1275. https://doi.org/10.1246/cl.2007.1274.

[139] E.P. Maris, R.J. Davis, Hydrogenolysis of glycerol over carbon-supported Ru and Pt catalysts, J. Catal. 249 (2007) 328-337. https://doi.org/10.1016/j.jcat.2007.05.008.

[140] E.P. Maris, W.C. Ketchie, M. Murayama, R.J. Davis, Glycerol hydrogenolysis on carbon-supported PtRu and AuRu bimetallic catalysts, J. Catal. 251 (2007) 281-294. https://doi.org/10.1016/j.jcat.2007.08.007.

[141] S. Sato, R. Takahashi, T. Sodesawa, N. Honda, H. Shimizu, Selective dehydration of diols to allylic alcohols catalyzed by ceria, Catal. Commun. 4 (2003) 77-81. https://doi.org/10.1016/S1566-7367(02)00260-1.

[142] S. Sato, R. Takahashi, T. Sodesawa, N. Honda, Dehydration of diols catalyzed by CeO2, J. Mol. Catal. A Chem. 221 (2004) 177-183. https://doi.org/10.1016/j.molcata.2004.07.004.

[143] W. Suprun, M. Lutecki, H. Papp, TPD-TG-MS Investigations of the Catalytic Conversion of Glycerol over MOx-Al2O3-PO4 Catalysts, Chem. Eng. Technol. 34 (2011) 134-139. https://doi.org/10.1002/ceat.201000316.

[144] K.N. Papageridis, G. Siakavelas, N.D. Charisiou, D.G. Avraam, L. Tzounis, K. Kousi, M.A. Goula, Comparative study of Ni, Co, Cu supported on γ-alumina catalysts for hydrogen production via the glycerol steam reforming reaction, Fuel Process. Technol. 152 (2016) 156-175. https://doi.org/10.1016/j.fuproc.2016.06.024.

[145] Y. Liu, X. Guo, G. Rempel, F. Ng, The Promoting Effect of Ni on Glycerol Hydrogenolysis to 1,2-Propanediol with In Situ Hydrogen from Methanol Steam Reforming Using a Cu/ZnO/Al2O3 Catalyst, Catalysts. 9 (2019) 412.

https://doi.org/10.3390/catal9050412.

[146] S. Ajaikumar, A. Pandurangan, Reaction of benzaldehyde with various aliphatic glycols in the presence of hydrophobic Al-MCM-41: A convenient synthesis of cyclic acetals, J. Mol. Catal. A Chem. 290 (2008) 35-43. https://doi.org/10.1016/j.molcata.2008.04.008.

[147] A.J. Gellman, M.T. Buelow, S.C. Street, T.H. Morton, Transition state for β-elimination of hydrogen from alkoxy groups on metal surfaces, J. Phys. Chem. A. 104 (2000) 2476-2485. https://doi.org/10.1021/jp993474x.

[148] R.M. Rioux, M.A. Vannice, Hydrogenation/dehydrogenation reactions: Isopropanol dehydrogenation over copper catalysts, J. Catal., 216 (2003) 362-376. https://doi.org/10.1016/S0021-9517(02)00035-0.

[149] L. Ott, V. Lehr, S. Urfels, M. Bicker, H. Vogel, Influence of salts on the dehydration of several biomass-derived polyols in sub- and supercritical water, J. Supercrit. Fluids. 38 (2006) 80-93. https://doi.org/10.1016/j.supflu.2005.11.004.

[150] C. Montassier, D. Giraud, J. Barbier, Polyol conversion by liquid phase heterogeneous catalysis over metals, Stud. Surf. Sci. Catal., 41 (1988) 165-170. https://doi.org/10.1016/S0167-2991(09)60811-9.

[151] R.B. Mane, C. V. Rode, Simultaneous glycerol dehydration and in situ hydrogenolysis over Cu-Al oxide under an inert atmosphere, Green Chem. 14 (2012) 2780-2789. https://doi.org/10.1039/c2gc35661a.

[152] R.B. Mane, A. Yamaguchi, A. Malawadkar, M. Shirai, C. V. Rode, Active sites in modified copper catalysts for selective liquid phase dehydration of aqueous glycerol to acetol, RSC Adv. 3 (2013) 16499-16508. https://doi.org/10.1039/c3ra42348d.

[153] P.A. Torresi, V.K. Díez, P.J. Luggren, J.I. Di Cosimo, Conversion of diols by dehydrogenation and dehydration reactions on silica-supported copper catalysts, Appl. Catal. A Gen. 458 (2013) 119-129. https://doi.org/10.1016/j.apcata.2013.03.031.

[154] Z. Xiao, X. Wang, J. Xiu, Y. Wang, C.T. Williams, C. Liang, Synergetic effect between Cu0 and Cu+ in the Cu-Cr catalysts for hydrogenolysis of glycerol, Catal. Today. 234 (2014) 200-207. https://doi.org/10.1016/j.cattod.2014.02.025.

[155] Z. Wang, X. Liu, D.W. Rooney, P. Hu, Elucidating the mechanism and active site of the cyclohexanol dehydrogenation on copper-based catalysts: A density functional theory study, Surf. Sci. 640 (2015) 181-189. https://doi.org/10.1016/j.susc.2015.01.004.

[156] J. Shan, H. Liu, K. Lu, S. Zhu, J. Li, J. Wang, W. Fan, Identification of the dehydration active sites in glycerol hydrogenolysis to 1,2-propanediol over Cu/SiO2 catalysts, J. Catal. 383 (2020) 13-23. https://doi.org/10.1016/j.jcat.2019.12.032.

[157] Y. Wang, S. Furukawa, X. Fu, N. Yan, Organonitrogen Chemicals from Oxygen-Containing Feedstock over Heterogeneous Catalysts, ACS Catal. 10 (2020) 311–335. https://doi.org/10.1021/acscatal.9b03744.

[158] X. Chen, S. Song, H. Li, G. Gözaydln, N. Yan, Expanding the Boundary of Biorefinery: Organonitrogen Chemicals from Biomass, Acc. Chem. Res. 54 (2021) 1711-1722. https://doi.org/10.1021/acs.accounts.0c00842.

[159] H. Li, H. Guo, Z. Fang, T.M. Aida, R.L. Smith, Cycloamination strategies for renewable N-heterocycles, Green Chem. 22 (2020) 582–611. https://doi.org/10.1039/c9gc03655e.

[160] G.W. Huber, S. Iborra, A. Corma, Synthesis of transportation fuels from biomass: Chemistry, catalysts, and engineering, Chem. Rev. 106 (2006) 4044-4098. https://doi.org/10.1021/cr068360d.

[161] A.B. Rao, E.S. Rubin, A technical, economic, and environmental assessment of amine-based CO2 capture technology for power plant greenhouse gas control, Environ. Sci. Technol. 36 (2002) 4467-4475. https://doi.org/10.1021/es0158861.

[162] X. Xu, C. Song, J.M. Andresen, B.G. Miller, A.W. Scaroni, Novel polyethylenimine-modified mesoporous molecular sieve of MCM-41 type as high-capacity adsorbent for CO2 capture, Energy and Fuels. 16 (2002) 1463-1469. https://doi.org/10.1021/ef020058u.

[163] X. Xu, C. Song, J.M. Andrésen, B.G. Miller, A.W. Scaroni, Preparation and characterization of novel CO2 "molecular basket" adsorbents based on polymer-modified mesoporous molecular sieve MCM-41, Microporous Mesoporous Mater. 62 (2003) 29-45. https://doi.org/10.1016/S1387-1811(03)00388-3.

[164] C. Chen, S.T. Yang, W.S. Ahn, R. Ryoo, Amine-impregnated silica monolith with a hierarchical pore structure: Enhancement of CO2 capture capacity, Chem. Commun. 24 (2009) 3627-3629. https://doi.org/10.1039/b905589d.

[165] P.J.E. Harlick, A. Sayari, Applications of pore-expanded mesoporous silica. 5. triamine grafted material with exceptional CO2 dynamic and equilibrium adsorption performance, Ind. Eng. Chem. Res. 46 (2007) 446-458. https://doi.org/10.1021/ie060774+.

[166] K. Okarf, H. Abe, Y. Yokota, Development of catalysts for direct amination of aliphatic alcohols, Stud. Surf. Sci. Catal. 44 (1989) 299-306. https://doi.org/10.1016/S0167-2991(09)61305-7.

[167] Y. Tao, P. Mao, Z. Cui, The application of cationic surfactant in the field of high technology, China Surfactant Deterg Cosmet. 6 (2001) 23–25.

[168] J. Zhang, Y. Zheng, P. Yu, L. He, H. Wang, R. Wang, Synthesis, characterization and surface-activity of a polyoxyethylene ether trimeric quaternary ammonium surfactant, J. Surfactants Deterg. 13 (2010) 155-158. https://doi.org/10.1007/s11743-009-1166-y.

[169] S. Farzadfar, J.D. Knight, K.A. Congreves, Soil organic nitrogen: an overlooked but potentially significant contribution to crop nutrition, Plant Soil. (2021) 1-17. https://doi.org/10.1007/s11104-021-04860-w.

[170] Metabolic Pathways of Agrochemicals, Chem. Int. -- Newsmag. IUPAC. 21 (1999). https://doi.org/10.1515/ci.1999.21.2.48a.

[171] P.J. Reeds, Dispensable and indispensable amino acids for humans, J. Nutr., 130 (2000) 1835S-1840S. https://doi.org/10.1093/jn/130.7.1835s.

[172] 2017 (in Million U.S. Dollars). Https://www.statista.com/statistics/, 258022/top-10-pharmaceutical-products-by-global-sales-2011/., In, Statista Top 15 Pharmaceutical Products by Sales Worldwide, (2017).

[173] J. Chen, Y. Huang, Asymmetric catalysis with N-heterocyclic carbenes as non-covalent chiral templates, Nat. Commun. 5 (2014) 1-8. https://doi.org/10.1038/ncomms4437.

[174] M. Frauenkron, J.-P. Melder, G. Ruider, R. Rossbacher, H. Höke, Ethanolamines and Propanolamines, Ullmann's Encycl. Ind. Chem., 2001. https://doi.org/10.1002/14356007.a10_001.

[175] R. Turakhia, L. Valette, S.W. King, C. Boyer, Ethyleneamine epoxy hardener, 0246999A1 (2013).

[176] T. Miyamoto, C. Ketterings, Q. Cherney, J. Kilcer, Nitrogen Fixation, Cornell Univ. Coop. 2008. http://nmsp.cals.cornell.edu/publications/%0Afactsheets/factsheet39.pdf.

[177] L.E. Apodaca, Nitrogen (Fixed) Ammonia, Mineral Commodity Summaries; U.S. Geological Survey, 2019. https://prd-wret.s3-us-west-2.amazonaws.com/assets/%0Apalladium/production/atoms/files/mcs-2019-nitro.pdf.

[178] A.L. Reznichenko, K.C. Hultzsch, Hydroamination of Alkenes, Org. React. 88 (2015) 1–554. https://doi.org/10.1002/0471264180.OR088.01.

[179] P. Roose, K. Eller, E. Henkes, R. Rossbacher, H. Höke, Amines, Aliphatic. Ullmann's Encyclopedia of Industrial Chemistry, 2015.

[180] D.C. Caskey, D.W. Chapman, Process for the preparation of arylhydroxylamines, 1984.

[181] K. Weissermel, H. Arpe, Industrial Organic Chemistry, 2008. https://doi.org/10.1002/9783527616688.

[182] T. Kahl, K. Schröder, F.R. Lawrence, W.J. Marshall, H. Höke, R. Jäck, "Aniline", Ullmann's Encycl. Ind. Chem., 2007.

[183] M. Rueping, B.J. Nachtsheim, A review of new developments in the Friedel-Crafts alkylation - From green chemistry to asymmetric catalysis, Beilstein J. Org. Chem. 6 (2010) 6. https://doi.org/10.3762/bjoc.6.6.

[184] J. Schranck, A. Tlili, Transition-Metal-Catalyzed Monoarylation of Ammonia, ACS Catal. 8 (2018) 405-418. https://doi.org/10.1021/acscatal.7b03215.

[185] A. Gamble, Ullmann's Encyclopedia of Industrial Chemistry, Charlest. Advis. 20 (2019) 46-50. https://doi.org/10.5260/chara.20.4.46.

[186] C.A.G.N. Montalbetti, V. Falque, Amide bond formation and peptide coupling, Tetrahedron. 61 (2005) 10827-10852. https://doi.org/10.1016/j.tet.2005.08.031.

[187] R.G. Carter, A.R. Doumaux, S.W. Kaiser, P.R. Umberger, Diamines and Higher Amines, Aliphatic, Van Nostrand's Encycl. Chem., 2005. https://doi.org/10.1002/0471740039.vec0802.

[188] Z. Sun, B. Fridrich, A. De Santi, S. Elangovan, K. Barta, Bright Side of Lignin Depolymerization: Toward New Platform Chemicals, Chem. Rev. 118 (2018) 614-678. https://doi.org/10.1021/acs.chemrev.7b00588.

[189] C. Zhang, F. Wang, Catalytic Lignin Depolymerization to Aromatic Chemicals, Acc. Chem. Res. 53 (2020) 470-484. https://doi.org/10.1021/acs.accounts.9b00573.

[190] Y. Jing, Y. Guo, Q. Xia, X. Liu, Y. Wang, Catalytic Production of Value-Added Chemicals and Liquid Fuels from Lignocellulosic Biomass, Chem. 5 (2019) 2520-2546. https://doi.org/10.1016/j.chempr.2019.05.022.

[191] C. Mondelli, G. Gözaydin, N. Yan, J. Pérez-Ramírez, Biomass valorisation over metal-based solid catalysts from nanoparticles to single atoms, Chem. Soc. Rev. 49 (2020) 3764-3782. https://doi.org/10.1039/d0cs00130a.

[192] A.M. Medway, J. Sperry, Heterocycle construction using the biomass-derived building block itaconic acid, Green Chem. 16 (2014) 2084-2101. https://doi.org/10.1039/c4gc00014e.

[193] S. Elangovan, A. Afanasenko, J. Haupenthal, Z. Sun, Y. Liu, A.K.H. Hirsch, K. Barta, From Wood to Tetrahydro-2-benzazepines in Three Waste-Free Steps: Modular Synthesis of Biologically Active Lignin-Derived Scaffolds, ACS Cent. Sci. 5 (2019) 1707-1716. https://doi.org/10.1021/acscentsci.9b00781.

[194] A. Afanasenko, T. Yan, K. Barta, Amination of β-hydroxyl acid esters via cooperative catalysis enables access to bio-based β-amino acid esters, Commun. Chem. 2 (2019) 1-9. https://doi.org/10.1038/s42004-019-0229-x.

[195] I. Scodeller, S. Mansouri, D. Morvan, E. Muller, K. de Oliveira Vigier, R. Wischert, F. Jérôme, Synthesis of Renewable meta-Xylylenediamine from Biomass-Derived Furfural, Angew. Chemie - Int. Ed. 130 (2018) 10670-10674. https://doi.org/10.1002/anie.201803828.

[196] M. Pelckmans, T. Renders, S. Van De Vyver, B.F. Sels, Bio-based amines through sustainable heterogeneous catalysis, Green Chem. 19 (2017) 5303-5331. https://doi.org/10.1039/c7gc02299a.

[197] J. Kühlborn, J. Groß, T. Opatz, Making natural products from renewable feedstocks: Back to the roots?, Nat. Prod. Rep. 37 (2020) 380-424. https://doi.org/10.1039/c9np00040b.

[198] B.G. Reed-Berendt, D.E. Latham, M.B. Dambatta, L.C. Morrill, Borrowing Hydrogen for Organic Synthesis, ACS Cent. Sci. 7 (2021) 570–585. https://doi.org/10.1021/acscentsci.1c00125.

[199] M.H.S.A. Hamid, P.A. Slatford, J.M.J. Williams, Borrowing Hydrogen in the Activation of Alcohols, Adv. Synth. Catal. 349 (2007) 1555–1575. https://doi.org/10.1002/ADSC.200600638.

[200] K. Murugesan, T. Senthamarai, V.G. Chandrashekhar, K. Natte, P.C.J. Kamer, M. Beller, R. V. Jagadeesh, Catalytic reductive aminations using molecular hydrogen for synthesis of different kinds of amines, Chem. Soc. Rev. 49 (2020) 6273–6328. https://doi.org/10.1039/c9cs00286c.

[201] X. Dai, F. Shi, Green synthesis of N-alkylamines and amides via the building and transformation of carbonyl-containing molecules, Curr. Opin. Green Sustain. Chem. 22 (2020) 1–6. https://doi.org/10.1016/j.cogsc.2019.11.001.

[202] J. He, L. Chen, S. Liu, K. Song, S. Yang, A. Riisager, Sustainable access to renewable N-containing chemicals from reductive amination of biomass-derived platform compounds, Green Chem. 22 (2020) 6714–6747. https://doi.org/10.1039/d0gc01869d.

[203] E. Scott, F. Peter, J. Sanders, Biomass in the manufacture of industrial products-the use of proteins and amino acids, Appl. Microbiol. Biotechnol. 75 (2007) 751–762. https://doi.org/10.1007/s00253-007-0932-x.

[204] M. Pera-Titus, F. Shi, Catalytic amination of biomass-based alcohols, ChemSusChem. 7 (2014) 720–722. https://doi.org/10.1002/cssc.201301095.

[205] B.W. Hoffer, E. Benne, H. Rutter, W. Schlindwein, J.P. Melder, Method for Producing an Ethylamine From Denatured Ethanol, US20080194879A1, 2008. https://patents.google.com/patent/US20080194879A1/en.

[206] N. Asprion, M. Julius, O. Bey, S. Werland, F. Stein, M. Kummer, W. Mägerlein, J.P. Melder, K. Huyghe, M. Moors, Process for Preparing Ethylamines and Monoisopropylamine (MIPA), US20130131385A1, 2013. https://patents.google.com/patent/US20130131385A1/en.

[207] F. Niu, S. Xie, Z. Yan, B.T. Kusema, V. V. Ordomsky, A.Y. Khodakov, Alcohol amination over titania-supported ruthenium nanoparticles, Catal. Sci. Technol. 10 (2020) 4396–4404. https://doi.org/10.1039/d0cy00709a.

[208] P.G. Dalev, Utilisation of waste feathers from poultry slaughter for production of a protein concentrate, Bioresour. Technol. 48 (1994) 265-267. https://doi.org/10.1016/0960-8524(94)90156-2.

[209] T.M. Lammens, M.C.R. Franssen, E.L. Scott, J.P.M. Sanders, Availability of protein-derived amino acids as feedstock for the production of bio-based chemicals, Biomass and Bioenergy. 44 (2012) 168–181. https://doi.org/10.1016/j.biombioe.2012.04.021.

[210] R.A. Sheldon, Green and sustainable manufacture of chemicals from biomass: State of the art, Green Chem. 16 (2014) 950–963. https://doi.org/10.1039/c3gc41935e.

[211] N. Yan, Y. Wang, Catalyst: Is the Amino Acid a New Frontier for Biorefineries?, Chem. 5 (2019) 739–741. https://doi.org/10.1016/j.chempr.2019.03.016.

[212] N. Yan, X. Chen, Sustainability: Don't waste seafood waste, Nature. 524 (2015) 155–157. https://doi.org/10.1038/524155a.

[213] R.H. Rødde, A. Einbu, K.M. Vårum, A seasonal study of the chemical composition and chitin quality of shrimp shells obtained from northern shrimp (Pandalus borealis), Carbohydr. Polym. 71 (2008) 388–393. https://doi.org/10.1016/j.carbpol.2007.06.006.

[214] X. Chen, N. Yan, Conversion of chitin to nitrogen-containing chemicals, Chem. Catal. Biomass Upgrad., wiley, 2019, 569–590. https://doi.org/10.1002/9783527814794.ch14.

[215] J. Dai, F. Li, X. Fu, Towards Shell Biorefinery: Advances in Chemical-Catalytic Conversion of Chitin Biomass to Organonitrogen Chemicals, ChemSusChem. 13 (2020) 6498–6508. https://doi.org/10.1002/cssc.202001955.

[216] X. Chen, S. Chew, F. Kerton, N.Yan, Direct conversion of chitin into a N-containing furan derivative, Green Chem. 18 (2014) 2204-2212. https://pubs.rsc.org/en/content/articlehtml/2014/gc/c3gc42436g.

[217] X. Chen, Y. Gao, L. Wang, H. Chen, N.Yan, Effect of treatment methods on chitin structure and its transformation into nitrogen-containing chemicals, ChemPlusChem. 10 (2015) 1565-1572. https://search.proquest.com/openview/45d30d27db1815663dc19b67f0a6a989/1?pq-origsite=gscholar&cbl=28000.

[218] J. Zhang, N.Yan, Formic acid-mediated liquefaction of chitin, Green Chem. 18 (2016) 5050-5058. https://pubs.rsc.org/en/content/articlehtml/2016/gc/c6gc01053a.

[219] X. Chen, H. Yang, Z. Zhong, N.Yan, Base-catalysed, one-step mechanochemical conversion of chitin and shrimp shells into low molecular weight chitosan, Green Chem. 19 (2017) 2783-2792. https://pubs.rsc.org/en/content/articlehtml/2017/gc/c7gc00089h.

[220] J. Zhang, N. Yan, Production of Glucosamine from Chitin by Co-solvent Promoted Hydrolysis and Deacetylation, ChemCatChem. 9 (2017) 2790–2796. https://doi.org/10.1002/cctc.201601715.

[221] H. Kobayashi, K. Techikawara, A. Fukuoka, Hydrolytic hydrogenation of chitin to amino sugar alcohol, Green Chem. 19 (2017) 3350–3356. https://doi.org/10.1039/c7gc01063j.

[222] G. Margoutidis, V.H. Parsons, C.S. Bottaro, N. Yan, F.M. Kerton, Mechanochemical Amorphization of α-Chitin and Conversion into Oligomers of N-Acetyl-D-glucosamine, ACS Publ. 6 (2017) 1662–1669. https://doi.org/10.1021/acssuschemeng.7b02870.

[223] M. Flork, Industrial process for the preparation of amino acids by hydrolysis of proteins in acid medium, U.S. Patent No 4,874,893, 1989.

[224] F. Weygaid, R. Geiger, Process for preparing optically active armeng aces from proteen hydrolysates, United States Patent Office 3,030,380, 1958.

[225] T.T. Pham, X. Chen, T. Söhnel, N. Yan, J. Sperry, Haber-independent, diversity-oriented synthesis of nitrogen compounds from biorenewable chitin, Green Chem. 22 (2020) 1978-1984. https://doi.org/10.1039/d0gc00208a.

[226] N. J. Race, I. R. Hazelden, Adele Faulkner, J. F. Bower, Recent developments in the use of aza-Heck cyclizations for the synthesis of chiral N-heterocycles, Chem. Sci. 8 (2017) 5248–5260. https://doi.org/10.1039/C7SC01480E.

[227] J.A. Joule, K. Mills, Heterocyclic Chemistry, 5th ed., Wiley Blackwell, 2010.

[228] V. Bhardwaj, D. Gumber, V. Abbot, S. Dhiman, P. Sharma, Pyrrole: a resourceful small molecule in key medicinal hetero-aromatics, RSC Adv. 5 (2015) 15233–15266. https://doi.org/10.1039/C4RA15710A.

[229] A.L. Harreus, Pyrrole, in: Ullmann's Encycl. Ind. Chem., Weinheim: Wiley-VCH., 2000.

[230] P. CHIU, M.S.-T. The synthesis and chemistry of azolenines. XVIII, Preparation of 3-ethoxycarbonyl-3H-pyrroles via the Paal-Knorr reaction, and sigmatropic rearrangements, Tetrahedron. 46 (1990) 3439-3456. https://pascal-francis.inist.fr/vibad/index.php?action=getRecordDetail&idt=19289861.

[231] F.G. Cirujano, A. Leyva-Pérez, A. Corma, F.X. Llabrés i Xamena, MOFs as Multifunctional Catalysts: Synthesis of Secondary Arylamines, Quinolines, Pyrroles, and Arylpyrrolidines over Bifunctional MIL-101, ChemCatChem. 5 (2013) 538–549. https://doi.org/10.1002/CCTC.201200878.

[232] N.T.S. Phan, T.T. Nguyen, Q.H. Luu, L.T.L. Nguyen, Paal–Knorr reaction catalyzed by metal–organic framework IRMOF-3 as an efficient and reusable heterogeneous catalyst, J. Mol. Catal. A Chem. 363 (2012) 178–185. https://doi.org/10.1016/J.MOLCATA.2012.06.007.

[233] P. Daw, S. Chakraborty, J.A. Garg, Y. Ben-David, D. Milstein, Direct Synthesis of Pyrroles by Dehydrogenative Coupling of Diols and Amines Catalyzed by Cobalt Pincer Complexes, Angew. Chemie. 128 (2016) 14585–14589. https://doi.org/10.1002/ANGE.201607742.

[234] J.C. Borghs, Y. Lebedev, M. Rueping, O. El-Sepelgy, Sustainable Manganese-Catalyzed Solvent-Free Synthesis of Pyrroles from 1,4-Diols and Primary Amines, Org. Lett. 21 (2018) 70–74. https://doi.org/10.1021/ACS.ORGLETT.8B03506.

[235] S.J. Pridmore, P.A. Slatford, J.E. Taylor, M.K. Whittlesey, J.M.J. Williams, Synthesis of furans, pyrroles and pyridazines by a ruthenium-catalysed isomerisation of alkynediols and in situ cyclisation, Tetrahedron. 65 (2009) 8981–8986. https://doi.org/10.1016/J.TET.2009.06.108.

[236] S.I. Murahashi, T. Shimamura, I. Moritani, Conversion of alcohols into unsymmetrical secondary or tertiary amines by a palladium catalyst. Synthesis of N -substituted

pyrroles, J. Chem. Soc. Chem. Commun. (1974) 931–932. https://doi.org/10.1039/C39740000931.

[237] G. Guillena, D.J. Ramón, M. Yus, Hydrogen Autotransfer in the N-Alkylation of Amines and Related Compounds using Alcohols and Amines as Electrophiles, Chem. Rev. 110 (2009) 1611–1641. https://doi.org/10.1021/CR9002159.

[238] K. Sun, H. Shan, G.-P. Lu, C. Cai, M. Beller, Synthesis of N-heterocycles via oxidant-free dehydrocyclization of alcohols using heterogeneous catalysts, Angew. Chemie Int. Ed. (2021). https://doi.org/10.1002/ANIE.202104979.

[239] D.C. Hargis, R.L. Shubkin, gem-cyclodialkylation A facile synthetic route to N-substituted heterocycles, Tetrahedron Lett. 31 (1990) 2991–2994. https://doi.org/10.1016/S0040-4039(00)89006-1.

[240] L. Tao, Z.J. Wang, T.H. Yan, Y.M. Liu, H.Y. He, Y. Cao, Direct Synthesis of Pyrroles via Heterogeneous Catalytic Condensation of Anilines with Bioderived Furans, ACS Catal. 7 (2017) 959–964. https://doi.org/10.1021/ACSCATAL.6B02953.

[241] N. Das Adhikary, S. Kwon, W.J. Chung, S. Koo, One-Pot Conversion of Carbohydrates into Pyrrole-2-carbaldehydes as Sustainable Platform Chemicals, J. Org. Chem. 80 (2015) 7693–7701. https://doi.org/10.1021/ACS.JOC.5B01349.

[242] S. Shimizu, N. Watanabe, T. Kataoka, T. Shoji, N. Abe, S. Morishita, H. Ichimura, Pyridine and Pyridine Derivatives, Ullmann's Encycl. Ind. Chem. (2000). https://doi.org/10.1002/14356007.A22_399.

[243] R.L. Frank, R.P. Seven, Pyridines. IV. A Study of the Chichibabin Synthesis, J. Am. Chem. Soc. 71 (2002) 2629–2635. https://doi.org/10.1021/JA01176A008.

[244] X. Zhang, C.W. Luo, C. Huang, B.H. Chen, D.G. Huang, J.G. Pan, Z.S. Chao, Synthesis of 3-picoline from acrolein and ammonia through a liquid-phase reaction pathway using SO42−/ZrO2-FeZSM-5 as catalyst, Chem. Eng. J. 253 (2014) 544–553. https://doi.org/10.1016/J.CEJ.2014.03.072.

[245] C.W. Luo, A. Li, J.F. An, X.Y. Feng, X. Zhang, D.D. Feng, Z.S. Chao, The synthesis of pyridine and 3-picoline from gas-phase acrolein diethyl acetal with ammonia over ZnO/HZSM-5, Chem. Eng. J. 273 (2015) 7–18. https://doi.org/10.1016/J.CEJ.2015.01.017.

[246] X. Zhang, Z. Wu, W. Liu, Z.S. Chao, Preparation of pyridine and 3-picoline from acrolein and ammonia with HF/MgZSM-5 catalyst, Catal. Commun. 80 (2016) 10–14. https://doi.org/10.1016/J.CATCOM.2016.02.011.

[247] W. Zhang, S. Duan, Y. Zhang, Enhanced selectivity in the conversion of acrolein to 3-picoline over bimetallic catalyst 4.6%Cu–1.0%Ru/HZSM-5 (38) with hydrogen as carrier gas, React. Kinet. Mech. Catal. 127 (2019) 391–411. https://doi.org/10.1007/S11144-019-01558-0.

[248] M. Saitoh, Y. Tanaka, A process for the preparation of pyridine, EP0764638A1, 1996. https://patents.google.com/patent/EP0764638A1/en.

[249] Lujiang Xu, Zheng Han, Qian Yao, Jin Deng, Ying Zhang, Yao Fu, Qingxiang Guo, Towards the sustainable production of pyridines via thermo-catalytic conversion of glycerol with ammonia over zeolite catalysts, Green Chem. 17 (2015) 2426–2435. https://doi.org/10.1039/C4GC02235A.

[250] Yuecheng Zhang, Xiang Yan, Baoqiang Niu, Jiquan Zhao, A study on the conversion of glycerol to pyridine bases over Cu/HZSM-5 catalysts, Green Chem. 18 (2016)

3139–3151. https://doi.org/10.1039/C6GC00038J.

[251] C.-W. Luo, C. Huang, A. Li, W.-J. Yi, X.-Y. Feng, Z.-J. Xu, Z.-S. Chao, Influence of Reaction Parameters on the Catalytic Performance of Alkaline-Treated Zeolites in the Novel Synthesis of Pyridine Bases from Glycerol and Ammonia, Ind. Eng. Chem. Res. 55 (2016) 893–911. https://doi.org/10.1021/IE504934N.

[252] Lujiang Xu, Qian Yao, Ying Zhang, Yao Fu, Producing pyridines via thermo-catalytic conversion and ammonization of glycerol over nano-sized HZSM-5, RSC Adv. 6 (2016) 86034–86042. https://doi.org/10.1039/C6RA18603C.

[253] C. Müller, V. Diehl, F.W. Lichtenthaler, Building blocks from sugars. Part 23. Hydrophilic 3-pyridinols from fructose and isomaltulose, Tetrahedron. 54 (1998) 10703–10712. https://doi.org/10.1016/S0040-4020(98)00634-6.

[254] J.H. Choi, W.Y. Lee, Pyridine synthesis from tetrahydrofurfuryl alcohol over a Pd/γ-Al2O3 catalyst: II. Effect of supports and palladium loading, Appl. Catal. A Gen. 98 (1993) 21–31. https://doi.org/10.1016/0926-860X(93)85022-H.

[255] A.-L. Harreus, R. Backes, J.-O. Eichler, R. Feuerhake, C. Jäkel, U. Mahn, R. Pinkos, R. Vogelsang, 2-Pyrrolidone, Ullmann's Encycl. Ind. Chem., Weinheim: Wiley-VCH., 2011.

[256] W. Schwarz, J. Schossig, R. Rossbacher, R. Pinkos, H. Höke, Butyrolactone, Ullmann's Encycl. Ind. Chem. (2019) 1–7. https://doi.org/10.1002/14356007.A04_495.PUB2.

[257] H. Gräfje, W. Körnig, H.-M. Weitz, W. Reiß, G. Steffan, H. Diehl, H. Bosche, K. Schneider, H. Kieczka, R. Pinkos, Butanediols, Butenediol, and Butynediol, Ullmann's Encycl. Ind. Chem. (2019) 1–12. https://doi.org/10.1002/14356007.A04_455.PUB2.

[258] S.V. de Vyver, Joice Thomas, Jan Geboers, Stefaan Keyzer, Mario Smet, Wim Dehaen, P. A. Jacobs, B. F. Sels, Catalytic production of levulinic acid from cellulose and other biomass-derived carbohydrates with sulfonated hyperbranched poly(arylene oxindole)s, Energy Environ. Sci. 4 (2011) 3601–3610. https://doi.org/10.1039/C1EE01418H.

[259] D. Martin Alonso, J.M. R. Gallo, M. A. Mellmer, S. G. Wettstein, J. A. Dumesic, Direct conversion of cellulose to levulinic acid and gamma-valerolactone using solid acid catalysts, Catal. Sci. Technol. 3 (2013) 927–931. https://doi.org/10.1039/C2CY20689G.

[260] B. Girisuta, L.P.B. M. Janssen, H. J. Heeres, A kinetic study on the decomposition of 5-hydroxymethylfurfural into levulinic acid, Green Chem. 8 (2006) 701–709. https://doi.org/10.1039/B518176C.

[261] K. W. Omari, J. E. Besaw, F. M. Kerton, Hydrolysis of chitosan to yield levulinic acid and 5-hydroxymethylfurfural in water under microwave irradiation, Green Chem. 14 (2012) 1480–1487. https://doi.org/10.1039/C2GC35048C.

[262] M. V. Bukhtiyarova, G.A. Bukhtiyarova, Reductive amination of levulinic acid or its derivatives to pyrrolidones over heterogeneous catalysts in the batch and continuous flow reactors: A review, Renew. Sustain. Energy Rev. 143 (2021) 110876. https://doi.org/10.1016/J.RSER.2021.110876.

[263] J.D. Vidal, M.J. Climent, A. Corma, P. Concepcion, S. Iborra, One-Pot Selective Catalytic Synthesis of Pyrrolidone Derivatives from Ethyl Levulinate and Nitro

Compounds, ChemSusChem. 10 (2017) 119–128. https://doi.org/10.1002/CSSC.201601333.

[264] A. Schmidt, A. Dreger, Recent Advances in the Chemistry of Pyrazoles. Properties, Biological Activities, and Syntheses, Curr. Org. Chem. 15 (2011) 1423–1463. https://doi.org/10.2174/138527211795378263.

[265] M. Nozari, A.W. Addison, G.T. Reeves, M. Zeller, J.P. Jasinski, M. Kaur, J.G. Gilbert, C.R. Hamilton, J.M. Popovitch, L.M. Wolf, L.E. Crist, N. Bastida, New Pyrazole- and Benzimidazole-derived Ligand Systems, J. Heterocycl. Chem. 55 (2018) 1291–1307. https://doi.org/10.1002/JHET.3155.

[266] N. Oikawa, C. Müller, M. Kunz, F.W. Lichtenthaler, Hydrophilically functionalized pyrazoles from sugars, Carbohydr. Res. 309 (1998) 269–279. https://doi.org/10.1016/S0008-6215(98)00137-2.

[267] E.S.H. El Ashry, K.F. Atta, S. Aboul-Ela, R. Beldi, MAOS of Sugar Phenylosazones and their Derived Pyrazoles and Triazoles, 26 (2008) 429–437. https://doi.org/10.1080/07328300701787164.

[268] X. Yang, P. Zhang, Y. Zhou, J. Wang, H. Liu, Synthesis and Antioxidant Activities of Novel 4,4′-Arylmethylene-bis(1H-pyrazole-5-ol)s from Lignin, Chinese J. Chem. 30 (2012) 670–674. https://doi.org/10.1002/CJOC.201280009.

[269] D.C. Schmitt, A.P. Taylor, A.C. Flick, J. Robert E. Kyne, Synthesis of Pyrazoles from 1,3-Diols via Hydrogen Transfer Catalysis, Org. Lett. 17 (2015) 1405–1408. https://doi.org/10.1021/ACS.ORGLETT.5B00266.

[270] A.J. Arduengo, F.P. Gentry Jr, P.K. Taverkere, H.E. Simmons, Process for manufacture of imidazoles, US6177575B1, 1998. https://patents.google.com/patent/US6177575B1/en.

[271] W.J. Darby, H.B. Lewis, J.R. Totter, The Preparation of 4(5)-Hydroxymethyl-imidazole, J. Am. Chem. Soc. 64 (1942) 463–464. https://doi.org/10.1021/JA01254A502.

[272] E. Dubost, D. Le Nouën, J. Streith, C. Tarnus, T. Tschamber, Synthesis of Substituted Imidazolo[1,2-a]piperidinoses and Their Evaluation as Glycosidase Inhibitors, European J. Org. Chem. (2006) 610–626. https://doi.org/10.1002/EJOC.200500414.

[273] A. Brust, E. Cuny, Conversion of reducing carbohydrates into hydrophilic substituted imidazoles, Green Chem. 15 (2013) 2993–2998. https://doi.org/10.1039/C3GC41203B.

[274] M. Ernst, B.W. Hoffer, J.-P. Melder, Method for producing amines from glycerin, US20100240894A1, 2008. https://patents.google.com/patent/US20100240894A1/en.

[275] V.M. Arredondo, P.J. Corrigan, A.C. Cearley, D.J. Back, M.S. Gibson, N.T. Fairweather, Processes for converting glycerol to amino alcohols, U.S. Patent Application No 11/810,778, 2007.

[276] M. Safariamin, S. Paul, K. Moonen, D. Ulrichts, F. Dumeignil, B. Katryniok, Novel direct amination of glycerol over heteropolyacid-based catalysts, Catal. Sci. Technol. 6 (2016) 2129–2135. https://doi.org/10.1039/C5CY01478F.

[277] J. Ding, M. Cui, T. Ma, R. Shao, W. Xu, P. Wang, Catalytic amination of glycerol with dimethylamine over different type ofheteropolyacid/Zr-MCM-41 catalysts, Mol. Catal. 457 (2018) 51–58. https://doi.org/10.1016/J.MCAT.2018.07.017.

[278] M. Ernst, B. Willem, J.-P. Melder, Method for producing amines from sugar alcohols, US20100311973A1, 2008. https://patents.google.com/patent/US20100311973A1/en.

[279] R. Pandya, R. Mane, C. V. Rode, Cascade dehydrative amination of glycerol to oxazoline, Catal. Sci. Technol. 8 (2018) 2954–2965. https://doi.org/10.1039/C8CY00185E.

[280] Y. Chen, C. Xu, C. Liu, X. Li, J. Liu, Y. Cao, J. Yang, Synthesis of 3-methylindole from glycerol cyclization with aniline over CuCr/Al2O3 catalysts modified by alkali earth oxides, Heteroat. Chem. 24 (2013) 263–270. https://doi.org/10.1002/HC.21090.

[281] C. Liu, C. Xu, T. Xia, Y. Guo, J. Liu, Glycerol catalytic cyclocondensation with ethanediamine to pyrazinyl compounds over the modified SiO2-Al2O3, Heteroat. Chem. 23 (2012) 377–382. https://doi.org/10.1002/HC.21026.

[282] X. Li, C. Xu, C. Liu, N. Zhang, J. You, Q. Wu, Reaction pathway in vapor-phase synthesis of pyrazinyl compounds from glycerol and 1,2-propanediamine over ZnO-based catalysts, J. Mol. Catal. A Chem. 371 (2013) 104-110. https://doi.org/10.1016/j.molcata.2013.01.032.

[283] V. Krishna, G. Naresh, V.V. Kumar, R. Sarkari, A.H. Padmasri, A. Venugopal, Synthesis of 2,6-dimethylpyrazine by dehydrocyclization of aqueous glycerol and 1,2-propanediamine over CuCrO catalyst: Rationalization of active sites by pyridine and formic acid adsorbed IR studies, Appl. Catal. B Environ. 193 (2016) 58-66. https://doi.org/10.1016/j.apcatb.2016.04.018.

[284] V. Krishna, S.N. Kumar, S. Reema, A.H. Padmasri, K.V.R. Chary, A. Venugopal, Bio-glycerol utilization: Synthesis of 2,6-dimethylpyrazine over MxOy-MCr2O4 (M = Mg, Fe, Co, Ni, Cu and Zn) catalysts, Appl. Catal. A Gen. 488 (2014) 275-284. https://doi.org/10.1016/j.apcata.2014.09.019.

[285] K. Vankudoth, A.H. Padmasri, R. Sarkari, V.K. Velisoju, N. Gutta, N.K. Sathu, C.N. Rohita, V. Akula, The role of Lewis acid-base pair sites in ZnO-ZnCr2O4 catalysts for cyclization: Via dehydrogenative condensation of crude glycerol and 1,2-propanediamine for the synthesis of 2,6-dimethylpyrazine, New J. Chem. 41 (2017) 9875-9883. https://doi.org/10.1039/c7nj01819c.

[286] K. Vankudoth, V.K. Velisoju, N. Gutta, N.K. Sathu, H.P. Aytam, S. Inkollu, V. Akula, Zn-Modified CuCr2O4 as Stable and Active Catalyst for the Synthesis of 2,6-Dimethylpyrazine: Valorization of Crude Glycerol Obtained from a Biodiesel Plant, Ind. Eng. Chem. Res. 56 (2017) 11664–11671. https://doi.org/10.1021/ACS.IECR.7B02594.

[287] X. Li, C. Xu, C. Liu, Y. Chen, J.Y. Liu, Synthesis of pyrazinyl compounds from glycerol and 1, 2-propanediamine over Cu–TiO2 catalysts supported on γ-Al2O3, Chinese Chemical Letters. 24 (2013) 751-754. https://www.sciencedirect.com/science/article/pii/S1001841713002040?casa_token=tV5UGrJuisYAAAAA:jMzbbiR5hPfJLOyoM45NcyVIuh9-vFn27KiOqnqvN6WJvYaj6Iou8zUj0jV7a1FrCOEzZdFrWIM.

[288] R. Sarkari, C. Anjaneyulu, V. Krishna, R. Kishore, M. Sudhakar, A. Venugopal, Vapor phase synthesis of methylpyrazine using aqueous glycerol and ethylenediamine over ZnCr2O4 catalyst: Elucidation of reaction mechanism, Catal. Commun. 12 (2011) 1067-1070. https://doi.org/10.1016/j.catcom.2011.03.021.

[289] V. Akula, R. Sarkari, A. Chatla, K. Vankudoth, K.K. Mandari, Synthesize 2-

methylpyrazine using aqueous glycerol and ethylenediamine over zinc oxide-zinc chromite catalysts: Structure-activity relationship, Appl. Catal. A Gen. 441 (2012) 108-118. https://doi.org/10.1016/j.apcata.2012.07.012.

[290] A. Venugopal, R. Sarkari, C. Anjaneyulu, V. Krishna, M.K. Kumar, N. Narender, A.H. Padmasri, Influence of acid-base sites on ZnO-ZnCr2O4 catalyst during dehydrocyclization of aqueous glycerol and ethylenediamine for the synthesis of 2-methylpyrazine: Kinetic and mechanism studies, Appl. Catal. A Gen. 469 (2014) 398-409. https://doi.org/10.1016/j.apcata.2013.10.023.

[291] R. Sarkari, V. Krishna, M. Sudhakar, T.V. Rao, H. Padmasri, D. Srinivas, A. Venugopal, The Effects of Thermal Treatment of ZnO-ZnCr 2 O 4 Catalyst on the Particle Size and Product Selectivity in Dehydrocyclization of Crude Glycerol and Ethylenediamine 1, Kinet. Catal. 57 (2016) 607–614. https://doi.org/10.1134/S0023158416050177.

[292] J. Hou, W. Luo, S. Luo, C. Lin, P. Liu, X. Liao, F. Jing, X. Li, Facile synthesis of CuMAl (M = Cr, Mn, Zn, and Co) with highly dispersed Cu and tailorable surface acidity for efficient 2-methylpyrazine synthesis, RSC Adv. 7 (2017) 48662-48669. https://doi.org/10.1039/c7ra08349a.

[293] G. Liang, A. Wang, L. Li, G. Xu, N. Yan, T. Zhang, Production of Primary Amines by Reductive Amination of Biomass-Derived Aldehydes/Ketones, Angew. Chemie. 129 (2017) 3096–3100. https://doi.org/10.1002/ANGE.201610964.

[294] A.S. Stålsmeden, J.L.B. Vázquez, K. van Weerdenburg, R. Rae, P.-O. Norrby, N. Kann, Glycerol Upgrading via Hydrogen Borrowing: Direct Ruthenium-Catalyzed Amination of the Glycerol Derivative Solketal, ACS Sustain. Chem. Eng. 4 (2016) 5730–5736. https://doi.org/10.1021/ACSSUSCHEMENG.6B01659.

[295] R.J. Martin, Modes of action of anthelmintic drugs, Vet. J. 154 (1997) 11–34. https://doi.org/10.1016/S1090-0233(05)80005-X.

[296] WHO, Helminths: Intestinal nematode infection: Piperazine., WHO Model Prescr. Inf. Drugs Used Parasit. Dis., 2nd ed., 1995.

[297] R.D. Taylor, M. MacCoss, A.D.G. Lawson, Rings in Drugs, J. Med. Chem. 57 (2014) 5845–5859. https://doi.org/10.1021/JM4017625.

[298] E. Vitaku, D.T. Smith, J.T. Njardarson, Analysis of the Structural Diversity, Substitution Patterns, and Frequency of Nitrogen Heterocycles among U.S. FDA Approved Pharmaceuticals, J. Med. Chem. 57 (2014) 10257–10274. https://doi.org/10.1021/JM501100B.

[299] K.E. Gettys, Z. Ye, M. Dai, Recent Advances in Piperazine Synthesis, Synthesis (Stuttg). 49 (2017) 2589–2604. https://doi.org/10.1055/S-0036-1589491.

[300] D.W. Keith, Why Capture CO2 from the Atmosphere?, Science. 325 (2009) 1654–1655. https://doi.org/10.1126/SCIENCE.1175680.

[301] S.A. Freeman, R. Dugas, D.H. Van Wagener, T. Nguyen, G.T. Rochelle, Carbon dioxide capture with concentrated, aqueous piperazine, Int. J. Greenh. Gas Control. 4 (2010) 119–124. https://doi.org/10.1016/J.IJGGC.2009.10.008.

[302] G. Rochelle, E. Chen, S. Freeman, D. Van Wagener, Q. Xu, A. Voice, Aqueous piperazine as the new standard for CO2 capture technology, Chem. Eng. J. 171 (2011) 725–733. https://doi.org/10.1016/J.CEJ.2011.02.011.

[303] F. Closmann, T. Nguyen, G.T. Rochelle, MDEA/Piperazine as a solvent for CO2

capture, Energy Procedia. 1 (2009) 1351–1357. https://doi.org/10.1016/J.EGYPRO.2009.01.177.

[304] L. Li, A.K. Voice, H. Li, O. Namjoshi, T. Nguyen, Y. Du, G.T. Rochelle, Amine blends using concentrated piperazine, Energy Procedia. 37 (2013) 353–369. https://doi.org/10.1016/J.EGYPRO.2013.05.121.

[305] R.D. Ashford, Ashford's Dictionary of industrial chemicals., 3rd ed., Wavelength, 2011.

[306] E.-L. Dreher, K.K. Beutel, J.D. Myers, T. Lübbe, S. Krieger, L.H. Pottenger, Chloroethanes and Chloroethylenes, Ullmann's Encycl. Ind. Chem. (2014) 1–81. https://doi.org/10.1002/14356007.O06_O01.PUB2.

[307] K. Weissermel, H.-J. Arpe, C.R. Lindley, S. Hawkins, Chap. 7. Oxidation Products of Ethylene. Industrial Organic Chemistry., in: Ind. Org. Chem., 2nd ed., Wiley-VCH, 2003, 159–161.

[308] C.B. Pollard, L.J. Kitchen, Derivatives of Piperazine. XXI. Synthesis of Piperazine and C-Substituted Piperazines, J. Am. Chem. Soc. 69 (1947) 854–855. https://doi.org/10.1021/JA01196A034.

[309] G. Bai, X. Fan, H. Wang, J. Xu, F. He, H. Ning, Effects of the preparation methods on the performance of the Cu–Cr–Fe/γ-Al2O3 catalysts for the synthesis of 2-methylpiperazine, Catal. Commun. 10 (2009) 2031–2035. https://doi.org/10.1016/J.CATCOM.2009.07.025.

[310] C.M. Subrahmanyam, G. Muralidhar, S.J. Kulkarni, V. Viswanathan, B. Srinivas, J.S. Yadav, A.V.R. Rao, 281/DEL/92, 1992.

[311] N. Narender, P. Srinivasu, S.J. Kulkarni, K. V. Raghavan, Intermolecular Cyclization of Diethanolamine and Methylamine to N,N′-Dimethylpiperazine over Zeolites under High Pressure, J. Catal. 202 (2001) 430–433. https://doi.org/10.1006/JCAT.2001.3291.

[312] K. Nagaiah, A.S. Rao, S.J. Kulkarni, M. Subrahmanyam, A.V.R. Rao, Intermolecular Cyclization of Diethanolamine and Methylamine to N-Methylpiperazine over Zeolites, J. Catal. 147 (1994) 349–351. https://doi.org/10.1006/JCAT.1994.1147.

[313] R.B. Chedid, J.-P. Melder, U. Abel, R. Dostalek, N. Challand, B. Stein, M. Jödecke, Process for preparing piperazine, 2013. https://patents.google.com/patent/US8981093B2/en.

[314] L. Forni, Ammoxidation of 2-methylpyrazine over oxide catalysts, Appl. Catal. 20 (1986) 219–230. https://doi.org/10.1016/0166-9834(86)80018-5.

[315] S.L. Lewis, S.R. Dirksen, M.M. Heitkemper, L. Bucher, Medical-surgical nursing : assessment and management of clinical problems., 9th ed., St. Louis, MO, 2014.

[316] H.-D. Belitz, P. Grosch, Werner, Schieberle, Food Chemistry., 4th ed., Springer, 2009.

[317] M. Amrani-Hemaimi, C. Cerny, L.B. Fay, Mechanisms of Formation of Alkylpyrazines in the Maillard Reaction, J. Agric. Food Chem. 43 (1995) 2818–2822. https://doi.org/10.1021/JF00059A009.

[318] M.R. Hellberg, A. Rusinko, H.Y. Decornez, Aminopyrazine analogs for treating glaucoma and other rho kinase-mediated diseases and conditions, 200633709A, 2005.

[319] V. Lotti, G.A. Showell, Substituted pyrazines, pyrimidines and pyridazines for use in the treatment of glaucoma, US5219849A, 1993. https://patents.justia.com/patent/5219849.

[320] K.T. Ong, Z.-Q. Liu, & Meng, G. Tay, Review on the Synthesis of Pyrazine and Its Derivatives, Borneo J. Resour. Sci. Technol. 7 (2017) 60–75.

[321] A. Anderson, S. Yurel, M. Shimanskaya. Catalytic synthesis of pyrazine, piperazine, and 1, 4-diaza[2, 2, 2]-bicyclooctane, Chem. Heterocycl. Compd. 3 (1967) 271-286. https://link.springer.com/content/pdf/10.1007/BF01172569.pdf

[322] B. Latha, V. Sadasivam, B. Sivasankar, A highly selective synthesis of pyrazine from ethylenediamine on copper oxide/copper chromite catalysts, Catal. Commun. 8 (2007) 1070-1073. https://www.sciencedirect.com/science/article/pii/S1566736706002068.

[323] J. Okada, 4925947, 1974.

[324] T. Shoji, T. Nakaishi, M. Mikata, Process for producing pyrazine compounds, 5693806A, 1996. https://patents.google.com/patent/US5693806A/en.

[325] K. Sato, Process for preparing pyrazines, 4097478A, 1977. https://patents.google.com/patent/US4097478A/en?oq=4097478%2C+++1978.

[326] I. Park, J. Lee, Y. Rhee, Y. Han, H. Kim, CuO/ZnO/SiO2 catalysts for cyclization of propyleneglycol with ethylenediamine to 2-methylpyrazine, Appl. Catal. A Gen. 253 (2003) 249–255. https://doi.org/10.1016/S0926-860X(03)00527-1.

[327] R. Anand, B.S. Rao, Synthesis of 2-methyl pyrazine over zinc-modified ferrierite (FER) catalysts, Catal. Commun. 3 (2002) 29-35. https://doi.org/10.1016/S1566-7367(01)00064-4.

[328] R. Anand, S.G. Hegde, B.S. Rao, C.S. Gopinath, Catalytic synthesis of 2-methyl pyrazine over Zn-modified zeolites, Catal. Letters. 84 (2002) 265-272. https://doi.org/10.1023/A:1021400624969.

[329] S.A. Raw, C.D. Wilfred, R.J.K. Taylor, Preparation of quinoxalines, dihydropyrazines, pyrazines and piperazines using tandem oxidation processes, Chem. Commun. 3 (2003) 2286–2287. https://doi.org/10.1039/B307177B.

[330] P. Ghosh, A. Mandal, R. Subba, γ-Maghemite-silica nanocomposite: A green catalyst for diverse aromatic N-heterocycles, Catal. Commun. 41 (2013) 146–152. https://doi.org/10.1016/J.CATCOM.2013.06.026.

Chapter 2
Objectives

2.1 Main Objective

Biomass is, together with CO_2, one of the primary and renewable sources of carbon. Therefore, its recovery and valorisation become a sustainable alternative to the evident and continuous decrease in the fossil reserves necessary for producing fuels and chemicals.

In this context, an extensive array of biofuels (i.e., bioethanol, biodiesel, biogas) have appeared in the market over the last decades in an attempt to reduce the worldwide dependence on fossil sources. Specifically, for biodiesel, the transformation of second-generation raw materials (i.e., cooking oils, animal fats, etc.) for its production has grown in the last years. Nevertheless, even in these innovative instances, a glycerol surplus is generated, and its valorisation continues to be essential for the biorefinery. On this basis, this polyalcohol must be transformed into higher added-value chemicals by using highly selective processes and reducing as many synthesis steps as possible.

Among different chemical products with high added-value and industrial interest, we focused on compounds of the N-heterocycle type, such as piperazines and pyrazines. These compounds are used as intermediates in the synthesis of pharmaceuticals and other fine chemicals. In most cases, these N-heterocycles are synthesised in several reaction stages by using homogeneous catalysts and enzymes or highly specific, toxic, and expensive solid catalysts. Additionally, the yields to N-heterocycles obtained are moderate.

This thesis aims to use glycerol and its derivative acetol to synthesise organonitrogen compounds using novel catalytic strategies. To achieve this objective, it is essential to develop new multi-functional catalysts and catalytic systems capable of efficiently and selectively carrying out several cascade-type reactions in a single stage. Consequently, multi-functional solid catalysts are promising candidates to carry out this type of process. In this way, it is intended to address the following specific objectives:

2.2 Specific Objectives

- Continuous selective glycerol dehydration to acetol will be studied with a series of hydrotalcite-derived Cu-, Ni-, and Co-Mg-Al mixed oxides as catalysts. The transition metal and its weight percentage, and the M^{II}/M^{III} ratio, will be varied to optimize acetol yields and understand the reaction mechanism and the role and true nature of redox and acid-base centres in the catalytic behaviour. In addition, the effect of certain doping elements (La, Ga, Ni, Fe, Co, Zn) on catalyst activity, selectivity and stability will be assessed.

- Activity, selectivity, and stability of CuO/MO_x (M: Si, Al, Zr) catalysts in the continuous selective glycerol dehydration to acetol will be tested. At the same time, structure-activity relationships will be established using specific characterization techniques. Furthermore, these catalysts will be structurally optimized, and a selection will be made to carry out the selective glycerol dehydration to acetol, maximizing yield and enabling working under industrially close conditions.

- Under mild conditions, the synthesis of 2-methylpiperazine *via* reductive amination of acetol with ethylenediamine will be studied and developed. Catalysts based on Pd nanoparticles supported on different metal oxides (Ti, Zr, Al, Mg) and mixed metal oxides (Ti-Al, Ti-Zr, Zr-Al) will be tested to obtain results and correlate them with acidity, metal particle morphology and hydrogen activation.

- An environmentally friendly catalytic process will be developed to produce 2-methylpyrazine from acetol and ethylenediamine in the absence of chromium-based catalysts. The strategy will comprise cycloamination of acetol with ethylenediamine followed by dehydrogenation. Solid catalysts CuO/MO_x (M: Mg, Si, Al, Zr) will be tested and their structural and compositional features carefully evaluated and optimized to combine understanding and selection of the best catalytic material.

Objectives

- The production of both N-heterocycles, i.e., 2-methylpiperazine and 2-methylpyrazine, starting from glycerol, will be studied. In the first case, the acetol coming from the selective dehydration of glycerol will be used in the second reductive amination step in a semi-continuous catalytic process. In the second case, a multi-bed catalytic reactor will be employed to design a cascade-type catalytic process for the direct glycerol transformation into the desired organonitrogen compound.

Chapter 3
Experimental Procedure

3.1 Commercial chemicals

Different commercial chemicals were used throughout this research. Unless otherwise specified, they were directly used without any other pre-treatment or purification steps.

Several commercial catalysts and supports, especially metallic oxides, were used either for comparative purposes or as supports of some other active phases (see Table 3.1).

Table 3.1. Commercial catalysts and supports used during this work.

Material	Supplier	Surface Area (m^2/g)	Pore volume (cm^3/g)
$2CuO{\cdot}Cr_2O_3$	Sigma-Aldrich	38	0.21
$1wt\%Pd/Al_2O_3$	Sigma-Aldrich	n/d	n/d
$1wt\%Pt/Al_2O_3$	Sigma-Aldrich	n/d	n/d
TiO_2 Nanoactive[a]	Nanoscale corp.	148	0.32
Al_2O_3 Nanopowder[a] (*npw*)	Sigma-Aldrich	134	0.43
Al_2O_3 Acid Activated[a] (*ac*)	Sigma-Aldrich	n/d	n/d
Al_2O_3 Basic Activated[a] (*bas*)	Sigma-Aldrich	139	0.28
ZrO_2-monoclinic[a]	Chempure	102	0.28
ZrO_2-tetragonal[a]	Chempure	138	0.20
MgO Nanoactive[a]	Nanoscale corp.	226	0.39
SiO_2 Catalyst support[a]	Chempure	224	0.90
SiO_2 Fumed[a]	Sigma-Aldrich	343	5.94

* These materials were calcined under an air flow (50 mL/min) at 250 ºC for 3h, with a heating rate of 3 ºC/min, to eliminate adsorbed water and other contaminants.

On the other hand, a wide set of reactants and solvents were used to carry out catalytic tests and develop the analytical methods needed to identify, quantify, and determine the catalytic performance of the different materials used in this thesis. Table 3.2 summarizes the main organic chemicals used during those catalytic tests included in *Chapters 4* and *5*, which are focused on the continuous selective dehydration of glycerol to acetol.

Table 3.2. Reactants used for the glycerol dehydration to acetol reaction and analysis.

Reactant	Supplier	Purity (wt%)	Main use
Glycerol	Sigma-Aldrich	≥99.5	Reactant
Methanol	Scharlab	>95	Solvent
Hydroxyacetone	Sigma-Aldrich	90	Standard for analysis
Methyl lactate	Sigma-Aldrich	≥97.0	Standard for analysis
Methyl glycolate	Sigma-Aldrich	98	Standard for analysis
Methyl acetate	Sigma-Aldrich	≥98	Standard for analysis
Acetic acid	Sigma-Aldrich	≥99	Standard for analysis
Propionic acid	Sigma-Aldrich	≥99.5	Standard for analysis
Acetoin	Sigma-Aldrich	≥95	Standard for analysis
1,2-propanediol	Sigma-Aldrich	≥99.5	Standard for analysis
1,3-propanediol	Sigma-Aldrich	98	Standard for analysis
Solketal	Sigma-Aldrich	≥97.0	Standard for analysis
Methyl formiate	Sigma-Aldrich	97	Standard for analysis
Dihydroxyacetone	VWR	98	Standard for analysis
Methyl pyruvate	Sigma-Aldrich	90	Standard for analysis
Glyceraldehyde	Sigma-Aldrich	≥98.0	Standard for analysis
Ethanol	Scharlab	>95	Standard for analysis
Acetone	Scharlab	>95	Standard for analysis
Acrolein DMA	Sigma-Aldrich	98	Standard for analysis
Chlorobenzene	Sigma-Aldrich	99.9	GC internal standard
1,4-butanediol	Sigma-Aldrich	99	GC internal standard

In the same way, Table 3.3 presents those chemicals used to carry out and determine the results corresponding to the synthesis of 2-methylpiperazine from acetol and ethylenediamine, excluding those mentioned in the tables above.

Table 3.3. Organic reactants used for 2-methylpiperazine catalytic synthesis and analysis.

Reactant	Supplier	Purity (%)	Main use
Ethylenediamine	Sigma-Aldrich	≥99	Reactant
Methanol	Scharlab	>95	Solvent
2-methylpiperazine	Sigma-Aldrich	95	Standard for analysis
Chlorobenzene	Sigma-Aldrich	99.9	GC internal standard

Likewise, Table 3.4 lists those organic chemicals employed in the synthesis of 2-methylpyrazine from acetol and ethylenediamine, together with the standards used in the analytical method, excluding those mentioned in the tables above.

Table 3.4. Organic reactants used for 2-methylpyrazine catalytic synthesis and analysis.

Reactant	Supplier	Purity (%)	Main use
Ethylenediamine	Sigma-Aldrich	≥99	Reactant
Methanol	Scharlab	>95	Solvent
2-methylpyrazine	Sigma-Aldrich	95	Standard for analysis
Pyrazine	Sigma-Aldrich	≥99	Standard for analysis
2,6-dimethylpyrazine	Sigma-Aldrich	98	Standard for analysis
2-propylpyrazine	Sigma-Aldrich	97	Standard for analysis
2,3,5,6-tetramethylpyrazine	Sigma-Aldrich	98	Standard for analysis

Finally, Table 3.5 shows metal precursors and other inorganic reactants used to synthesize the many different catalysts that will appear in this work.

Table 3.5. Reactants used for catalyst preparation.

Reactant	Supplier	Purity (wt%)
Sodium hydroxide pellets	Emplura	99.99
Sodium carbonate anhydrous	Fisher Scientific	≥99.5
Ammonia solution	ITW Reagents	25 wt% NH_3
Magnesium nitrate hexahydrate	Sigma-Aldrich	99
Aluminum nitrate nonahydrate	Sigma-Aldrich	99.997
Copper (II) nitrate pentahemihydrate	Sigma-Aldrich	≥99.99
Zinc nitrate hexahydrate	Acros Organics	98
Iron (III) nitrate nonahydrate	Sigma-Aldrich	≥99.95
Lanthanum nitrate hexahydrate	Sigma-Aldrich	99.999
Gallium nitrate hydrate	Sigma-Aldrich	99.9
Manganese (II) nitrate tetrahydrate	Alfa-Aesar	98
Cobalt(II) nitrate hexahydrate	Sigma-Aldrich	≥98
Copper (II) nitrate trihydrate	Sigma-Aldrich	99-104
Nickel (II) nitrate hexahydrate	Sigma-Aldrich	≥97.0
n-hexane	Scharlab	≥95
Brij L4	Sigma-Aldrich	-
APTES	Sigma-Aldrich	99
Urea	Sigma-Aldrich	99.0-100.5
Hydrazine	Sigma-Aldrich	64-65 wt% N_2H_4
Zyrconium oxychloride	Sigma-Aldrich	98
Titanium (IV) oxychloride-HCl acid solution	Sigma-Aldrich	15% (Ti basis)
Tetraamminepalladium (II) chloride monohydrate	Sigma-Aldrich	>99.99
Tetraammineplatinum (II) nitrate	Sigma-Aldrich	99.995

3.2 Catalyst synthesis

3.2.1 Hydrotalcite-derived mixed oxides

Hydrotalcite-type materials were prepared by the co-precipitation method under well-optimized synthesis (and ageing) conditions, following the procedure described in refs.[1,2]. The corresponding gels were achieved by mixing two aqueous solutions: Solution A, containing the metallic species (Al, Mg and whichever other divalent o trivalent cation: Cu/Ni/Co/Zn/La/Ga/Fe) in the desired molar ratios as nitrates and not exceeding 1.5 of total cationic concentration; and solution B, containing sodium hydroxide and sodium carbonate in adequate amounts to accomplish a CO_3^{2-}/(total cationic number) ratio always equal to 0.66. Both solutions were slowly mixed at 20 mL/h (addition rate) to an empty plastic beaker, continuously stirring at 200 rpm. The basic solution concentration was adjusted to obtain a final pH ≈14 and the precipitates were aged at 60 ºC overnight in a thermostatic bath. The resulting products were filtered and washed thoroughly with deionized water until pH ≈7. Depending on the transition metal to be incorporated in the hydrotalcite, the corresponding nitrates specified in Table 3.5 were used as precursors.

Pure Mg-Al hydrotalcites were calcined at 450 ºC (2 ºC/min, for a total time of 10 h) under an air flow (airflow (100 mL/min) to attain the corresponding Mg-Al mixed oxide, as usually performed for simple Mg-Al hydrotalcites[1,3]. Other metal-based hydrotalcites were calcined at 550 ºC for 6 h in static air to yield the corresponding metal-based mixed oxides used in the catalytic tests. Additionally, and in the case of Cu-based samples, one material was reduced under a H_2 flow (100 mL/min) at 450 ºC during 3 h, and another amount of the same material was partially reduced at 200 ºC during 3 h under a MeOH flow (2 mL/h), before their use in specific catalytic experiments.

3.2.2 High surface area mixed metal oxides *via* co-precipitation

A general co-precipitation procedure adapted from ref.[4] was used to synthesize the rest of the mixed oxides employed in this work, except those derived from hydrotalcites. In this sense, an aqueous solution containing the desired relation of metal precursors (see Table 3.5) was firstly prepared. Metal precursors (30 mmol of metals) were dissolved in 300 mL of distilled water, being stirred for 10 minutes until homogenization. Afterwards,

an aqueous ammonia solution (25 vol%) was added dropwise (1000 ml/h) until the pH was approximately 9, and the solution was stirred for another 15 minutes. The resulting slurry was kept at 60 ºC for 12 h and then filtered and washed with distilled water until pH ≈7, and dried at 100 ºC overnight. Finally, synthesized catalysts were calcined at 500 ºC for 3 h (airflow, 100 mL/min, 2 ºC/min) to obtain the corresponding metallic mixed oxide. This procedure has been used for mixed oxide supports employed in *Chapter 6* (Ti-Al, Ti-Zr and Zr-Al).

3.2.3 Supported metal and metal oxide catalysts *via* incipient wetness impregnation

Several catalysts were prepared in this work by dispersing one active phase on another with a higher surface area. The preferred method was the incipient wetness impregnation. In this method, the volume of the solution containing the metallic precursor must be the same as the total pore volume of the selected support. For this purpose, the volume of water that the support can admit must be measured before preparing the solution. This step is known as a water test, as it is carried out by adding water to a certain mass of support. Once the saturation point has been reached, a ratio of pore volume per gram of material can be obtained. Then, the precursor mass needed to achieve the desired percentage of active metal in the material is calculated. With the water test value and the volume of solid precursor, the remaining amount of water necessary to cover the volume is added. This solution is impregnated drop by drop and homogenized to obtain the desired percentage of metal on the entire material. After the addition step, the catalyst was dried at 100 ºC overnight. Expressly, CuO and Pd were incorporated into different high surface area oxides using this methodology.

On the one hand, $Cu(NO_3)_2 \cdot 2.5H_2O$ was selected as Cu precursor, at adequate concentrations to obtain a nominal 2.5-5.0 wt% over each support. After the drying step, synthesized catalysts were calcined under static air at 550 ºC for 6 hours (heating rate = 3 ºC/min). On the other hand, $Pd(NH_3)_4Cl_2 \cdot 6H_2O$ was selected as Pd precursor, at adequate concentrations to get a metal loading of ≈1.0 wt% in the final solid. After the drying step, synthesized catalysts were calcined in airflow for 3 hours (450 ºC for Pd/Al_2O_3 and Pd/MgO; 400 ºC for Pd/TiO_2, Pd/ZrO_2 and Pd supported on mixed oxides) (heating rate

= 3 ºC/min). Additionally, all these catalysts were thermally activated at 400 ºC (3 ºC/min) under a H_2 flow of 100 ml/min for 2 h before their use in catalytic experiments.

3.2.4 CuO supported on SiO_2 *via* precipitation-deposition method.

In a typical synthesis, 2 g of porous silica were dispersed in 100 mL of H_2O, 2.7 g of urea and the appropriate amount of $Cu(NO_3)_2 \cdot 3H_2O$ to obtain catalysts with Cu loading of around 5 wt.%. Subsequently, the suspension was stirred at 90 ºC for 2 h to favour the thermal decomposition of urea into CO_2 and NH_3, causing an increase in the pH leading to the formation of small $Cu(OH)_2$ particles. After this time, the solid was filtered and dried overnight in a stove at 80 ºC.

The samples were calcined at 400 ºC by using a heating rate of 2 ºC/min and maintaining this temperature for 2h.

3.2.5 CuO supported on SiO_2 *via* grafting with APTES.

2 g of porous silica were dried overnight under a He flow, at 115 ºC, and added to a three-neck flask with a solution of 3 aminopropyltriethoxysilane (APTES), by using dry toluene (15 mL) as the solvent, under reflux at 110 ºC for 24 h. In this process, APTES molecules are grafted to the silanol groups of the porous silica. After the grafting, the solid was filtered, washed with toluene, and dried overnight at 120 ºC. In the next step, the porous silica-APTES was stirred with an aqueous solution of Cu^{2+} species in the form of $Cu(NO_3)_2 \cdot 3H_2O$ (5 wt% to the porous silica) for 2 h. Finally, the solid was filtered, discarding the presence of Cu in the filtered liquid, and then dried overnight in a stove at 80 ºC.

The samples were calcined at 400 ºC by using a rate of 2 ºC/min and maintaining this temperature for 2h.

3.2.6 CuO supported on ZrO_2 or Al_2O_3 *via* reverse micelle formation

This methodology was developed by adapting that reported in ref.[5]. Reverse micelles were prepared in water-in-oil microemulsions with n-hexane as the continuous oil phase at room temperature mixed with a surfactant (poly(ethylene glycol) dodecyl ether, Brij®

L4). The oil/surfactant molar ratio had a constant value of 16. This solution was always under a N_2 atmosphere until the moment of breaking the micelles.

A solution of copper nitrate trihydrate ($Cu(NO_3)_2 \cdot 3H_2O$, Sigma Aldrich) with a total metal concentration of 0.65 mol/l was prepared and added to the above-described mixture. Required amounts of copper were added to yield a Cu loading of 2.5-5.0 wt%, and the mixture was stirred at 500 rpm for 20 minutes. The support (ZrO_2-*m* or Al_2O_3-*npw*) was added and, after 20 min of stirring at 500 rpm, precipitation of Cu was achieved by adding hydrazine monohydrate (64-65% aqueous solution, Sigma Aldrich). Hydrazine to metal molar ratio of 10.5 : 1.0 was employed. The addition of hydrazine was performed rapidly under vigorous stirring (up to 800 rpm). The solution was kept stirring overnight (800 rpm). Subsequently, the micelles were broken by adding approximately 500 mL of acetone, stirring 2 h at 200 rpm (until the colour keeps constant). The colour progressively changes from dark brown to purplish brown to green/cyan to light blue. The resulting precipitate was filtered and washed with additional acetone (3 L) and dried 3 h at 100 ºC. The sample (light blue) was calcined at 350 ºC (heating rate 2 ºC/min) under static air for 4 h to eliminate surfactant residues.

3.2.7 Synthesis of ZrO_2 (mixture of tetragonal and monoclinic phases)

Due to a shortage in the commercial tetragonal zirconium oxide from Chempur, a zirconia containing a mixture of phases was synthesized.

15.45 grams of zirconium oxychloride were weighed and diluted in 300 mL of deionized water. This solution was stirred at 400 rpm, and a 5M NaOH solution was slowly added, at a rate of 0.5 mL/min until a pH: 10.23 (about 20 mL). Next, it is left in a 100 ºC oven for 22 hours and subsequently filtered and washed with deionized water up to pH 7. Then, the solid is left for 12 hours in a 100 ºC oven, drying. Finally, it is calcined at 450 ºC in a muffle (for 5h), with a 5 ºC /min ramp.

3.3 Catalyst characterization

3.3.1 Inductively Coupled Plasma Atomic Emission Spectroscopy (ICP-AES)

This technique can determine most of the periodic table elements by vaporisation and ionisation of a liquid sample. It is a type of emission spectroscopy technique, where inductively coupled plasma produces excited atoms and ions, which emit electromagnetic radiation at given wavelengths characteristic of each element[6]. A fluid sample is pumped into the nebuliser with the help of a peristaltic pump. This nebuliser generates an aerosol mist, while an argon gas current is injected into the chamber and subsequently transferred into the torch along with the sample. As a result, the Ar plasma is formed and causes the excitation of the electrons, emitting energy at specific wavelengths when returning to the ground state. This light emitted by the atoms of an element is converted into an electrical signal that can be measured quantitatively by the spectrometer. The intensity of the energy emitted is proportional to that element concentration in the analysed sample. ICP-AES analysis requires the sample to be in solution.

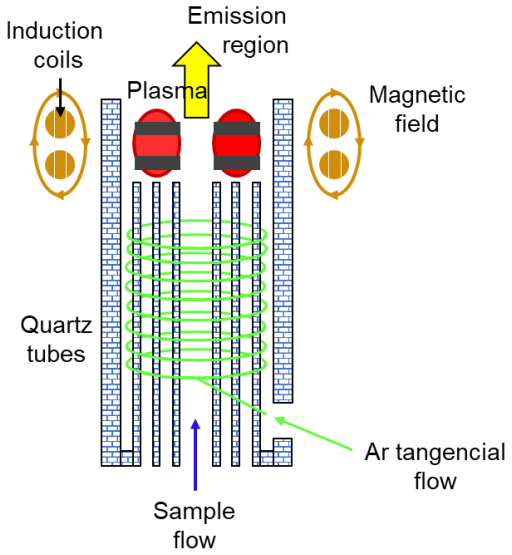

Figure 3.1. Schematic cross-section of an ICP.

ICP was used in this work to quantify the metal content of fresh and used catalysts using a Varian 715-ES ICP (inductively coupled plasma-optical emission spectrometer)

equipment after solid dissolution in HNO_3/HCl/HF aqueous solution (1: 1: 1 vol), except for samples containing Mg (where the same acid mixture but without HF was used). The instrument was previously calibrated with solutions containing knowing concentrations of the elements of interest.

3.3.2 X-Ray Diffraction (XRD)

X-ray crystallography is a technique regularly used to determine the atomic and molecular periodical structure of a solid. X-ray wavelength interval goes from 10 to 100 Å, being in a comparable order of magnitude to interplanar spacing in most crystalline structures. Then, when monochromatic X-ray radiation incises on a solid, dispersion phenomenon may take place. Concretely, X-ray is based on the elastic scattering of X-ray photons by atoms arranged in a periodic lattice[7]. Diffraction can be considered an interference phenomenon in which constructive interference occurs between the incident (i.e., transmitted) beam and the scattered beam. This is observed when the path difference between both waves is an integer of the radiation wavelength, i.e. when Bragg´s law is satisfied (Equation 3.1). In other words, regular scattering produces waves that will cancel each other in most directions through destructive interference, whereas they will add constructively in a few specific directions, dictated by Bragg´s law[8]:

$$n\lambda = 2d_{hkl}\,\mathrm{sen}\theta \quad \textbf{(Equation 3.1)}$$

where d_{hkl} is the spacing between diffraction planes, θ is the incident angle, n is an integer, and λ is the beam wavelength.

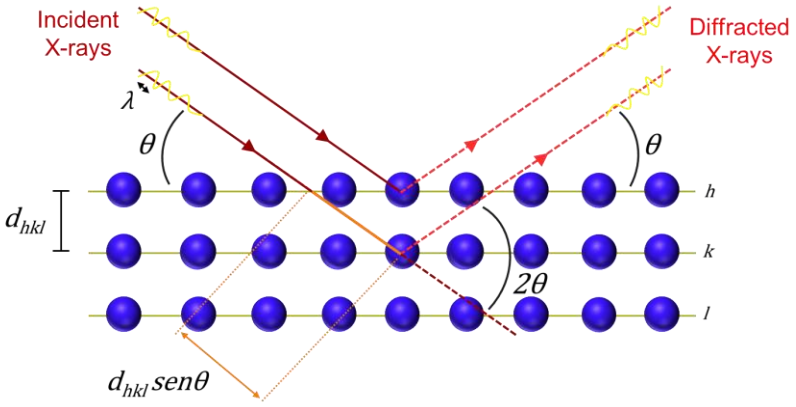

Figure 3.2. Illustration of the diffraction phenomena determined by Bragg´s Law : ($n\,\lambda = 2d_{hkl}\,sen\,\theta$).

Then, X-ray diffraction consists of an incident X-ray beam with varying angles, which causes a dispersion phenomenon, whose intensity is measured and converted into an X-ray diffraction pattern, specific for every crystalline phase. Hence, this pattern allows for elucidating the crystalline phases in a catalyst structure by comparison to an already reported database. Additionally, crystal structures are defined in terms of the geometrical arrangement of the particles present in the unit cell (the smallest repeating unit having complete symmetry in the structure). In this sense, the three values Miller indexes notation (hkl) describe vectors and planes in a crystal lattice. All crystalline materials nowadays recognised fit in one of the 14 Bravais lattices, where interplanar spacing (d) between adjacent (hkl) planes is given by known equations depending on the catalyst structure (i.e., cubic, tetragonal, hexagonal). Then, if λ is experimentally known and (hkl) and θ are known for a specific lattice plane, interplanar spacing can be calculated applying Braggs's Law, and the unit cells lattice dimensions (a, b, and c) can be elucidated from this data and the corresponding equation for a determined crystal structure. This is valuable information in catalysis, for instance to analyse the incorporation of metals in a crystalline structure during mixed oxide synthesis.

In order to identify the crystalline phases, present in hydrotalcites, mixed oxides and supported metal and metal oxide catalysts, an X-ray analysis of said samples was carried out. The equipment chosen for the analysis was a PANalytical Cubix Pro diffractometer

equipped with a PANalytical X-Celerator detector, at a scan rate of 2 min^{-1}, operating at 40 kV and 35 mA, provided with a variable divergence slit and working in fixed irradiated area mode. The diffractograms were obtained at room temperature, using the K_α radiation of Cu, in a range of 2θ = 2-90º and with a step size of 0.04º. The obtained diffractograms were compared and indexed with those found at the PDF2 database, thereby identifying the crystalline phases.

3.3.3 Electron microscopy

The operation principle of this technique is based on an electron emission source, which is accelerated with a specific potential until condensing lenses, which force the beam to converge in an effective section. Each of the different electron microscopy techniques takes advantage of one or more of the events when this beam of high-energy electrons interacts with a given sample to obtain different information (Figure 3.3), counting on a detector or several specific detectors[9].

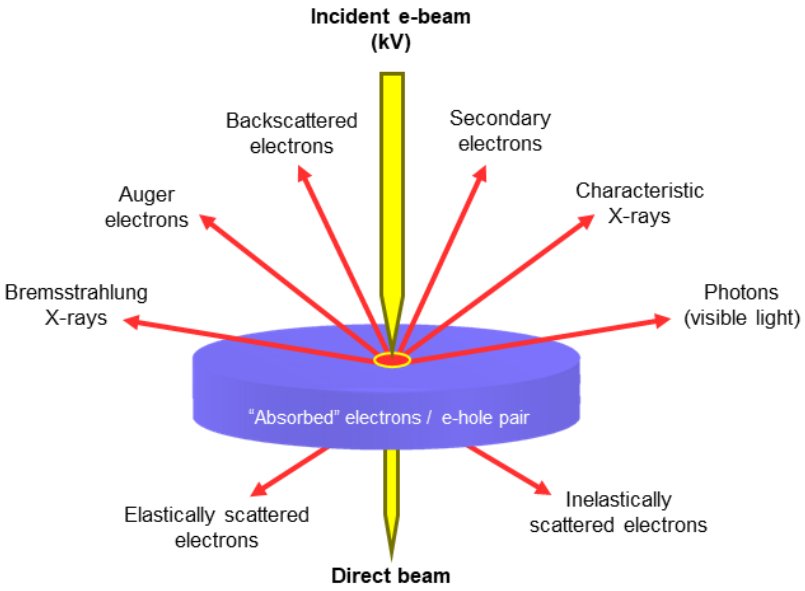

Figure 3.3. Physical phenomena arising when an electron beam interacts with a specimen.

3.3.3.1 Scanning electron microscopy (SEM)

Scanning electron microscopy (SEM) scans the sample with an electron beam along its entire surface, detecting secondary or backscattered electrons. The images are formed by contrast, which has its cause in the orientation of the particles. That is, areas of the surface facing directly at the detector will appear brighter than areas that point outward from the detector. In imaging, secondary electrons give better results as they originate primarily from the surface of the samples, while backscattered electrons come from deeper in the sample. However, the latter gives more visual information about the composition. In this sense, as far as the backscattered electron detector is concerned, heavier elements will appear brighter in the images than those lighter.

A JEOL 6300 scanning electron microscope (SEM) equipped with an Oxford LINK ISIS detector was used, but mainly to focus on obtaining compositional information of the analysed samples, as discussed in *Section 3.3.3.3*. The sample was prepared by simply sprinkling the sample onto a carbon tape.

3.3.3.2 Transmission electron microscopy (TEM)

When a high-energy electron beam passes through a sample, many electrons are transmitted and scattered by the material. Transmission electron microscope (TEM) uses dispersed and transmitted electrons to form an image focused onto a phosphor screen for direct observation by the operator and optionally on an image recording system such as a fluorescent film or a CCD retina combined with a phosphor screen. Its operation can be compared to an optical microscope that uses electrons instead of visible light as a light source, which implies a higher resolution due to the shorter wavelength of the electrons and magnetic lenses to orient them in rather than optical lenses. TEM image contrast is due to the differential absorption of electrons by different element compositions or thicknesses of the material. Then, the signal is magnified to create the final image. Importantly, TEM microscopes can image at a significantly higher resolution than SEM images, owing to the smaller wavelength of electrons (high-energy electron beams >200 keV)[9,10].

Scan Transmission Mode (STEM) enables illumination of more significant areas of the sample (by scanning the electron beam across the sample), which is optimal for Z-

contrast analysis (annular darkfield mode high angle, HAADF) and Energy-Dispersive X-ray spectroscopy (XEDS) compositional mapping. In HAADF mode, the image comprises electrons scattered at high angles larger than those where Bragg diffraction occurs. In this way, the image contrast is directly related to the weight of the elements in the sample, generating a brighter contrast for heavier ones. Therefore, the scan transmission mode is the best setting to elucidate the phase distribution in the catalysts[11].

High-resolution electronic transmission microscopy (HR-TEM) study of fresh and used catalysts was performed in Jeol JEM-2100F equipment, working at 200 kV. The microscope was also equipped with a high-angle annular dark-field (HAADF) detector and an EDS X-Max 80 detector. Images from HAADF detector running the microscope in STEM mode were used to achieve better compositional contrast. In this way, a distribution of the particle sizes for each of the samples was obtained together with its statistical parameters. Besides, the EDS X-Max 80 detector, with a resolution of 127 eV, supplied qualitative information about which elements were at particular points of the sample. For the analysis, a suspension was prepared through the ultrasonic stirring of the material to be studied and, by depositing a drop on a copper grid (3mm in diameter) covered by a perforated amorphous carbon film, some particles were partially located in the holes. In this way, they could be studied without major interferences. HR micrograph analysis, lattice spacing measurement, first Fourier transform (FFT) and phase interpretation were done using the Gatan Digital Micrograph software (Gatan Inc.), the ImageJ software and the Java version of the electron microscope software (JEM).

3.3.3.3 Energy-Dispersive X-ray spectroscopy (XEDS)

Since all the microscopes used during this doctoral thesis had connected X-ray detectors to perform XEDS measurements, it is essential to comment on the underlying principle for this technique.

The XEDS microanalysis exploits the information derived from the elastic interaction of electrons with the matter, in which energy exchange takes place[9]. In this way, the electron beam interacts with core-level electrons and transfers a specific amount of energy, promoting a core-electron to an unoccupied state above the Fermi level (that is, the atom is in an excited state). The atom can return to the ground state by transferring an

electron from the outer shell to the generate hole. This phenomenon can be accompanied by the emission of X-rays or Auger electrons. Since the energy of the emitted X-rays is specific for each chemical element, we can use them to detect and quantify the concentration of metal species in catalysts.

In *Chapter 4*, the Jeol JEM-2100F equipment with the EDS X-Max 80 detector, with a resolution of 127 eV, was used to check the copper dispersion along the catalyst surface by compositional mapping. This detector has also been used to carry out single-point analysis, helping to identify the supported metal and metal oxide nanoparticles prepared throughout this thesis. A focused beam of electrons (20 kV) and a counting time of 5 mins for compositional mappings were also selected. Additionally, in *Chapter 5*, X-ray energy-dispersive spectroscopy has checked mixed metal oxide homogeneity by acquiring elemental mappings using a JEOL 6300 scanning electron microscope (SEM) equipped with an Oxford LINK ISIS detector. With this purpose, compositional mapping images were obtained with a focused beam of electrons (20 kV) and a counting time of 50–100 s.

3.3.4 N_2-physisorption

When gas encounters the surface of a solid, an equilibrium occurs between adsorbed molecules and molecules in the gas phase, which depends on pressure and temperature. The relationship between the adsorbed molecules (adsorbed volume) and the partial pressure of the gas at constant temperature can be registered in an adsorption isotherm. The mathematical adjustment of these isotherms to different theoretical models can provide information on the volume adsorbed at a given pressure, enabling the calculation of values such as the surface area of the solid, the size and shape of the pore and its distribution.

Concretely, the BET method, established by Brunauer, Emmett and Teller, allows for determining the surface area based on the adsorption of inert gas, generally N_2, at low temperature[12]. This BET theory can be considered an extension of the Langmuir model but considering that in multilayer adsorption of the gas molecules, it is not necessary to complete a layer to begin the formation of the next. The equation that defines the model is the following:

$$\frac{p}{V(p-p^0)} = \frac{1}{V_m \cdot C} + \frac{(C-1)}{V_m \cdot C} + \frac{p}{p^0} \quad \textbf{(Equation 3.2)}$$

Where V is the volume adsorbed at pressure p, V_m is the volume required to form a complete monolayer, p^0 is the vapour pressure of the gas, and C is a constant associated with the difference between the heats of adsorption of the different monolayers.

Representing $p/V(p^0\text{-}p)$ against p/p^0, V_m and C are obtained through the slope and the ordinate at the origin. Once the volume of the monolayer V_m has been obtained, the surface area can be calculated from the following equation:

$$S = \frac{V_m \cdot N \cdot A_m}{M} \quad \textbf{(Equation 3.3)}$$

where V_m is the monolayer adsorbed gas quantity, N is Avogadro's number, A_m is the cross-sectional area of each adsorbed N_2 molecule (0.162 nm^2) and M is the molar volume of the adsorbate gas.

On the other hand, pore volumes and pore size distributions can be estimated using the Barrett-Joyner-Halenda (BJH) method based on the Kelvin equation[13]. In general, the BJH method is the first derivative of the cumulative adsorbed volume. The procedure calculates the pore radius (r) derived from the Kelvin equation and the representation of dV/dr as a function of r (or pore diameter), that is, the slope of the variation adsorbed volume for each calculated pore size. This gives an estimate of the pore size distribution and accumulated volumes in selected pore size.

In this thesis, the N_2 adsorption isotherms were obtained using a Micromeritics ASAP2420 and TriStar 3000 equipment. The surface areas were calculated using the BET method (Brunauer-Emmet-Teller), but fulfilling the criterion established by Rouquerol *et al.*[14], according to which the relative pressure range for BET surface area determination was limited to the range p/p^0= 0.05–0.25 of the N_2 adsorption isotherms. Likewise, pore size distributions and pore volumes were obtained using the Barrett – Joyner – Halenda (BJH) method. Importantly, the BJH method has been applied to the adsorption branch of isotherms, seeking to avoid a false pore size distribution derived from physical phenomena produced in the desorption branch, such as tensile strength, which produces a fast release of N_2[15].

3.3.5 Pulse chemisorption and ammonia temperature programmed desorption (NH_3-TPD)

NH_3-TPD is a widespread technique to study the acid characteristics of a catalyst. It permits the quantification of surface acid sites by quantifying the amount of chemisorbed ammonia (i.e., NH_3 mol/g). In this sense, ammonia is a hard base that can interact with Lewis acid sites (*via* electron lone pairs on the nitrogen atom) and with Brønsted acid sites (by accepting a surface proton). In addition, it is possible to assess the relative strength of those surface acid sites by monitoring NH_3 desorption. In this respect, ammonia will be desorbed at higher temperatures as the acid strength of the site to which it is chemisorbed increases. That is to say, the higher the strength of the acid site, the higher the stability of NH_3 in the chemisorbed state. However, although it is an advantageous technique, it does not distinguish between Lewis and Brønsted-type acid sites. To differentiate between both sites, spectroscopic techniques with probe molecules, such as pyridine-FTIR are needed, discussed in *Section 3.3.7.1*.

Acid centres in our materials were determined by pulse chemisorption of NH_3 followed by temperature-programmed desorption (NH_3-TPD) on a TPD/2900 apparatus from Micromeritics. First, nearly 0.100 g of sample were pre-treated in an Ar stream at 300 ºC for one h. Next, ammonia was chemisorbed by pulses at 100 ºC until equilibrium was reached. The sample was then fluxed with a helium stream for 15 min before increasing the temperature to 500 ºC in a 100 mL/min helium stream, working with a heating rate of 10 ºC/min. Gas adsorption was monitored with a calibrated thermal conductivity detector (TCD), representing a quantitative value. Besides, a non-calibrated mass-spectrometer (MS) was used to follow ammonia desorption, providing us with a spectrum obtained from the m/z=15 signal, having qualitative information about the strength distribution of acid sites.

3.3.6 Pulse chemisorption and CO_2 temperature programmed desorption (CO_2-TPD)

CO_2 is acknowledged as a mildly acidic molecule, and the basic sites of solid surfaces attract it so that it can be used to probe these sites on a solid catalyst. The electron-deficient C atom of the CO_2 molecule is prone to be attacked by electron-rich atoms. As in the NH_3-

TPD, it is also possible to estimate the relative strength of those surface base sites by following CO_2 desorption. Again, CO_2 will be desorbed at higher temperatures as the acid strength of the site to which it is chemisorbed increases. To be exact, the higher the strength of the acid site, the higher the stability of CO_2 in the chemisorbed state. However, when the carbon atom of CO_2 interacts with basic materials, the CO_2 can be activated as a carbonate (CO_3^{2-}), formed through reaction with O site, and bicarbonate (HCO_3^-), formed through reaction with surface OH[16]. Consequently, and due to the continuous exposure of samples to atmospheric CO_2, interpretation of the desorption experiment might not be as straightforward as in the case of NH_3.

Pulse chemisorption of CO_2 and subsequent temperature-programmed desorption (CO_2-TPD) were applied to study the base properties of the materials. Experiments were conducted in a Micromeritics TPD/2900 instrument. First, the catalysts (0.100 g) were pre-treated at 300 ºC under Ar stream for 1h. Next, the carbon dioxide was chemisorbed at room temperature. Then, the sample was fluxed with a helium stream for 15 min, before increasing the temperature to 650 ºC in a helium stream of 100 mL/min and using a heating rate of 10 ºC/min. Gas adsorption was monitored with a calibrated thermal conductivity detector (TCD), representing a quantitative value. On the other hand, a non-calibrated mass-spectrometer (MS) was used to monitor CO_2 desorption, following the m/z=44 signal, providing qualitative information about the strength distribution of basic sites.

3.3.7 Fourier-transform infrared (FTIR) spectroscopy

Infrared spectroscopy studies the interaction between matter and infrared radiation, which corresponds to the region of the electromagnetic spectrum that covers wavelengths between 30 and 14000 cm^{-1} and is used to determine the nature of surface chemical species. The infrared region of the electromagnetic spectrum comprises molecular and rotational vibrations that radiation absorption can produce. IR active vibration modes remain determined by the symmetry characteristics of the species; for a vibratory mode in a sample to be "active IR", it must be associated with changes in the dipole moment. Two basic categories of vibrations can be distinguished: stress and bending. Stress vibrations are changes in the interatomic distance along the axis of the bond between two atoms. Bending vibrations are caused by changes in the angle between two links. Also, a molecule

will absorb the energy of a beam of infrared light when said incident energy is equal to that necessary for a vibrational molecule transition to occur[17].

3.3.7.1 Fourier-transform infrared (FTIR) spectroscopy of adsorbed pyridine

Infrared (FT-IR) spectroscopy can be used to monitor the adsorption-desorption of pyridine, a commonly used characterization technique for evaluating the acidity of solid catalysts. The pyridine molecule can interact with Lewis acid sites via the donation of the electron lone pair on the N atom and with Brønsted sites via its protonation and subsequent absorption. Therefore, both Brønsted acid sites (BAS) and Lewis acid sites (LAS) can be distinguished. Thus, a characteristic band of pyridine ring bending vibrational modes coordinatively bonded to Lewis acid sites (LAS) can be identified at 1450 cm^{-1}. Furthermore, another signal corresponding to the ring bending vibrational modes of pyridinium ion (PyH+) can appear due to its interaction with Brønsted acid sites (1555 cm^{-1}). These bands are used for determining the type of acidity exhibited by the sample. With this objective, Lewis and Brønsted acid site concentration were calculated from integrated absorbance of signals at 1450 and 1555 cm^{-1}, according to the methodology proposed by Emeis (Equations 3.4 and 3.5) and the extinction coefficients determined therein[18].

$$\mathrm{C(L)} = 1.42\ \mathrm{A(L)}\ \mathrm{R}^2\ \mathrm{W}^{-1} \quad \textbf{(Equation 3.4)}$$

$$\mathrm{C(B)} = 1.88\ \mathrm{A(B)}\ \mathrm{R}^2\ \mathrm{W}^{-1} \quad \textbf{(Equation 3.5)}$$

These equations allow for calculating the concentration of Lewis (C(L), in mmol/g) and Brønsted acid sites (C(B), in mmol/g); where A(L) and A(B) are the integrated absorbances of FTIR signals of pyridine coordinated to Lewis or Brønsted sites; R is the pellet radius; and W its weight.

Moreover, the acid strength distribution of these acid sites can be investigated by the desorption of pyridine at different temperatures. The pyridine molecules remaining absorbed at higher temperatures would correspond to stronger acid sites.

Specifically, acid sites present in our materials were probed by FTIR measurements with adsorption-desorption of pyridine in a Nicolet Is-10 Thermo FT-infrared spectrophotometer. First, self-supported pellets (ca. 10 mg) were outgassed under vacuum

(10^{-2} Pa) at 300 ºC for 12 h. Pyridine was then introduced into the cell ($6.5 \cdot 10^2$ Pa) and, when equilibrium was achieved, the cell was degassed at 150 ºC and cooled down to room temperature. At this point, FTIR spectra of adsorbed pyridine were recorded. Usually, the degassing process (followed by acquisition at r.t.) was also carried out at 250 ºC and 350 ºC. In all cases, a spectrum was collected under vacuum before pyridine adsorption was used as background. The background was subtracted from each spectrum, and the absorbance was normalized to weight (10 mg) before calculations.

3.3.7.2 Fourier-transform infrared (FTIR) spectroscopy of adsorbed CO

Carbon monoxide is a soft base and, therefore, highly polarizable (despite its small size). Consequently, it shows low interaction with solid surfaces, presenting low adsorption heats and making the use of low temperatures necessary. As a result, the CO molecule is very sensitive to the interaction with protic and aprotic acid sites, especially with Lewis or coordinatively unsaturated metal sites (CUS) and to the strength of these sites on the same material. Interestingly, carbonyl stretching frequency can vary significantly to its gas-phase frequency (2143 cm^{-1}) depending on the specific interaction with a surface site (especially with CUS sites). In this way, CO allows for discriminating between different exposed crystal facets and other highly unsaturated sites present in metal oxide and metal oxide surfaces (i.e., nanoparticles). CO firstly forms donor bonds of σ-character (*via* its 5σ orbital) with surface metal centers. Then metal-carbon bond is usually stabilized *via* a π-back donation from d orbitals from the metal to antibonding π* orbital of CO, which will shift carbonyl frequencies to lower values (constantly comparing with gas-phase frequency carbonyl, 2143 cm^{-1})[19,20].

Considering the above-mentioned points, this thesis used FTIR of adsorbed CO for the analyses of unsaturated metal sites to qualitatively assess metal particle morphologies in Pd-based materials. Moreover, this technique was also used to determine the relative amount of Cu^{1+} in those catalysts containing copper and assess the Lewis acidity in hydrotalcite-derived materials. IR spectra of adsorbed CO were recorded at 25 ºC or -170 ºC with a Nexus 8700 FTIR spectrometer using a DTGS detector and 4 cm^{-1} resolution. An IR cell allowing for *in-situ* treatments in controlled atmospheres and at temperatures from 25 to 500 ºC has been connected to a vacuum system with a gas dosing facility. For IR studies, the samples were pressed into self-supported wafers and i*n-situ* reduced at 250

ºC under a H_2 flow (10 ml min^{-1}) for 1.5 h (in the case of Pd-based samples) or at 150 ºC under air flow (in the case of Cu-based samples), followed by evacuation at 10^{-4} mbar at 300 ºC for 1 h. After activation, the samples were cooled down to 25 ºC or -170 ºC under dynamic vacuum conditions. IR spectra were recorded after each dosage.

3.3.7.3 Fourier-transform infrared (FTIR) spectroscopy of adsorbed $CHCl_3$

On the other hand, $CHCl_3$ is classified as a hard acid, found suitable to act as a probe molecule for the strength of basic sites[21].

For the experiments of adsorption of $CHCl_3$ on the surface of the hydrotalcite-derived mixed metal oxides, an IR cell that allows in situ pre-treatments under controlled atmosphere and temperatures from 25 to 600 ºC was connected to a vacuum system with a gas dispenser. The pellets were prepared from the powdered samples treated at 250 ºC under a dynamic vacuum (10^{-4} mbar). After activation, the samples were cooled down to 25 ºC. During the IR studies with $CHCl_3$, the gas was adsorbed at different pressures (1-30 mbar). IR spectrum was registered after each dose.

3.3.7.4 Fourier-transform infrared (FTIR) spectroscopy of adsorbed NO

Although surface probing potentialities of NO have been less utilized than some other molecules such as CO, $CHCl_3$ or pyridine, this molecule also fulfils the requirements for a probe molecule such as small size and accordingly good accessibility to surface sites, softness, and low chemical reactivity. Additionally, and compared to CO, NO shows greater sensitivity to the electronic state of the cation where it coordinates due to an unpaired electron in the NO antibonding 2π orbital[22].

In the present study, different types of copper species could be identified thanks to the use of NO as a probe molecule in FT-IR. The samples were pressed into self-supported wafers and treated at 300 ºC in Nitrogen flow (20 mL/min) during 1 h, followed by evacuation at 10^{-4} mbar at 100 ºC during 1 h. After activation, the samples were cooled down to −156 ºC under dynamic vacuum conditions followed by NO dosing at increasing pressure (0.05–0.60 mbar) for NO adsorption studies. IR spectra were recorded after each dosage. After maximum NO dosing, the samples were evacuated under dynamic vacuum conditions at 10^{-5} mbar and IR spectra acquired at controlled times.

3.3.7.5 In-situ Fourier-transform infrared (FTIR) spectroscopy using hydroxyacetone (gas phase), 1,2-PDO as probe molecule (gas phase), and glycerol (impregnated)

With the aim of understanding the catalyst behavior in the selective glycerol dehydration to acetol, some *in-situ* FT-IR spectrometry studies were registered with a Bruker 70 V spectrometer working with a DTGS detector and acquiring at 4 cm^{-1} resolution. An IR cell allowing *in-situ* treatments in controlled atmospheres and temperatures from 25 ºC to 500 ºC was connected to a vacuum system with a gas/liquid dosing facility.

In the studies carried out with either hydroxyacetone or 1,2-propanediol, the samples were pressed into self-supported wafers and treated at 300 ºC in N_2 flow (20 mL/min) for 1 h followed by evacuation at 10^{-4} mbar at 100 ºC for one hour, except in one ex-situ H_2 reduced sample, which was activated in vacuum at 100 ºC for one hour. After activation, the samples were cooled down to 25 ºC under dynamic vacuum conditions and exposed to 1.5 mbar of 1,2-propanediol and/or hydroxyacetone, followed by evacuation at 25 ºC for 5 min. In the case of 1,2-propanediol, temperature rose under static vacuum conditions to 160 ºC, taking IR spectra at 45 min of each temperature step. Once completed 45 min at 160 ºC, the sample was evacuated and cooled down to 25 ºC where ten mbar of CO have been adsorbed to titrate the catalyst surface. To avoid surface reduction by CO, IR spectra were recorded at once.

Additionally, to check the competitive adsorption between a polyol and different solvents on the CuO/ CuO/*m*-ZrO_2 catalyst, the samples were pressed into self-supported wafers and treated at 150 ºC in airflow. After this activation, the samples were cooled down to 50 ºC under dynamic vacuum conditions and exposed to calibrated MeOH/water volumes until saturation. Then, calibrated volumes of 1,2-propanediol (1,2-PDO) were introduced, and IR spectra were acquired after each dosage.

For CuO/*m*-ZrO_2, to assess the reactivity of the real molecule (i.e., glycerol) and the effect of MeOH on the true characteristics displayed by the working catalyst, the solid sample was impregnated with a mixture of 90 wt.% solvent (MeOH or water) and 10wt.% glycerol. 100 mg of catalyst was weighed, and 100 µL of the above-described mixtures were homogeneously added. The catalyst was dried at 50 ºC for 20 minutes. For IR studies

the samples were pressed into self-supported wafers and treated without further activation. Then, the temperature rose under static vacuum conditions from r.t. to 60 ºC and from 60 ºC to 160 ºC with 20 ºC steps, acquiring IR spectra at each temperature step.

3.3.8 Temperature-programmed reduction (TPR)

The analysis by reduction with H_2 at a programmed temperature is used to characterise metallic oxides, mixed metallic oxides and metals or metallic oxides dispersed on a support. It is carried out by reduction with a gaseous stream of H_2/Ar at increasing temperatures. This analysis provides information on the number and type of reducible species present in the catalyst, their reduction temperature (i.e., their reducibility), and their reduction kinetics. Based on these findings, it is possible to draw interesting conclusions about the nature and strength of the metal-support interactions, the degree of dispersion of the metal species, or their oxidation state.

The reduction behaviour of the most effective catalysts was studied by temperature-programmed reduction (TPR) in a Micromeritics Autochem 2910 equipment. Approximately 50 mg of the calcined catalyst were initially cleaned with 30 cm^3/min of Ar at room temperature for 30 min. Then, a mixture of 10 vol% of H_2 in Ar was passed across the sample at a total flow rate of 50 cm^3/min, while the temperature was increased up to 800 ºC at a heating rate of 10 ºC/min. The H_2 consumption rate was monitored in a thermal conductivity detector (TCD), previously calibrated using the reduction of CuO as a reference.

3.3.9 X-ray photoelectron spectroscopy (XPS)

X-ray photoelectron spectroscopy is one of the most widely used surface analytical techniques. This technique has aroused great interest in the science of catalysis due to its high selectivity for analysing the upper layers of materials. This spectroscopy is based, like all spectroscopies, on the interaction between matter and photons with a specific frequency. In this case, the photoelectric effect is the applied physical principle (Hertz, 1887)[23]. When a sample is irradiated with photons of higher energy than the binding energy of the electrons in the atoms, they emerge from the sample with a kinetic energy

equal to the energy excess of the incident photon. In the case of XPS, the sample is irradiated with X-rays (generally Al K_α, 1486.6 eV; or Mg K_α radiation, 1253.6 eV), which promote electrons at the nucleus level to beyond the Fermi level (EF). The energy required to promote an electron from an inner orbital to EF is called the binding energy (B.E.), which is characteristic of every element in the periodic table. Notoriously, X-rays penetrate microns into the sample, but only the photoelectrons which escape the sample without energy loss provide readily interpretable chemical information. In fact, only electrons from the first few layers can escape without inelastic collisions, whereas electrons from deeper in the sample end up in the spectrum background. As a result, XPS is considered a semi-bulk technique, usually allowing for analysing a sample region that ranges from its very top surface to 2-5 nm in depth, depending on the material[24].

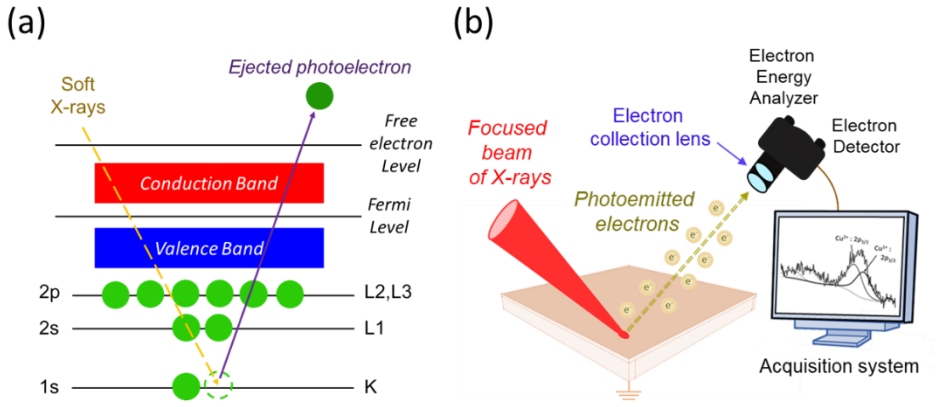

Figure 3.4. (a) Scheme of X-ray induced photoelectron emission. (b) Simplified experimental XPS set-up.

Notably, the energy measured by a hemispherical detector is the photon's kinetic energy. In this sense, the electron's binding energy can be calculated through the energy of the irradiated photon and the work function of the spectrometer Φspec, which in turn can be approximated to a constant for each device, the value of which must be periodically demonstrated. Therefore, the kinetic energy (Ec) can be expressed by the following equation:

$$\mathrm{Ec} = \mathrm{hv} - \mathrm{BE} - \Phi_{\mathrm{spec}} \quad \textbf{(Equation 3.6)}$$

where Φ_{spec} $r$epresents the spectrometer's work function, and BE is the binding energy. This formula allows for the immediate conversion of the detected kinetic energy to the commonly represented binding energy. In this way, a typical XPS spectrum shows the number of electrons versus the binding energy of the internal levels of the atoms present in the solid[23].

Each element emits in a characteristic spectral range with an intensity dependant on the relative sensitivity factor (R.S.F) of each of its electrons. Therefore, measurements of the kinetic energies of the emitted electrons provide an elemental quantitative analysis for all the elements of the periodic table, except nitrogen and helium.

A more detailed analysis of the emitted photoelectron reveals the correlation between the element's kinetic energy and its chemical state in its compounds. In this sense, an XPS spectrum can be interpreted in terms of initial and final effects that can cause changes in the kinetic energy detected. The effects of the initial state mainly comprise effects related to the charge on the atom under study, which can cause modifications in the binding energy: i) oxidation state of the element or ii) chemical environment. Therefore, the different species of the same element, those present in different chemical environments, will give rise to different shifts with respect to the BE expected for the pure element. In general, higher oxidation states show higher binding energy. That is, electrons are more attracted to the nucleus. In the same way, bonded electron attractor species will promote shifts towards higher bond energies, while electron donors will follow the opposite trend, shifting signals to lower bond energies. However, the most intricate part of XPS is related to the interpretation of the final state effects, which occur after the photoemission process, and are factors that affect the atom once the electron is gone or the photoelectron leaving the atom. These effects include relaxation processes, hole screening, shaking-up or shaking-off processes, and multiplet splitting[24]. Nonetheless, as long as the proper fitting rules and restrictions are applied, XPS allows for conducting a qualitative analysis of a test sample where we can have information of the present elements, oxidation states and even the coordination environments of a specific element.

Remarkably, internal charge corrections are necessary because the sample gets charged, especially insulators or semiconductors, by the loss of electrons. Generally, the C*1s* signal of the adventitious carbon present in all samples is taken as a reference. In addition, there are significant effects due to differential charging when having inhomogeneity in electrical conductivity throughout the sample. This charge problem can be partially or totally neutralised using a low energy electron flood-gun on the sample, but this can lead to misinterpretation when dealing with species susceptible to reduction.

As well as spectral peaks originated by primary photoemission processes, other peaks corresponding to diverse electronic processes are observed. Among them, it should be noted the Auger effect. When a photoelectron is emitted, an inner hole is generated, occupied by an electronic transition from an outer layer. The energy associated with this transition can be dissipated by electron emission from a third layer, known as the Auger effect[24,25].

In this work, X-ray photoelectron spectroscopy (XPS) was used to conclude the oxidation state of copper species at the catalyst surface. XPS data were collected on a SPECS spectrometer equipped with a 150-MCD-9 detector and using a non-monochromatic Mg Kα (1253.6 eV) and Al Kα (1486.6 eV) as X-ray sources. Spectra were recorded at 25 ºC, using an analyzer pass energy of 30 eV, an X-ray power of 50 W (to avoid photo-reduction) and under an operating pressure of 10^{-9} mbar. During data processing of the XPS spectra, binding energy (BE) values were referenced to the Al*2p* peak settled at 73.5 eV. Spectra treatment was performed using the CASA software.

Additionally, an *in-situ* study was carried out at RMIT (Melbourne, Australia) using a KRATOS spectrometer with monochromatic Al Kα. Approximately 1 gram of glycerol was dissolved in methanol (1 gram) and sonicated for 3 minutes, giving a mixture of 50wt.% of glycerol and 50wt.% of methanol. For the impregnation of glycerol on the CuO/*m*-ZrO_2 catalyst, 100 mg of catalyst was weighed, and then added 100 µL of the above-described glycerol-methanol mixture to the catalyst. Then the catalyst was dried at 50 ºC for 20 minutes. For the XPS acquisition, the XPS instrument is equipped with a flexilock chamber that can achieve pressures as low as 1 x 10^{-8} Torr. The flexilock pressure should be <1 x 10^{-7} Torr before transferring to the sample analysis chamber

(SAC). All heating treatments were done in a flexilock chamber before transferring the sample to SAC. There are three temperatures (1) 25 ºC, (2) 100 ºC and (3) 200 ºC. Initially, the fresh CuO/*m*-ZrO_2 catalyst was transferred to flexilock chamber. After achieving the required pressure, the sample was transferred to SAC and analyzed at 25 ºC. Then, the same catalyst was brought back to the flexilock chamber and heated to 100 ºC for 30 minutes under vacuum, cooled down to room temperature and transferred to SAC for analysis. Last, the sample was again brought back to the flexilock chamber and heated to 200 ºC for 30 minutes under vacuum and cooled down to room temperature. Afterwards, the catalyst was transferred to SAC and analyzed. Similarly, the glycerol impregnated catalyst was analyzed by XPS at 25 ºC, 100 ºC and 200 ºC.

3.3.10 Chemisorption

Some catalytic surfaces show sufficient reactivity to chemisorb some gases, a phenomenon different from physisorption, involving chemical bonds between the adsorbate and the active centres. Thus, knowing the stoichiometry between absorbate and absorbent, these techniques can be used to determine the density of active surface sites and their dispersion.

3.3.10.1 CO chemisorption

Chemisorption of CO on the late transition-metal surfaces is one of the most common tools to calculate metal dispersion and particle size. As previously said, CO is a soft acid that can interact with coordinatively unsaturated metal sites. Therefore, when knowing the endpoint for chemisorption, i.e., when chemisorbed molecules occupy all the active sites on the solid surface, the metal dispersion can be estimated[26]:

$$\mathrm{D}(\%) = \frac{\text{no.surface atoms}}{\text{Total no.atoms}} \cdot 100$$

$$\mathrm{D}(\%) = \mathrm{S} \cdot \frac{\mathrm{N} \cdot \mathrm{Mw}_{\mathrm{metal}}}{\mathrm{X}_{\mathrm{metal}}} \cdot 100 \qquad \textbf{(Equation 3.7)}$$

where S is a stoichiometric factor (assumed to be one for CO:Pd), N is the amount of monolayer, experimentally obtained from Langmuir isotherm (in static experiments) or directly from dynamic (flow experiments) in mol/g, Mw is the molecular weight of the

metal (g/mol) and X_{metal} is the mass fraction of metal in the solid sample (measured, for example, by ICP).

Surface-averaged chemisorption diameters can be calculated from this dispersion as:

$$d_{chem} = \frac{f_{shape}}{D}\frac{v_m}{a_m} \quad \textbf{(Equation 3.8)}$$

where f is a particle shape correction factor (six for spherical particles), v_m and a_m are the volume and surface area of a metal atom[26].

Additionally, the specific active surface area AA is determined by multiplying the area a_m occupied by one surface molecule by the number of adsorbed molecules per gram N[26].

Unfortunately, the issue with CO chemisorption is the selection of the metal : gas ratio, as there is a linear and bridged chemisorbed form possible. The ratio between absorption modes is not constant as it is likely to change as one metal is diluted with the other. Furthermore, modifications take place when a late transition metal is deposited on a more electropositive transition-metal substrate. In this work, the stoichiometry Pd : CO was assumed to be 1, as typically considered in the literature. Nonetheless, the highly likely possibility of underestimating Pd dispersion and, correspondingly, overestimating the particle size should make the reader take the values as relatives, and they must only be compared with each other[27].

In *Chapter 5*, CO chemisorption was carried out on Pd-based materials by using the double isotherm method on Quantachrome Autosorb-1C equipment. Before adsorption, 300 mg of the sample (0.45–0.8 mm) were reduced in flowing hydrogen (100 mL/min) using the same reduction temperature applied before for catalysts (i.e., 400 ºC for 2 h and 3 ºC/min). After reduction, samples were degassed at 1333×10^{-3} Pa for 2 h at 400 ºC, and then, the temperature was lowered to 35 ºC. Next, pure CO was admitted, and the first adsorption isotherm (i.e., the total CO uptake) was measured. After the evacuation at 35 ºC, the second isotherm (i.e., the reversible CO uptake) was taken. Finally, the amount of chemisorbed CO was calculated by subtracting the two isotherms. The pressure range

studied was 0.5–11 × 10^4 Pa. Pd dispersion was calculated from the amount of irreversibly adsorbed CO.

3.3.10.2 N_2O chemisorption

Standard chemisorption methods are not believed to be practical techniques for characterizing copper catalysts. Neither CO nor H_2 have been shown to chemisorb strongly on copper. Therefore, the classic method for determining copper surface areas uses the decomposition of nitrous oxide to selectively oxidize the surface copper atoms to Cu_2O with a stoichiometry of one oxygen atom to two copper surface atoms *via* the following reaction[28]:

$$N_2O(g) + 2Cu_s \xrightarrow{60\text{-}90\ ^oC} N_2(g) + Cu_s\text{-}O\text{-}Cu_s$$

Usually, the samples are pretreated by reducing the copper surface with flowing hydrogen at temperatures ranging from 200-300 ºC for 1-2 hours. Then the sample is cooled down to the analysis temperature (60-90 ºC). Nitrous oxide is then introduced to oxidize the copper surface selectively. Traditionally, a thermal conductivity detector (TCD) measures the nitrogen evolved from this reaction but, if carrying out a last hydrogen reduction of Cu_2O to Cu^0, the hydrogen uptake can also be monitored by TCD and used to calculate the amount of surface copper.

In this manner, copper dispersion (D_{Cu}), defined as a ratio of Cu exposed at the surface to total Cu, can be calculated by dividing the H_2 uptake from the second TPR (A_2: Cu_2O to Cu) by the H_2 uptake from the first TPR (A_1: CuO to Cu^0), taking into account the stoichiometry of every process.

$$D_{Cu}(\%) = \frac{2A_2}{A_1} \cdot 100 \qquad \textbf{(Equation 3.9)}$$

The specific surface area of metallic copper ($S_{Cu}^{N_2O}$) was calculated using the following expression:

$$S_{Cu}^{N_2O}(m^2/g) = \frac{M_{H_2}\ SF\ N_A}{10^4\ C_M\ W_{Cu}} \qquad \textbf{(Equation 3.10)}$$

,where M_{H2}, SF, N_A, C_M, and W_{Cu} are moles of hydrogen consumed per unit mass of catalyst (μmol H_2/g cat), stoichiometric factor (2), Avogadro's number (6.022×10^{23} mol^{-1}), number of copper atoms per unit surface area (1.46×10^{19} atoms·m^{-2}) and Cu content (wt%), respectively.

Also, by assuming a spherical shape of particles, the average size of copper particles ($d_{Cu}^{N_2O}$) was determined by the following expression:

$$d_{Cu}^{N_2O}(nm) = \frac{6 \cdot 10^3}{S_{Cu}^{N_2O} \cdot \rho_{Cu}} \qquad \textbf{(Equation 3.11)}$$

where ρ is copper density (8.92 g/cm^3).

Therefore, copper dispersion in some of the CuO-based materials was measured by N_2O chemisorption. The technique comprised three steps: reduction to Cu^0, oxidation of Cu^0 to Cu_2O using N_2O, and temperature-programmed reduction of Cu_2O surface species. With this objective, 80 mg of sample were loaded into a flow microreactor. Next, the reduction was carried out with a H_2/Ar mixture (10 vol % at 50 mL/min) passed through the sample. The temperature was increased at a rate of 10 ºC/min until the minimum temperature needed to reduce CuO to Cu^0 (followed by TCD) completely was reached. Reduced samples were purged under a He flow, cooled down to 60 ºC and exposed to N_2O (5 vol% N_2O/He) for 45 min. The last TPR was done on the freshly oxidized Cu_2O surface up to 500 ºC with a H_2/Ar mixture (10 vol% at 50 mL/min) and a heating rate of 10 ºC/min. Again, the uptake of hydrogen was followed by a thermal conductivity detector.

3.3.11 Thermogravimetric analysis (ATG)

In general, *thermal analysis* can be defined as the measurement of the physicochemical properties of a material as a function of temperature. The properties most frequently evaluated by this type of analysis are mass, enthalpy, heat capacity, and coefficient of thermal expansion. In particular, we will focus on studying the variation of mass against temperature to use the technique of thermogravimetry.

The ATG is a technique in which a substance weight change is measured as a function of temperature or time, thus detecting the events that imply a change in mass. In ATG, the

weights of a particular transformation M_f and M_i and the difference in weight (ΔM) are the fundamental data of the sample, and they are used for qualitative and quantitative calculations of compositional changes.

In our case, ATG was mainly used to quantify the organic matter deposition after using the catalysts. The analyses were carried out in a Mettler Toledo TGA/SDTA 851 apparatus, using a heating rate of 10 ºC/min under an air stream, until a temperature of 800 ºC was reached.

3.3.12 Elemental analysis (EA)

Elemental analysis (EA) is a process in which a catalyst sample is analysed to determine its carbon, hydrogen, nitrogen, and sulphur content. This method consists of an oxidation process, which is accomplished by combustion analysis. The sample is instantaneously burned in an excess of oxygen, and gas combustion products are *in-situ* reduced to produce N_2, SO_x, CO_2 and H_2O, separated in a chromatographic column and quantified in a TCD detector. Therefore, it can be used to determine the percentage of N, C, H and S, thereby contributing to the confirmation of the structure, the purity of the sample, and, in our case, allowing us to determine the amount of carbon present in the catalytic material after the reaction.

In the work herein presented, Elemental analysis (EA) was carried out in a Fisons EA1108CHN-S apparatus to determine organic matter deposition (C wt.%) on the catalysts after their use in different catalytic reactions.

3.3.13 Nuclear magnetic resonance analyses (NMR)

Nuclear Magnetic Resonance (NMR) spectroscopy is based on the interaction of a nuclear magnetic moment with an external magnetic field, which leads to the generation of different energy levels. The response to the transition between these levels due to the radiofrequency energy absorption by the atomic nucleus can be detected. In this way, the NMR spectra are generated for compounds with nucleus with a non-zero magnetic moment. Interestingly, the resonance frequencies are different for the same type of nucleus since the chemical environments are different. Hence the chemical shift (δ) is defined.

Molecular information is obtained from a variety of spectra obtained from different types of NMR experiments[29].

Specifically, Nuclear Magnetic Resonance (NMR) spectroscopy of liquids is one of the most powerful techniques for the structural elucidation of compounds molecular techniques by characterizing chemical shifts, couplings, and the resonance peaks' relative intensities[29].

With the objective of identifying a chemical intermediate, one reaction mixture from the selective glycerol dehydration to acetol was characterized by ^{1}H and ^{13}C NMR spectroscopy. Spectra were recorded using a Bruker Avance 300 (^{1}H 300 MHz, ^{13}C 75 MHz) in $CDCl_3$.

3.3.14 Isotopic exchange experiments H/D

Over the last decades, the improvement in high-resolution mass spectrometry systems has resulted in more extended use of the isotopic exchange Hydrogen/Deuterium reaction to provide both structural and mechanistic insights. In particular, the reaction between H_2 and D_2 to give HD has been accepted as an indicator of the catalyst ability to dissociate H_2[30,31].

Hydrogen/deuterium (H_2/D_2) exchange experiments were carried out in a flow reactor to study the H_2 activation potential of the Pd-based catalysts. The feed gas was composed of a mixture of H_2 (4 ml/min), D_2 (4 ml/min), and Ar (17 ml/min). The total catalyst weight was 0.4 mg. The reactor outlet was coupled with a mass spectrometer (Balzer, Tecnovac), operating in the multi-ion detection mode (MID) and registering the mass signals (m/z) of 2(H_2), 3(HD) and 4(D_2). The samples were pre-reduced by heating at 400 ºC with a H_2 flow of 100 ml/min. After sample activation, temperature was decreased to 25 ºC under Ar flow (25 ml/min), and once the mass signal was stable, the Ar flow was switched to the H_2/D_2/Ar reaction mixture. After 30 min at 25 ºC, temperature was gradually raised to 60 ºC, 90 ºC and 120 ºC, maintaining each temperature for at least 30 min.

3.4 Catalytic tests

3.4.1 Continuous glycerol dehydration to acetol

Catalytic experiments were done in a stainless-steel tubular fixed-bed reactor (Figure 3.5; length = 25 cm and diameter = 0.5 cm), with the catalyst (0.500 g) pelletized in particles of 0.425-0.600 mm in size diluted with SiC (0.600-0.800 mm). Typically, catalytic tests were carried out by feeding the reactor a liquid mixture of glycerol and methanol (with variable ratios) at 240 ºC for different times, depending on the experiment. The reaction is considered to start when the first drop is collected at the reactor outlet. Importantly, experiments have always been performed under strict kinetic limitations. In this sense, the *Annex* (Figures A1-A4) shows the different internal and external diffusion tests carried out for the different families of catalysts applied in this reaction under their typical working conditions. For each experiment, cumulative fractions (corresponding to 0-1 h, 1-2 h, 2-3 h, etc.) were collected in a glass recipient submerged in an ice bath. In a typical experiment, the feed flow was 2.0 mL/h, and the fraction from 0 to 1 h was considered an induction-stabilization time and, therefore, disregarded in calculations.

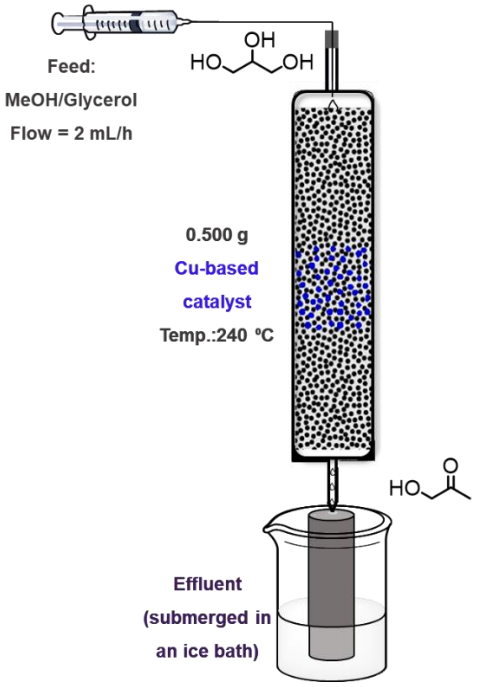

Figure 3.5. Scheme of the reaction system for continuous glycerol dehydration to acetol.

After the reaction, selected solid catalysts were washed with 20 mL of methanol (2 mL/h) in the same reactor, and then calcined at 550 ºC during 6 h (hydrotalcite-derived mixed oxides) or 4 h (CuO-supported materials) in airflow (3 ºC/min, 50 mL/min). The catalytic experiments together with the analytics corresponding to the re-usability tests were performed in the same way as the common experiments already described.

3.4.2 Reductive cycloamination of acetol with ethylenediamine to 2-methylpiperazine

Reductive cycle-amination reactions were carried out in a "batch" type micro-reactor of 6 ml with a probe for sampling and a pressure gauge for pressure measurements (Figure 3.6). The reproducibility of the system was carefully evaluated with a commercial catalyst (see Annex, Figure A5). Different samples were collected throughout a common experiment. Nonetheless, the amount of sample collected was always between 0.040 and 0.050 g. In this manner, kinetic experiments were done by avoiding removing more than 15% of the total weight of the reaction mixture. A test to discard any effect of the sampling on the catalytic activity can also be found in the *Annex* (Table A1). The reactor was purged twice with 10 bar of N_2 before feeding H_2. The H_2 pressure in the system was kept practically constant during all experiments by recharging H_2 every 30 minutes. Normally, reactions were carried out in the presence of 13 bar of H_2, at 90 ºC for 7 h at a stirring rate of 800 rpm. In preliminary experiments, 0.325 g of acetol (3.9 mmol), 0.227 g of ethylenediamine (3.8 mmol) and 0.056 g of catalyst were added at the same time, in the presence of 1.250 g of solvent (methanol). Afterwards, the improved standard protocol was established. In this procedure, acetol was not initially introduced into the batch reactor but slowly added at an addition rate of 100 μl/h during the first three hours. Then, the reaction was continued until 7 h. Also, the catalyst loading was decreased to 0.011 in some experiments to further discriminate between catalyst activity.

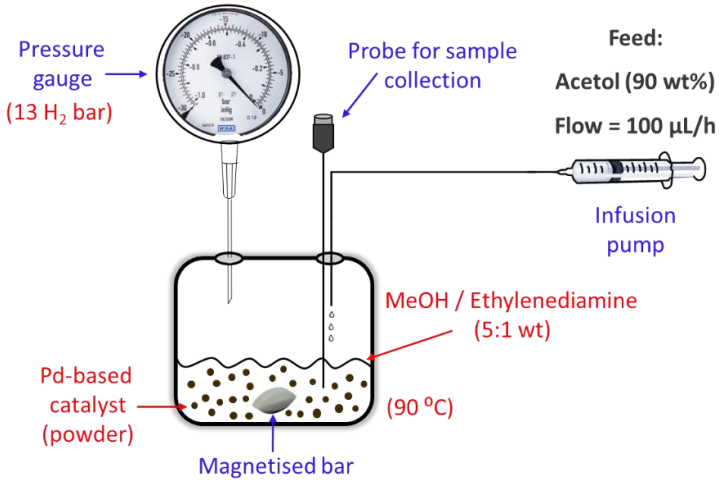

Figure 3.6. Scheme of the reaction system for reductive cycloamination of acetol with ethylenediamine to 2-methylpiperazine.

In addition, some experiments were done using water instead of MeOH as the reaction solvent. More importantly, some recyclability tests were carried out for selected catalysts. With this aim, four successive catalytic cycles were usually completed; the first three correspond to the direct separation and recovery of the solid catalyst after reaction through filtration, followed by a thorough washing using MeOH (3 mL, 10 min); and final catalyst recovery by centrifugation. After that, an additional (fourth) catalytic cycle was done, involving the same steps previously described together with a catalyst regeneration step under identical conditions employed for sample activation before reaction usage (i.e., 400 ºC, under H_2 flow for 2 h, 3 ºC/min). It is worth noting that, to compensate catalyst losses during the consecutive recycles and the consequent scaling down of the other reactants participating in the reaction, a pyramidal scheme was followed with four repetitions for the first use, three for the second one, etc., by this means guaranteeing to work with equal catalyst loading all through a specific reusability test.

3.4.2.1 Coupling with the dehydration product

The coupling of the reductive amination reaction with the glycerol dehydration reaction was accomplished by simply feeding the mixture obtained at the exit of the first continuous reactor (Figure 3.5) to the second batch reactor (Figure 3.6), thereby attaining a “semicontinuous” catalytic process. Thus, taking into account that, at the reactor outlet,

the average weight percentage of acetol achieved with the best catalyst is around 20%, to keep the equimolarity between reactants, 1.6 mL of the solution coming from the first reactor were slowly added to a mixture of 0.227 g of ethylenediamine and 0.227 g of MeOH. Again, the reactor was purged twice with 10 bar of N_2 before feeding H_2. The H_2 pressure in the system was kept practically constant during all experiments by recharging H_2 every 30 minutes. Reactions were carried out in the presence of 13 bar of H_2 at 90 ºC for 7 h at a stirring rate of 800 rpm. In this case, and to keep the addition rate of acetol, the selected rate for the infusion pump was 550 µL/h.

3.4.3 Cycloamination of acetol with ethylenediamine and dehydrogenation to 2-methylpyrazine

A stainless-steel tubular fixed-bed reactor (length = 25 cm and diameter = 0.5 cm) was used for catalytic tests with ethylenediamine and acetol aqueous solutions, which were added equimolarly to the reactor. This reactor has two inlets. On the one hand, an inlet with 40% in weight of aqueous ethylenediamine and introduced into the system with a flow rate of 1.00 mL/h. The other input comprises an aqueous solution with a 40% in weight of acetol. Since the reaction mixture was planned to be equimolar, the flow rate of this second solution is 1.24 mL/h. Both solutions were added to a mixing pre-reactor (length = 6 cm and diameter = 0.1 cm) at room temperature, allowing the imine formation under mild conditions and avoiding undesired reactions. Later, they arrived at the catalytic fixed-bed reactor, working at a temperature of 350 ºC. A schematized illustration of the reactor can be found in Figure 3.7. The catalyst was pelletized (0.425-0.600 mm) and diluted with SiC (0.600-0.800 mm) without additional pre-treatment. In a previous master thesis experimentally supervised by the PhD candidate, these conditions were ensured to be within the kinetic regime[32]. The catalytic experiment could last between 4.5 and 8 hours, depending on the material and the information to be obtained. For each experiment, cumulative samples were taken at the reactor outlet corresponding to periods of 0.5, 1.0 or 1.5 h of reaction, respectively. Sampling was done inside a glass recipient submerged in an ice bath. Again, the reaction is considered to start when the first drop is collected at the reactor outlet. In a typical experiment, the fraction collected from the start until 0.5 h was induction-stabilization time and therefore, not considered in cumulative calculations.

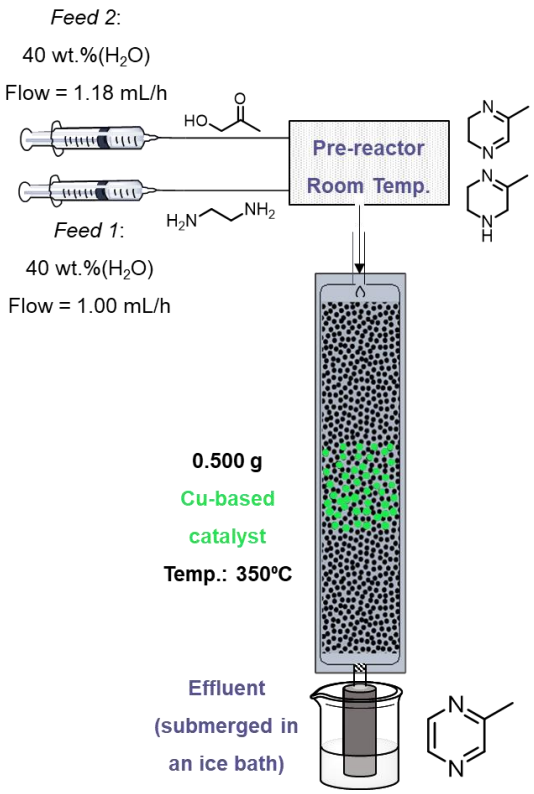

Figure 3.7. Scheme of the reaction system for reductive cycloamination of acetol with ethylenediamine and dehydrogenation to yield 2-methylpyrazine.

3.4.3.1 One pot two-step process from glycerol

In order to yield 2-methylpyrazine directly from glycerol, a multi-bed continuous reactor was designed (Figure 3.8). The constituent parts of the reactor are mainly three. On the one hand, the first bed where *Cat1* is working at 240 ºC to selectively dehydrate glycerol to acetol. This first part of the reactor is fed with a mixture of glycerol : H_2O : MeOH (2:1:1 in wt.) at 1.8 mL/h (to roughly keep the equimolarity between acetol and ethylenediamine in the second stage). The diameter of the bed is 0.5 cm and the height 14.1 cm. The second bed, with *Cat2*, shares the characteristics of the first, but, in this case, the height (12.6 cm) and the working temperature (350 ºC) are different. A long (8.0 cm height) hollow three-way junction connects the two independent beds, with a frit in the upper part that allows liquids to circulate but prevents the bottom part of the silicon carbide (inert) from moving which, together with the catalyst, constitutes the first fixed bed. The

other entry of the three-way junction is used as access for the ethylenediamine probe (1.0 mL/h, 40 wt.% aqueous solution). The two inlets are mixed on the walls of the three-way junction at a much lower temperature than that of both beds, even though it does not reach room temperature due to their proximity to them. In this way, upon reaching the second bed, the reagents are well mixed, and the imines formed at relatively low temperatures. Finally, the second bed has a grid at the outlet of the second bed itself to prevent, in the same way that the frit in the first bed did, the passage of solid that could obstruct the exit of liquid products from the system and cause catalyst-loading losses. The reactor outlet has a length of 5 cm, where the reaction mixture is cooled down before being collected in a flask submerged in an ice bath. Cumulative samples were collected every 30 minutes.

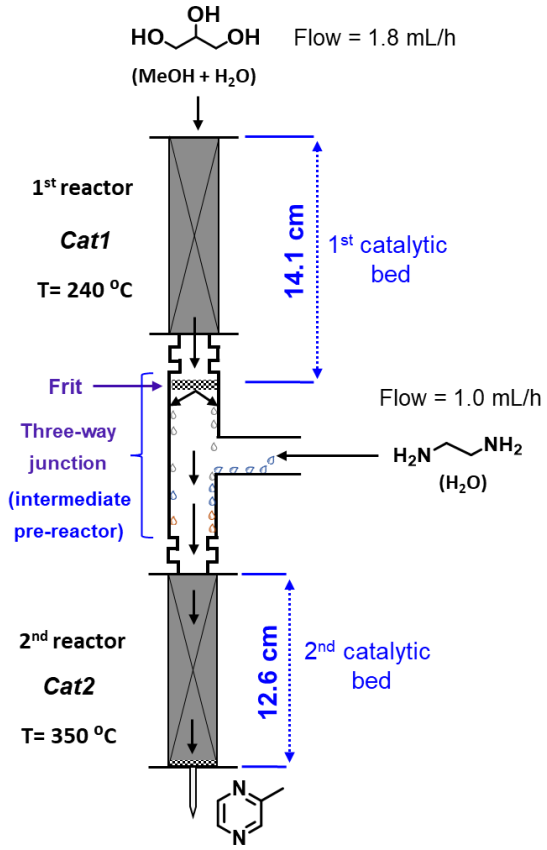

Figure 3.8. Scheme of reaction system for the overall process to produce 2-methylpyrazine starting from glycerol in a multi-bed reactor.

3.5 Reaction mixture analyses

3.5.1 Continuous glycerol dehydration to acetol

As previously mentioned, collection flasks were attached to the outlet of the reactor and immersed in an ice bath to maximize the condensation of volatile products. Once the sampling flask changed, two small aliquots were taken out and dissolved in a quantity of internal standard solution, in line with that used in obtaining the calibration range.

A combination of two GC instruments was used to analyse liquid samples. Most polar compounds were analysed with a Varian CP-3800, equipped with an FID detector and a CARBOWAX Column (15 m x 3.2 mm). On the other hand, non-polar compounds, and the desired product (acetol) were determined with an Agilent Technologies 7890A GC system with an FID detector equipped with an HP-5 MS capillary column (30 m x 250 µm x 0.25 µm). Figures 3.9 and 3.10 illustrate the chromatograms obtained in each case. Either way, the internal standard methodology determines the different compounds. Chlorobenzene is the internal standard used in the HP-5 column (1.0 wt%, MeOH), while 1,4-butanediol is selected in the analysis carried out by using the CARBOWAX column (1.5 wt%, MeOH). Accordingly, 0.100 g of sample were diluted in 0.700 g of internal standard solution in the case of the instrument having an HP-5 column, and 0.400 g of sample in 0.400 of internal standard solution in the case of the CARBOWAX column. Product identification was done by GC–MS (Agilent 6890N GC System, with an HP-5 column and coupled with an Agilent 5973N mass detector). Silylation with ethyl acetate diluted N,O-Bis(trimethylsilyl)trifluoroacetamine with 1 wt.% trimethylsilyl chloride (ACROS Organics) was carried out on some MeOH-previously evaporated samples to identify the most polar compounds.

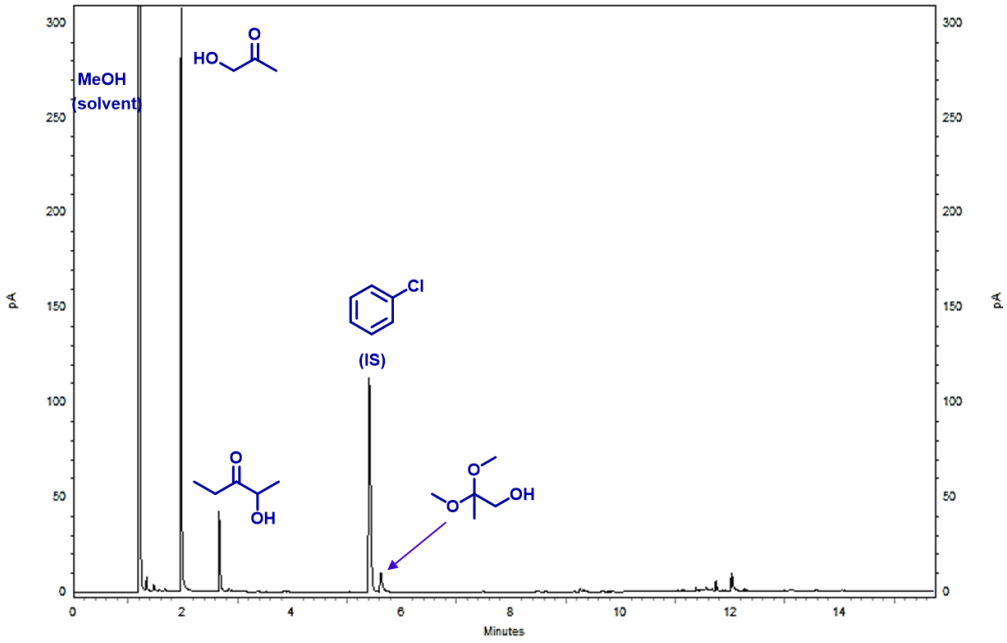

Figure 3.9. Chromatogram obtained with an Agilent Technologies 7890A GC, equipped with an FID detector and an HP-5 MS capillary column (30m x 250µm x 0.25µm). Fraction corresponding to 7-8 h when using a CuO/*m*-ZrO_2 catalyst. Reaction conditions: feed = methanol/glycerol (50/50 in weight), flow = 2 ml/h, with 0.500 g of catalyst, at 240 ºC.

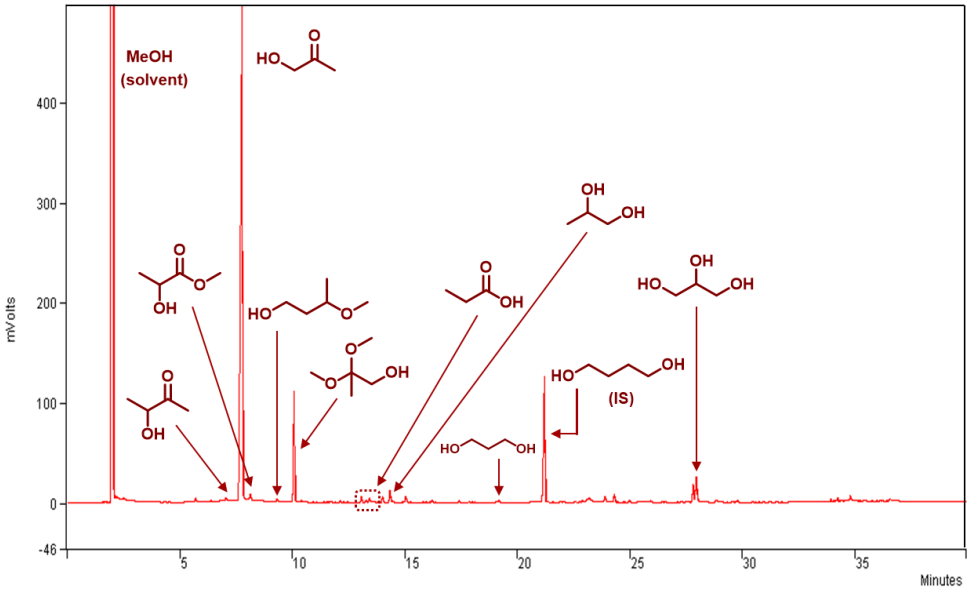

Figure 3.10. Chromatogram obtained with a Varian CP-3800, equipped with an FID detector and a CARBOWAX Column (15 m x 3.2 mm). Fraction corresponding to 7-8 h when using a CuO/*m*-ZrO_2 catalyst. Reaction conditions: feed = methanol/glycerol (50/50 in weight), flow = 2 ml/h, with 0.500 g catalyst, at 240 ºC.

Additionally, gaseous products in some specific experiments were analysed at the exit of the reactor. The gas composition was determined using a GC fitted with 3 detection lines: (i) one for H_2 separated on a 5A molecular sieve column (with Ar as carrier) and quantified on a TCD, (ii) a second one for N_2 separated on a 13X molecular sieve column (with He as carrier) and quantified on a second TCD, and iii) a third one equipped with Al-plot column (with He as carrier) and a FID detector for hydrocarbon quantification. This, together, with the TG analysis allowed us to calculate the carbon balance of the reaction relating to the total amount of glycerol fed into the reactor.

In all cases, glycerol conversion (X), selectivities (S_i), and yields (Y_i) of the different products "i" have been calculated through the GC analysis of the different aliquots corresponding to different fractions of times on stream ("t"):

$$X^{t}_{glycerol}(mol.\%) = \frac{n^{outlet,t}_{glycerol}}{n^{inlet,t}_{glycerol}} \cdot 100 \qquad \textbf{(Equation 3.12)}$$

$$Y_i^t(\text{mol.}\%) = \frac{n_i^{outlet,t} \cdot a_i}{n_{glycerol}^{inlet,t}} \cdot 100 \qquad \textbf{(Equation 3.13)}$$

Being a_i the stoichiometric correction factor for the product "i".

Selectivity to acetol (and to the different products) was calculated both considering the amount of glycerol converted as well as a function of the total amount of products in the liquid fraction:

$$S_{acetol}^{t,T}(\text{mol.}\%) = \frac{n_{acetol}^{outlet,t}}{n_{glycerol}^{inlet,t} - n_{glycerol}^{outlet,t}} \cdot 100 \qquad \textbf{(Equation 3.14)}$$

$$S_{acetol}^{t,L}(\text{mol.}\%) = \frac{n_{acetol}^{outlet,t}}{n_{liquid\ products}^{outlet,t}} \cdot 100 \qquad \textbf{(Equation 3.15)}$$

Importantly, considering that a significant fraction of the glycerol fed is retained on the catalytic surface and later transformed into coke, the yield to liquid products was also estimated:

$$YL^t(\%) = \frac{\sum n_{liquid\ product_i}^{outlet,t} a_i}{n_{glycerol}^{inlet,t}} \cdot 100 \qquad \textbf{(Equation 3.16)}$$

Also, carbon balances of the reaction to the total amount of glycerol fed into the reactor were also calculated as follows:

$$CB_{glycerol}(\text{mol}\%) = \frac{\sum n_{product_i}^{outlet} \cdot x_i\ \text{C atoms}}{n_{glycerol}^{inlet} \cdot 3\ \text{C atoms}} \cdot 100 \qquad \textbf{(Equation 3.17)}$$

Being x_i the number of carbon atoms in the $product_i$ coming from glycerol reaction.

Last, and with the aim of refining the comparison between catalysts, specific activities (SA) towards acetol production were calculated:

$$SA = \frac{n_{acetol}^t}{n_{Cu}} \qquad \textbf{(Equation 3.18)}$$

n_{Cu} are the mols of Cu in the catalyst and n_{acetol}^t are the mols acetol produced during a specific time (t).

3.5.2 Reductive cycloamination of acetol with ethylenediamine to 2-methylpiperazine

In this reaction, different aliquots (≈0.050-0.060 g) were collected at different reaction times (usually 1, 3, 5, and 7 h), and diluted in an internal standard solution (chlorobenzene, 1 wt.%, MeOH) before analysis. GC analyses of the reaction mixtures were carried out using a 3900-Varian GC equipped with an FID and a HP-5 MS capillary column (30 m x 250 µm x 0.25 µm). A typical chromatogram is exemplified in Figure 3.11. Product identification was accomplished by GC-MS (Agilent 6890N GC system coupled with an Agilent 5973N mass detector).

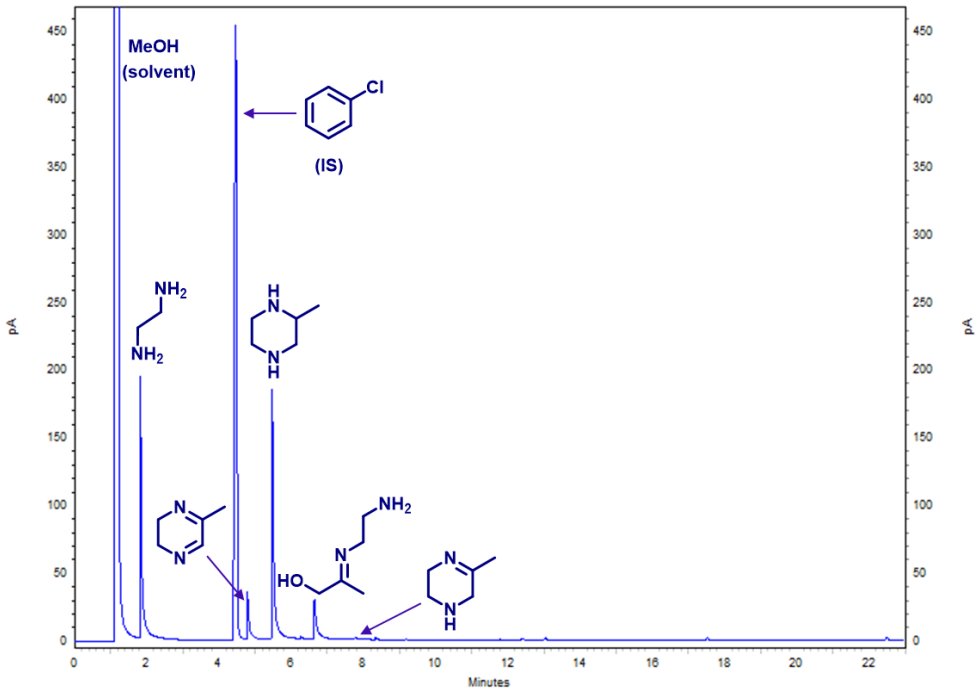

Figure 3.11. Chromatogram obtained with 3900-Varian GC equipped with an FID and a HP-5 MS capillary column (30 m x 250 µm x 0.25 µm). Reaction conditions: 0.325 g acetol, 0.227 g ethylenediamine, 1.250 g MeOH, 0.056 g of catalyst: Pd/Al_2O_3 (1 wt.% Pd, third use), at 13 bars of H_2, 90 ºC, and with slow addition of acetol (100 µL/h). Reaction time = 1h.

Ethylenediamine conversion (X), selectivities (S_i) and yields (Y_i) to the different products "$_i$" have been calculated through GC analysis of the various aliquots collected at

specific reaction times ("t"), (see equations 3.19, 3.20, 3.21, and 3.22), using ethylenediamine as the reference reactant, owing to the labile nature of acetol, whose conversion is always 100%.

$$X^t(\text{mol.}\,\%) = \frac{n^0_{\text{ethylenediamine}} - n^t_{\text{ethylenediamine}}}{n^0_{\text{ethylenediamine}}} \cdot 100 \qquad \textbf{(Equation 3.19)}$$

$$S^t_i(\text{mol.}\,\%) = \frac{n^t_i}{n^t_{\text{total products}}} \cdot 100 \qquad \textbf{(Equation 3.20)}$$

$$Y^t_i(\text{mol.}\,\%) = \frac{n^t_i}{n^0_{\text{ethylenediamine}}} \cdot 100 \quad \text{or} \quad Y^t_i(\text{mol.}\,\%) = \frac{X^t \cdot S^t_i}{100} \text{ if } CB > 95\%$$

(**Equations 3.21** and **3.22**)

Finally, carbon balances were calculated for each reaction, weighing the total amount of products by their mols of carbon along with the remains of ethylenediamine (see equation 3.23).

$$CB(\text{mol.}\,\%) = \frac{\left[(n^0_{\text{ethylenediamine}} - n^f_{\text{ethylenediamine}}) \cdot 3\text{ C atoms}\right] + \sum(n^f_{\text{product}} \cdot \text{X C atoms})}{n^0_{\text{ethylenediamine}} \cdot 3\text{ C atoms}} \cdot 100$$

(**Equation 3.23**)

Being X de total number of C atoms in the molecules corresponding to the different by-products coming from ethylenediamine.

It is necessary to point out that the reaction between ethylenediamine and acetol to give rise to the corresponding cyclic and linear imines is thermal and does not need hydrogen or a catalyst. Ethylenediamine instantly attacks acetol (nucleophilic addition) to yield an equilibrium of the corresponding imines along with other nitrogenated by-products. Consequently, most of the catalytic comparisons herein proposed use the yield to 2-methylpiperazine as the comparative parameter if working with values not exceeding 80% by much, being this a measure of the "effective activity" of the catalyst.

3.5.2.1 Coupling with the glycerol dehydration product

Analyses for the reaction consisting of coupling the reductive amination with the product attained in the glycerol dehydration reactor were carried out with the same methodology and instrumentation described above. Nonetheless, a previous analysis of

the feed to be introduced in the reductive amination batch reactor is always carried out according to the methodology described in *Section 3.5.1*. Additionally, those oxygenates accompanying glycerol (those properly separated and observed by using an HP-5 column) were added to the analysis method in the 3900-Varian GC instrument (i.e., methyl lactate, methyl acetoin, acetoin, acetol dimethyl acetal) to avoid the misinterpretation of their signals.

Importantly, to simplify the analyses of the reaction mixture, all the nitrogenated compounds detected but not properly identified were supposed to come from acetol reaction with ethylenediamine. This simplification is based on the greater reactivity exhibited by acetol compared to the other by-products and, in particular, its specific affinity for the condensation with ethylenediamine seen throughout the present work.

3.5.3 Cycloamination of acetol with ethylenediamine and dehydrogenation to 2-methylpyrazine

Usually, cumulative samples were collected at the reactor outlet corresponding to periods of 0.5, 1.0 or 1.5 h, respectively. As in the glycerol dehydration reactor, the collection containers were connected to the reactor outlet and submerged in an ice bath to maximize the condensation of volatile products. Once the bottle for sampling has been changed, a quantity of internal standard is introduced. Considering the heterogeneity of the sample, the preparation is carried out with the total amount of liquid collected for a particular time fraction, which is approximately one gram every 30 minutes, and dissolved in 7 grams of internal standard solution.

For this acetol cyclo-amination with ethylenediamine, the internal standard used is chlorobenzene in a 1 wt.% solution using methanol as solvent. The instrument used to analyse the samples was an Agilent 7890A gas chromatograph equipped with an FID detector and an HP-5 MS capillary column (30 m x 250 µm x 0.25 µm). Figure 3.12 illustrates a typical example of the chromatograms registered for these reaction mixtures. Product identification was done by GC-MS (Agilent 6890N GC system coupled with an Agilent 5973N mass detector).

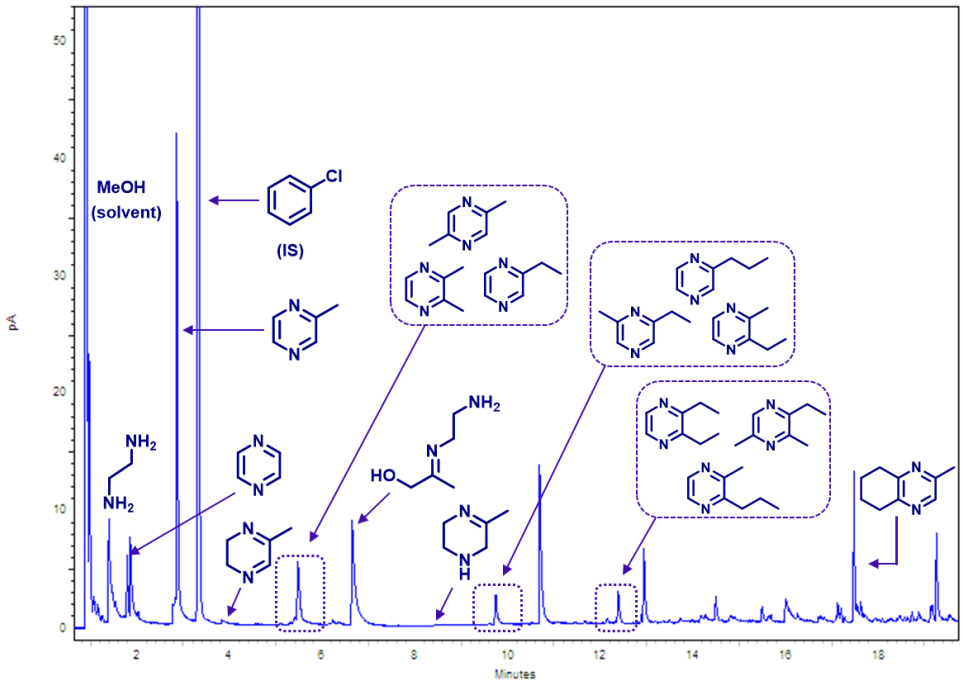

Figure 3.12. Chromatogram obtained with an Agilent Technologies 7890A GC, equipped with an FID detector and an HP-5 MS capillary column (30m x 250µm x 0.25µm). Reaction conditions: feed = H_2O/ethylenediamine (60/40 wt., 1.00 mL/h) + a glycerol dehydration reactor outlet (26 wt.% acetol, 1.83 mL/h), 0.500 g of catalyst: 2.2Ga-5Cu/ZrO_2, 350 ºC, TOS=1.5 h.

By using gas chromatography, calculations of the most important catalytic parameters were carried out for the different fractions of times on stream ("t") as follows:

$$X^{t}_{ethylenediamine}(mol.\,\%) = \frac{n^{outlet,t}_{ethylenediamine}}{n^{inlet,t}_{ethylenediamine}} \cdot 100 \qquad \textbf{(Equation 3.24)}$$

$$Y^{t}_{i}(mol.\,\%) = \frac{n^{outlet,t}_{i} \cdot a_i}{n^{inlet,t}_{ethylenediamine}} \cdot 100 \qquad \textbf{(Equation 3.25)}$$

Being a_i the stoichiometric correction factor for the product "i".

Selectivity to 2-methylpyrazine (and to the different products) was calculated both considering the amount of ethylenediamine converted as well as a function of the total amount of products in the liquid fraction:

$$S^{t,T}_{2-\text{methylpyrazine}}(\text{mol.}\,\%) = \frac{n^{\text{outlet,t}}_{\text{2-methylpyrazine}}}{n^{\text{inlet,t}}_{\text{ethylenediamine}} - n^{\text{outlet,t}}_{\text{ethylenediamine}}} \cdot 100 \qquad \textbf{(Equation 3.26)}$$

$$S^{t,L}_{i}(\text{mol.}\,\%) = \frac{n^{\text{outlet,t}}_{i}}{n^{\text{outlet,t,}}_{\text{liquid products}}} \cdot 100 \qquad \textbf{(Equation 3.27)}$$

$$YL^{t}(\text{mol}\%) = \frac{\sum n^{\text{outlet,t}}_{\text{liquid product}_i} a_i}{n^{\text{inlet,t}}_{\text{ethylenediamine}}} \cdot 100 \qquad \textbf{(Equation 3.28)}$$

Also, carbon balances of the reaction to the total amount of ethylenediamine fed into the reactor were also calculated as follows:

$$CB_{\text{Ethylenediamine}}(\text{mol}\%) = \frac{\sum n^{\text{outlet}}_{\text{product}_i} \cdot x_i \text{ C atoms}}{n^{\text{inlet}}_{\text{ethylenediamine}} \cdot 2 \text{ C atoms}} \cdot 100 \qquad \textbf{(Equation 3.29)}$$

Being x_i the number of carbon atoms in the product_i coming from ethylenediamine.

3.5.3.1 One pot two-step process from glycerol (multi bed reactor)

Bearing in mind that the process comprises, as the first stage, the glycerol dehydration to acetol, to adequately quantify the oxygenated by-products formed in the first bed as well as the organonitrogen chemicals synthesized in the second bed, two types of gas chromatographs were used. The analysis scheme is quite similar to that reported in Section *3.5.1*. The first of these devices is a Varian CP-3800, equipped with an FID detector and a CARBOWAX column (15 m x 3.2 mm). This equipment was used for identifying and quantifying polar oxygenates (i.e., glycerol, methyl-lactate, 1,2-propanediol and methyl glycolate). On the other hand, the less polar oxygenates (acetals, ethers) together with organonitrogen compounds (alkyl pyrazines, imines and other nitrogenated by-products) are determined with the Agilent Technologies 7890A GC System that has an FID detector equipped with an HP-5 capillary column (30 m x 250 µm x 0.25 µm). In both cases, as in all the previous analyses, the standard internal method is used to quantify the various

components of the reaction mixture. A 1.0 wt.% chlorobenzene solution in MeOH was selected as internal standard for the analysis done with the HP-5 column, whereas a 1.5 %wt. 1,4-butanediol was chosen for the CARBOWAX column.

With the information acquired in optimizing the individual stages, the products already known formed in the first stage were individually injected into the chromatograph equipped with the HP-5 column to know the retention times of each one and add them to the new processing method. In the same way, the equipment with the CARBOWAX column individually injected the products of the second stage to identify them, check retention times with the method used in the first stage, and add them to the new processing method to avoid peak misinterpretation.

Again, and due to the heterogeneity of the sample, it was necessary to homogenize by dissolving the total amount of sample collected at the reactor outlet with the standard solution. In this case, the standard internal method was carried out with a single solution having the internal standards corresponding to each one of the methods. Thus, the methanol solution contained 1 wt.% chlorobenzene and 1.5 wt.% 1,4-butanediol. Cumulative liquid samples collected at the end of the reactor every 30 minutes, with a mass of around 1.5 grams, were diluted in approximately 7 grams of the solution that includes both internal standards. Once the new solution was homogenized, it was injected in the two instruments already defined.

Regarding the calculations, as both reactants (glycerol and ethylenediamine) were intended to be added equimolarly to the system, the calculations for conversion (X), selectivities (S_i) and yields (Y_i) to the different products "$_i$" have been calculated by applying the same formulas defined in the last section, always referred to ethylenediamine. Nevertheless, glycerol conversion was also calculated, the yield to liquids referred to the total amount of carbon contributed by both reactants (glycerol and ethylenediamine), and

the carbon balance was also considered with respect to the total amount carbon mols fed into the reactor.

$$YL^{t}(mol\%) = \frac{\sum n^{outlet}_{liquid\ product_i} \cdot x_i\ C\ atoms}{\left(n^{inlet}_{ethylenediamine} \cdot 2\ C\ atoms\right) + \left(n^{inlet}_{glycerol} \cdot 3\ C\ atoms\right)} \cdot 100$$

(**Equation 3.30**)

$$CB_{Total}(mol\%) = \frac{\sum n^{outlet}_{product_i} \cdot x_i\ C\ atoms}{\left(n^{inlet}_{ethylenediamine} \cdot 2\ C\ atoms\right) + \left(n^{inlet}_{glycerol} \cdot 3\ C\ atoms\right)} \cdot 100$$

(**Equation 3.31**)

Being x_i the number of carbon atoms in the $product_i$.

3.6 References

[1] M.J. Climent, A. Corma, P. De Frutos, S. Iborra, M. Noy, A. Velty, P. Concepción, Chemicals from biomass: Synthesis of glycerol carbonate by transesterification and carbonylation with urea with hydrotalcite catalysts. The role of acid-base pairs, 269 (2009) 140-149. https://doi.org/10.1016/j.jcat.2009.11.001.

[2] N. Blanch-Raga, A.E. Palomares, J. Martínez-Triguero, G. Fetter, P. Bosch, Cu Mixed Oxides Based on Hydrotalcite-Like Compounds for the Oxidation of Trichloroethylene, Ind. Eng. Chem. Res. 52 (2013) 15772–15779. https://doi.org/10.1021/IE4024935.

[3] E. Dumitriu, V. Hulea, C. Chelaru, C. Catrinescu, D. Tichit, R. Durand, Influence of the acid–base properties of solid catalysts derived from hydrotalcite-like compounds on the condensation of formaldehyde and acetaldehyde, Appl. Catal. A Gen. 178 (1999) 145–157. https://doi.org/10.1016/S0926-860X(98)00282-8.

[4] X. Zhang, T. Wang, L. Ma, Q. Zhang, X. Huang, Y. Yu, Production of cyclohexane from lignin degradation compounds over Ni/ZrO2–SiO2 catalysts, Appl. Energy. 112 (2013) 533–538. https://doi.org/10.1016/J.APENERGY.2013.04.077.

[5] J. C. Medina, Manuel Figueroa, Raydel Manrique, J.R. Pereira, P. D. Srinivasan, J. J. Bravo-Suárez, V.G.B. Medrano, Romel Jiménez, Alejandro Karelovic, Catalytic consequences of Ga promotion on Cu for CO 2 hydrogenation to methanol, Catal. Sci. Technol. 7 (2017) 3375–3387. https://doi.org/10.1039/C7CY01021D.

[6] V.A. Fassel, R.N. Knfseley, Inductively Coupled Plasma: Optical Emission Spectroscopy, Anal. Chem. 46 (1974) 1110A-1120a. https://doi.org/10.1021/AC60349A023.

[7] Y. Waseda, E. Matsubara, K. Shinoda, X-ray diffraction crystallography: introduction, examples and solved problems, Springer, Berlin Heidelberg, 2011.

[8] N.W. Gregory, Elements of X-Ray Diffraction, J. Am. Chem. Soc. 79 (1957) 1773–1774. https://doi.org/10.1021/JA01564A077.

[9] D.B. Williams, C.B. Carter, Transmission electron microscopy: A textbook for materials science, Springer US, 2009. https://doi.org/10.1007/978-0-387-76501-3.

[10] B. Imelik, J.C. Vedrine, Catalyst Characterization Physical Techniques for Solid Materials, Springer, New York, 1994. https://doi.org/10.1007/978-1-4757-9589-9_1.

[11] M.T. Otten, HighAngle annular darkfield imaging on a tem/stem system, J. Electron Microsc. Tech. 17 (1991) 221–230. https://doi.org/10.1002/JEMT.1060170209.

[12] S. Brunauer, P.H. Emmett, E. Teller, Adsorption of Gases in Multimolecular Layers, J. Am. Chem. Soc. 60 (2002) 309–319. https://doi.org/10.1021/JA01269A023.

[13] J. Rouquerol, F. Rouquerol, P. Llewellyn, G. Maurin, Adsorption by powders and porous solids: principles, methodology and applications, Academic Press, Kidlington, Oxford, 2013.

[14] J. Rouquerol, P. Llewellyn, F. Rouquerol, Characterization of Porous Solids VII, in: Stud. Surf. Sci. Catal., Elsevier, Amsterdam and Oxford, 2007: pp. 49–56.

[15] J.C. Groen, L.A.A. Peffer, J. Pérez-Ramírez, Pore size determination in modified micro- and mesoporous materials. Pitfalls and limitations in gas adsorption data analysis, Microporous Mesoporous Mater. 60 (2003) 1–17. https://doi.org/10.1016/S1387-1811(03)00339-1.

[16] A. Álvarez, M. Borges, J.J. Corral-Pérez, J.G. Olcina, L. Hu, D. Cornu, R. Huang, D. Stoian, A. Urakawa, CO2 Activation over Catalytic Surfaces, ChemPhysChem. 18 (2017) 3135–3141. https://doi.org/10.1002/CPHC.201700782.

[17] T. Chafik, Infrared Spectroscopy - Materials Science, Engineering and Technology, InTech, 2012. https://doi.org/10.5772/2055.

[18] C.A. Emeis, Determination of Integrated Molar Extinction Coefficients for Infrared Absorption Bands of Pyridine Adsorbed on Solid Acid Catalysts, J. Catal. 141 (1993) 347–354. https://doi.org/10.1006/JCAT.1993.1145.

[19] A. Davydov, N.T. Sheppard, Molecular spectroscopy of oxide catalyst surfaces, Wiley, Chichester, West Sussex, England, 2003.

[20] K.I. Hadjiivanov, G.N. Vayssilov, Characterization of Oxide Surfaces and Zeolites by Carbon Monoxide as an IR Probe Molecule, Adv. Catal. 47 (2002) 307–511.

[21] M. Tamura, K. Shimizu, A. Satsuma, Comprehensive IR study on acid/base properties of metal oxides, Appl. Catal. A: Gen. 433-434 (2012), 135-145. https://doi.org/10.1016/j.apcata.2012.05.008

[22] P. Concepción, M. Boronat, R. Millán, M. Moliner, A. Corma, Identification of Distinct Copper Species in Cu-CHA Samples Using NO as Probe Molecule. A Combined IR Spectroscopic and DFT Study, Top. Catal. 60 (2017) 1653–1663. https://doi.org/10.1007/S11244-017-0844-7.

[23] M. Faraldos, C. Goberna, Técnicas de análisis y caracterización de materiales, 2nd ed., Consejo Superior de Investigaciones Científicas, 2019.

[24] D. Briggs, J.T. Grant, Surface analysis by Auger and x-ray photoelectron

spectroscopy, IM Publications, Chichester, 2003.

[25] J. Moulder, Standard XPS Spectra of the Elements, Physical Electronics Division Perkin-Elmer Corp., Eden Prairie Minnesota, 1992.

[26] P.A. Webb, Introduction to Chemical Adsorption Analytical Techniques and their Applications to Catalysis, MIC Tech. Publ. (2003).

[27] P. Canton, G. Fagherazzi, M. Battagliarin, F. Menegazzo, F. Pinna, N. Pernicone, Pd/CO Average Chemisorption Stoichiometry in Highly Dispersed Supported Pd/γ-Al2O3 Catalysts, Langmuir. 18 (2002) 6530–6535. https://doi.org/10.1021/LA015650A.

[28] K. Narita, N. Takezawa, H. Kobayashi, I. Toyoshima, Adsorption of nitrous oxide on metallic copper catalysts, React. Kinet. Catal. Lett. 19 (1982) 91–94. https://doi.org/10.1007/BF02065064.

[29] B. I. Ionin, NMR Spectroscopy in Organic Chemistry, Springer, Boston, MA, 1970.

[30] P. Serna, P. Concepción, A. Corma, Design of highly active and chemoselective bimetallic gold–platinum hydrogenation catalysts through kinetic and isotopic studies, J. Catal. 265 (2009) 19-25. https://doi.org/10.1016/j.jcat.2009.04.004

[31] M. Boronat, P. Concepción, A. Corma, Unravelling the Nature of Gold Surface Sites by Combining IR Spectroscopy and DFT Calculations. Implications in Catalysis, J. Phys. Chem. C, 113 (2009) 16772–16784. https://doi.org/10.1021/jp905157r

[32] L. De Lange, Trabajo fin de máster en ingeniería industrial: The designing of a novel continuous flow catalytic process for the direct synthesis of pyrazines from glycerol, Universidad Politécnica de Valencia, 2018.

Chapter 4
Hydrotalcite-derived Cu-based mixed oxides as catalysts for the selective glycerol dehydration to acetol

4.1 Introduction

Mineral hydrotalcites are Mg and Al hydroxides with a structure derived from brucite ($Mg(OH)_2$). Brucite comprises neutral dioctahedral sheets of magnesium hydroxide where the hydroxyls are located at the vertexes shared by 2 octahedra, each with a Mg atom in its centre. A number of water molecules are located between the sheets. In a hydrotalcite (HT), Mg^{2+} cations are isomorphically replaced by Al^{3+}, and, as a result, the layers acquire a positive charge. To restore electroneutrality to this system, an appropriate number and type of anions (in the nature OH^- and CO_3^{2-}) are located between the aforementioned positively charged layers, balancing charges in this way. This structure is familiar to numerous synthetic and natural materials that have the following compositional formula[1]:

$$M_a{}^{2+}M_b{}^{3+}(OH)_{2a+2b}(X^-)_{2b}\cdot xH_2O$$

Interestingly, after calcination, this structure collapses and yields a low-crystalline mixed oxide with cationic vacancies, produced because of the need to equilibrate the excess of positive charge induced by replacing some Mg^{2+} with Al^{3+}. Therefore, with respect to MgO, the material presents some stronger Lewis basic sites, corresponding to unsaturated O^{2-}, and some weak acid sites, corresponding to Al^{3+}[2].

The most common preparation method for the hydrotalcite precursor is co-precipitation, which is used in this work (see Experimental Procedure, *Section 3.2.1*). Synthetically, there are many variables: the M^{2+} cation(s), the M^{3+} cation(s), a possible presence of M^{4+}, the M^{2+}/M^{3+} ratio, the type or types of compensation anions, the amount of interstitial water, as well as the morphology and the crystallite size[3].

Among their many advantages, hydrotalcite-type and hydrotalcite-derived materials have an easy and low-cost synthesis procedure; they are non-toxic and possess the capacity to modify their physicochemical properties by controlling their composition efficiently. Thus, the amount and strength of both basic and acid sites can be adapted to the needs of the catalytic process by changing the M^{2+}/M^{3+} molar ratio. In addition, different metals (others than Mg and Al) can also be incorporated in the hydrotalcite precursor during the synthesis or post-synthesis steps, thus extending the versatility of these materials. According to these properties, hydrotalcites have broad applicability as

catalysts in biomass conversion, either as tuneable acid-base catalysts or as precursors to mixed metal oxide catalysts[3,4].

In this regard, it makes perfect sense that a combination of redox, acid, and basic Lewis centres in mixed metallic oxides derived from hydrotalcites may constitute an excellent alternative to carrying out the selective dehydration of glycerol to acetol effectively. At the very least, the opportunities offered by this family of materials in terms of the large number of variables to optimize is a great advantage to provide new insights into the role of the different active centres that may be involved in this reaction.

In our case, the main hydrotalcites with which we worked were Mg, Al, and small proportions of Cu, owing to the beneficial effect of this metal in the glycerol dehydration to acetol. Nonetheless, Ni or Co were also tried instead of Cu, since these transition metals had been reported to help produce acetol as an intermediate during glycerol reforming[5,6]. Therefore, their corresponding hydrotalcite-derived metallic mixed oxides were tested and evaluated to produce the desired acetol from glycerol in a fixed bed reactor and without using hydrogen. Special attention is paid to the role of copper in the formation of acetol and the influence of its oxidation state in that process, as it might be a pivotal point to accomplish the dehydration, as thoroughly discussed during the introduction of this thesis. However, there are indeed many variables where optimization was pursued: M^{2+}/M^{3+} ratio, Cu/Ni/Co content, reaction system, etc. Additionally, different metallic species (Ga, La, Ni, Co, Fe, Zn) were added to improve as maximum as possible the material in terms of activity, selectivity, and stability for acetol production while understanding the parameter(s) the new dopant was somehow modifying.

4.2 Compositional, structural, and textural characterization

First, a group of hydrotalcite-type (HTs) materials including different M^{2+}/M^{3+} molar ratios, copper loadings close to 5 wt.%, and surface areas of approximately 200 m^2/g were synthesized and characterized. Table 4.1 shows the main physicochemical and textural properties of these Cu-based hydrotalcite-derived materials following calcination.

Table 4.1. Main physicochemical and textural properties of Cu-based HT-derived calcined materials with different M^{II}/M^{III} ratios.

Catalyst	Cu content (wt%)[a]	M^{II}/M^{III} molar ratio[a]	Surface area (m^2/g)[b] [BET method]
5.0%Cu-HT-1	4.9	1.0	218
5.0%Cu-HT-2	4.6	2.3	245
5.0%Cu-HT-3	4.9	3.3	212
5.0%Cu-HT-4	4.9	4.1	205
5.0%Cu-HT-5	5.1	5.5	224
5.0%Cu-HT-6	4.8	6.3	177

[a] Cu content and chemical composition measured by ICP. [b] Values calculated from N_2 adsorption isotherms by applying the BET method.

XRD analysed the structural characteristics of the Cu-based hydrotalcite-type materials. For the non-calcined Cu-HTs samples, the X-ray diffractograms of Figure 4.1a show a typical Mg/Al layered doubled hydroxide (LDH, hydrotalcite) structure in practically all samples. Only in the case of the 5.0%Cu-HT-1 sample, some diffraction peaks from aluminium hydroxide are observed. This fact is the consequence of a significant amount of Al^{3+} precipitated separately from the main phase of Cu-Mg-Al hydrotalcite.

After calcination of the Cu-based HT-precursors, the corresponding Cu-Mg-Al mixed oxides were attained, and their XRD patterns are depicted in Figure 4.1b. For Cu-based mixed oxides, the desired phase with a defectively crystalline MgO structure comprising the cationic species in the proper ratios has been accomplished in nearly all the evaluated materials, being essential to highlight the higher level of crystallization when rising the Mg content. As regards the 5.0%Cu-HT-1 calcined sample, its X-ray diffractogram presents some peaks matching aluminium oxide, as anticipated after analysing the diffractogram belonging to the hydrotalcite precursor. Apparently, some Al^{3+} cations from

bayerite contribute to the MgO crystal lattice after the calcination process, but others remained apart, giving rise to this aluminium oxide.

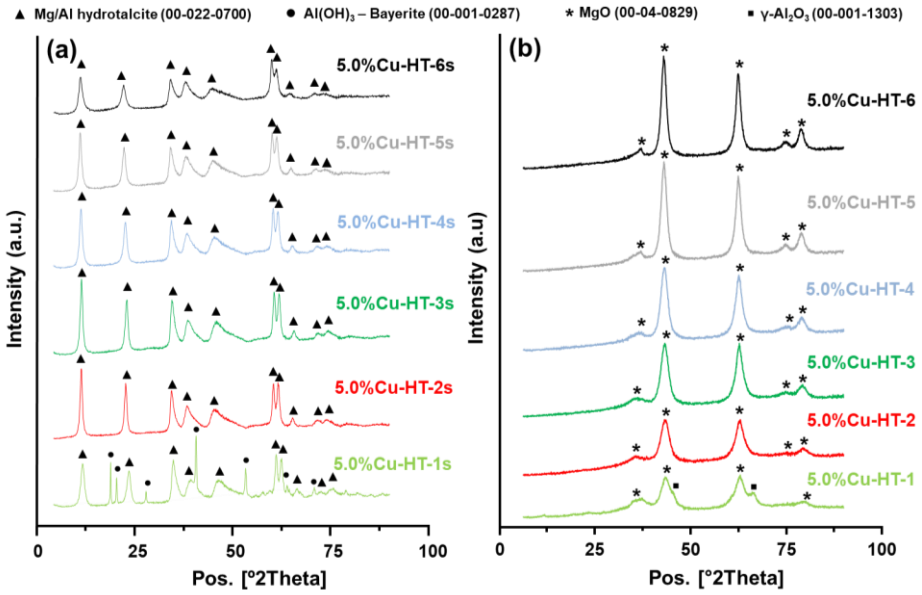

Figure 4.1. a) XRD patterns of as-synthesized Cu-based hydrotalcites with different M^{II}/M^{III} ratios (the "s" at the end of the name indicates a material analysed just after the synthesis). b) XRD patterns of Cu-based hydrotalcite-derived mixed oxides with different M^{II}/M^{III} ratios.

The second set of hydrotalcite-type materials has 5.0 wt.% for the calcined material of varying transition metals (i.e., Cu, Co, and Ni) and, settling the molar ratio M^{2+}/M^{3+} equal to 4; they were prepared and characterized. The main physicochemical and textural properties of 5.0%Cu-HT-4, 5.0%Co-HT-4, and 5.0%Ni-HT-4 calcined samples are summarized in Table 4.2. The chemical composition of this material series is again comparable to the theoretical one, while all surface areas are around 200 m^2/g.

As shown in Figure 4.2a, the XRD patterns of the three Cu-HT-4, Co-HT-4 and Ni-HT-4 as-prepared samples presented the characteristic peaks belonging to well-crystallized LDH with a hydrotalcite structure. Accordingly, the 5.0%Ni-HT-4 and the 5.0%Co-HT-4 samples are supposed to contain most either Ni^{2+} or Co^{3+} cations in the

hydrotalcite structure, partially replacing Mg^{2+} and Al^{3+} ions, respectively. In the same line, in the case of Ni- and Co-based mixed oxides after calcination, the X-ray diffractograms of Figure 4.2b only show peaks matching the MgO structure. This meaning that Ni^{2+} and Co^{3+} ions are well dispersed on the Mg-Al-O structure in both cases.

Table 4.2. Main physicochemical and textural properties of HT-derived calcined materials containing different transition metals.

Catalyst	Metal content (wt%)[a]	M^{II}/M^{III} molar ratio[a]	Surface area (m^2/g)[b] [BET method]
5.0%Cu-HT-4	4.9	4.1	205
5.0%Co-HT-4	4.9	4.2	198
5.0%Ni-HT-4	5.1	4.2	190

[a] Metal (Cu, Co, or Ni) content and chemical composition measured by ICP.
[b] Values calculated from N_2 adsorption isotherms by applying the BET method.

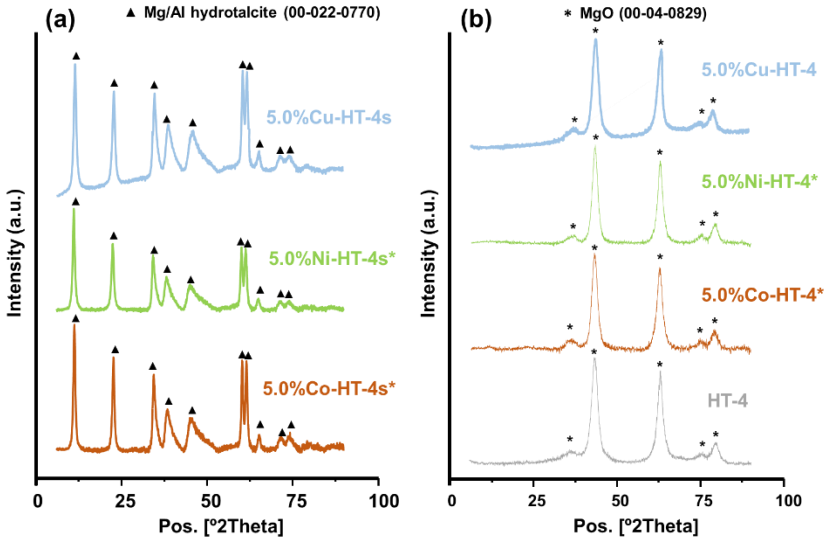

Figure 4.2. a) XRD patterns of as-synthesized Mg/Al hydrotalcites with different transition metals. (the "s" at the end of the name indicates a material analyzed just after the synthesis). b) XRD patterns of hydrotalcite-derived mixed oxides with different transition metals. (*): Background corrected to avoid strong fluorescence effects.

In addition, several hydrotalcite-type materials with an M^{II}/M^{III} molar ratio of ≈4 and varying Cu loadings (from 1.0 to 12.8wt%) were synthesized and characterized. The main physicochemical and textural features of these Cu-based HT-4 calcined samples are reported in Table 4.3, showing that the Cu was incorporated in the expected amounts into the hydrotalcite precursors, maintaining an M^{II}/M^{III} molar ratio around four and surface areas close to 200 m^2/g.

Table 4.3. Main physicochemical and textural properties of Cu-based HT-derived calcined materials with different copper loadings.

Catalyst	Cu content (wt%)[a]	M^{II}/M^{III} molar ratio[a]	Surface area (m^2/g)[b] [BET method]
HT-4	-	4.3	249
1.0%Cu-HT-4	1.0	4.4	196
2.5%Cu-HT-4	2.4	4.1	199
5.0%Cu-HT-4	4.9	4.1	205
7.0%Cu-HT-4	6.7	4.1	193
10.0%Cu-HT-4	9.9	4.2	196
12.0%Cu-HT-4	12.8	4.1	186

[a] Cu content and chemical composition measured by ICP.
[b] Values calculated from N_2 adsorption isotherms by applying the BET method.

The XRD patterns of the Cu-based materials with various Cu loadings before and after calcination treatment are represented in Figures 4.3a and 4.3b. The desired hydrotalcite and the mixed oxide phase with MgO structure are seen for the non-calcined and calcined material for this Cu-based collection of samples, respectively. Interestingly, even for the materials containing quantities of copper beyond 5.0 wt.%, no isolated copper oxide phases are distinguished.

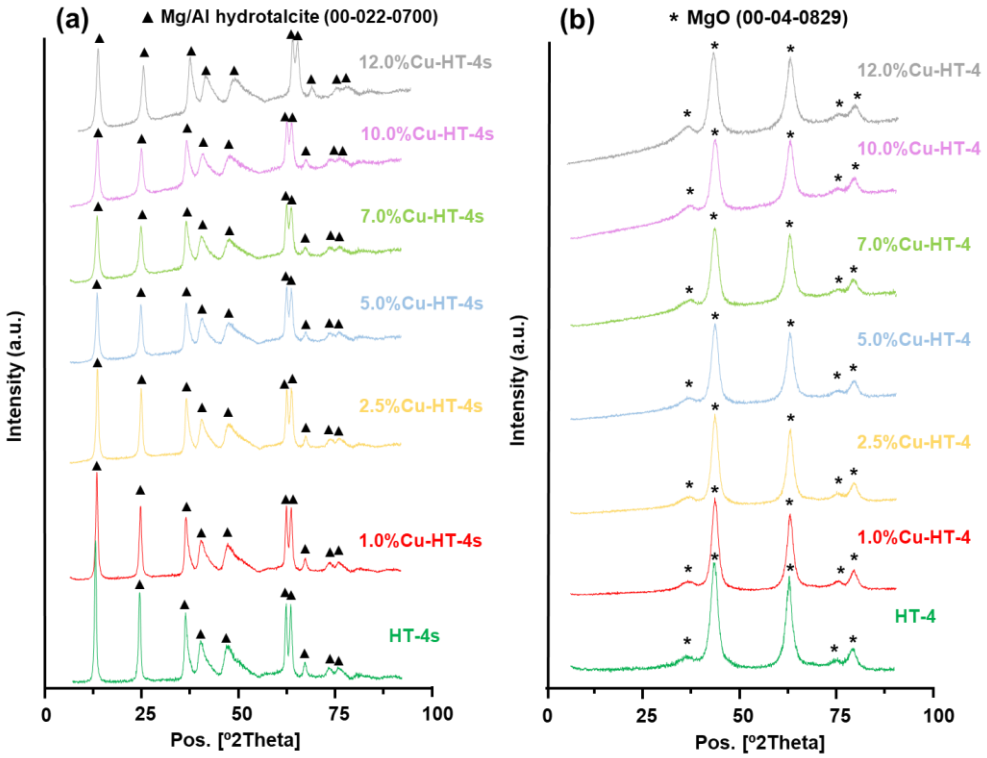

Figure 4.3. a) XRD patterns of as-synthesized hydrotalcites (s) containing different copper loadings. b) XRD patterns of hydrotalcite-derived mixed oxides containing different copper loadings.

Lending support to what has been seen by XRD, microscopy analyses of the materials 5.0%Cu-HT-4, 10.0%Cu-HT-4 and 12.0%Cu-HT-4 (Figure 4.4) proved that the materials were primarily homogeneous, with a MgO structure, and presenting a high copper dispersion inside this crystalline structure. However, a meticulous analysis by using HR-TEM allowed us to identify a few CuOx nanoparticles in 12.0%Cu-HT-4 (Figure 4.5a). For materials containing lower copper loadings, those nanoparticles were not visible with this technique but, when using a more sensitive technique capable of examining all the material surface, such as NO adsorption (see Figure 4.5a), isolated CuO_x species arise again. Nonetheless, XRD data and microscopy suggest most copper is inside the crystalline lattice in materials carrying less than 12.0 wt.% Cu.

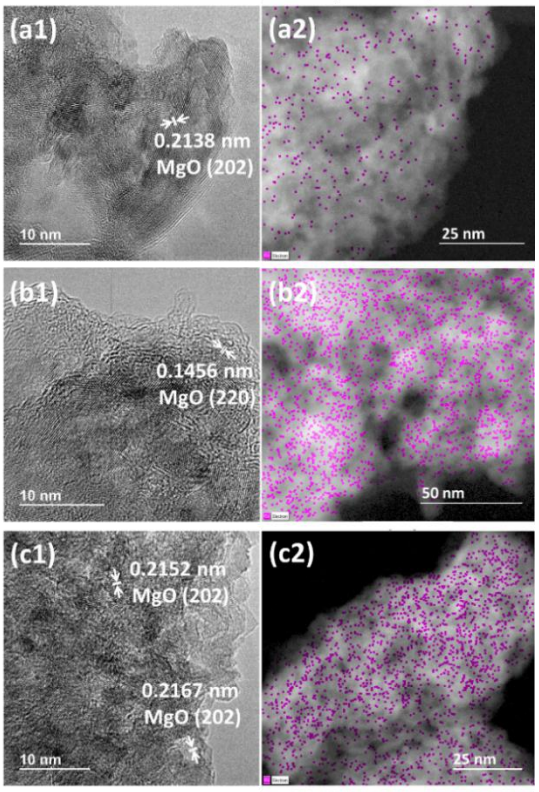

Figure 4.4. HR-TEM (1) and STEM (2) images of (a) 5.0%Cu-HT-4, (b) 10.0%Cu-HT-4, (c) 12.0%Cu-HT-4. (▪) Copper detected by EDS mapping.

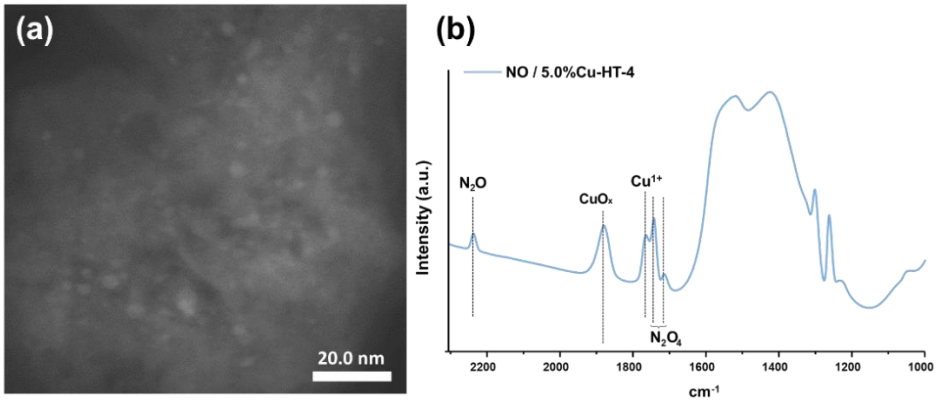

Figure 4.5. (a) CuO_x nanoparticles by HR-TEM for 12.0%Cu-HT-4 material. (b) NO adsorption FTIR spectra on 5.0%Cu-HT-4. Interpretation according to references[7,8].

Finally, the introduction of small quantities of other metals (Co, Fe, Ga, La, Ni, Zn) used as dopants during the synthesis of 10%Cu-HT-4 was essayed, and the physicochemical properties can be found in Table 4.4.

Table 4.4. Main physicochemical and textural properties of doped Cu-HT-derived calcined materials with different auxiliary metals.

Catalyst	M content (wt%)[a]	Cu content (wt%)[a]	M^{II}/M^{III} molar ratio[a]	Surface area (m^2/g)[b] [BET method]
10.0%Cu-HT-4	-	9.9	4.2	196
Ni-10.0%Cu-HT-4	1.7	10.0*	4.0*	181
Zn-10.0%Cu-HT-4	1.5	9.8	4.2	179
Co-10.0%Cu-HT-4	1.4	8.9	4.1	195
Fe-10.0%Cu-HT-4	1.8	9.9	4.1	193
Ga-10.0%Cu-HT-4	1.2	9.5	4.0	183
La-10.0%Cu-HT-4	1.1	9.8	4.0	185

[a] Cu content and chemical composition measured by ICP.

[b] Values calculated from N_2 adsorption isotherms by applying the BET method.

* Theoretical values.

Additionally, X-ray diffraction data of the metal-doped Cu-HT-derived catalytic samples here prepared are shown in Figure 4.6. Similar to those observed with the bare Cu-HT samples, the crystalline phase corresponding to the cubic MgO phase is detected. In addition, the presence of signals corresponding to CuO_x or MO_x (M: Ni, Zn, Co, Fe, Ga, La) species was complicated to distinguish, thus indicating high dispersion of these metal species either onto or into these supports.

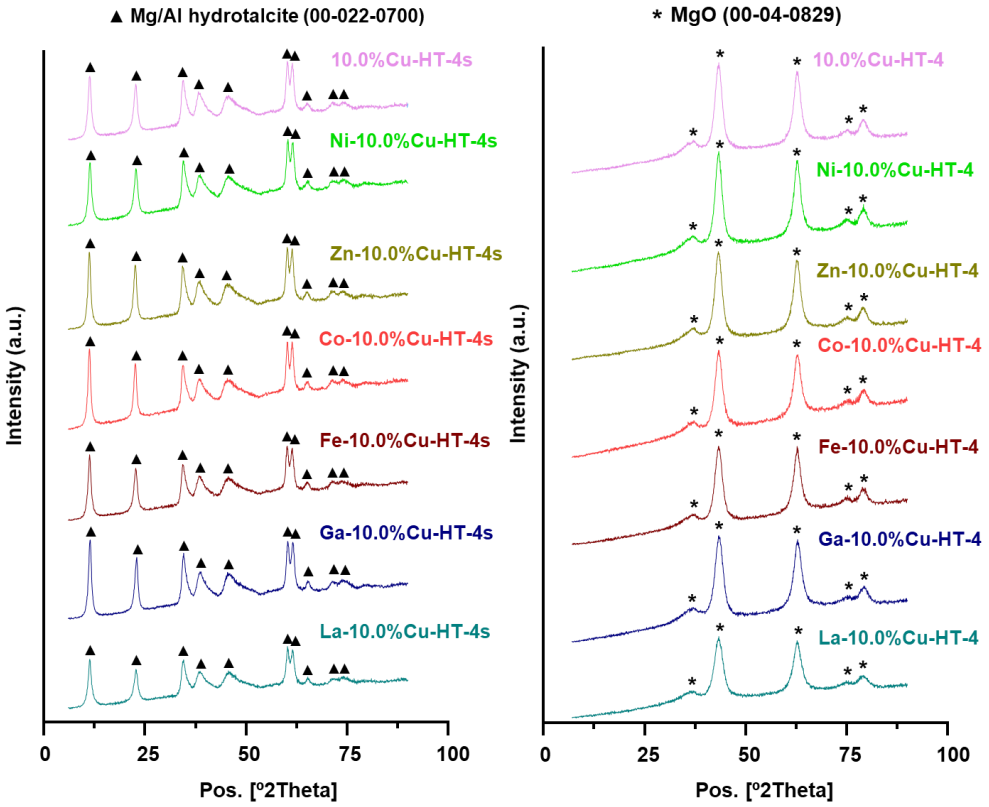

Figure 4.6. a) XRD patterns of as-synthesized hydrotalcites (s) and b) of hydrotalcite-derived mixed oxides, containing 10 wt.% Cu and around 1.5 wt.% of copper doping agents.

In the same line, EDS-STEM measurements have also checked this successful dispersion, and illustrative examples can be found in Figure 4.7. All elemental mappings acquired have shown a homogeneous presence of every element. This finding suggests that all the metallic species composing the different mixed oxides are, if not entirely inside the same crystalline structure, very intimately mixed with each other.

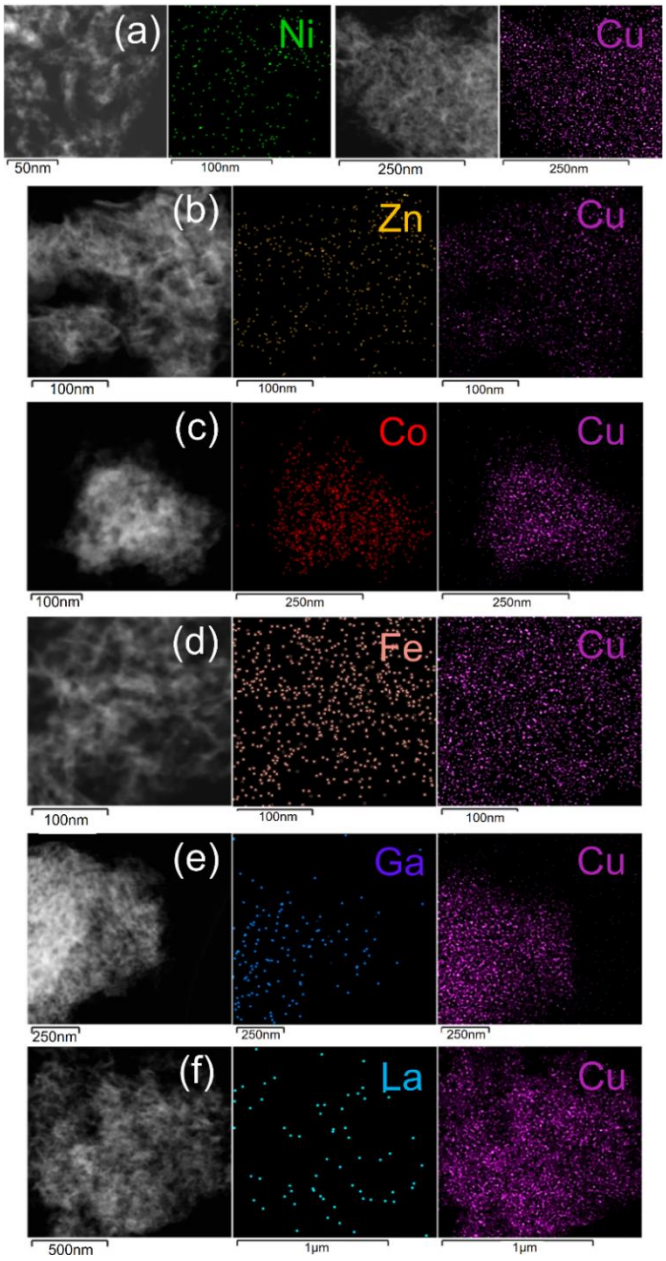

Figure 4.7. EDS mappings of: (a) Ni-10.0%Cu-HT-4, (b) Zn-10.0%Cu-HT-4, (c) Co-10.0%Cu-HT-4, (d) Fe-10.0%Cu-HT-4, (e) Ga-10.0%Cu-HT-4. (e) La-10.0%Cu-HT-4. Note: For Ni-10.0%Cu-HT-4 two different analysis were needed with a Cu-grid and a Ni-grid.

4.3 Catalytic results and discussion

4.3.1 Optimizations and catalytic results in continuous-flow fixed-bed reactor

Catalytic experiments for selective dehydration of glycerol (GLY) to acetol were performed in the continuous-flow fixed-bed reactor already represented in *Experimental Procedure - Section 3.4.1*. Methanol (MeOH) was chosen as the solvent for feeding into the reactor together with glycerol. In a first attempt and aiming at optimizing the most critical reaction conditions, different operational parameters, such as glycerol dilution in methanol and temperature, were varied by always operating with the 5.0%Cu-HT-4 calcined material as the catalyst. The results in catalytic activity (i.e., glycerol conversion), stability, and, more importantly, selectivity to acetol were evaluated. Importantly, as previously mentioned in *Experimental Procedure - Section 3.5.1*, a significant fraction of fed glycerol is retained in the reactor, although not converted into products. Consequently, the yield to liquids was usually preferred over glycerol conversion to measure the actual catalyst activity more reliably.

Table 4.5. Catalytic results on the selective dehydration of glycerol in a continuous-flow fix-bed reactor over 5%Cu-HT-4 catalyst with different methanol/glycerol (MeOH/GLY) ratios.

MeOH / GLY ratio (wt%)	TOS = 3 h		TOS = 5 h		TOS = 8 h	
	Yield to Liquids (mol%)	Select. to acetol* (mol%)	Yield to Liquids (mol%)	Select. to acetol* (mol%)	Yield to Liquids (mol%)	Select. to acetol* (mol%)
95/5	87	34	72	49	44	59
90/10	67	53	71	53	48	53
85/15	67	52	63	59	12	52
75/25	50	67	38	59	-	-
50/50	37	52	23	45	-	-

Reaction conditions: Temperature = 240 ºC, liquid flow = 2 mL/h, catalyst = 0.5 g (5.0%Cu-HT-4). *Calculated over the total amount of products in the liquid fraction.

Primary data for the study of the dilution degree are compiled in Table 4.5. As expected, an apparent decrease in the yield to liquids was observed by decreasing the MeOH/GLY (methanol/glycerol) ratio from 95/5 to 50/50. This means by increasing the glycerol concentration in the feed. At the same time, some slight increase in the selectivity to acetol was achieved when decreasing MeOH/GLY weight ratio from 95:5 to 85:15 or even 75:25, this fact mainly occurring at short times on streams (TOS = 3 h). These significant differences in acetol selectivity that appeared at short TOS were practically not observed when the reaction reached TOS = 5 h. In fact, acetol yields at TOS = 5 h calculated for different MeOH/GLY ratios in the feed (from 95/5 to 85/15) were similar and close to 35%. More interestingly, beneficial effects on catalyst stability were observed when increasing the quantity of methanol in the feed (see Table 4.5). Experiments with streams containing less than 20wt% of glycerol allowed the catalyst to be working up to 8 h keeping acceptable yield to liquid values and selectivity levels to acetol higher than 52%. From these results, the mixture MeOH/GLY = 90:10 (weight ratio) was selected as the optimal for further studies because it permits the system to work up to longer TOS with acceptable productivities, preserving good catalyst stability.

Once the optimum dilution degree of glycerol in methanol was founded, a series of experiments were done to determine which temperature could improve both glycerol conversion and selectivity to acetol. Tests of selective dehydration of glycerol over the 5.0%Cu-HT-4 catalyst in the fix-bed reactor were carried out by varying temperature from 220 to 280 ºC, keeping constant all the other reaction parameters (feed: MeOH/GLY = 90/10, flow = 2 mL/h, catalyst = 0.5 g, TOS = 9 h). The results are shown in Figure 4.8 regarding yield to liquids (cumulative during all the experiments, TOS = 1-9 h) and average selectivity to acetol (cumulative during all reactions, TOS = 1-9 h). The temperature of 240 ºC turned out to be the best by a slight deviation in glycerol conversion and clearly better as far as selectivity to acetol is concerned during most of the reaction. Significantly, no significant differences were noticed concerning the catalyst stability.

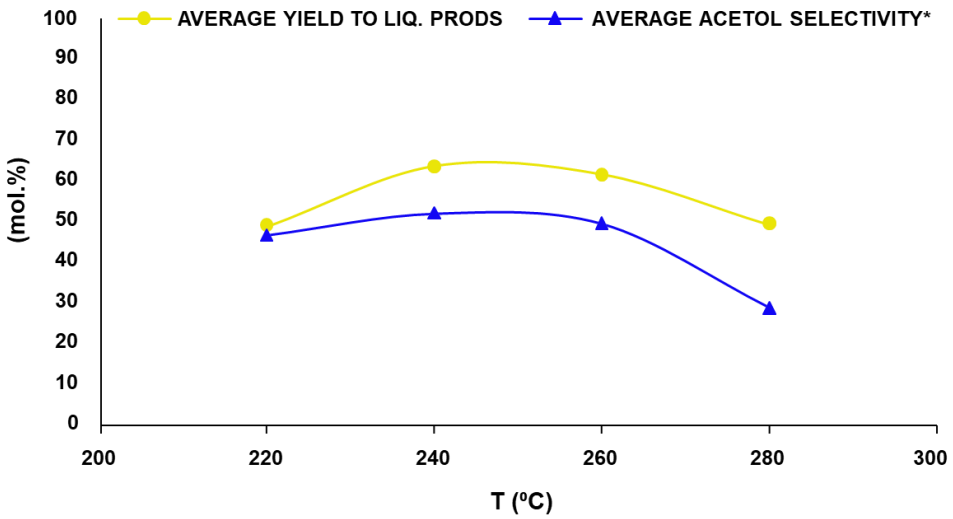

Figure 4.8. Effect of temperature in the selective dehydration of glycerol over 5.0%Cu-HT-4 catalyst. Average data. Reaction conditions: feed: MeOH/GLY = 90/10 wt., flow = 2 mL/h, catalyst = 0.5 g, TOS = 1-9 h. *Calculated over the total amount of products in the liquid fraction. Note: Average glycerol conversions were less than 90 % in every case.

The product distribution for the glycerol dehydration reaction under the aforementioned optimal conditions (and adopted as standard reaction conditions since now) and the proposed reaction network can be found in Figure 4.9 and Scheme 1 (appearing in color all the identified compounds), respectively. Although not showed in Figure 4.9, the starting glycerol conversion is 98% (TOS = 1 h) and the final conversion 76% (TOS = 9 h).

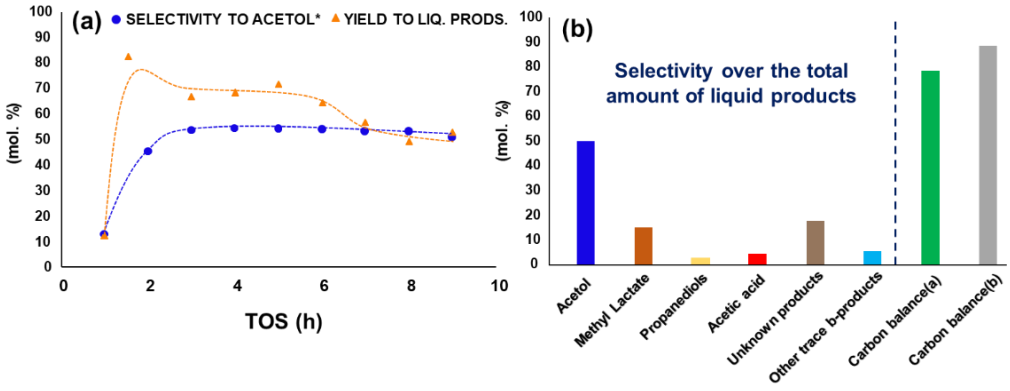

Figure 4.9. a) Yield to liquids and selectivity to acetol with TOS under the optimal reaction conditions over the 5.0%Cu-HT-4 catalyst b) Product distribution and carbon balance: (a) Carbon balance calculated with the total amount of products quantified during the reaction, and (b) Carbon balance calculated including also the carbonaceous matter deposited on the catalytic surface and the gas products coming from glycerol. Reaction conditions: feed: MeOH/GLY = 90/10 wt., flow = 2 mL/h, temperature = 240 ºC, catalyst = 0.5 g. *Calculated over the total amount of products in the liquid fraction. Note: Dashed traces in (a) only serve as visual guidelines.

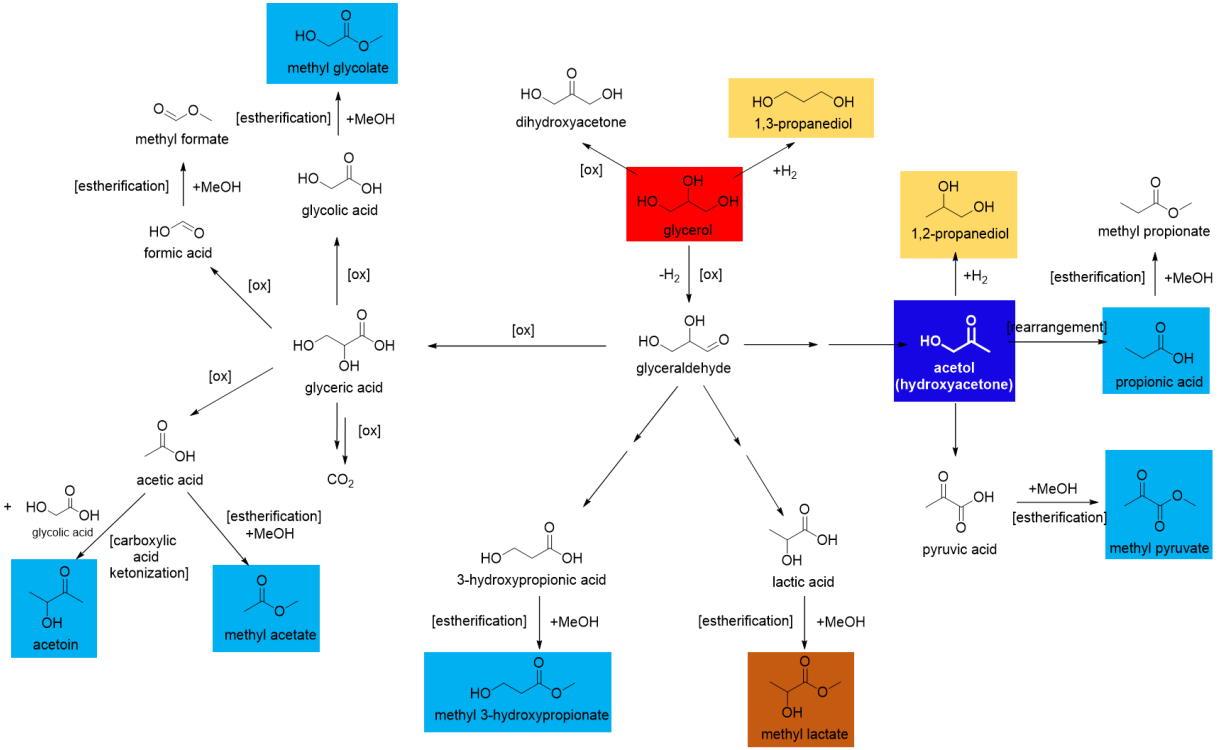

Scheme 1. Reaction network describing the different pathways when using 0.5 g of 5.0%Cu-HT-4 as catalyst under the following reaction conditions: T=240 ºC, Feed: MeOH/Gly (9:1 wt.), F= 2mL/h, p.size= 0.425-0.600 mm. Colors correspond with detected products and match with colors of Figure 4.9.

4.3.2 Ascertaining the effect of M^{II}/M^{III} molar ratio in Cu-based catalysts

As already explained, the thermal decomposition of Mg-Al hydrotalcite precursor generates a high surface area Mg-Al mixed oxide, which largely exposes Lewis basic sites and some weak acid sites. The acid-base properties of these sites depend on the M^{II}/M^{III} molar ratio in the hydrotalcite precursor[2,3,9]. Therefore, to optimize these M^{II}/M^{III} ratios in Cu-Mg-Al mixed oxides, hydrotalcites with (Cu+Mg)/Al ratios from 1 to 6 were prepared, calcined, and tested selective dehydration of glycerol in a continuous flow fixed-bed catalytic reactor. The catalytic results as regards yield to liquids and selectivity to acetol (at 240 ºC and TOS = 4 h) achieved for Cu-Mg-Al mixed oxides (5.0%-HTs) with different (Cu+Mg)/Al ratios are represented in Figure 4.10 and compared with CuO/Al_2O_3 and CuO/MgO (with 5wt% Cu in both cases), as reference materials. In addition, the average yield to liquids and selectivity to acetol attained for the different Cu-Mg-Al mixed oxides here studied during 9 h of reactor operation at 240 ºC are also shown in Figure 4.11. As can be seen, M^{II}/M^{III} molar ratios around 4 offered the highest yield to liquids and acetol selectivity (the highest yield of acetol) achieved. Especially, the acetol selectivity attained with 5.0%Cu-HT catalysts with Mg/Al ratios from 3 to 5 is more significant than the values achieved with CuO/Al_2O_3 reference material, while CuO/MgO material offered the worse results. However, the catalyst stability allows for discerning between these values as Cu-Mg-Al materials with higher M^{II}/M^{III} molar ratios ((Cu+Mg)/Al ratios ≥4) are slightly more appropriate to keep the catalytic performance over 9 hours.

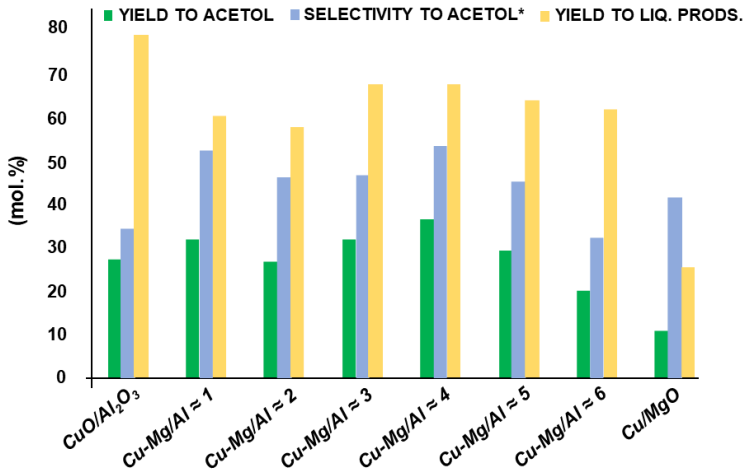

Figure 4.10. Yield to liquids, selectivity, and yield to acetol in the selective dehydration of glycerol over 5.0%Cu-HT catalysts with different (Cu+Mg)/Al molar ratios at TOS = 4 h. Reaction conditions: feed: MeOH/GLY = 90/10 wt., flow = 2 mL/h, temperature = 240 ºC, catalyst = 0.5 g. *Calculated over the total amount of products in the liquid fraction.

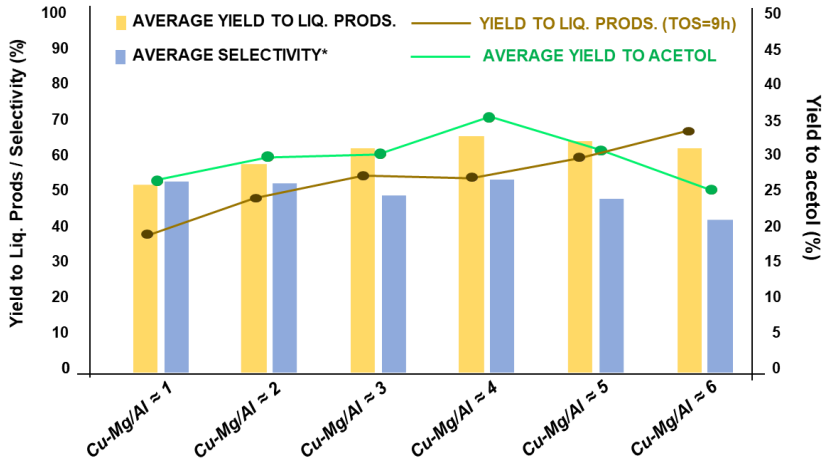

Figure 4.11. Average yield to liquids and selectivity to acetol in the selective dehydration of glycerol over 5.0%Cu-HT catalysts with different (Cu+Mg)/Al molar ratios during TOS =1-9 h. Reaction conditions: feed: MeOH/GLY = 90/10 wt., flow = 2 mL/h, temperature = 240 ºC, catalyst = 0.5 g. *Calculated over the total amount of products in the liquid fraction.

As for the acid properties of the Cu-Mg-Al samples with different (Cu+Mg)/Al molar ratios, inspecting the NH_3-TPD profiles (Figure 4.12a), two different peaks can be defined the first one appearing at temperatures around 200 ºC and the second at temperatures above 350 ºC. As reported for calcined hydrotalcites, the acidity in-between this range can be ascribed to weak and moderate Lewis acid sites matching mainly to different Al^{3+} species[10,11], although the participation of copper to the moderate acid sites cannot be dismissed[12]. As far as the basic sites are concerned, from the CO_2-TPD profiles attained from Cu-Mg-Al samples, the two peaks at lower temperatures rising in Figure 4.12b could be attributed to MgO (weak, physiosorbed CO_2) and O^{2-} unsaturated (moderate, chemisorbed CO_2). Similar sites can be found in MgO[13].

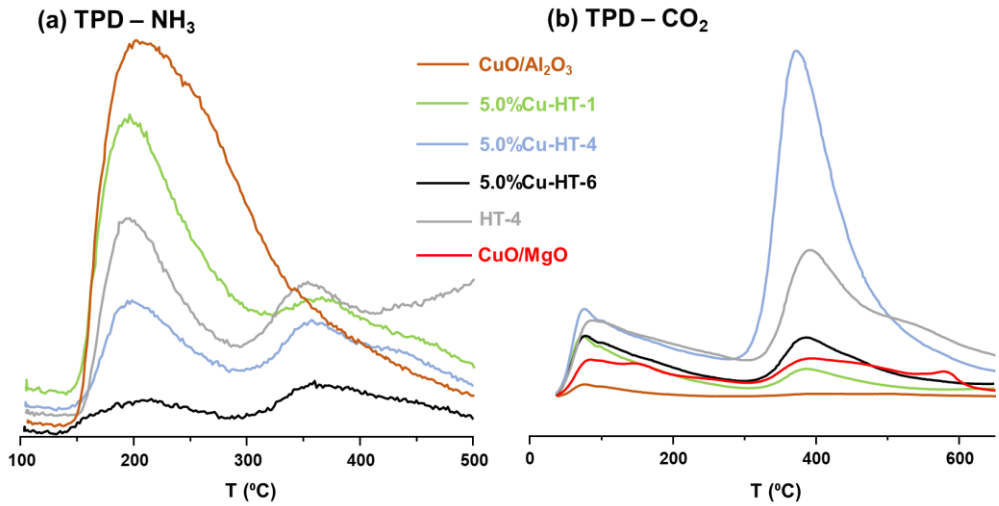

Figure 4.12. NH_3-TPD (a) and CO_2-TPD (b) profiles of Cu-Mg-Al hydrotalcite-derived mixed oxides with different M^{II}/M^{III} ratios. Note-1: non-calibrated mass-spectrometer (MS); qualitative information about the strength distribution of acid sites. Note-2: Baseline drift in HT-4 due to NO_x formation ($T \geq 450$ ºC).

Hence, the higher performance of these mixed oxides having M^{II}/M^{III} molar ratios between 3-4 could be explained based on the different distribution of active sites exhibited by each material, thus being more beneficial a material containing mainly weak Lewis acid sites and moderate Lewis basic sites. This good combination of Lewis acid and basic sites can be encountered in the samples as mentioned earlier with M^{II}/M^{III} molar ratios ≈3-4 (see

Figure 4.12 and Table 4.6). On the contrary, higher ratios make the material lose both total acidity (concretely weak centers) and basicity, the former because of the lower aluminum loading, the latter due to the decrease of the vacancies in the mixed oxide structure generated by the presence of aluminum[3][14]. Nevertheless, the MgAl mixed oxides having a combination of Lewis, both basic and acid sites, but without Cu in the structure, cannot carry out the selective dehydration of glycerol to acetol. Thus, the role of Cu is essential to accomplish this process.

Table 4.6. Quantitative data for temperature programmed desorption (NH_3-TPD and CO_2-TPD) of Cu-Mg-Al hydrotalcite-derived materials with different M^{II}/M^{III} molar ratios.

Catalyst	Acid site density (µmol/g)	Basic site density (µmol/g)	Acid sites (weak/medium)	Basic sites (weak/medium)
CuO/Al_2O_3	102	33	100	77:23
5.0%Cu-HT-1	122	111	68:32	66:34
5.0%Cu-HT-4	87	159	42:58	21:79
5.0%Cu-HT-6	63	153	37:63	44:56
CuO/MgO	-	111	-[a]	39:61

[a] MgO can be considered as having almost zero acidity[15].

The presence of Cu in the hydrotalcite-derived mixed oxide reduces the acidity and basicity of the samples compared to the MgAl mixed oxide (see Table 4.7). This behavior can be explained by different effects co-occurring. When Cu^{2+} replacing Mg^{2+} in the mixed oxide structure is close to Al^{3+} sites, Cu works as the base, but the acid site ascribed to the Al is less acid to the corresponding site in the only presence of Mg. Thus, the Cu-HT material's acidity (mainly week acidity) is lower than that observed in the corresponding HT sample without Cu (see Table 4.7). Moreover, replacing Mg^{2+} by Cu^{2+} in the mixed oxide structure diminishes the amount and strength of basic sites in the material, mainly because CuO_x species have lower basicity than MgO species (see Table 4.7). In brief, the presence of Cu in the structure of MgAl mixed oxides leads to a decrease in the acidity and

the basicity of the materials, being this effect more pronounced in the case of the basic properties. It is also possible that the Lewis acidity of the copper species could contribute to the total acidity presented by the Cu-HT samples, but this influence should be minor compared to the amount of Al contained in the samples. In that case, the effect would be more relevant only in Cu-HT samples with a meager amount of Al (i.e., Cu-HT-6).

Table 4.7. Comparison of NH_3-TPD and CO_2-TPD quantitative data and catalytic activity of hydrotalcite-derived Cu-Mg-Al and Mg-Al mixed oxides with the same Mg/Al ratio.

Catalyst	Acid sites (μmol/g) (weak:medium)	Basic sites (μmol/g) (weak:medium)	Yield to Liquids[a] (mol.%)	Selectivity to acetol[a]* (mol.%)
5.0%Cu-HT-4	87 (42:58)	159 (21:79)	64	52
HT-4	124 (56:44)	245 (31:69)	7	39

[a]Average glycerol conversion and selectivity to acetol during TOS =1-9 h. Reaction conditions: feed: MeOH/GLY =90/10 wt., flow =2 mL/h, temperature =240 ºC, catalyst =0.5 g. *Calculated over the total amount of products in the liquid fraction.

In summary, also considering the differences noted in Figures 4.10 to 4.12, the material 5.0%Cu-HT-4, which has an adequate combination of weak acid and moderate basic sites, presents a medium activity (in terms of yield to liquids) between Al_2O_3-based (mainly acid) and MgO-based (basic) materials. Also, if taking the glycerol conversion as a definitory parameter, the conclusions reached are equivalent (≈50% for CuO/MgO, ≈90% for 5.0%Cu-HT-4, and ≈100% for CuO/Al_2O_3, average results TOS =1-9 h).

With this 5.0%Cu-HT-4 material, the best catalytic results (maximum selectivity values and yield to acetol) can be reached. Therefore, weak acid sites corresponding to Al^{3+} can be concluded as the main responsible for glycerol conversion as they are almost the only ones present on the most active material (CuO/Al_2O_3). In fact, the activity reached for MgO, without any acid site, was the worst among all the materials tested. In this sense, a compromise between acid and basic centres in the solid is needed to produce a good acetol yield. Apparently, low catalyst Mg/Al molar ratios do not present the necessary basicity to perform the reaction with good selectivity. On the other hand, higher Mg/Al ratios and pure MgO lack the acid site density needed to react and generate the desired acetol.

Regarding the catalytic deactivation detected in these Cu-based catalysts, one possible interpretation that fits with the tendency observed for these HT-derived materials would be the deactivation occurring on the weak acid sites, whose ratio rises with decreasing of (Cu+Mg)/Al in the solids. However, the deactivation happening on the weak basic sites cannot be cast aside with the handled data. Actually, it is challenging neither to discriminate between both options nor to discard any of them. Besides, literature reports claim both acid and basic sites could cause catalytic deactivation in similar reactions, as coke formation would occur on acid sites, and polyglycerols or acetalization products of glycerol would be formed and remain adsorbed on basic sites[16].

Finally, as previously mentioned in this section, it must be emphasized that the MgAl mixed oxide (HT-4) cannot carry out the reaction to almost any extent (≈20% av. conversion vs ≈89% for 5.0%Cu-HT-4, see also Table 4.7), despite offering both weak acids and moderate basic centers. This fact unveils the need for copper to somehow interplay with glycerol through a specific interaction apart from an acid-base effect. This fact will be the subject of further discussions in the following sections.

4.3.3 The role of Cu in Cu-Mg-Al mixed oxides

4.3.3.1 Comparison between Cu-, Ni-, and Co-based catalysts

The viability of using other divalent transition metals with redox features and a recognized capacity to produce acetol in the glycerol reforming, such as nickel or cobalt[5,6], was investigated. For that, 5.0%Ni-HT-4 and 5.0%Co-HT-4 materials were synthesized, calcined, and assayed in the selective dehydration of glycerol in the continuous-flow fixed-bed reactor (at 240 ºC and TOS = 4 h), constantly comparing with the 5.0%Cu-HT-4 catalyst. The catalytic results for these three analogous samples are compiled in Table 4.8. The experiments conducted using 5.0%Ni-HT-4 and 5.0%Co-HT-4 hydrotalcite-derived mixed oxides exposed the need to utilize copper in this system. At this stage, the significant differences in catalytic performance could not be ascribed to either the different acid-base properties (Figure 4.13 and Table 4.9) or the reducibility of the samples (Figure 4.14). Slight glycerol conversions with poor selectivities to acetol were accomplished with both Co- and Ni-based catalysts (in Ni-HT-4, negligible amounts of acetol were detected).

Table 4.8. Catalytic activity data for hydrotalcite-derived mixed oxides containing different transitions metals.

Catalyst	Yield to Liquids (mol.%)	Selectivity to acetol (mol.%)*
5.0%Cu-HT-4	74	51
5.0%Co-HT-4	6	17
5.0%Ni-HT-4	<5	-

Reaction conditions: Temperature = 240 ºC, feed: MeOH/GLY (90:10 w.), flow = 2mL/h, catalyst: 0.5 g, TOS= 1-4 h. *Calculated over the total amount of products in the liquid fraction.

Nonetheless, previous literature reports claim some goods result in glycerol conversion to either acetol or 1,2-propanediol for Co- and Ni-containing materials[17,18]. These results could be justified based on two facts. First, the higher contact times in a batch reactor instead of the shorter contact times in a fixed bed reactor, thus allowing Co and Ni to interact with the glycerol molecule differently as it is taking place in our system. In addition, H_2 could also assist in increasing Ni and Co reactivity. Either way, most literature reports about glycerol transformation to propane-diols agree that copper is essential when working with mixed metal oxides in fixed-bed reactors[19,20]. Therefore, studying the different Cu species existing in the Cu-based mixed oxide materials and how they interact with glycerol to produce acetol selectively becomes imperative to understand Cu catalysis and its role in the solid material.

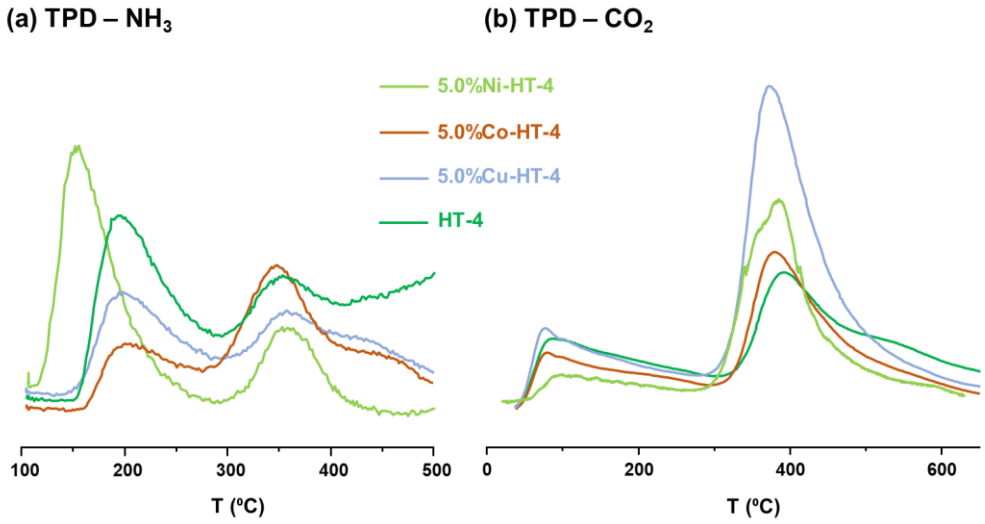

Figure 4.13. TPD-NH_3 (a) and TPD-CO_2 (b) profiles of Mg-Al hydrotalcite-derived mixed oxides pure and with different transition metals. Note-1: non-calibrated mass-spectrometer (MS); qualitative information about the strength distribution of acid sites. Note-2: Baseline drift in HT-4 due to NO_x formation (T ≥ 450 ºC).

Table 4.9. Quantitative data for temperature programmed desorption (NH_3-TPD- and CO_2-TPD) of Mg-Al HT-derived (HT-4) pure material and with the incorporation of different Cu, Co, and Ni metals.

Catalyst	Acid site density (µmol/g)	Basic site density (µmol/g)	Acid sites (weak/medium)	Basic sites (weak/medium)
5.0%Cu-HT-4	87	159	42:58	21:79
5.0%Co-HT-4	165	198	26:74	28:72
5.0%Ni-HT-4	115	290	74:26	18:82
HT-4	139	245	56:44	31:69

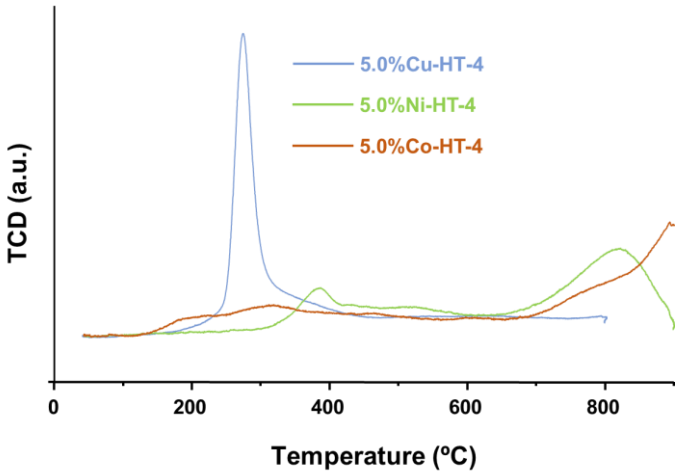

Figure 4.14. TPR traces for 5.0%Cu-HT-4 (blue), 5.0%Co-HT-4 (brown) and 5.0%Ni-HT-4 (green) samples.

4.3.3.2 Effect of the oxidation state of Cu in Cu-Mg-Al mixed oxides

The coexistence of Cu^0, Cu^{1+} and Cu^{2+} species in a partially reduced Cu-Al oxide catalyst has been stated as the cause of its multifunctional behavior, thus catalyzing, for example, the simultaneous dehydration to acetol and the hydrogenolysis (hydrogenation) to 1,2-propanediol[19]. Therefore, the effect of having different copper species in our Cu-based mixed oxides was evaluated through a detailed XPS study combined with different catalyst pretreatments and catalytic tests.

XPS experiments were carried out by using: a) 5.0%Cu-HT-4, a fresh calcined material; b) 5.0%Cu-HT-4U, the same material recuperated after reaction; c) 5.0%Cu-HT-4R, again the same material but this time reduced *ex-situ* at 450 ºC under H_2 atmosphere and without previous reaction testing; and finally d) 5.0%Cu-HT-4R-INSITU, the same material but reduced at 450 ºC under H_2 atmosphere in the instrument's cell, to assure that the sample has not had contact with atmospheric air before analysis. The results obtained through XPS measurements are shown in Figure 4.15 and recapitulated in Table 4.10. Figure A6 in *Annex* also presents a stability study of the reduction state of Cu species in the solids under the experiment conditions, thus discarding Cu photoreduction during these measurements.

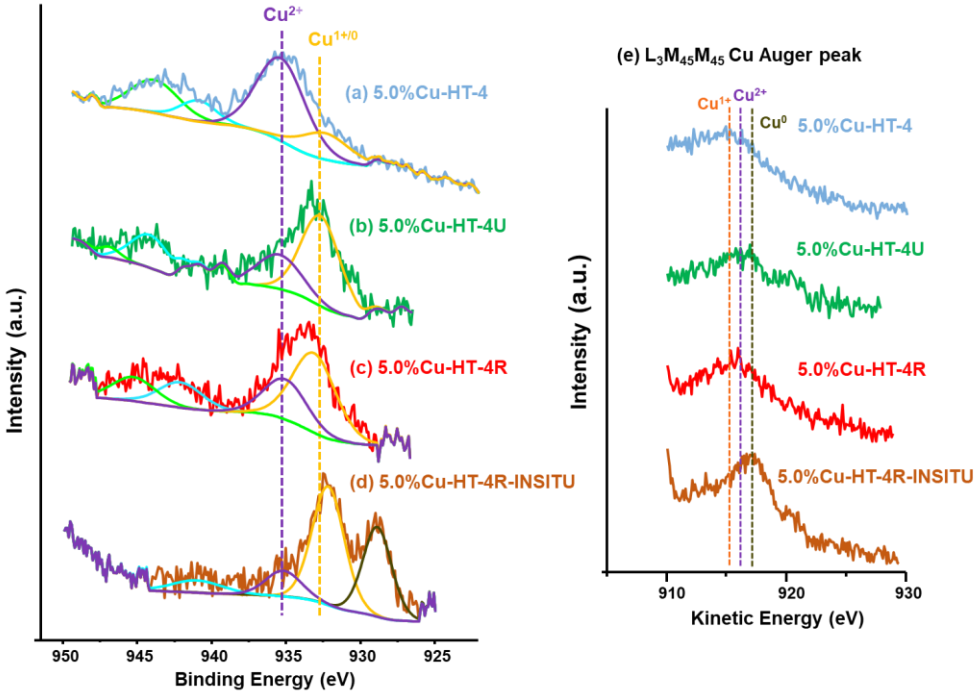

Figure 4.15. Cu2p$_{3/2}$ XPS peak of (a) 5.0%Cu-HT-4 (fresh, calcined), (b) 5.0%Cu-HT-4U (used), (c) 5.0%Cu-HT-4R (H_2 reduced *ex-situ*), (d) 5.0%Cu-HT-4R-INSITU (H_2 reduced *in-situ*), (e) $L_3M_{45}M_{45}$ Cu Auger peak for the studied Cu-Mg-Al samples.

In the fresh sample, the Cu2p$_{3/2}$ main peak appears at 935.7 eV, which, jointly with a shoulder at higher BE (943.5 eV, shake-up peak) and the value for the modified Auger Parameter of 1850.9 eV, confirms the assignation as Cu^{2+} predominately [48]. The lower BE signal (932.6 eV) is related to a minor amount of reduced copper species (Cu^{1+}/Cu^0). The high BE shift of the Cu^{2+} ion (935.7 eV) is due to final state effects related to their high dispersion in the HT matrix[21]. An opposite situation is observed in the case of the used material (5.0%Cu-HT-4U), where the central peak appears at low BE (932.9 eV) together with a shoulder at high BE (935.6eV). The lower shake-up intensity (s/m = 0.30) and the value of the modified Auger Parameter of 1849.5 eV indicate the presence of reduced copper species Cu^{1+} predominately, whereas the shoulder at higher BE corresponds to Cu^{2+}. On the other hand, in the "ex situ" H_2 reduced sample (5.0%Cu-HT-4R), two peaks at 935.6 eV and 933.5 eV are observed, associated with Cu^{2+} and reduced $Cu^{1+/0}$, respectively. The

presence of reduced copper as mostly Cu^{1+} is confirmed by the value of the modified Auger Parameter in 1849.6eV. Finally, in the *in-situ* H_2 reduced sample (5.0%Cu-HT-4R-INSITU), two prominent peaks corresponding to Cu reduced species can be distinguished at 928.9 and 932.2 eV, as well as one shoulder at 935.5 (Cu^{2+}). The value of the modified Auger Parameter at 1850.2 eV unveils the majority presence of Cu^0 versus Cu^{1+}. In addition, the splitting of the $Cu2p_{3/2}$ XPS peak into two components (928.9 and 932.2 eV) is related to differential charging of the sample because of the presence of Cu metal species in different environments and/or particle sizes. Minor amounts of Cu^{2+} are also detected, based on the XPS component at BE of 935.5 eV and its shake-up peak.

Table 4.10. XPS data of the $Cu2p_{3/2}$ core level and surface composition.

Catalyst	Cu ($2p_{3/2}$)			α^a	Molar ratio		Molar ratio Cu: Al: Mg
	B.E. (eV) Cu^{2+}	B.E. (eV) $Cu^{1+/0}$	s/m	(eV)	Cu^{2+}	$Cu^{1+/0}$	
5.0%Cu-HT-4	935.7	932.6	0.45	1850.9	84	16	3: 58: 39
5.0%Cu-HT-4U	935.6	932.9	0.30	1849.5	47	53	2: 56: 42
5.0%Cu-HT-4R	935.6	933.5	0.42	1849.6	47	53	2: 56: 42
5.0%Cu-HT-4R-INSITU	935.5	932.3/928.9	0.12	1850.2	20	80	1: 57: 42

[a] $Cu2p_{3/2}$ XPS (BE) + $L_3M_{45}M_{45}$ CuAES (KE).

The prevalent presence of Cu^{1+} in the 5.0%Cu-HT-4U material (used catalyst) illustrates that the reduction of Cu^{2+} species present in the fresh (calcined) sample occurs during the reaction. However, since the used catalyst has been analyzed after being exposed to atmospheric air, and metallic copper (Cu^0) quickly oxidizes to either Cu^{1+} or Cu^{2+}[22], the extent of the copper species reduction through this "on reaction" reduction is difficult to determine. The TPR analysis of the fresh (calcined) material and the "ex-situ" H_2 reduced material (see Figure 4.16) also confirms the presence of Cu^{2+} species (peak at 285 ^oC)[23,24] in the former (5.0%Cu-HT-4) and segregated Cu^{2+} and/or Cu^{1+} species (peak at

190 ºC)[25,26] in the later (5.0%Cu-HT-4R). Most likely, both Cu^0 and Cu^{1+} are present in the reduced material 5.0%Cu-HT-4R. Cu^0 would be formed during the reduction with H_2 at 450 ºC (see XPS Cu-HT4-R-INSITU, Figure 4.15), whereas Cu^{1+} would result from the oxidation of Cu^0 to Cu^{1+} in the presence of air (see XPS Cu-HT4-R, Figure 4.15). Moreover, if the used material (5.0%Cu-HT4U) also suffers a reduction during the glycerol dehydration process, as it seems, this could also be applied to it.

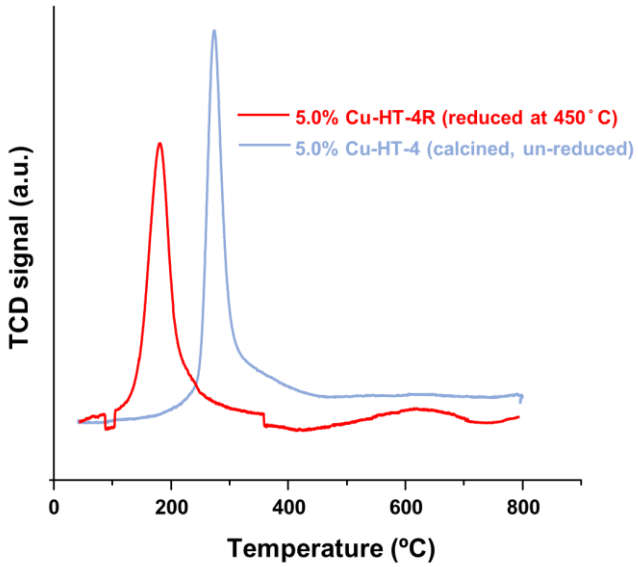

Figure 4.16. TPR traces for 5.0%Cu-HT-4 (fresh, calcined) and 5.0%Cu-HT-4R (calcined + reduced at 450 ºC under a H_2 atmosphere) samples.

With the aim of finding out if these reduced copper species detected in Cu-Mg-Al mixed oxides are active or not in the selective dehydration of glycerol, the 5.0%Cu-HT-4R ("ex situ" H_2 reduced) material having mainly Cu^{1+} species (see XPS data, Figure 4.15, and Table 4.10) was tested in reaction. The material displayed similar catalytic behavior, especially in yield to liquids and selectivity to acetol (i.e., acetol yield) to the original 5.0%Cu-HT-4 calcined or un-reduced material (see Figure 4.17). Another experiment with the 5.0%Cu-HT-4R-INSITU material (reduced in the same fix-bed catalytic reactor at 450 ºC under H_2 atmosphere during 4 h, before the reaction), having mainly Cu^0 (see XPS data, Figure 4.15, and Table 4.10), was carried out. A significant decrease in acetol yield was

observed in this case, falling the average yield to liquid product values from ≈65% to ≈45% regarding the other two samples discussed above. As for the acetol selectivity, a lower value was obtained (from ≈50% to ≈45% on average) over this reduced sample mainly possessing Cu^0 species.

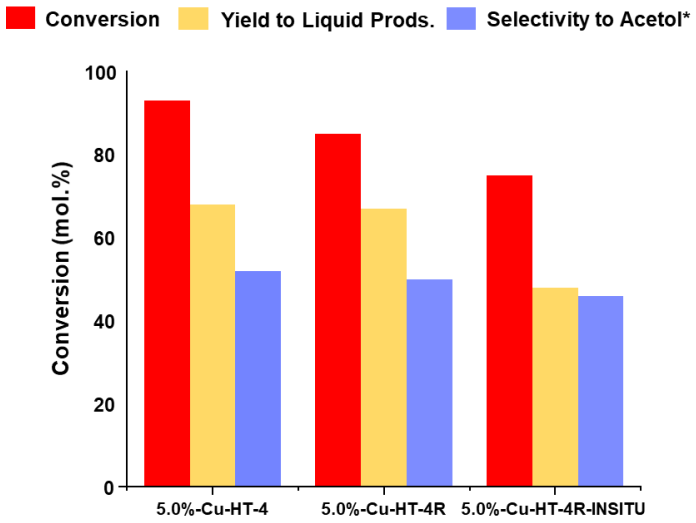

Figure 4.17. Glycerol conversion (a), yield to liquid products (b), and selectivity to acetol (c) for 5.0%Cu-HT-4, 5.0%Cu-HT-4R and 5.0%Cu-HT-4R-INSITU materials. Reaction conditions: Temperature = 240 ºC, feed: MeOH/GLY (90/10 w.), flow = 2 mL/h, TOS =1-7 h, catalyst: 0.5 g. *Calculated over the total amount of products in the liquid fraction.

From the results obtained up to now, it is sensible to think that Cu^{2+} species initially in the 5.0%Cu-HT-4 (calcined) catalyst are *in-situ* reduced to Cu^{1+} and/or Cu^0 species along the glycerol dehydration process. The experiments herein described have set Cu^{1+} and Cu^{2+} appearing to be more active for this reaction than metallic copper, being the catalyst when the Cu is found mainly as Cu^0 much less active and slightly less selective towards acetol than the solids having mostly cationic Cu species.

4.3.3.3 Additional tests and measurements

In order to shed some light on the role of copper species in the Cu-Mg-Al mixed oxides during the selective catalytic dehydration of glycerol in a continuous flow fix-bed reactor, three additional catalytic experiments were carried out. First, the liquid and gaseous

fractions were analyzed at the reactor outlet. First, the gas composition was determined using a specific GC-TCD system fitted with 3 detection lines to detect H_2, N_2 and light hydrocarbons. On the other hand, the standard GC-FID system determined the liquid composition (see *Experimental procedure*, *Section 3.5.1*).

For the first experience, the reactor previously charged with 5.0%Cu-HT-4 catalyst was fed for one hour with absolute methanol (MeOH pre-treatment). The results thus obtained are shown in Figure 4.18. As can be seen, ≈30% of the methanol fed is converted in the presence of Cu-Mg-Al material, which initially mainly contains Cu^{2+} species, into gaseous products, such as CO, CO_2, and H_2, together with meager amounts of methyl-formate.

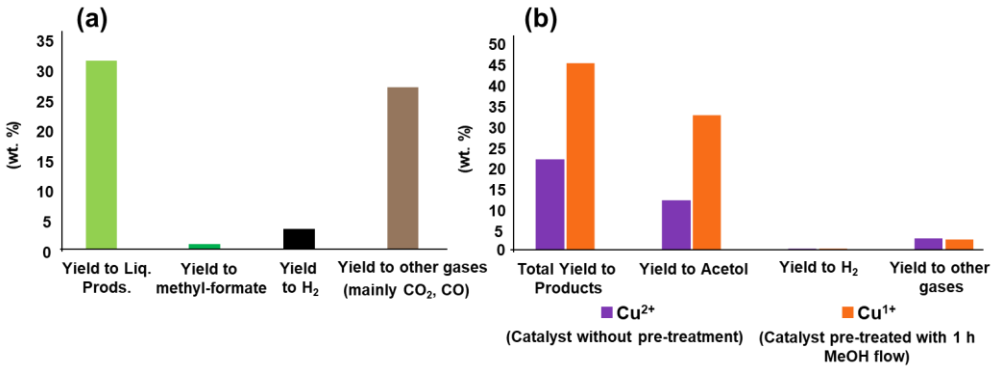

Figure 4.18. (a) Pre-treatment test of 5.0%Cu-HT-4 catalyst with methanol. Reaction conditions: Feed: methanol, temperature = 240 ºC, flow = 2 mL/h, catalyst: 0.5 g, TOS = 1 h. (b) Catalytic results of selective glycerol dehydration over 5.0%Cu-HT-4 with and without methanol pre-treatment. Reaction conditions: Feed: water/glycerol (90/10 wt.), temperature = 240 ºC, flow = 2 mL/h, catalyst: 0.5 g, TOS = 6 h.

Then, the same 5.0%Cu-HT-4 catalyst (already pre-treated with MeOH at 200 ºC) was fed with a mixture of GLY/Water (10/90 in weight) for 6 h, and the catalytic results were compared to another experiment performed by feeding a fresh 5.0%Cu-HT-4 catalyst (without the previous pre-treatment with methanol) with the same GLY/Water (10/90 wt.) mixture during 6, as well. The attained results are depicted in Figure 4.18, and they make clear that the pre-treatment had beneficial effects on the catalytic performance. This could be attributed to the presence of either Cu(I) or Cu(0) instead of Cu(II) species due to the

hydrogen formation when feeding with MeOH during the catalyst pre-treatment (see Figure 4.18). Thus, these copper reduced species would be more active than Cu^{2+} species for this reaction and, since Cu^{1+} has been found to be more active than Cu^{0} (*Section 4.3.3.2*, Figure 4.17), Cu^{1+} can be concluded as the most active species for this reaction. These shreds of evidence are in good agreement with recent results reported by Batiot-Dupeyrat and co-workers based on catalytic results together with DFT calculations[27].

TPR measurements of the 5.0%Cu-HT-4 calcined sample before and after pre-treatment with methanol (at 200 ºC) unveils the reduction of Cu(II) when comparing with the original calcined sample (Figure 4.19). Therefore, it is reasonable to think that the methanol feeding used throughout this work can make the corresponding Cu(II) → Cu(I), Cu(0) transformation. In fact, during the pre-treatment with MeOH, approximately 25 mmol of H_2 were produced. Hence, since 0.4 mmol of copper are present in our catalyst, this quantity should be enough to reduce most of the Cu^{2+} species inside the catalyst.

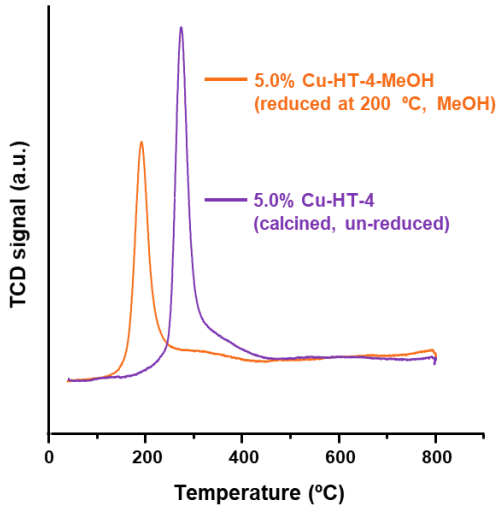

Figure 4.19. TPR traces for 5.0%Cu-HT-4 (calcined, un-reduced) and 5.0%Cu-HT-4R (calcined + reduced at 200 ºC with MeOH).

In summary, under the reaction conditions here employed, the Cu^{2+} species present in the catalyst endure the corresponding reduction to Cu^{1+} (and Cu^{0}) species, owing to the presence of MeOH, thus promoting the selective catalytic dehydration of glycerol to acetol.

Although it is hard to distinguish between Cu^{1+} and Cu^{0} due to the oxidation behavior of copper once exposed to the air, results shown in Figure 4.17 point to Cu^{1+} as a more active species to carry out the reaction than Cu^{0}.

4.3.3.4 "in-situ" FTIR measurements

In order to explain the catalytic behavior of the 5.0%Cu-HT-4 sample and provide additional information concerning the reaction mechanism and the role of copper in the reaction pathway, IR spectroscopic studies were carried out using 1,2-propanediol as probe molecule instead of glycerol. In addition, the HT-4 (Mg/Al = 4), 5.0%Ni-HT-4 and 5.0%Co-HT-4 samples displaying much lower catalytic activity have also been investigated. First, 1,2 propanediol has been adsorbed at 25 ºC on all samples until saturation coverage, and then the temperature has been stepwise increased from 25 ºC to 160 ºC, acquiring IR spectra at each temperature.

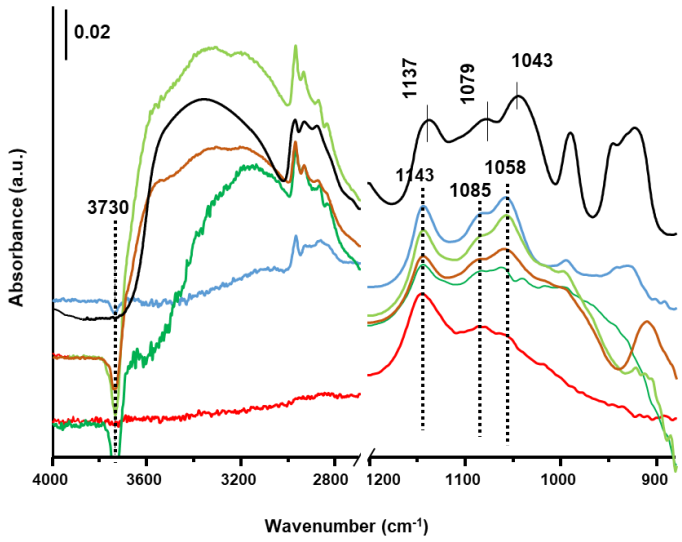

Figure 4.20. IR spectra of 1,2-propanediol adsorbed at 25 ºC on 5.0%Cu-HT-4 (blue), 5.0%Ni-HT-4 (light green), 5.0%Co-HT-4 (brown), HT-4 (dark green) and 5.0%Cu-HT-4R (ex situ H_2 reduced, red). In black, gas phase spectra of 1,2-propanediol as reference.

Gas-phase 1,2 propanediol shows a complicated group of IR bands in the low-frequency region with maxima at 1654, 1137, 1079, 1043, 989, 924 and 839 cm^{-1}. After adsorption at 25 ºC, IR bands corresponding to υ_{C-O} vibration (1137, 1079 and 1043 cm^{-1}) are shifted to

higher frequencies (1143, 1085 and 1058 cm^{-1}) on all samples, with a corresponding downshift in the OH band in every case (3730 cm^{-1}, Figure 4.20). Since the interaction of 1,2 propanediol is relatively strong in all cases (i.e., stable toward evacuation at 10^{-6} mbar and 25ºC), the redshift of the υ_{C-O} IR bands may correspond to interaction with Lewis acid sites, along with OH groups. Moreover, the shift in the υ_{C-O} IR bands is the same in all samples, meaning similar adsorption sites in every material. This fact is consistent with what has been pointed out about the weak acid sites corresponding to Al^{3+} as the main responsible for the catalytic activity. Since these acid sites are present in all studied materials (see NH_3-TPD measurements, Figures 4.12 and 4.13), they could be held accountable for reactant adsorption.

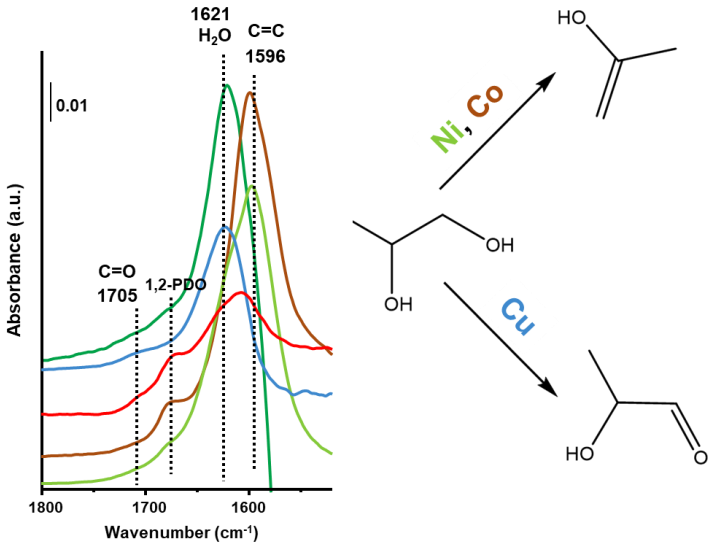

Figure 4.21. IR spectra of 1,2-propanediol at 160 ºC on 5.0%Cu-HT-4 (blue), 5.0%Ni-HT-4 (light green), 5.0%Co-HT-4 (brown), HT-4 (dark green) and 5.0%Cu-HT-4 "ex situ" H_2 reduced (red). 1,2-PDO: IR peak related to 1,2-propanediol.

Nonetheless, when the evolution of the adsorbed 1,2-propanediol is analyzed at increasing temperatures, a different behavior could be observed depending on the nature of the transition metal site (Cu, Ni, and Co), thereby predicting different reaction mechanisms and, hence, reaction intermediate species and reaction rates. Accordingly, in the 5.0%Cu-HT-4 sample, increasing the reaction temperature up to 160 ºC leads to the appearance of a

band at 1705 cm^{-1} corresponding to a carbonyl functional group, whereas under the same conditions in the Ni and Co-based catalysts, a band at 1596 cm^{-1} is seen, corresponding to C=C bond, while no additional band could be observed in the HT-4 sample (Figure 4.21). This finding may correspond to a different activation mode of the 1,2-propanediol. In this sense, we propose that a hydride abstraction could be promoted by Cu species, whereas OH^- abstraction catalyzed by Lewis acid sites would take place on Ni and Co catalysts. Moreover, using CO as probe molecule, Cu^{1+} species have been evidenced in the IR studies after 1,2-propanediol adsorption at 160 ºC on the 5.0%Cu-HT-4 sample (IR band at 2098 cm^{-1})[28], which may be related to Cu^{2+} reduction by the aforementioned Cu-hydride interaction (Figure 4.22). In opposition, no reduced species Ni^{1+} nor $Co^{2+/1+}$ have been discerned in the 5.0%Ni-HT-4 and 5.0%Co-HT-4 samples under similar conditions. However, this fact was fully expected considering the very low reducibility of these samples, as very short amounts of Ni^{2+} and Co^{3+} are available to be reduced at low temperatures (see TPR, Figure 4.14 in *Section 4.3.3.1*). Thus, it can be concluded that weak acid sites are important because they are 1,2-propanediol adsorption centers (see NH_3-TPD, Figure 4.13 in *Section 4.3.3.1*), and that the additional proximity of reducible centers, such as Cu^{2+} (but not Ni^{2+} and Co^{3+}), could favor the abstraction of H^-, in that way accelerating the carbonyl group formation pathway.

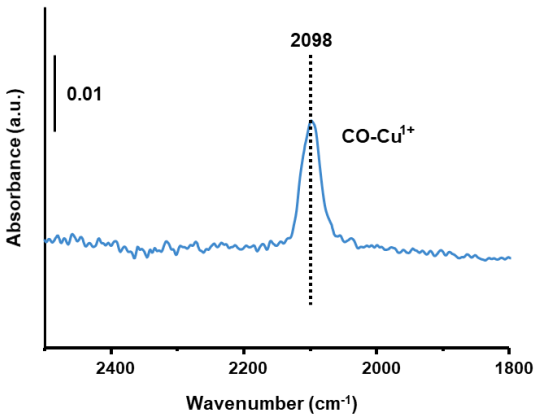

Figure 4.22. IR spectra of CO adsorption at 25 ºC as probe molecule on the 5.0%Cu-HT-4 sample after 1,2-propanediol adsorption and increasing the temperature to 160 ºC.

Once Cu^{2+} and Cu^{1+} are identified as the two main species present in the catalyst when the reaction is taking place, and in order to assess if Cu^{2+} or Cu^{1+} are involved in the possible intermediate formation step, the 5.0%Cu-HT-4 sample has been "ex situ" reduced in H_2 flow (containing mainly Cu^{1+}, see XPS data of 5.0%Cu-HT-4R in Figure 4.15) and analyzed in the IR study. Analogously to the Cu-based non-reduced sample, a band at 1705 cm^{-1} due to carbonyl group has been observed in the 1,2-propanediol temperature-dependent reaction profile. Nevertheless, the onset of the carbonyl group formation appears at a slightly lower temperature, i.e., 120 ºC, in the "ex situ" reduced sample versus 160 ºC in the calcined sample (see Figure 4.23). Therefore, while Cu^{2+} and Cu^{1+} can be considered active sites in the 5.0%Cu-HT-4 sample, a slightly higher reactivity could be observed for Cu^{1+}, which is in line with the improvement already seen when reducing the Cu-containing catalyst with MeOH at 240 ºC (see *Section 4.3.3.3*). Based on the IR data, it is essential to remark that the enhanced catalytic activity in the glycerol dehydration observed with the 5.0%Cu-HT-4 sample can be ascribed to the distinct role of copper versus other transition metals to promote the carbonyl group formation pathway.

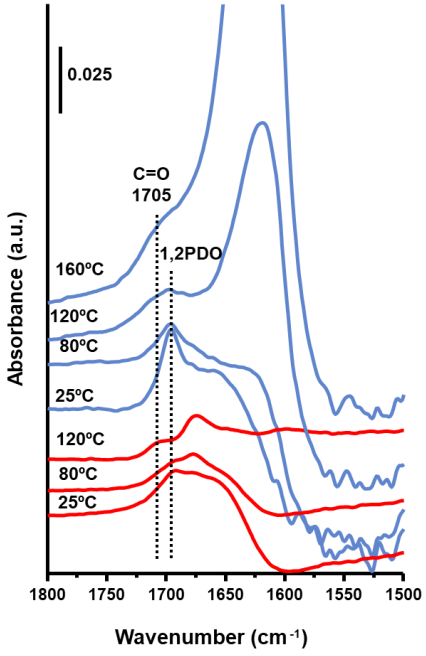

Figure 4.23. FT-IR spectra of 1,2-propanediol at 25 ºC, 80 ºC and 160 ºC on 5.0%CuHT-4 (blue) and 5.0%Cu-HT-4 "ex situ" H_2 reduced (red). 1,2-PDO: IR peak of 1,2-propanediol.

However, despite displaying different reaction pathways, such mechanisms cannot fully explain the considerably lower activity of 5.0%Co-HT-4 and 5.0%Ni-HT-4 catalysts. Therefore, another aspect that could influence the catalytic activity is the interaction strength of the reaction products with the catalyst surface so that a more robust interaction would result in fast catalyst deactivation. Thus, and aiming at analyzing the reaction product interaction strength, hydroxyacetone (acetol) has been adsorbed on the 5.0%Cu-HT-4 and 5.0%Ni-HT-4 samples and followed by FT-IR spectroscopic measurements. As shown in Figure 4.24, hydroxyacetone interacts on both catalysts, although the interaction is lower on the 5.0%Cu-HT-4 sample and firmer on the 5.0%Ni-HT-4 sample, probably because of the higher density of acid sites in this sample (see NH_3-TPD, Table 4.9 in *Section 4.3.3.1*).

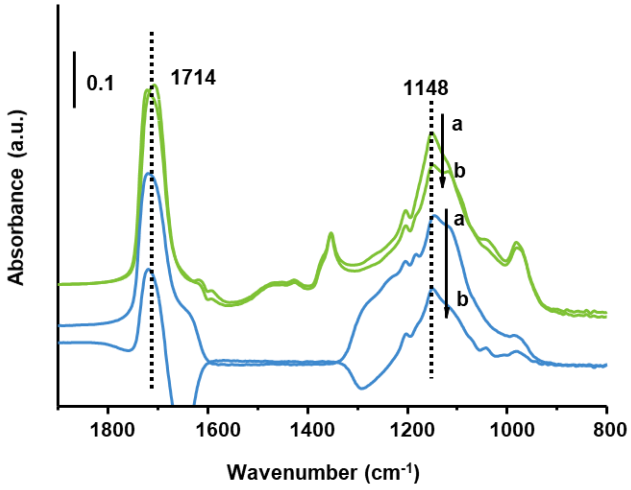

Figure 4.24. IR spectra of hydroxyacetone adsorbed at 25 ºC on 5.0%Cu-HT-4 (blue) and 5.0%Ni-HT-4 (green) (a), and after evacuation at 25 ºC for 5 min (b).

In summary, it can be postulated that weak acid sites are relevant for adsorption of 1,2-propanediol and that the presence of specific copper sites in the Cu-HT sample could favor hydride abstraction in the first reaction step. Moreover, Cu^{1+} species show higher reactivity than Cu^{2+}, and since Cu^{2+} species are reduced during the reaction helped by methanol, we can consider and confirm Cu^{1+} as the main active sites in the glycerol dehydration reaction over a 5.0%Cu-HT-4 catalyst. In addition, the reaction product desorption is enhanced in the 5.0%Cu-HT-4 sample compared to the 5.0%Ni-HT-4 and 5.0%Co-HT-4 materials. This

stronger acetol adsorption could be related to the different distribution of acid-base sites in both Co- and Ni-based samples (see NH_3-TPD measurements, Table 4.9 in *Section 4.3.3.1*) that could have too much acid density, thus making it difficult for acetol to leave the catalytic surface. Thus, the essential role of copper species and the higher interaction of the products on the Co- and Ni-based catalysts may explain the markedly higher catalytic activity observed with the Cu-containing catalyst.

4.3.4 Reaction mechanism proposal

The preceding results indicated that the presence Cu is crucial in the studied hydrotalcite-derived mixed oxides to achieving good conversion and selectivity to acetol, mainly due to giving rise an intermediate possessing a carbonyl group at the beginning of the process. In this sense, and according to the FTIR studies, we have hypothesized a plausible reaction pathway where glyceraldehyde is this reaction intermediate (Scheme 2). Nonetheless, to further clarify the function of Cu and elucidate some insights into the mechanism, catalytic tests with a very small amount of glyceraldehyde in the starting feed were carried out.

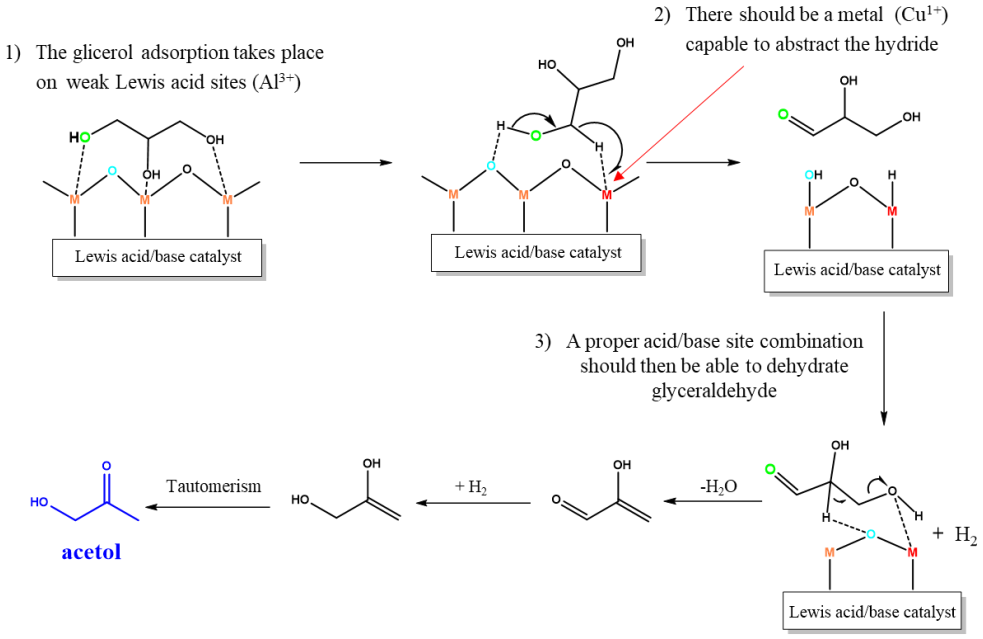

Scheme 4.2. Proposed reaction mechanism when using 5.0%Cu-HT-4 as catalyst for the selective dehydration of glycerol to acetol.

For this experiment, the most active material so far reported in this work, i.e., 5.0%Cu-HT-4, was selected, and the reaction carried out under previously established standard conditions. The experiment was followed by ^{13}C NMR at a shorter reaction time, i.e., 45 min, observing a signal that could be related to the presence of a low amount of glyceraldehyde (see Figure 4.25). However, because of the glyceraldehyde nature that results in a very high reactivity in that reaction medium, it was impossible to isolate or accumulate more glyceraldehyde during the reaction. Therefore, ^{1}H NMR data were unclear and valuable information could only be extracted from ^{13}C NMR.

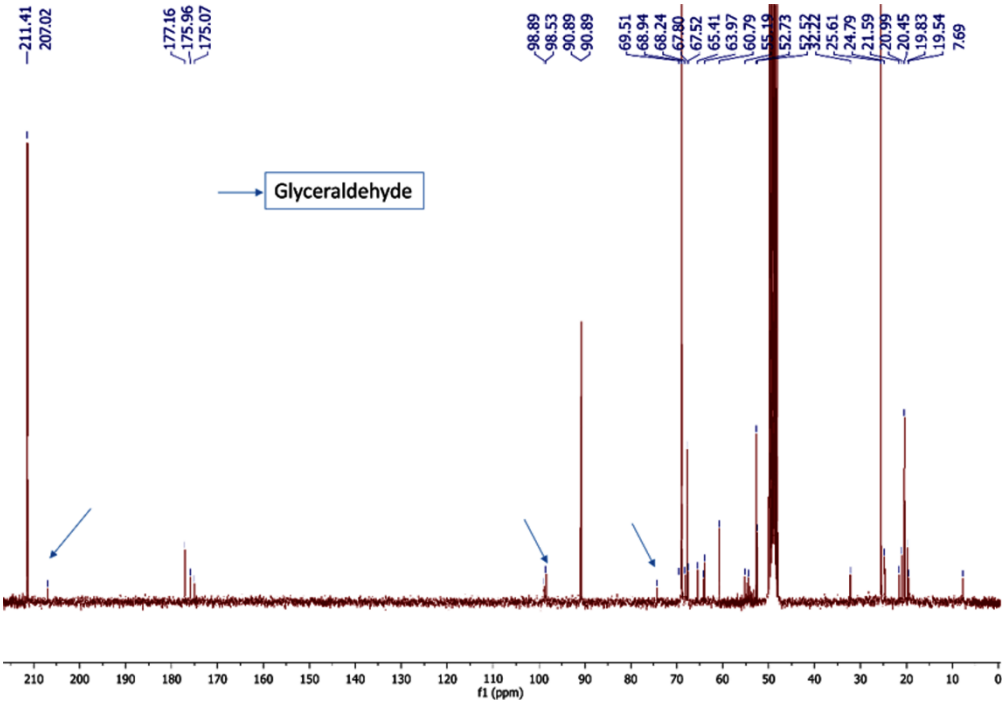

Figure 4.25. ^{13}CNMR of the selective glycerol dehydration over 5.0%Cu-HT-4 at 45 min. Reaction conditions: Feed: MeOH/GLY (90/10 w.), temperature = 240 ºC, flow = 2 mL/h, catalyst: 0.5 g of 5.0%Cu-HT-4.

Aiming at supporting this hypothesis, experiments in continuous flow with the less active catalyst 5.0%Co-HT-4 were carried out with a mixture of glycerol + 0.45 wt.% glyceraldehyde. The results showed an improvement in the yield towards acetol (Figure

4.26). This improvement has approximately the same percentage value as the amount introduced on the feed: 0.45%. In these cases, it was necessary to use a small amount of water to dissolve the glyceraldehyde in the initial mixture.

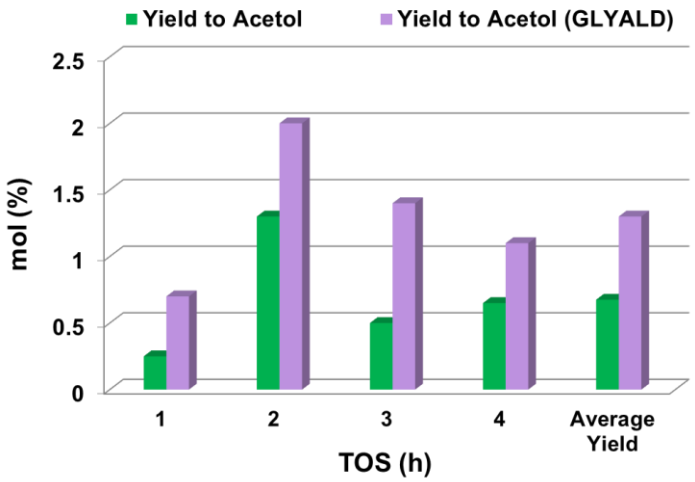

Figure 4.26. Catalytic results of selective glycerol dehydration over 5.0%Co-HT-4 with (purple) and without (glyceraldehyde) glyceraldehyde co-feed. Reaction conditions: Feed: MeOH/GLY (90/10 wt.), Feed-GLYALD: methanol/glycerol/glyceraldehyde/water (87.8/9.5/0.45/2.2 wt.), temperature = 240 ºC, flow = 2 mL/h, catalyst: 0.5 g.

These results provided us with decent proof about the reaction mechanism: Co cannot activate the C-OH bond of glycerol towards the formation of glyceraldehyde, the intermediate to acetol. However, apparently, by skipping the first step, Co-HT was able to transform glyceraldehyde to acetol.

4.3.5 Effect of the amount of Cu in Cu-Mg-AlO_x catalysts

Once the adequate Cu-Mg-Al mixed oxide with the satisfactory Mg/Al molar ratio in its structure was determined as the best composition for the selective dehydration of glycerol to acetol, the effect of the amount of Cu in these materials was studied. The Cu loading in the catalysts was varied from 0.0 to 12.0wt%, finding out that, although the selectivity to acetol is barely affected when increasing the quantity of copper, the more copper the solid contains, the higher both conversion and yield to acetol are reached.

Nonetheless, this is only true until reaching Cu loading of 10wt% (see Figure 4.27a). From this amount of copper onwards, no further increase is observed for glycerol conversion and the selectivity to acetol. Thus, a mixed oxide containing 10.0wt% of copper would correspond to the optimal composition, keeping the proper glycerol conversion and acetol selectivity balance. More importantly, it provided the best catalytic stability during 9 hours of reaction in acetol selectivity, with practically no deviation (≈55%, see Figure 4.27b). Nonetheless, the difference between the conversion value at the beginning of the experiment (100%, TOS = 1h) and the end (90%, TOS = 9h), and the yield to liquid evolution (Figure 4.27b), reveals a catalyst deactivation. Although slower than what was observed for 5.0%Cu-HT-4, this catalyst deactivation is still relevant and, therefore, the following sections will address the catalyst regeneration issue.

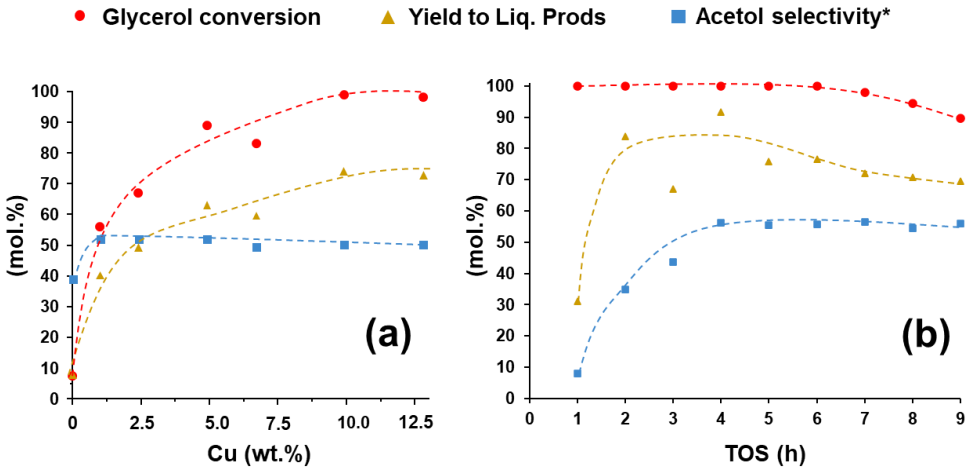

Figure 4.27. (a) Average glycerol conversion, yield to liquid products, and acetol selectivity for Cu-Mg-Al calcined materials with different Cu contents during TOS = 1–9 h. Reaction conditions: feed = methanol/glycerol (90/10 in weight), flow = 2 mL/h, with 0.5 g of catalyst at 240 ºC. (b) Catalytic performance of 10.0%Cu-HT-4 in the selective dehydration of glycerol to acetol. Reaction conditions: feed = MeOH/GLY (90/10 in weight), flow = 2 ml/h, with 0.5 g of catalyst at 240 ºC. *Calculated over the total amount of products in the liquid fraction. Note: Dashed traces only serve as visual guidelines.

Notably, a comparison of acidity and basicity data employing TPD analysis of both 5.0%Cu-HT-4 and 10.0%Cu-HT-4 calcined samples (see Table 4.11 and Figure 4.28) shows introducing more copper into the structure does not affect the amount and force of the active acid-basic centers significantly. In fact, the two Cu-based materials exhibit almost the same acid/basic sites distribution, being slightly more acid and less basic than the one containing the lower amounts of copper (5.0%Cu-HT-4 sample). Therefore, we can associate the higher activity observed for 10.0%Cu-HT-4 catalyst with increasing quantities of copper, as no significant effect of this increasing amount of copper in the acid-base properties of our materials was observed. In this sense, it was noted that the more copper the material has, the more reducible it is, and, therefore, a higher amount of copper is available to carry out the reaction. Nevertheless, once the 10wt% of Cu is exceeded, part of the copper needs higher temperatures to be reduced (peak at a higher temperature, in Figure 4.29), thereby showing more difficulties to take part in the reaction. Furthermore, the position of this TPR peak, together with the CuO_x nanoparticles seen for the material 12.0%Cu-HT-4 in the HR-TEM measurements (Figure 4.5a), made us think about large CuO_x aggregates as the most probable cause of this behavior[26].

Table 4.11. Quantitative data for temperature programmed desorption (NH_3-TPD and CO_2-TPD) of 5.0%Cu-HT-4 and 10.0%Cu-HT-4 calcined materials.

Catalyst	Acid site density (μmol/g)	Basic site density (μmol/g)	Acid peaks (weak/strong)	Basic peaks (weak/medium)
5.0%Cu-HT-4	87	159	42:58	21:79
10.0%Cu-HT-4	80	165	45:55	33:67

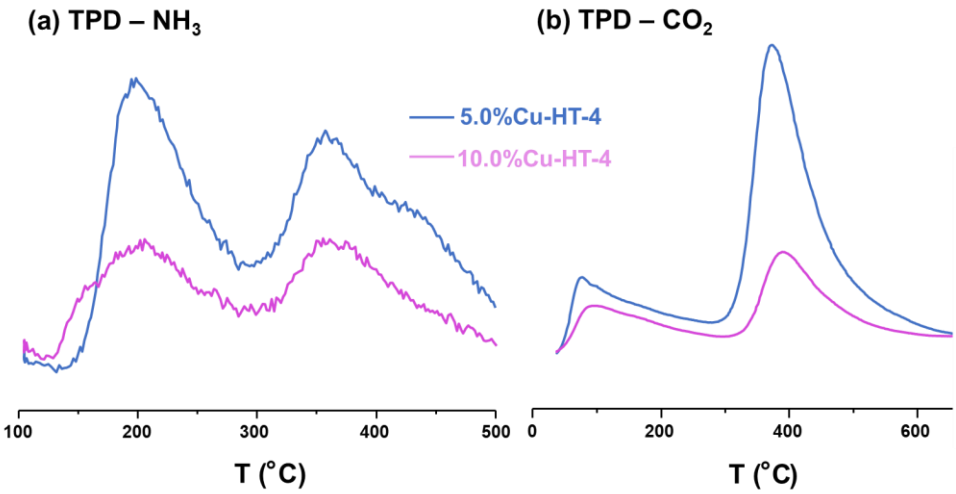

Figure 4.28. NH_3-TPD (a) and CO_2-TPD (b) profiles of Cu-Mg-Al hydrotalcite-derived mixed oxides with different Cu contents. Note: non-calibrated mass-spectrometer (MS); qualitative information about the strength distribution of acid sites.

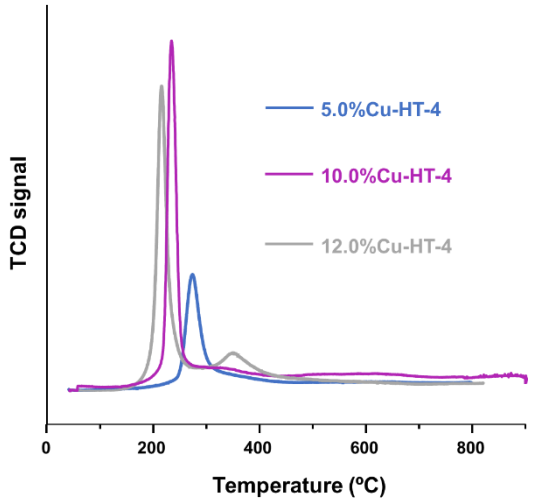

Figure 4.29. TPR traces for 5.0%Cu-HT-4 (green), 10.0%Cu-HT-4 (brown) and 12.0%Cu-HT-4 (blue) samples.

4.3.6. Significance of choosing MeOH as solvent

Results make it necessary to comment that the preference for methanol, although it could be considered arbitrary, is a crucial factor. Evidence up to now indicates that methanol is helping in the reduction of Cu^{2+} to Cu^{1+}, which has already been pointed out as the most active species (see *Sections 4.3.3.2-4*). In fact, the less amount of methanol, the lower extent of this reduction and, therefore, a lower reaction rate is attained. In this sense, several reactions for the selective glycerol dehydration to acetol were carried out to investigate the effects of the presence of water in the feed. Water was added to the GLY/MeOH mixture to assess if it could eventually replace, at least to some extent, the use of MeOH as solvent. Figure 4.30 summarizes glycerol conversion results for various water-MeOH mixtures. The presence of water resulted in a decrease in the amount of glycerol converted. It was also observed that the introduction of water had a significant effect on catalyst stability. Overall, when the catalyst activity reaches a maximum, both glycerol conversion and yield to liquids significantly decrease when even a small quantity of water is in the reaction medium.

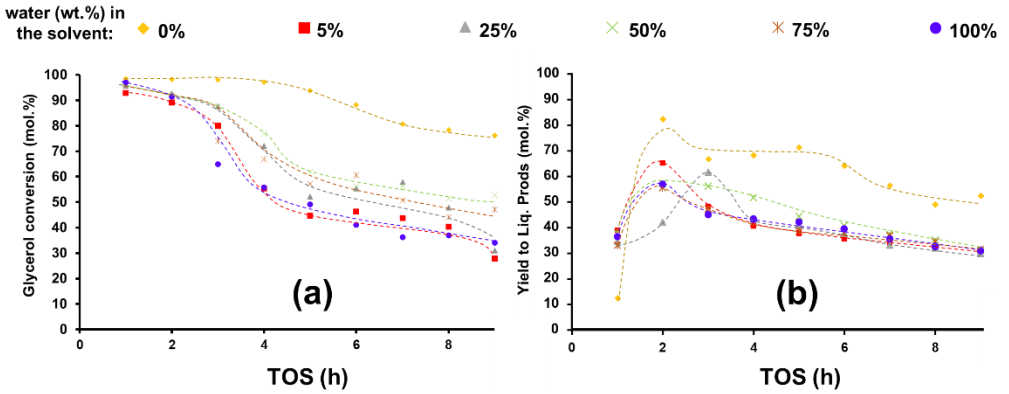

Figure 4.30. (a) Glycerol conversion and (b) yield to liquid products over 5.0%Cu-HT-4 calcined material by feeding the reactor with different MeOH/H_2O ratios. Reaction conditions: Temperature = 240 ºC, flow = 2 mL/h, catalyst: 0.5 g. Note: Dashed traces only serve as visual guidelines.

This phenomenon could be explained by the total or partial absence of methanol and the rehydration of the hydrotalcite-type material[29] when introducing water in the reaction

media. In this situation, water molecules could block acid centers needed for the first glycerol adsorption. Although the formation of the corresponding Cu-Mg-Al hydrotalcite phase could not be detected, even for the reaction carried out in pure water (see Figure 4.31), an experiment with the Cu-Mg-Al hydrotalcite precursor in pure MeOH allows for making sure the much less activity of this precursor (Figure 4.32a) compared to the corresponding mixed oxide (Figure 4.27b). Even when considering the lower amount of copper in the non-calcined material, by representing specific activities normalized by the quantity of copper in the catalyst (Figure 4.32b), the comparison states the better performance of the mixed oxide to the corresponding hydrotalcite. However, another possible source of this decline could be the effect that water could exert on the thermodynamic equilibrium, whose study is beyond the scope of this work.

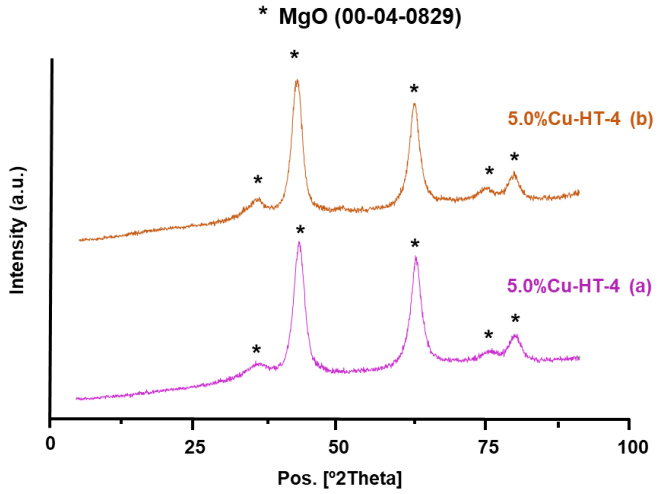

Figure 4.31. XRD patterns of 5.0%Cu-HT-4 materials. (a, green): Material after having been used in catalytic reaction (<u>feed:</u> MeOH/GLY = 90:10 wt.)., (b, blue): Material after having been used in catalytic reaction (<u>feed:</u> of H_2O/GLY = 90:10 wt.).

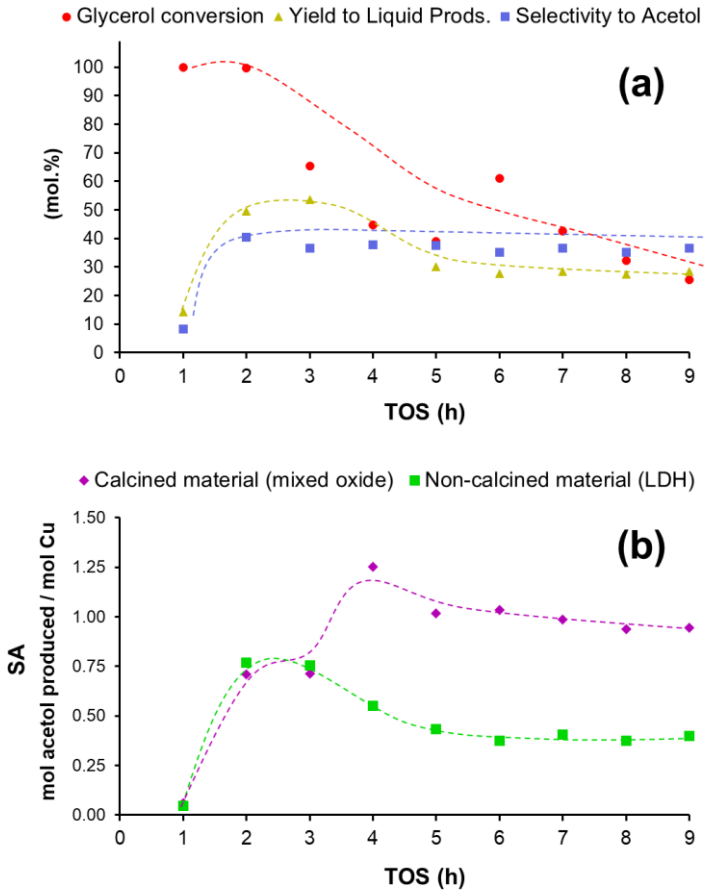

Figure 4.32. (a) Glycerol conversion, yield to liquids and acetol selectivity with TOS over the 10.0%Cu-HT-4s catalyst (hydrotalcite precursor) (b) Specific activity comparison over the 10.0%Cu-HT-4 catalyst before and after calcination. Reaction conditions: feed: MeOH/GLY = 90/10 wt., flow = 2 mL/h, temperature = 240 ºC, catalyst = 0.5 g. *Calculated over the total amount of products in the liquid fraction. Note: Dashed traces only serve as visual guidelines.

4.3.7. Catalyst re-usability

The 10.0%Cu-HT-4 catalyst displayed a high catalytic activity that comes with good selectivity to acetol in the selective dehydration of glycerol in continuous flow fixed bed reactor. Nevertheless, some deactivation was detected over time on stream. Then, the question was whether the Cu-Mg-Al material could be used several times in reaction by

introducing regeneration cycles in-between catalytic cycles. In this sense, catalyst re-cycles were carried out by washing the catalyst used in the reaction with MeOH and then regenerating by using the same calcination procedure used for the fresh material (before its first use). Five consecutive re-uses of the 10%Cu-HT-4 catalyst with the preceding catalyst regenerations in each case were completed under standard reaction conditions for the selective glycerol dehydration, and the attained results are given in Figure 4.33. Basically, both glycerol conversion and selectivity to acetol values remain practically unaltered during the five consecutive catalytic re-uses.

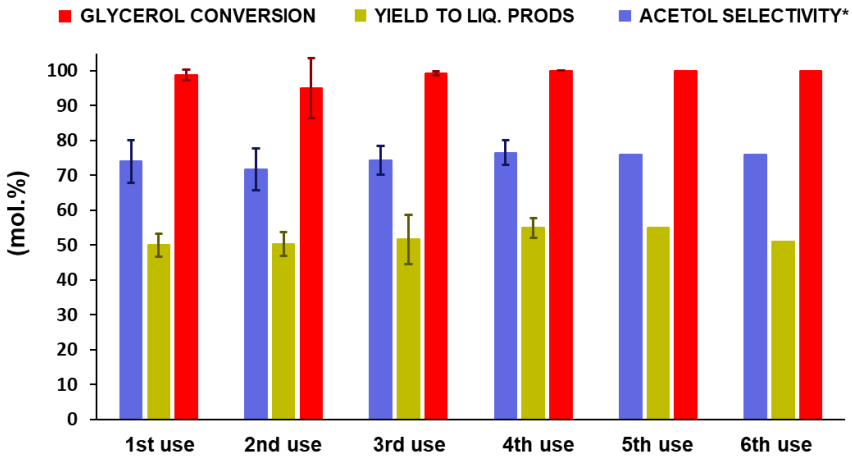

Figure 4.33. Glycerol conversion and acetol selectivity accumulative data during reusability tests of 10.0%Cu-HT-4 catalyst (Average values from several repetitions). Reaction conditions: feed = MeOH/GLY (90/10 in weight), flow = 2 mL/h, with 0.5 g of catalyst at 240 ºC. *Calculated over the total amount of products in the liquid fraction. Note: For uses 5^{th} and 6^{th} only one experiment was carried out, therefore no error bars are presented.

The occurrence of metallic leaching (i.e., Cu, Mg and Al) together with the deposition of carbonaceous compounds during the catalyst re-cycling tests was investigated through further comparative analysis of the catalysts before and after re-uses. Thus, thermogravimetric (TGA) and elemental (EA) analysis, together with ICP and surface area measurements of 5.0%Cu-HT-4 and 10.0%Cu-HT-4 re-used materials, reveal that our Cu-Mg-Al materials are principally deactivated by carbonaceous matter deposition, thus

making possible the recovery of the initial catalytic performance employing a calcination process (see Table 4.12) allowing for cleaning the catalyst surface. Furthermore, no significant metal leaching was detected for both 5.0%Cu-HT-4 and 10.0%Cu-HT-4 catalysts after several re-uses, while after a primary surface area loss during the first use, the surface area values stabilize around 150 m^2/g (Table 4.13). Furthermore, due to the extensively described "memory effect"[29], the rehydration of the calcined hydrotalcite could also have a part in catalytic deactivation. However, a retrotopotactic transformation when feeding the reactor with a mixture containing water (see Figure 4.34) was not noticed, even though water is generated throughout the reaction. However, this phenomenon occurring just at the catalyst surface, thus not being detected by bulk techniques, cannot be discarded. By XRD measurements, the only structural difference observed after reaction is the formation of a minimal amount of CuO, probably originating from the mixed oxide phase and sintering during the reaction (see Figure 4.34). Nevertheless, this effect does not impair the re-usability of the material. All these findings lead us to conclude that the carbonaceous compounds deposition on the solid surface could be considered, at this stage, as the leading cause of catalyst deactivation in this process.

Table 4.12. Results of elemental (EA) and thermogravimetric (TGA) analysis of Cu-Mg-Al materials after reaction and further regeneration (550 ºC, 6 h, air).

Catalyst	***%C/ After reaction***	***%C/ After regeneration***
5.0%Cu-HT-4	12.1 (22.3[a])	1.6
10.0%Cu-HT-4	16.2 (27.3[a])	1.5

[a] Total amount of carbonaceous matter on the catalytic surface (measured by TGA).

Table 4.13. Surface area and metallic content evolution over several catalytic cycles of Cu-Mg-Al materials.

Catalyst	Surface area (m^2/g)			Cu (wt%)[a]		Mg (wt%)[a]		Al (wt%)[a]	
	Before react.	*After 1 react.*	*After 2 react.*	Before used	After used	Before used	After used	Before used	After used
5.0%Cu-HT-4	205	172	-	4.7	4.7	43.9	42.1	12.1	11.9
10.0%Cu-HT-4	192	153	150	9.9	9.6	41.7	39.7	12.1	11.7

[a] Before reaction and after 24 h on continuous stream for Cu-HT-4 type catalyst.

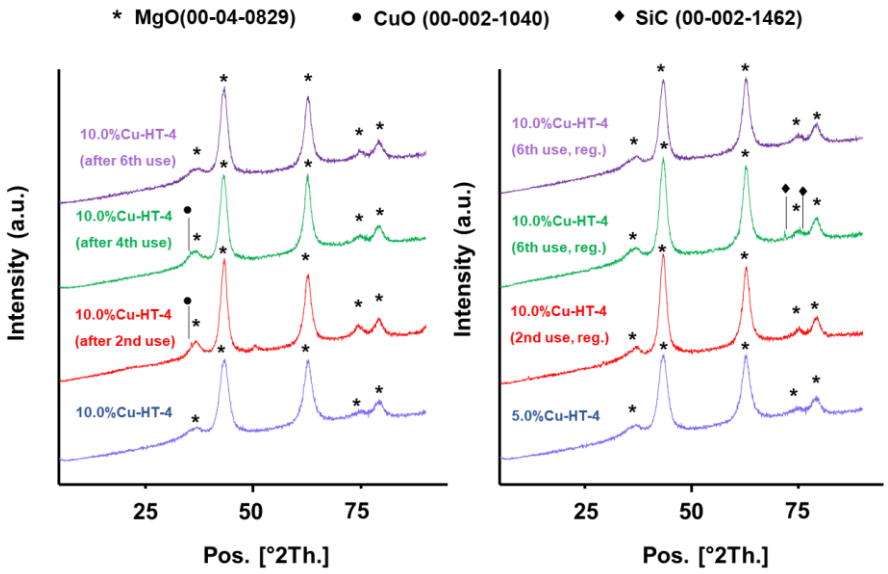

Figure 4.34. XRD patterns of 10.0%Cu-HT-4 materials. (a): Materials after having been used in catalytic reaction (b): Materials after having been used in catalytic reaction and regenerated.

In summary, the 10.0%Cu-HT-4 catalyst has been demonstrated to be an efficient and reusable catalyst for the selective dehydration of glycerol to acetol. Catalyst deactivation mainly due to the carbonaceous compounds deposition during reaction could be overcome

by thermal regeneration of the material, thus allowing performing several consecutive use/regeneration cycles of the Cu-Mg-Al catalyst without significant loss in the acetol yield.

4.3.8 Effect of doping elements in Cu-Mg-Al mixed oxides

4.3.8.1 First catalytic screening

After Cu-Mg-Al proved to be highly active, selective, and re-usable in the selective dehydration of glycerol in a continuous flow fixed bed reactor, the introduction of other metals during the synthesis of 10.0%Cu-HT-4 was essayed. Consequently, different doping metals (Co, Fe, Ga, La, Ni, Zn) were incorporated in the range of 1.0 to 2.0 wt.% in the 10%Cu-HT-4 sample (see Table 4.4). Then, the effect on the catalytic dehydration of glycerol was evaluated over these materials, with results shown in Figure 4.35. A slight improvement in acetol yield was observed when introducing gallium and zinc, while a significant amelioration was attained when adding a small amount of nickel or iron. However, Zn offers a higher risk of leaching compared to the others[30]. Consequently, the research mainly focused on Fe, Ga, Ni to continue studying.

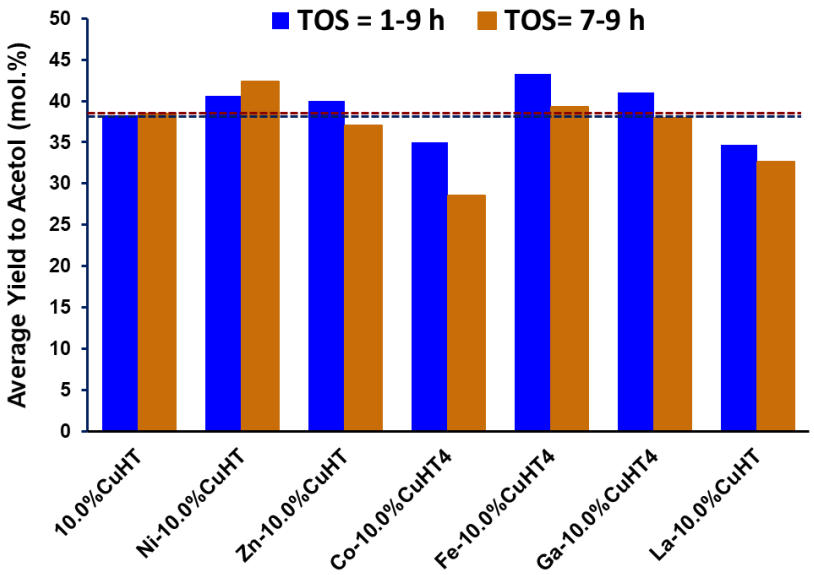

Figure 4.35. Effect of introducing other metals on the catalytic performance. Reaction conditions: feed = MeOH/GLY (90/10 in weight), flow = 2 mL/h, with 0.5 g of catalyst at 240 ^{o}C.

The introduction of auxiliary metals in Cu-HT-4 is expected to influence the acid-base properties of the mixed oxide, the copper reducibility, and the resistance to the already mentioned "memory effect". For instance, the systems ZnAl- and MgGa-LDHs have been reported to offer broader acidity than their analogous MgAl counterparts[4]. Also, the presence of small Ga_2O_3 nanoparticles may favor generating an intermediate state of copper between Cu^0 and Cu^{2+}[31,32]. In the case of Ni, it has been described that hydrotalcite type materials based on Ni display an increased proportion of strong acid sites, and a declining number of basic sites[33]. Last, as for Fe, in addition to the already known synergy for the redox couple Fe/Cu[34], Pavel *et al.*[35] described a MgFeAl mixed oxide showing an increase in the total number of acid sites due to the appearance of a separated spinel or Fe_2O_3 phase. On the contrary, León *et al.*[36] reported a MgFe mixed oxide with Mg/Fe molar ratio close to 3 with negligible ammonia adsorption. The authors associated this low acidity value with Fe^{3+} ions difficulty occupying a tetrahedral site because of its larger ionic radius.

Therefore, the metal-doped mixed oxides (M-Cu-Mg-Al) were further characterized by FTIR, TPD (NH_3), TPR, and XRD measurements to fully understand the effect of each one of these additions on the physicochemical properties of the original material 10.0%Cu-HT-4.

4.3.8.2 Acid-base properties after doping

The effect that the tiny amount of dopant could exert on the acid-base properties of the original 10.0%Cu-HT-4 was believed to be minimal. Consequently, FTIR with CO and $CHCl_3$ as probe molecules was a highly sensitive technique chosen to analyze these minor modifications on the acid and basic sites, respectively.

As far as basicity is concerned, no significant changes could be noted when introducing the dopants (see $CHCl_3$ FTIR spectra at *Annex*, Figure A7). Nonetheless, the FTIR measures using CO as the probe molecule established differences between the samples in terms of their acidity. Interestingly, after normalization, a second, less significant contribution to the Lewis acidity could be detected in those samples having an additional metal (Contribution **1**, in Figure 4.36). Unfortunately, the assignment and quantification of these two bands is highly risky and, therefore, NH_3-TPD analyses were carried out to

quantify and qualitatively ascertain the effect of this modification in the acid strength and distribution.

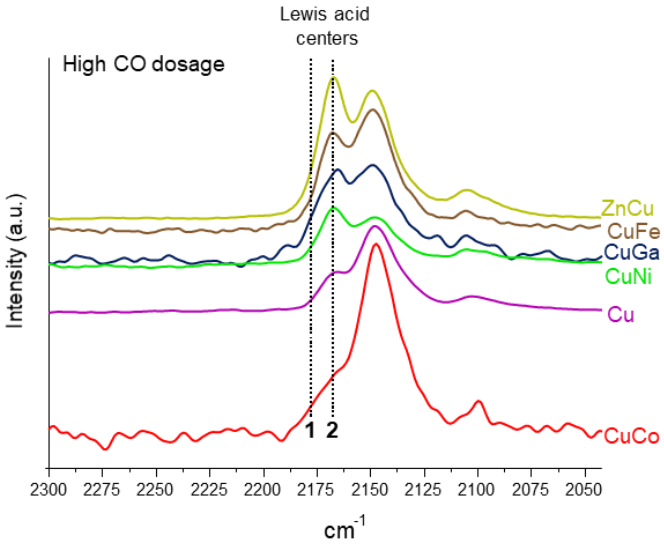

Figure 4.36. IR spectra of CO adsorption at 25 ºC and saturation coverage for M-Cu-Mg-Al mixed oxides.

NH_3-TPD analyses of the doped materials show that the dopant contribution to the acidity is nowhere near to be negligible. Table 4.14 and Figure 4.37 expose that the addition of the auxiliary metal makes a difference in the number and distribution of the acid sites. As already postulated, the first glycerol adsorption could be ascribed to the weak acidity (peak between 150 and 250 ºC), which is the only one common to all the active materials so far reported in this thesis. As a remarkable fact, Co-10.0%Cu-HT-4 is the only material whose weak acidity is equal to or below the reference material 10.0%Cu-HT-4, which is in line with the impaired specific activity seen for this material in Figure 4.35. Interestingly, for the rest of the analyzed materials (GaCu, FeCu, NiCu) the weak acidity is more significant than that exhibited by the reference material, which also aligns with the higher yield to acetol (Figure 4.35). Therefore, these results suggest enhanced glycerol adsorption could arise when introducing some doping agents, which is a plausible explanation for the slightly superior acetol production.

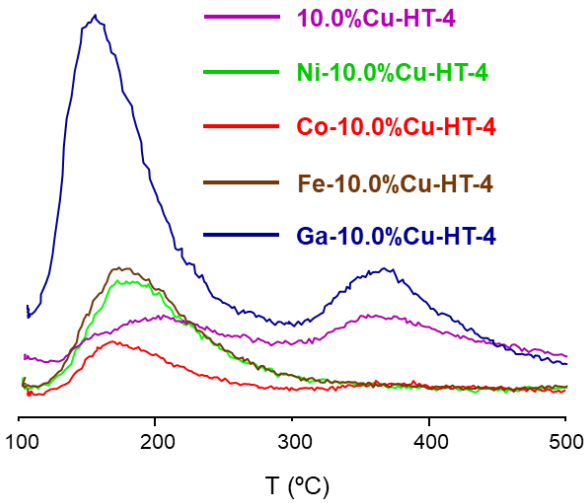

Figure 4.37. NH_3-TPD of M-Cu-Mg-Al hydrotalcite-derived mixed oxides. Note: non-calibrated mass-spectrometer (MS); qualitative information about the strength distribution of acid sites.

Table 4.14. Quantitative data for temperature programmed desorption (NH_3-TPD) of M-Cu-Mg-Al HT-derived materials.

Catalyst	Acid site density (μmol/g)	Acid sites (weak/medium)
10.0%Cu-HT-4	80	45:55
Ni-10.0%Cu-HT-4	98	100:0
Co-10.0%Cu-HT-4	56	83:17
Fe-10.0%Cu-HT-4	107	100:0
Ga-10.0%Cu-HT-4	182	74:26

4.3.8.3 Redox properties after doping

As already seen throughout this chapter, the nature of copper species generated during the reaction as well as the reducibility of the starting Cu(II), are key parameters that determine the catalyst behavior. In that sense, temperature-programmed reduction (TPR) experiments were carried out to check whether the enhancement in the yield to acetol seen for some of the doped samples could be associated with improved reducibility. Remarkably, for those doped samples showing the best results (Ni, Fe, Ga), a reduction temperature equal or below to that of 10.0%Cu-HT-4 was detected (Figure 4.38). This finding might be unraveling easier active species generation throughout the reaction. In this line, XPS measurements were carried out on the catalyst 10.0%Cu-HT-4 and Fe-10.0%Cu-HT-4 at several times on stream (Figure 4.39). Importantly, the samples after reaction did not have contact with atmospheric air before being analyzed so that the changes in the reduction state of Cu with respect to the fresh material can be ascribed to the catalytic process exclusively.

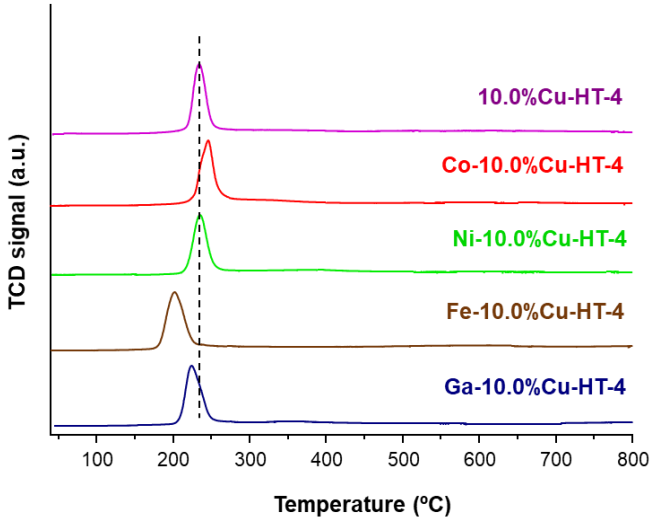

Figure 4.38. TPR traces for Cu-Mg-Al samples containing different doping elements.

The interpretation of the XPS is not straightforward due to the coexistence of different copper species, such as Cu(II), Cu(I)/(0), and some Cu(0) that seems to be differentially charged, probably associated with the formation of Cu^0 nanoparticles. Nevertheless, interestingly, the absence of this copper differentially charged in the Fe-10.0%Cu-HT-4

sample might be suggesting Fe plays a role as a redox promoter, acting as a stabilizer of the Cu active species. However, since a significant part of Cu(0) can also photoemit at the same B.E. as Cu(I), each try to ascertain if the catalyst generates more Cu(I) when iron is present, shall remain as a mere suggestion.

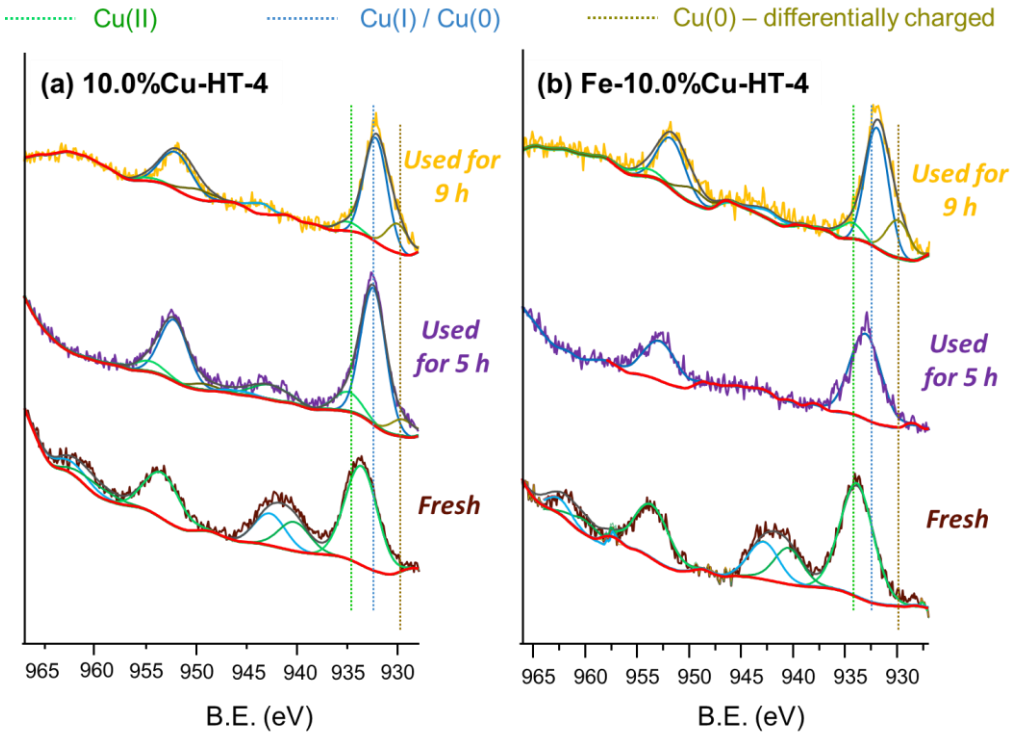

Figure 4.39. XPS data of (a) 10.0%Cu-HT-4, (b) 1.5Fe-10.0%Cu-HT-4 fresh materials and after having been used for several hours in the selective dehydration of glycerol to acetol.

Table 4.15. XPS data of the $Cu2p_{3/2}$ core level and Cu species distribution at the surface. (AlK_{α} source).

Catalyst	Cu ($2p_{3/2}$)				α^*
	B.E. (eV)				(eV)
	Cu^{2+}	$Cu^{1+/0}$	Cu^0	s/m*	
10.0%Cu-HT-4	933.6	-	-	0.59	1850.2
Fe-10.0%Cu-HT-4	933.9	-	-	0.55	1850.1
10.0%Cu-HT-4-used(5h)[a]	934.9	932.4	929.5	0.16	1848.8
Fe-10.0Cu-HT-used(5h)[a]	-	933.0		0	1848.9
10.0%Cu-HT-4-used(9h)[b]	935.1	932.2	930.0	0	1849.1
Fe-10.0%Cu-HT-4-used(9h)[b]	934.5	932.0	929.9	0.05	1849.5

*$Cu2p_{3/2}$ XPS (BE) + $L_3M_{45}M_{45}$ CuAES (KE).

[a]Auger parameter calculated by changing to a Mg anode.

[b] Fully analyzed with a Mg anode.

Despite the XPS results show a different distribution of copper species, thus revealing that Fe is modifying the copper redox activity, the ambiguity of the data does not allow for an explicit quantification of the exposed Cu(I) active species. With this objective, CO adsorption at low temperature was followed by FTIR after a catalyst pre-treatment with the reaction solvent (i.e., MeOH). After spectra deconvolution (see *Annex*, Figure A8) and mass normalization, Figure 4.40 shows the Cu^{1+} data in each catalyst. The enclosed comparison indicates that those materials achieving higher acetol yields (NiCu, NiFe and NiGa) can keep higher amounts of Cu as Cu^{1+} at working conditions.

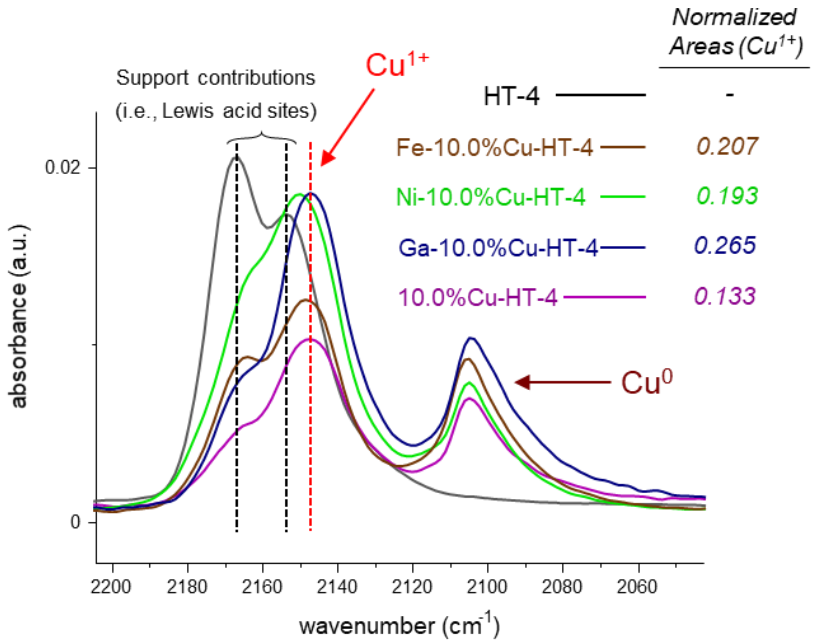

Figure 4.40. IR spectra of CO low temperature adsorption at saturation coverage normalized to sample weight on several M-10.0%Cu-HT-4 samples after a pre-treatment with 0.1 mbar of MeOH (240 ºC, 30 minutes).

4.3.8.4 Endurance to retrotopotactic transformation after doping

Because of water produced during the reaction, the mixed oxide can turn back to its hydrotalcite form, which has been found to be less active (see Figure 4.32). In this context, it has been reported that the presence of di- and tri-valent metals different from Mg and Al can influence this so-called "memory effect", usually reducing the rate at which this process occurs[37,38]. Aiming at studying this effect, the mixed oxides showing better results than the reference material 10.0%Cu-HT-4 were rehydrated with several amounts of water to force this memory effect and establish a comparison with the non-doped sample. The XRD patterns after rehydration and its comparison with the corresponding starting mixed oxide are shown in Figures 4.41-44. Interestingly, the XRD patterns for the mixed oxides containing an additional doping element (i.e., Ga, Ni, Fe) qualitatively show that the rehydration is occurring to less extent, this meaning a higher resistance to the retrotopotactic transformation. Therefore, another useful feature of the dopant that could be having a positive effect on the catalytic performance is the preservation of the mixed oxide

structure during the catalytic process, thereby preventing it to be rehydrated, with the consequent activity loss.

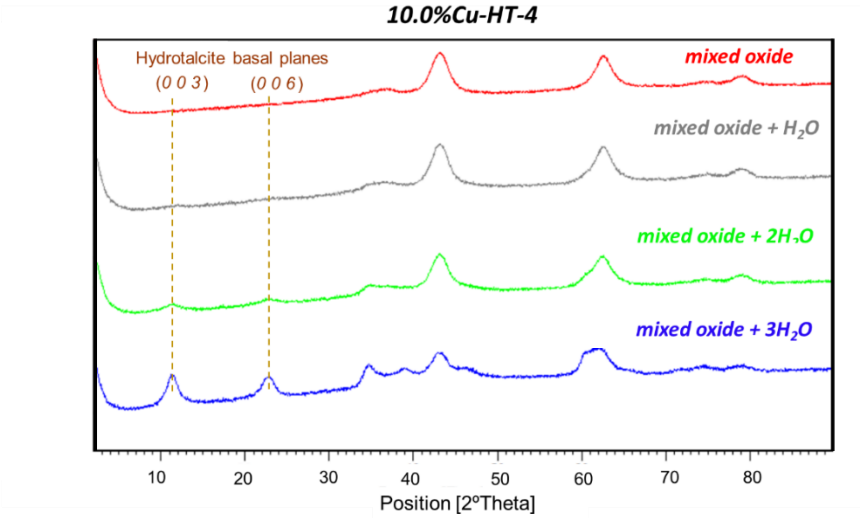

Figure 4.41. XRD patterns of hydrotalcite-derived mixed oxides 10.0%Cu-HT-4 after being rehydrated with different equivalents of water. Note: An equivalent of water corresponds to that amount formed per g of catalyst when achieving a 40% yield to acetol (Feed: MeOH/Gly =9:1, TOS = 9 h).

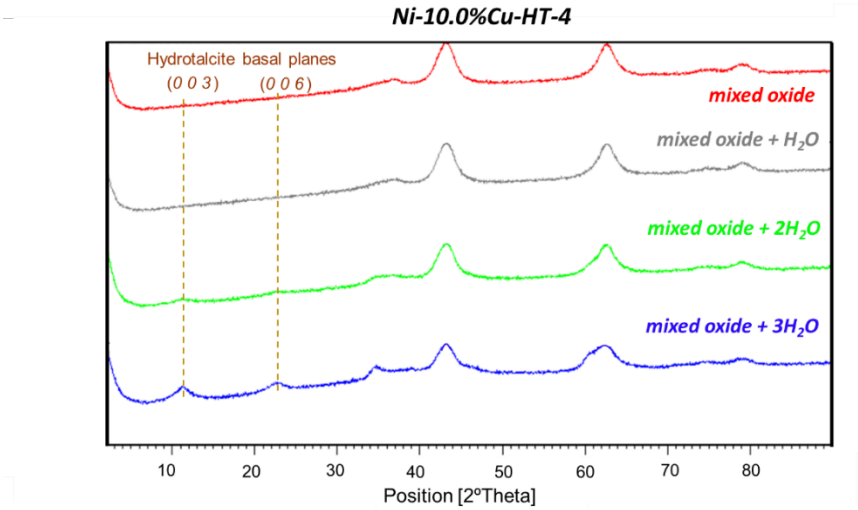

Figure 4.42. XRD patterns of hydrotalcite-derived mixed oxides Ni-10.0%Cu-HT-4 after being rehydrated with different equivalents of water. Note: An equivalent of water corresponds to that amount formed per g of catalyst when achieving a 40% yield to acetol (Feed: MeOH/Gly =9:1, TOS = 9 h).

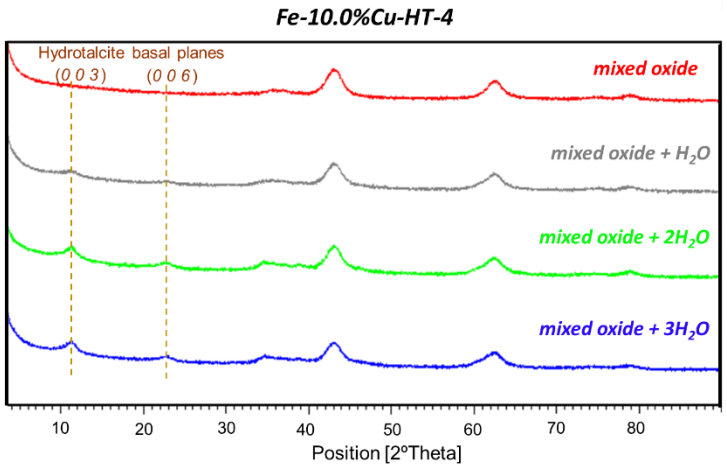

Figure 4.43. XRD patterns of hydrotalcite-derived mixed oxides Fe-10.0%Cu-HT-4 after being rehydrated with different equivalents of water. Note: An equivalent of water corresponds to that amount formed per g of catalyst when achieving a 40% yield to acetol (Feed: MeOH/Gly =9:1, TOS = 9 h).

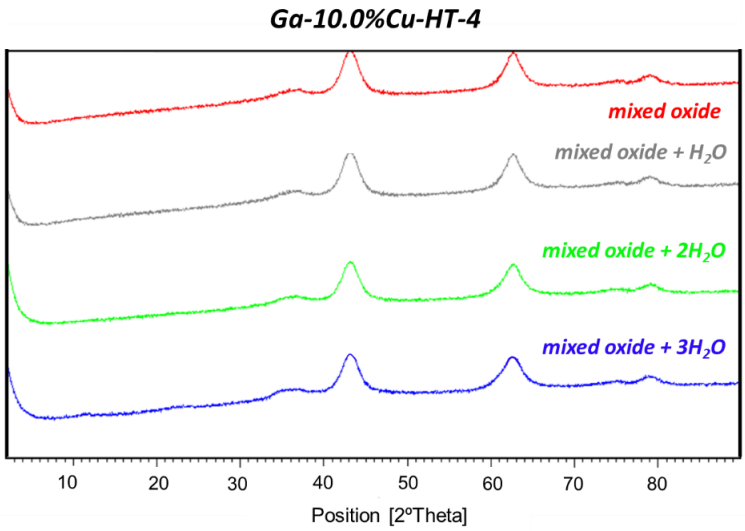

Figure 4.44. XRD patterns of hydrotalcite-derived mixed oxides Ga-10.0%Cu-HT-4 after being rehydrated with different equivalents of water. Note: An equivalent of water corresponds to that amount formed per g of catalyst when achieving a 40% yield to acetol (Feed: MeOH/Gly =9:1, TOS = 9 h).

4.4 Conclusions

- A glycerol surplus from biodiesel production can be transformed into acetol in a continuous flow fix-bed reactor using environmentally friendly Cu-based mixed oxides derived from hydrotalcites as catalysts.
- The 10.0%Cu-HT-4 catalyst offered ≈55% acetol selectivity at >90% glycerol conversion (≈80% yield to liquids), remaining stable for 9 h. Remarkably, the catalyst could be regenerated by calcination, achieving full activity recovery after five re-cycles.
- Valuable contributions to understanding the reaction mechanism have been made; finding that copper is essential for a high reaction rate glycerol dehydration to

acetol. The preferred generation of an intermediate with C=O instead of the C=C group makes this metal different from Co/Ni.

- A combination of well-selected catalytic experiments together with *in-situ* XPS and FTIR measurements allowed us to conclude that Cu^{1+} are the most active Cu species present in the catalyst. These species are generated at the beginning of the reaction by reducing Cu^{2+} species. However, minor contributions to the reaction of the other two Cu-species (Cu^0 and Cu^{2+}) cannot be discarded.

- The role of weak acid sites seems to be related to providing anchoring sites for glycerol adsorption. Then, once copper has interacted with the molecule, through a (hypothetic) hydride abstraction, and the intermediate containing a C=O group is generated, an acid/base interaction (not entirely ascertained yet) onto the catalyst surface could facilitate the final generation of acetol.

- Interestingly, acetol yield could be slightly improved by introducing other doping metals such as Fe, Ni or Ga. These three metals increase the number of weak acid sites necessary for glycerol adsorption, facilitate the stabilization of the Cu^{1+} active species, and prevent the mixed oxide from going back to its hydrotalcite precursor, found to be less active.

4.5 References

[1] W.T. Reichle, Synthesis of anionic clay minerals (mixed metal hydroxides, hydrotalcite), Solid State Ionics. 22 (1986) 135–141. https://doi.org/10.1016/0167-2738(86)90067-6.

[2] J.I. Di Cosimo, V.K. Díez, M. Xu, E. Iglesia, C.R. Apesteguía, Structure and Surface and Catalytic Properties of Mg-Al Basic Oxides, J. Catal. 178 (1998) 499–510. https://doi.org/10.1006/JCAT.1998.2161.

[3] B.F. Sels, D.E. De Vos, P.A. Jacobs, Hydrotalcite-like anionic clays in catalytic organic reactions, Catal. Rev. - Sci. Eng. 43 (2001) 443–488. https://doi.org/10.1081/CR-120001809.

[4] Y. Song, S.K. Beaumont, X. Zhang, K. Wilson, A.F. Lee, Catalytic applications of layered double hydroxides in biomass valorisation, Curr. Opin. Green Sustain. Chem. 22 (2020) 29–38. https://doi.org/10.1016/J.COGSC.2019.11.005.

[5] R. L. Manfro, T.P.M. D. Pires, N.F. P. Ribeiro, M.M. V. M. Souza, Aqueous-phase reforming of glycerol using Ni–Cu catalysts prepared from hydrotalcite-like precursors,

Catal. Sci. Technol. 3 (2013) 1278-1287. https://doi.org/10.1039/C3CY20770F.

[6] M. Araque, L.M. Martínez T, J.C. Vargas, M.A. Centeno, A.C. Roger, Effect of the active metals on the selective H2 production in glycerol steam reforming, Appl. Catal. B Environ. 125 (2012) 556-566. https://doi.org/10.1016/J.APCATB.2012.06.028.

[7] A.A. Davydov, A.A. Budneva, IR spectra of CO and NO adsorbed on CuO, React. Kinet. Catal. Lett. 25 (1984) 121–124. https://doi.org/10.1007/BF02076552.

[8] S. Bordiga, C. Pazé, G. Berlier, D. Scarano, G. Spoto, A. Zecchina, C. Lamberti, Interaction of N2, CO and NO with Cu-exchanged ETS-10: a compared FTIR study with other Cu-zeolites and with dispersed Cu2O, Catal. Today. 70 (2001) 91-105. https://doi.org/10.1016/S0920-5861(01)00410-2.

[9] F. Cavani, F. Trifiro, A.V.-C. today, undefined 1991, Hydrotalcite-type anionic clays: Preparation, properties and applications, Catal. Today. 11 (1991) 173-301. https://doi.org/10.1016/0920-5861(91)80068-K

[10] J. Shen, M. Tu, C.H.-J. of S.S. Chemistry, undefined 1998, Structural and surface acid/base properties of hydrotalcite-derived MgAlO oxides calcined at varying temperatures, J. Solid State Chem. 137 (1998) 295-301. https://doi.org/10.1006/jssc.1997.7739

[11] D. Yuan, X. Li, Q. Zhao, J. Zhao, S. Liu, M. Tadé, Effect of surface Lewis acidity on selective catalytic reduction of NO by C3H6 over calcined hydrotalcite, Appl. Catal. A Gen. 451 (2013) 176-183. https://doi.org/10.1016/J.APCATA.2012.11.001.

[12] M. Trombetta, G. Ramis, G. Busca, B. Montanari, A. Vaccari, Ammonia Adsorption and Oxidation on Cu/Mg/Al Mixed Oxide Catalysts Prepared via Hydrotalcite-Type Precursors, Langmuir. 13 (1997) 4628-4637. https://doi.org/10.1021/LA960673O.

[13] M.D. Romero, J.A. Calles, M.A. Ocaña, J.M. Gómez, Epoxidation of cyclohexene over basic mixed oxides derived from hydrotalcite materials: Activating agent, solvent and catalyst reutilization, Microporous Mesoporous Mater. 111 (2008) 243-253. https://doi.org/10.1016/J.MICROMESO.2007.07.041.

[14] B. Sels, D. De Vos, P.J.-C. Reviews, undefined 2001, Hydrotalcite-like anionic clays in catalytic organic reactions, Taylor Fr. 43 (2007) 443-488. https://doi.org/10.1081/CR-120001809.

[15] I. Popescu, N. Tanchoux, D. Tichit, I.C. Marcu, Total oxidation of methane over supported CuO: Influence of the MgxAlyO support, Appl. Catal. A Gen. 538 (2017) 81-90. https://doi.org/10.1016/J.APCATA.2017.03.012.

[16] P. Lauriol-Garbay, J.M.M. Millet, S. Loridant, V. Bellire-Baca, P. Rey, New efficient and long-life catalyst for gas-phase glycerol dehydration to acrolein, J. Catal. 280 (2011) 68-76. https://doi.org/10.1016/J.JCAT.2011.03.005.

[17] S. Mészáros, J. Halász, Z. Kónya, P. Sipos, I. Pálinkó, Reconstruction of calcined MgAl- and NiMgAl-layered double hydroxides during glycerol dehydration and their recycling characteristics, Appl. Clay Sci. 80-81 (2013) 245-248. https://doi.org/10.1016/j.clay.2013.04.010.

[18] A. Lähde, R.J. Chimentão, T. Karhunen, M.G. Álvarez, J. Llorca, F. Medina, J. Jokiniemi, L.B. Modesto-López, Co-Al spinel-based nanoparticles synthesized by flame spray pyrolysis for glycerol conversion, Adv. Powder Technol. 28 (2017) 3296–3306. https://doi.org/10.1016/J.APT.2017.10.009.

[19] R.B. Mane, C. V. Rode, Simultaneous glycerol dehydration and in situ hydrogenolysis

over Cu-Al oxide under an inert atmosphere, Green Chem. 14 (2012) 2780-2789. https://doi.org/10.1039/c2gc35661a.

[20] A. Bienholz, H. Hofmann, P. Claus, Selective hydrogenolysis of glycerol over copper catalysts both in liquid and vapour phase: Correlation between the copper surface area and the catalyst's activity, Appl. Catal. A Gen. 391 (2011) 153–157. https://doi.org/10.1016/J.APCATA.2010.08.047.

[21] W. Grünert, N.W. Hayes, R.W. Joyner, E.S. Shpiro, M. Rafiq, H. Siddiqui, G.N. Baeva5, Structure, Chemistry, and Activity of Cu-ZSM-5 Catalysts for the Selective Reduction of NO* * in the Presence of Oxygen, J. Phys. Chem. 98 (1994) 10832–10846.

[22] P. Keil, D. Lützenkirchen-Hecht, R. Frahm, Investigation of Room Temperature Oxidation of Cu in Air by Yoneda-XAFS, AIP Conf. Proc. 882 (2007) 490. https://doi.org/10.1063/1.2644569.

[23] L. Chmielarz, P. Kuśtrowski, A. Rafalska-Łasocha, R. Dziembaj, Influence of Cu, Co and Ni cations incorporated in brucite-type layers on thermal behaviour of hydrotalcites and reducibility of the derived mixed oxide systems, Thermochim. Acta. 395 (2002) 225-236. https://doi.org/10.1016/S0040-6031(02)00214-9.

[24] S. Kannan, A. Dubey, H. Knozinger, Synthesis and characterization of CuMgAl ternary hydrotalcites as catalysts for the hydroxylation of phenol, J. Catal. 231 (2005) 381-392. https://doi.org/10.1016/J.JCAT.2005.01.032.

[25] G. Fierro, M. Lo Jacono, M. Inversi, P. Porta, R. Lavecchia, F. Cioci, A Study of Anomalous Temperature-Programmed Reduction Profiles of Cu2O, CuO, and CuO-ZnO Catalysts, J. Catal. 148 (1994) 709-721. https://doi.org/10.1006/JCAT.1994.1257.

[26] A. Alejandre, F. Medina, P. Salagre, X. Correig, J. E. Sueiras, Preparation and Study of Cu−Al Mixed Oxides via Hydrotalcite-like Precursors, Chem. Mater. 11 (1999) 939-948. https://doi.org/10.1021/CM980500F.

[27] S. Célerier, S. Morisset, I. Batonneau-Gener, T. Belin, K. Younes, C. Batiot-Dupeyrat, Glycerol dehydration to hydroxyacetone in gas phase over copper supported on magnesium oxide (hydroxide) fluoride catalysts, Appl. Catal. A Gen. 557 (2018) 135-144. https://doi.org/10.1016/j.apcata.2018.03.022.

[28] K.I. Hadjiivanov, G.N. Vayssilov, Characterization of Oxide Surfaces and Zeolites by Carbon Monoxide as an IR Probe Molecule, Adv. Catal. 47 (2002) 307–511.

[29] S. Miyata, Physico-Chemical Properties of Synthetic Hydrotalcites in Relation to Composition, Clays Clay Miner. 1980 281. 28 (1980) 50–56. https://doi.org/10.1346/CCMN.1980.0280107.

[30] W.Y. Hernández, F. Aliç, A. Verberckmoes, P. Van Der Voort, Tuning the acidic–basic properties by Zn-substitution in Mg–Al hydrotalcites as optimal catalysts for the aldol condensation reaction, J. Mater. Sci. 2016 521. 52 (2016) 628–642. https://doi.org/10.1007/S10853-016-0360-3.

[31] J. Toyir, P. Ramírez De La Piscina, J.L.G. Fierro, N. Homs, Highly effective conversion of CO2 to methanol over supported and promoted copper-based catalysts: influence of support and promoter, Appl. Catal. B Environ. 29 (2001) 207–215. https://doi.org/10.1016/S0926-3373(00)00205-8.

[32] R. Zhang, H. You, D. Wu, Advanced treatment of coking wastewater by heterogeneous photo-Fenton technology with Cu/Fe oxide catalysts, New Pub Balaban. 57 (2015)

12010-12018. https://doi.org/10.1080/19443994.2015.1048535.

[33] W. Gac, Acid–base properties of Ni–MgO–Al2O3 materials, Appl. Surf. Sci. 257 (2011) 2875-2880. https://doi.org/10.1016/J.APSUSC.2010.10.084.

[34] Z. Han, Y. Dong, S. Dong, Copper–iron bimetal modified PAN fiber complexes as novel heterogeneous Fenton catalysts for degradation of organic dye under visible light irradiation, J. Hazard. Mater. 189 (2011) 241-248. https://doi.org/10.1016/J.JHAZMAT.2011.02.026.

[35] O.D. Pavel, D. Tichit, I.C. Marcu, Acido-basic and catalytic properties of transition-metal containing Mg–Al hydrotalcites and their corresponding mixed oxides, Appl. Clay Sci. 61 (2012) 52-58. https://doi.org/10.1016/J.CLAY.2012.03.006.

[36] M. León, E. Díaz, A. Vega, S. Ordóñez, A. Auroux, Consequences of the iron–aluminium exchange on the performance of hydrotalcite-derived mixed oxides for ethanol condensation, Appl. Catal. B Environ. 102 (2011) 590-599. https://doi.org/10.1016/J.APCATB.2010.12.044.

[37] Javier Pérez-Ramírez, and Sònia Abelló, N.M. van der Pers, Influence of the Divalent Cation on the Thermal Activation and Reconstruction of Hydrotalcite-like Compounds, J. Phys. Chem. C. 111 (2007) 3642-3650. https://doi.org/10.1021/JP064972Q.

[38] S.N. Golovin, M.N. Yapryntsev, I.G. Ryl'tsova, S. V. Savilov, K.I. Maslakov, O.E. Lebedeva, Synthesis and thermal behavior of Co/AlCe layered double hydroxide, Solid State Sci. 111 (2021) 106498. https://doi.org/10.1016/J.SOLIDSTATESCIENCES.2020.106498.

Chapter 5
Copper oxide supported on metal oxides as catalysts for the selective glycerol dehydration to acetol

5.1 Introduction

In the previous *Chapter 4*, Cu-Mg-Al catalysts have been developed and their catalytic activity in the selective glycerol dehydration fully investigated. Unfortunately, although Cu-based materials derived from hydrotalcites proved to be helpful materials to study, understand and carry out the selective dehydration of glycerol to acetol, they were limited to work at a particular operative window. In fact, when increasing the glycerol concentration in the feed, an arbitrarily selected CuO/Al_2O_3 (with 5wt% Cu), showed better results in terms of stability than the two best optimized catalysts 10.0%Cu-HT-4 and Fe-10.0%Cu-HT-4 (Figure 5.1). Probably, when adding more glycerol per time unit in the reactor, either the need to have many more acid sites to enable glycerol adsorption or the quantity of by-products formed at basic sites become more critical. Moreover, the low resistance of these catalysts to the presence of water in the feed has been notoriously observed, which also impairs catalytic performance when aiming at producing more acetol per time unit and, therefore, more water.

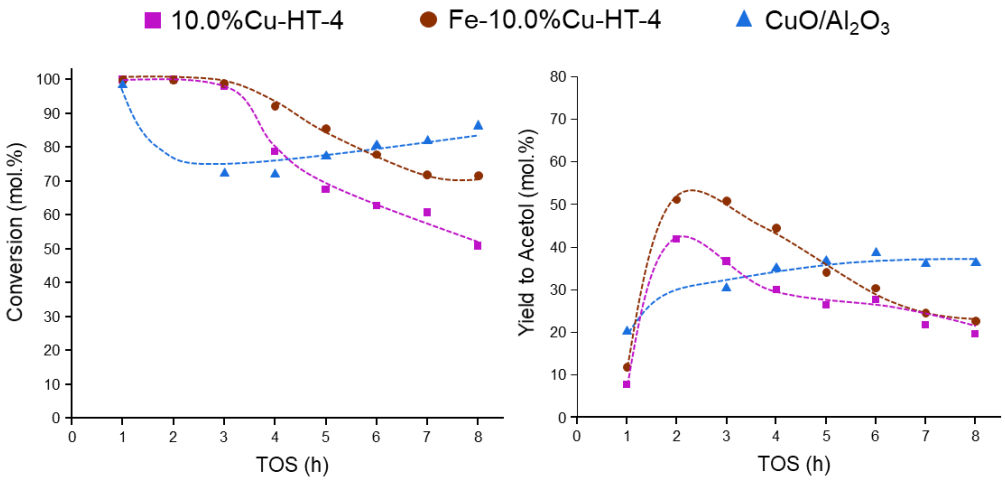

Figure 5.1. Catalytic performance of hydrotalcite-derived catalysts with 10.0 wt.% Cu compared to CuO/Al_2O_3. Reaction conditions: feed = MeOH/GLY (80/20 in weight), flow = 2 ml/h, with 0.5 g of catalyst at 240 ºC. Note: Dashed traces only serve as visual guidelines.

In that context, it was highly desirable to continue the lookout for materials providing enough acidity to allow for working with high glycerol concentrations, thereby enhancing

acetol productivity. All this bearing in mind the subsequent synthesis of N-heterocycles from this chemical.

Consequently, the idea was to design copper oxide supported catalysts. Supported catalysts are an alternative to overcome the surface limitation that certain materials inherently present or that they acquire after thermal treatment. They consist of a support with a high surface area, greater temperature resistance, and active surface species (metal oxides, metals, exchanged ions, anchored molecules…). On certain occasions, a support may modify the catalytic action of the active species through what is called "strong metal-support interactions" (SMSI) or can even act as a co-catalyst. The main reason to consider using this type of catalyst is the better dispersion of active centers to other heterogeneous catalysts, which positively influences activity and selectivity and increases the stability of the active phase[1].

The synthesis of supported catalysts consists of preparing the support (usually an inorganic oxide or an organic polymer), then incorporating the active phase precursor and, finally, a thermal process of catalyst activation (i.e., calcination, pyrolysis, reduction, among others). In our case, the incipient wetness impregnation method will be normally preferred to incorporate the precursor. Therefore, the synthesis of our CuO supported catalysts will consist of activating the support (inorganic oxide) at 250 ºC under an air flow, then incorporating the proper mass of active phase precursor dissolved in the amount of water required to fill the material total pore volume, a drying step and, finally, a thermal catalyst activation (calcination in air).

Hence, the objective pursued throughout this chapter was selecting, understanding, and optimizing a highly active catalyst to carry out the selective glycerol dehydration to acetol with high acetol productivities, without hydrogen pre-activation, and containing low copper loadings (≈5 wt.%). First, three families of supports from negligible to abundant acidity (SiO_2, Al_2O_3 and ZrO_2) were selected. Then, each of the families was optimized to achieve the best catalyst in each case. In the case of SiO_2, the particle size of CuO was decided to be tuned to maximize the yield to acetol. For Al_2O_3, different commercial aluminum oxides were used as supports for CuO nanoparticles with similar sizes. And finally, in the case of

ZrO_2, the different zirconium oxide phases were employed as support and their effect in the catalytic activity was studied.

5.2 Preparation and characterization of CuO supported on silica materials

Not long ago, N. Ravasio and co-workers observed that unanticipated acidic properties could arise in CuO/SiO_2 by improving the CuO dispersion degree[2,3]. They claim that this novel relationship between dispersion and acidity could dictate a new basis for their use in a broad range of applications, preserving other ordinary properties of Cu. This is especially interesting for our reaction, given that $Cu\text{-}SiO_2$ systems have been reported as materials that can be highly selective to acetol[4]. However, they lack the necessary acidity to react achieving high glycerol conversions, compared to other systems such as $Cu\text{-}ZrO_2$[5]. Thus, in this section, we tried to find a suitable acidity to boost catalyst activity without impairing selectivity on the $Cu\text{-}SiO_2$ system, by enhancing metal oxide dispersion.

In this sense, several catalysts were prepared by supporting an aqueous Cu precursor, i.e. $Cu(NO_3)\cdot 2.5H_2O$, on SiO_2 from Chempur (SiO_2-CH, ≈225 m^2/g, see Table 3.1) and SiO_2 from Sigma-Aldrich (SiO_2-AL, ≈350 m^2/g, see Table 3.1). Such incorporation was carried out, for the SiO_2-CH, by the incipient wetness impregnation (IW) method (CuO-IW/SiO_2-CH), see *Section 3.2.3*. Moreover, the precipitation-deposition method (PD) with urea as the precipitant agent was applied to obtain two different samples (CuO-PD/SiO_2-CH and CuO-PD/SiO_2-AL) from SiO_2-CH and SiO_2-AL, respectively, see *Section 3.2.4*. Additionally, for the SiO_2-AL, functionalization of the silica with aminopropyl groups (AP) was conducted before adding the Cu precursor (CuO-AP/SiO_2-AL), see *Section 3.2.5*. By employing these methodologies, a copper oxide percentage of around 5 wt.% was included in every case.

The main physicochemical and textural properties of the different CuO supported on silica materials are listed in Table 5.1. Similar characteristics can be found regarding surface area and copper content for all samples.

Table 5.1. Main physicochemical and textural properties of different SiO_2-supported CuO materials.

Catalyst	Cu loading (wt%) [a]	BET area (m^2/g) [b]	Pore volume (cm^3/g)[b]
CuO-IW/SiO_2-CH	5.0	219	0.92
CuO-PD/SiO_2-CH	5.8	242	0.73
CuO-PD/SiO_2-AL	5.8	218	0.92
CuO-AP/SiO_2-AL	5.8	245	0.71

[a] Calculated by ICP. [b] Calculated from N_2-adsorption isotherms data (BET method).

Figure 5.2 shows the XRD patterns of the four CuO/SiO_2 samples containing ≈5wt.% copper. Invariably, an amorphous structure is seen for SiO_2-based catalysts. On the contrary, the differences prompted by copper oxide from one material to another are noticeable. Whilst in those materials in which the copper has been incorporated by the precipitation-deposition method (PD) and by a previous grafting with APTES (AP), the signals corresponding to copper (II) oxide are barely detected, the material made by incipient wetness impregnation (IW) clearly displays the characteristics lines of CuO. These measurements point out the higher dispersion degree of CuO accomplished when employing the precipitation-deposition method (PD) or a previous grafting with APTES (AP), compared to that achieved by incipient wetness (IW).

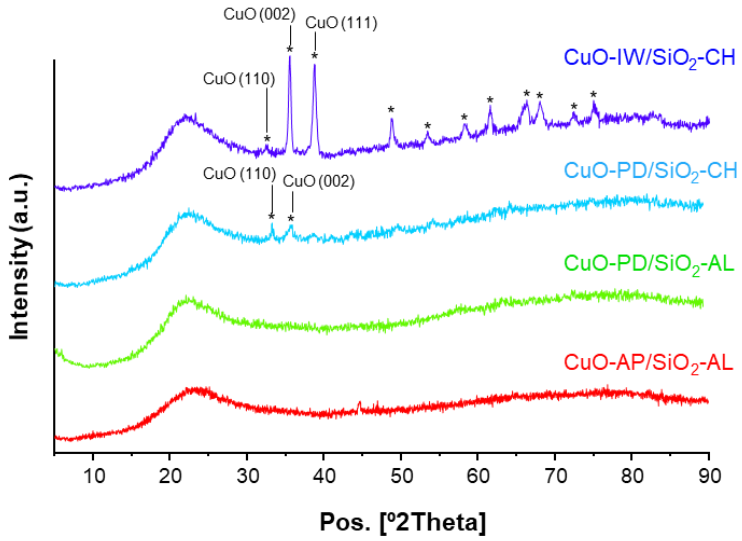

Figure 5.2. XRD patterns of CuO supported on SiO_2 materials. *: CuO (JCPDS: 00-048-1548).

In addition to the qualitative information deduced from the XRD diffraction patterns, titration with N_2O and particle size distribution by STEM imaging (Figure 5.3) were used to establish quantitative differences in CuO dispersion (Table 5.2). For CuO-IW/SiO_2-CH and CuO-PD/SiO_2-CH materials, there is a good agreement between the XRD, STEM and the N_2O titration data. Every technique showing the higher efficiency of the precipitation-deposition method (PD) to achieve higher dispersions than the incipient wetness approach (IW). Additionally, CuO-PD/SiO_2-AL presents higher dispersion and smaller particle size values (by both N_2O and STEM) than CuO-PD/SiO_2-CH, also in good agreement with the intensity of XRD peaks corresponding to CuO, which can be seen just for the former one. This fact was also predictable since SiO_2-AL is a SiO_2 with a larger surface area than the SiO_2-CH (see Table 3.1), allowing for a better dispersion of the CuO nanoparticles when incorporated by the same methodology. Finally, although N_2O titration hardly sees disparities between CuO-PD/SiO_2-AL and CuO-AP/SiO_2-AL, STEM imaging reveals the incorporation of CuO by the previous functionalization of the silica surface (SiO_2-AL) with APTES (CuO-AP/SiO_2-AL) is the methodology that gives rise to the smallest CuO particles. In that direction, CuO-AP/SiO_2-AL is the sole sample where this technique could not see particles above 3 nm (see Figure 5.4).

Table 5.2. CuO dispersion on several SiO_2 materials.

Catalyst	**STEM Particle size (nm)[a,b]**	**N_2O titration Particle size (nm)[c]**	**Dispersion (m^2 Cu/g Cu)[c]**
CuO-IW/SiO_2-CH	9.4 ± 6.8	12.2	55
CuO-PD/SiO_2-CH	6.2 ± 10.6	9.5	71
CuO-PD/SiO_2-AL	2.1 ± 1.5	5.8	117
CuO-AP/SiO_2-AL	1.6 ± 0.6	6.3	106

[a] Average particle size measured by HR-STEM ± the 2σ value (a minimum number of 200 particles was considered).
[b] Particle size distributions obtained by analyses of STEM micrographs.
[c] Measured by surface N_2O oxidation of the reduced catalyst and subsequent reduction.

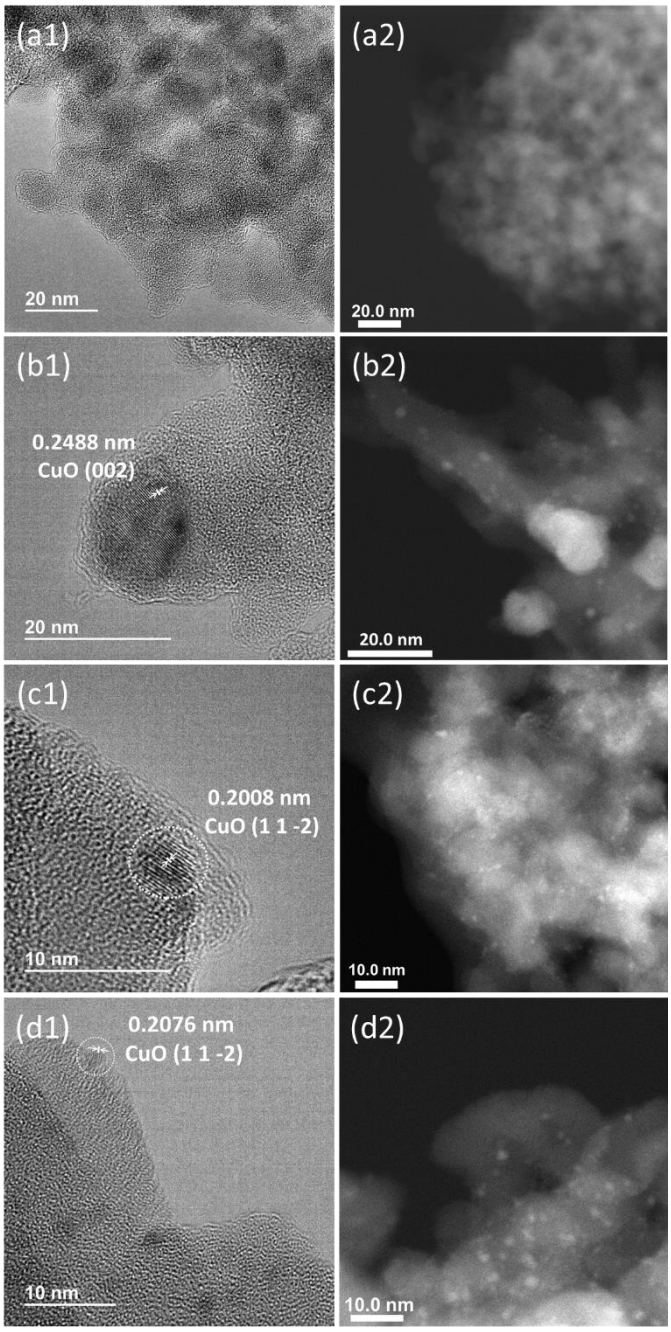

Figure 5.3. (1) HR-TEM and (2) HR-STEM micrographs for (a) CuO-IW/SiO_2-CH, (b) CuO-PD/SiO_2-CH, (c) CuO-PD/SiO_2-AL and (d) CuO-AP/SiO_2-AL.

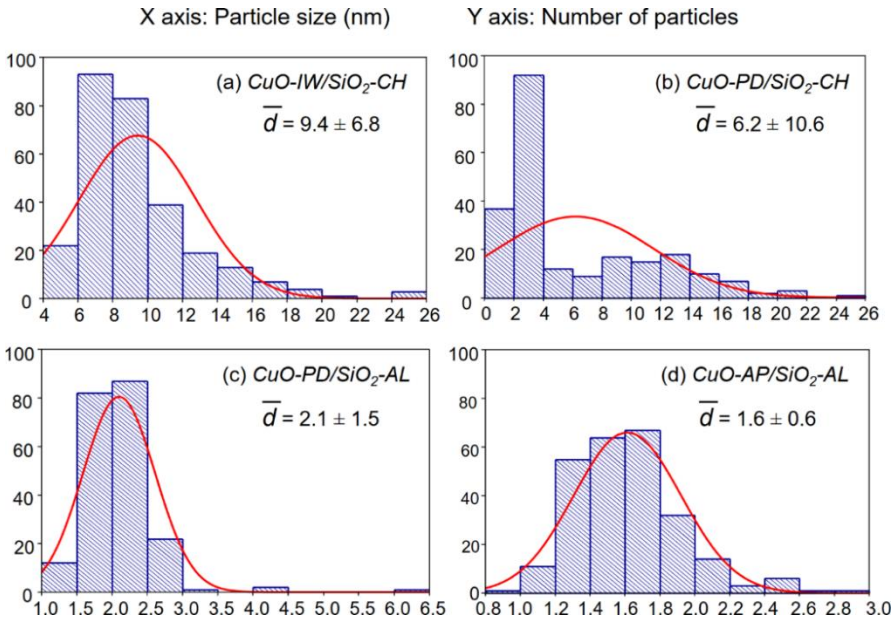

Figure 5.4. Histograms with Gaussian fitting for Cu/SiO_2 materials obtained by analysis of STEM micrographs by measuring (a): 284, (b): 223, (c): 207, (d): 255 particles.

On the other hand, a study of the acidic properties was conducted, first, by FTIR-followed pyridine adsorption-desorption experiments. The first cycle of pyridine adsorption and desorption at 150 ºC (Figure 5.5) allowed us to establish that Lewis acid sites predominate for these materials, the Brønsted acidity being insignificant. Moreover, the analyses unravel how, as reported by earlier studies[2,3], the smaller the particle size, the larger the number of acid sites. However, peak intensities and shapes arouse difficulties at discriminating real Lewis acid centers from physiosorbed pyridine at higher temperatures. Hence, this technique does not secure the distinction between weak, medium, and strong acid centers. Thus, to ensure a better approach to discriminate between the materials, a study of their acidic properties was carried out through adsorption and temperature-programmed desorption of ammonia (TPD-NH_3). The similar profiles for the qualitative desorption curves in Figure 5.6 essentially reveal a similar strength for the acid sites displayed by these catalysts. The main differences are then seen in the quantity of ammonia adsorbed, that is, in the total number of acid sites. In this regard, Table 5.3 shows the total ammonia adsorbed for each catalyst and the same value but normalized by each of the

catalyst BET areas, both columns pointing out the same trend. This data, consistent with the tendency observed by pyridine adsorption-desorption at 150 ºC, allows for ascertaining relevant differences between the various materials, whose total acidity can be ordered as follows: CuO-AP/SiO_2-AL > CuO-PD/SiO_2-AL > CuO-PD/SiO_2-CH >> CuO-IW/SiO_2-CH. As can be observed, while acid sites offered by CuO-IW supported on SiO_2-CH (with CuO particle sizes ≈8-9 nm by STEM, as seen in Table 5.2, and Figs. 5.3 and 5.4) are nearly negligible, in the sample showing the smaller particle size and the thinner dispersion (CuO-AP/SiO_2-AL, see Figure 5.4), a substantial amount of Lewis acid sites is detected. In all cases, the sites range from weak to moderate acid strength. Revealingly, as the acidity provided by the SiO_2 is insignificant (see FTIR-pyridine analyses for the supports, Annex, Table A2), differences can be attributed to the different nature of the CuO moieties supported in each material. Consequently, these findings support previous affirmations stating that higher copper oxide dispersions lead to increasing acidities, as reported by N. Ravasio and co-workers[36,37].

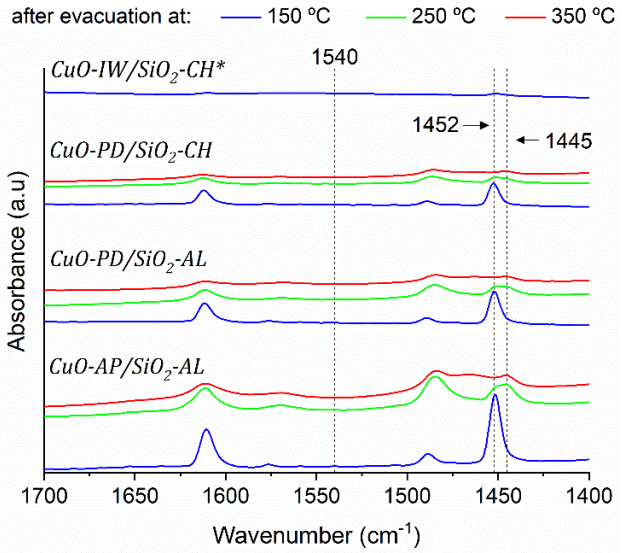

Figure 5.5. Infrared spectra of the pyridine region following pyridine adsorption-desorption cycles on CuO/SiO_2 materials. 1540 cm^{-1}: pyridine chemisorbed on Brønsted acid sites, 1452 cm^{-1}: pyridine chemisorbed on Lewis sites, 1445 cm^{-1}: physiosorbed pyridine. *Since insignificant pyridine adsorption was observed at 150 ºC, the temperature was not further increased.

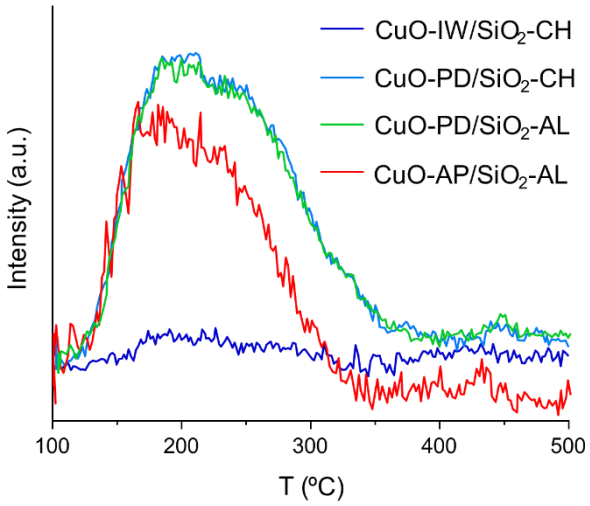

Figure 5.6. NH_3-TPD profiles of CuO/SiO_2 materials. Note: non-calibrated mass-spectrometer (MS); qualitative information about the strength distribution of acid sites.

Table 5.3. Acid site analyses for different CuO supported on SiO_2 catalysts.

Catalyst	Acid sites (µmol PYR/g)[a]	Acid sites (µmol NH_3/g)[b]	Acid site density (µmol NH_3/m^2)[c]
CuO-IW/SiO_2-CH	4	14	0.06
CuO-PD/SiO_2-CH	41	83	0.34
CuO-PD/SiO_2-AL	71	127	0.58
CuO-AP/SiO_2-AL	99	279	1.14

[a] Measured by FTIR with pyridine (PYR) as probe molecule.

[b] Measured by NH_3 adsorption pulses until saturation.

[c] Calculated as µmol NH_3/g divided by the catalyst surface area (m^2/g)

Finally, the redox features of the materials herein prepared were investigated by TPR analyses (Figure 5.7). Notably, TPR traces of the materials prepared by those methods leading to higher dispersions, specifically precipitation-deposition (PD) and grafting with APTES (AP), display an absolute maximum at ≈190 ºC. Contrarily, the material prepared

using the incipient wetness impregnation methodology (CuO-IW/SiO_2-CH) presents its maximum at ≈235 ºC. These maximums have already been reported to correspond to the complete reduction of Cu (Cu^{2+}→Cu^0) [44]. Importantly, these TPR graphs are logical when taking into account that higher CuO dispersions (i.e., smaller particle sizes) give as a result higher reducibilities [45,46].

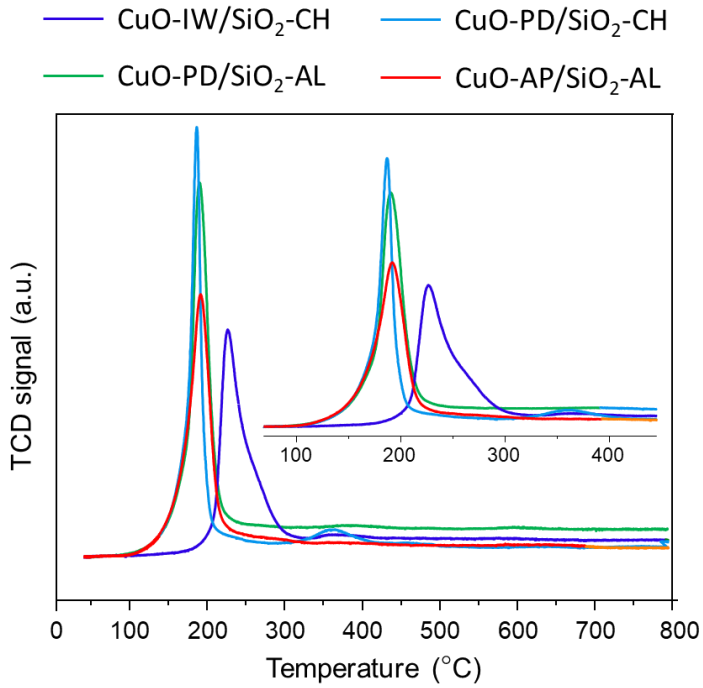

Figure 5.7. TPR traces for CuO supported on SiO_2 materials.

5.3 Preparation and characterization of CuO supported on alumina materials

Although remarkable catalytic activity has been reported for specific Cu-Al_2O_3 catalysts with high copper loadings[4,6,7], not great efforts have been put on testing different CuO/Al_2O_3 enabling working with lower copper percentages and thus allowing for achieving higher TONs. For that purpose, and due to the wide variety of existing commercial alumina, different commercial aluminium oxides from Sigma-Aldrich were

used; Al_2O_3 Nanopowder (Al_2O_3-*npw*), Al_2O_3 Acid Activated (Al_2O_3-*ac*), and Al_2O_3 Basic Activated (Al_2O_3-*bas*). A 5 wt.% Cu was incorporated in all cases by incipient wetness impregnation (see *Section 3.2.3*). Interestingly, since the same chemical support (synthesized differently) was going to be tested, the CuO/Al_2O_3 materials could also be helpful to provide us with some additional insight into the role of acidity and basicity, as no other factor complicating the discussion, such as the different chemical nature of the centres, was going to exert a significant influence.

The main properties of three materials prepared by incorporating CuO onto commercial Al_2O_3 supports are presented in Table 5.4. Copper weight percentages ranging from 4.0 and 6.0 wt.% and surface areas around 120-130 m^2/g were found for this family of samples.

Table 5.4. Main physicochemical and textural properties of different Al_2O_3-supported CuO materials.

Catalyst	**Cu loading (wt%)** [a]	**BET area (m^2/g)** [b]	**Pore volume (cm^3/g)** [c]
CuO/Al_2O_3-*ac*	4.2	125	0.24
CuO/Al_2O_3-*bas*	5.2	119	0.23
CuO/Al_2O_3-*npw*	5.6	130	0.35

[a] Calculated by ICP. [b] Calculated from N_2-adsorption isotherms data (BET method).

Figure 5.8 shows how the diffraction patterns for acid alumina and basic alumina are practically identical, mainly showing characteristic peaks of the γ phase, a cubic crystalline system. On the other hand, the nanopowder alumina shows a diffractogram different from the previous two, with characteristic peaks of the δ phase, a tetragonal-type crystalline system. Furthermore, none of the diffraction peaks associated with copper (II) oxide was observed for the three catalysts prepared. These results indicate the possibility that the copper oxide particles are very well dispersed in the support, with a relatively small size.

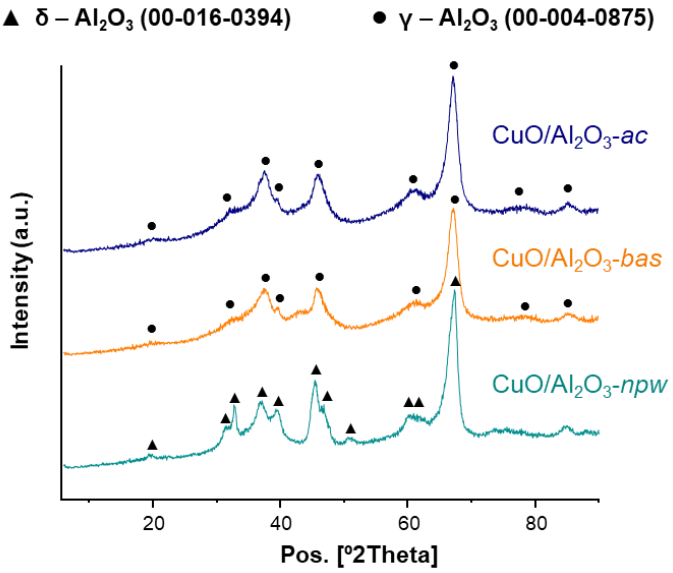

Figure 5.8. XRD patterns of CuO supported on Al_2O_3 materials.

Figure 5.9 shows in detail the different information obtained by high-resolution electron microscopy. The size distribution (histograms) is represented in Figure 5.9(c). These distributions were determined by measuring approximately 200 particles randomly on the STEM images. As can be seen in the histograms, the mean size of the CuO nanoparticles and the distribution range is similar in the case of the CuO/Al_2O_3-*ac* and CuO/Al_2O_3-*bas* samples, being slightly higher in average and amplitude in the case of CuO/Al_2O_3-*npw*. The small particle size detected by HR-TEM and STEM images aligns with XRD measurements. Considering that all catalysts have roughly similar sizes of CuO nanoparticles, the different catalytic activity must be attributed to the support's different physicochemical properties (mainly acidity and basicity).

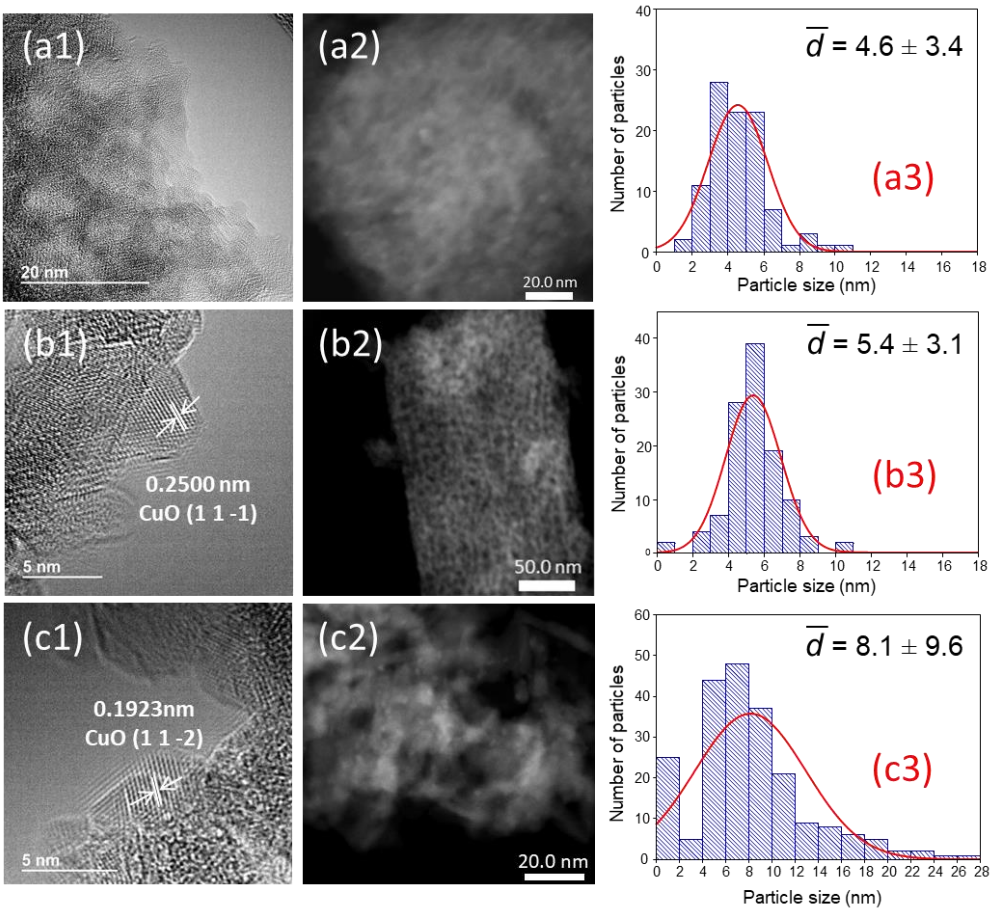

Figure 5.9. (1) HR-TEM micrographs, (2) HR-STEM micrographs and (3) histograms with Gaussian fitting from STEM imaging for (a) CuO/Al_2O_3-*ac*, (b) CuO/Al_2O_3-*bas*, and (c) CuO/Al_2O_3-*npw*.

As in the case of materials based on copper oxide supported on silica, the materials containing alumina as support were analyzed by infrared of pyridine (Figure 5.10) and absorption-desorption of ammonia at programmed temperature (Figure 5.11). Table 5.5 shows a consistent trend in terms of the acid sites measured by the two techniques (the different accessibility of the molecules must be taken into account). After examining the pyridine spectrum is clear that these materials mainly have Lewis-type acid centers, the Brønsted acidity being practically insignificant. However, a more detailed analysis of the

pyridine spectrum reveals physisorption of the probe molecule even after evacuation at 150 ºC, which is why the temperature programmed adsorption-desorption of ammonia was preferred to analyze both qualitatively and quantitatively the acidity in this series. The corresponding NH_3-TPD profiles of the CuO-supported on the three different alumina samples are depicted in Figure 5.11.

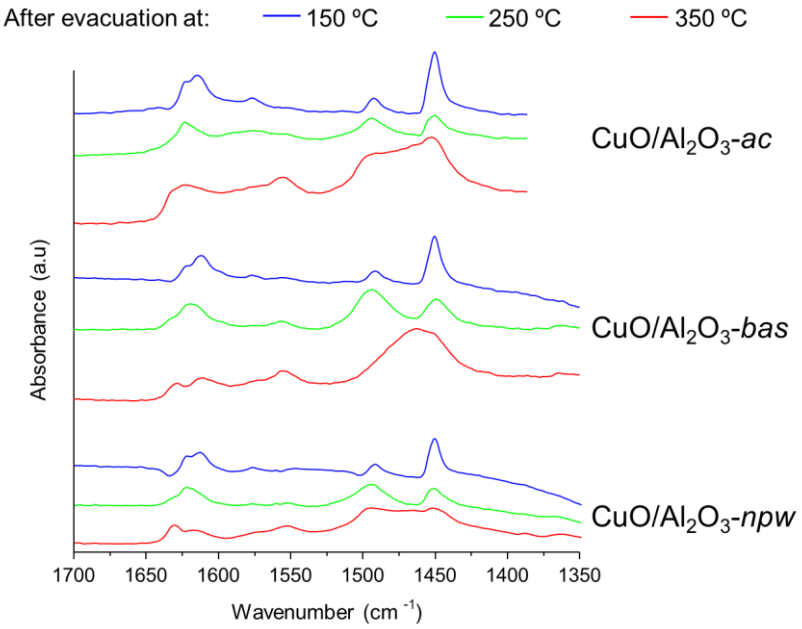

Figure 5.10. Infrared spectra of the pyridine region following pyridine adsorption-desorption cycles on CuO/Al_2O_3 materials. 1540 cm^{-1}: pyridine chemisorbed on Brønsted acid sites, 1452 cm^{-1}: pyridine chemisorbed on Lewis sites, 1445 cm^{-1}: physiosorbed pyridine.

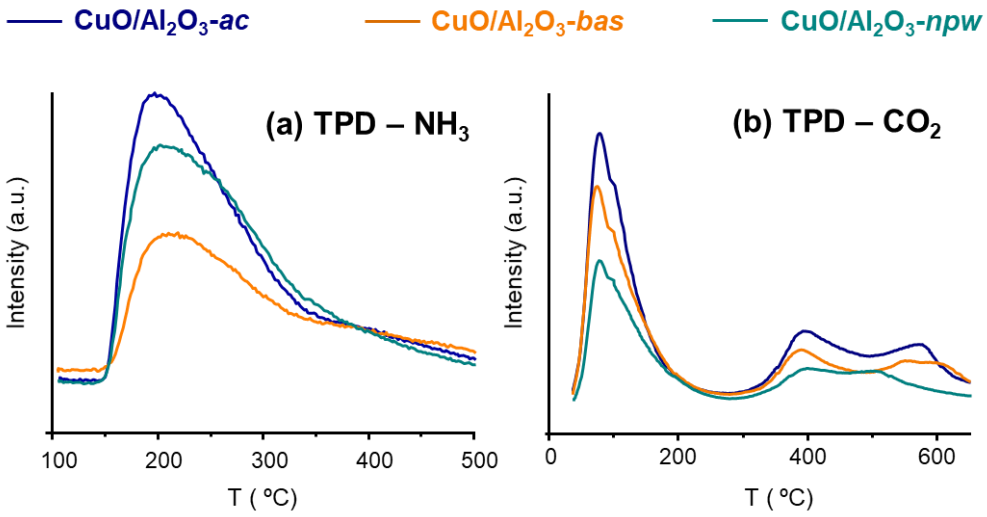

Figure 5.11. (a) NH_3-TPD and (b) CO_2-TPD profiles of CuO/Al_2O_3 materials. Note: non-calibrated mass-spectrometer (MS); qualitative information about the strength distribution of acid sites.

Table 5.5. Acid-base site analyses for different CuO supported on Al_2O_3 catalysts.

Catalyst	**Acid sites (µmol PYR/g)[a]**	**Acid sites (µmol NH_3/g)[b]**	**Basic sites (µmol CO_2/g)[b]**
CuO/Al_2O_3-*ac*	87	200	54
CuO/Al_2O_3-*bas*	43	192	33
CuO/Al_2O_3-*npw*	32	102	33

[a] Measured by FTIR with pyridine (PYR) as probe molecule.

[b] Measured by NH_3 (acid sites) and CO_2 (basic sites) adsorption pulses until saturation.

In general, what is seen in the analysis with ammonia is that the CuO/Al_2O_3-*npw* material presents a lower number of acid centers than the other two materials (CuO/Al_2O_3-*ac* and CuO/Al_2O_3-*bas*). However, the ammonia desorption profiles are indeed very similar in both cases, which reveals a similar acid strength distribution for the three catalysts studied in this section. Thus, the general trends observed with both FT-IR (PYR) and NH_3-

TPD measurements are similar and show that CuO/Al_2O_3-*ac* and CuO/Al_2O_3-*bas* samples present higher acidity than CuO/Al_2O_3-*npw* material. In addition, no remarkable differences are observed in terms of basicity for the three materials here studied, which generally present low basicity.

Finally, the reduction profiles at programmed temperature (TPR) for the three catalysts in which alumina has been used as support present an analogous appearance (Figure 5.12). A prominent peak at around 195 ºC can be observed, corresponding to most copper species reduction. This fact shows that, on this support, regardless of the type of commercial alumina used, very similar copper oxide reducibility is obtained. Since the reducibility will be a function mainly of the degree of dispersion and the interaction of the reducible species with the support, this possibly indicates at the same time a very similar dispersion of the metal oxide and a similar interaction between support and copper oxide in all three cases.

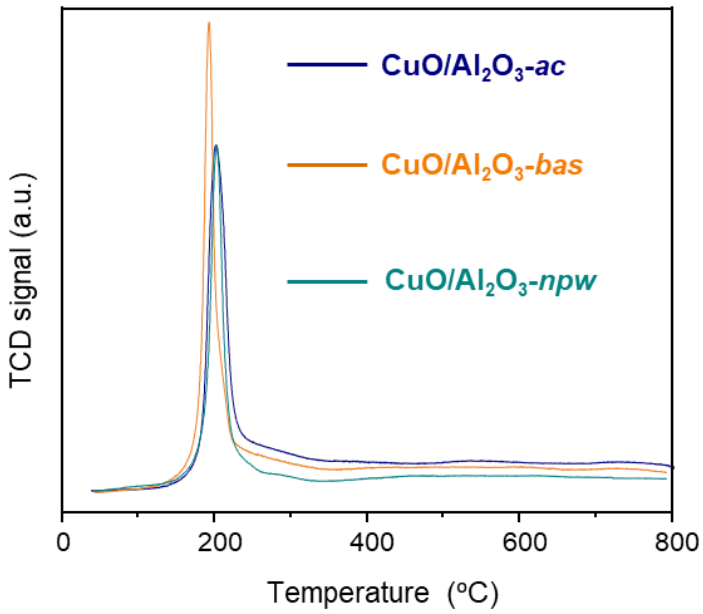

Figure 5.12. TPR traces for CuO supported on Al_2O_3 materials.

5.4 Preparation and characterization of CuO supported on zirconia materials

Another attractive matrix for CuO to be assessed is ZrO_2. In this sense, Sato *et al.* tested a pre-reduced mixed oxide Cu-Zr (3:1 mol.) prepared by co-precipitation in a fixed bed reactor, achieving 80% yield to acetol without further optimizations concerning either reaction conditions or catalyst composition[4]. Additionally, at the same time as the development of this study, R.J. Chimentão and co-workers achieved promising results by working in a batch reactor with supported CuO (Cu wt.% ≤ 5) on tetragonal zirconia, and reported the Cu-Zr sites as key active centres for the process success[5,8].

Interestingly, it is widely known that zirconium oxide can occur in two phases or stable polymorphs at room temperature called monoclinic and tetragonal phase. Furthermore, it is also well known in the scientific literature that these zirconia polymorphs have distinct acid-base properties and different concentrations of hydroxyl groups on the surface[9,10], being indisputable that these factors can somehow influence catalytic activity. Taking this previous information into account, in this section, several CuO/ZrO_2 samples have been prepared by incipient wetness impregnation using as supports: i) a pure monoclinic ZrO_2 from Chempur, ii) a pure tetragonal ZrO_2 from Chempur, and iii) a physical mixture of these both commercial polymorphs (60 *monoclinic (Chempur)* : 40 *tetragonal (Chempur)*, in weight). The resulting catalysts have been named CuO/*m*-ZrO_2, CuO/*t*-ZrO_2 and CuO/*mxt*-ZrO_2, respectively.

The characterisation analyses in Table 5.6 show similar results regarding the weight percentage of incorporated copper (between 5.7 and 5.9%). On the other hand, there appears to be a slight increase in the surface area caused by the presence of the tetragonal phase. In the same line to what was reported in *Section 5.3*, the pore volume impregnation method is sufficient to achieve a good dispersion of CuO on this type of supports. This can be deduced from the absence of characteristic peaks of CuO in the XRD patterns, which are illustrated in Figure 5.13.

Table 5.6. Main physicochemical and textural properties of different ZrO_2-supported CuO materials.

Catalyst	Cu loading (wt%) [a]	BET area (m^2/g) [b]	Pore volume (cm^3/g)[c]
CuO/*t*-ZrO_2	5.7	123	0.17
CuO/*mxt*-ZrO_2	5.9	105	0.20
CuO/*m*-ZrO_2	5.7	75	0.26

[a] Calculated by ICP. [b] Calculated from N_2-adsorption isotherms data (BET method).

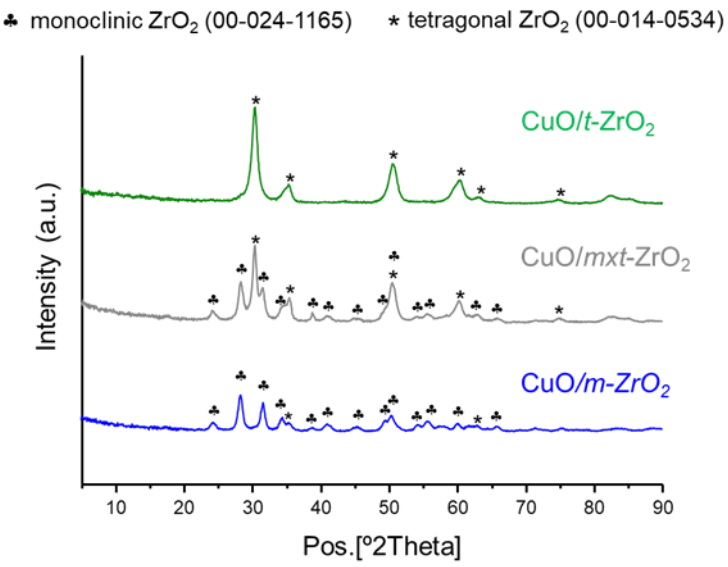

Figure 5.13. XRD patterns of CuO supported on ZrO_2 materials.

Figure 5.14 presents some electron micrographs for the ZrO_2-supported materials. Unfortunately, due to the similarities in shape and size and the lousy contrast between ZrO_2 nanoparticles composing the support and the supported CuO nanoparticles, establishing particle size distributions by counting CuO nanoparticles was non-viable. Instead, particles were to be identified one by one by lattice spacing comparison against patterns. In all cases, CuO nanoparticles with sizes between 5 and 10 nm were detected. Additionally, a hydrogen

reduction followed by N_2O oxidation plus reduction (see *Section 3.3.10.2*) was carried out for CuO/*mxt*-ZrO_2, establishing the average particle size around 11.0 nm, slightly above the values observed by punctual HR-TEM measurements.

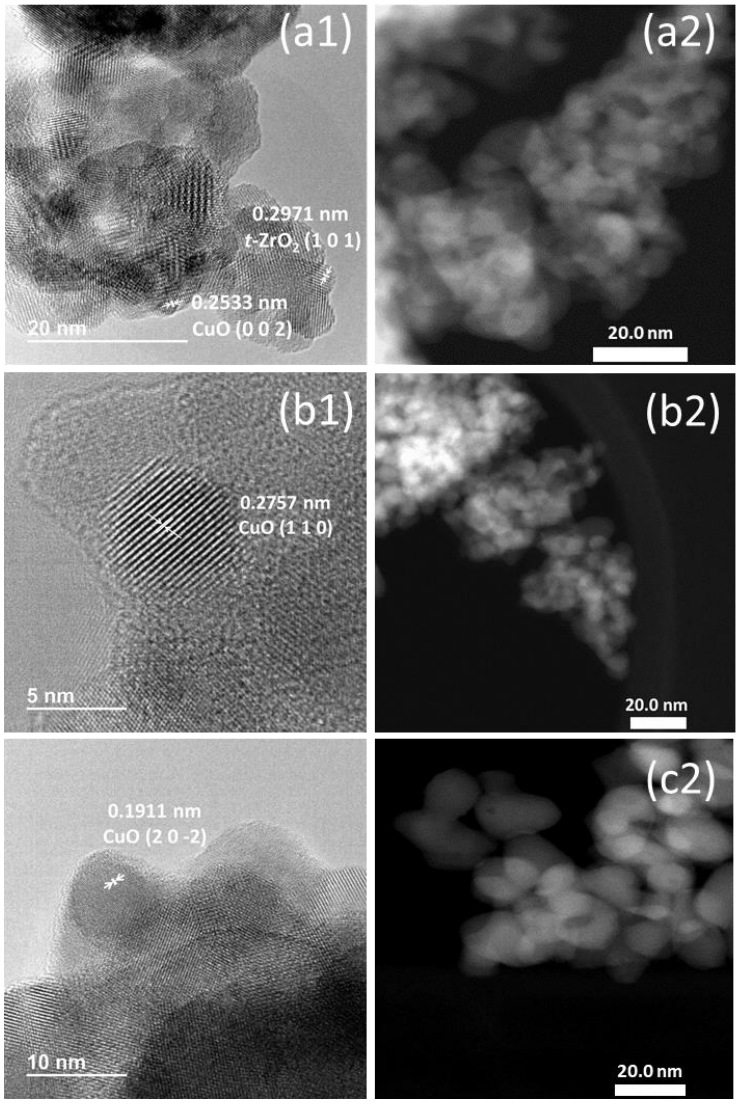

Figure 5.14. (1) HR-TEM micrographs, (2) HR-STEM micrographs for (a) CuO/*t*-ZrO_2, (b) CuO/*mxt*-ZrO_2, and (c) CuO/*m*-ZrO_2.

Figure 5.15 shows the pyridine adsorption-desorption experiments, followed by infrared spectroscopy. Unfortunately, once again, pyridine physisorption (at 1443 cm^{-1}) is very important in these analyses and does not allow for an adequate quantification of the Lewis centers of the catalyst in any of the cases. However, pyridine analysis reveals that, in these catalysts, the contribution of Brönsted acid centers, although minor, is not negligible.

In order to complement the pyridine analyses, absorption-desorption experiments were carried out at a programmed temperature (TPD) for NH_3 and CO_2. The maxima for temperature programmed desorption curves are centered around 200 ºC in all cases (Figure 5.16), which simplifies the discussion to the total number of acid sites. In Table 5.7, significant differences can be observed in this respect. Based on their total acidity per area unit, the materials can be ordered following the next sequence: CuO/*m*-ZrO_2 < CuO/*mxt*-ZrO_2 < CuO/*t*-ZrO_2. Again, these differences will allow us to establish structure-activity relationships and discern the role of each of the active centers in catalytic behavior.

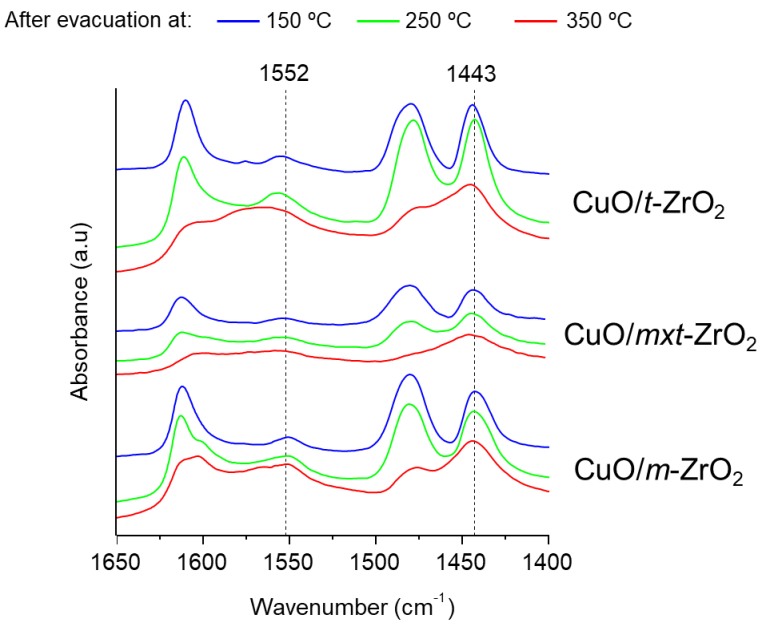

Figure 5.15. Infrared spectra of the pyridine region following pyridine adsorption-desorption cycles on CuO/ZrO_2 materials. 1540 cm^{-1}: pyridine chemisorbed on Brønsted acid sites, 1452 cm^{-1}: pyridine chemisorbed on Lewis sites, 1445 cm^{-1}: physiosorbed pyridine.

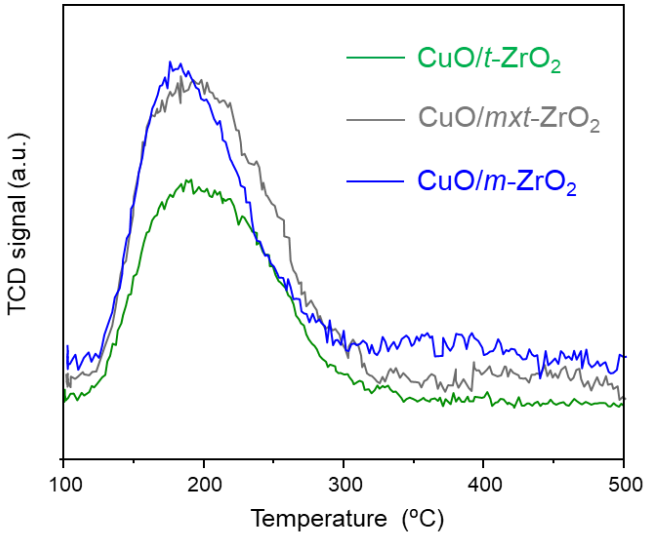

Figure 5.16. (a) NH_3-TPD profiles of CuO/ZrO_2 materials. Note: non-calibrated mass-spectrometer (MS); qualitative information about the strength distribution of acid sites.

Table 5.7. Acid site analyses for different CuO supported on ZrO_2 catalysts.

Catalyst	**Acid sites (μmol NH_3/g)[a]**	**Basic sites (μmol CO_2/g)[a]**	**Acid site density (μmol NH_3/m^2)[d]**
CuO/*t*-ZrO_2	311	n/d	2.53
CuO/*mxt*-ZrO_2	177	n/d	1.69
CuO/*m*-ZrO_2	115	123	1.53

[a] Measured by NH_3 adsorption pulses until saturation.

On the other hand, in the case of the family of materials based on copper oxide supported on zirconium oxide, it was only possible to carry out one adsorption and desorption experiment at a programmed temperature with CO_2. Therefore, this experiment was only carried out for the most promising catalyst in the dehydration reaction of glycerol to acetol (CuO/*m*-ZrO_2, see following Sections).

With respect to reducibility capacity for these ZrO_2-based materials, in Figure 5.17, two peaks can be observed for the three materials analyzed with maximas around 137 and 175 ºC, respectively. The peak at lower temperature has been reported to be characteristic of extremely dispersed CuO species[11]. Interestingly, the second peak corresponding to less reducible copper species, probably more poorly dispersed crystalline copper oxide[11], becomes more prominent in the case of CuO/*m*-ZrO_2. This fact may exert an influence on the material capability to generate the active copper species (i.e., Cu^{1+}) during the reaction and should be further studied. Nonetheless, it must be said that both peaks have reduction temperatures that are below the working temperature at which the reaction takes place.

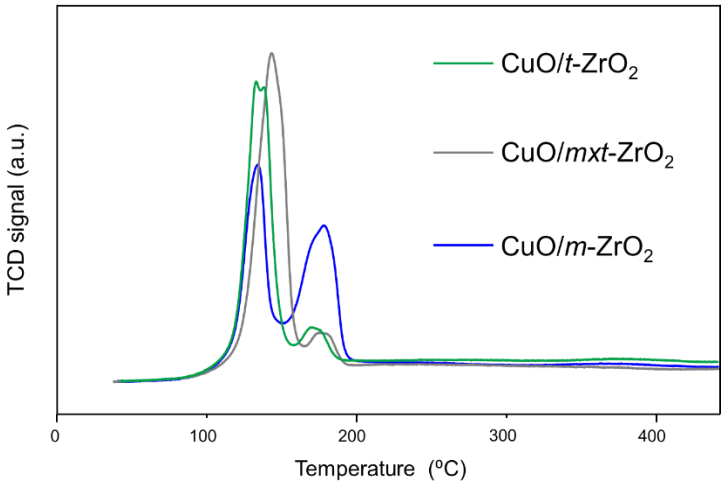

Figure 5.17. TPR traces for CuO supported on ZrO_2 materials.

5.5 Results and discussion for CuO supported on silica materials

5.5.1 Catalytic activity for CuO supported on silica materials

As previously said, the remarkable selectivity towards acetol observed for some Cu-SiO_2[4] materials encouraged us to find alternative ways to boost the catalyst activity in this type of materials without worsening their good selectivity.

Based on the previous articles reporting acidity arising in these systems when improving copper oxide dispersion[2,3], it was decided to decrease the CuO particle size, thereby achieving a double consequence consisting of increasing the active surface area and introducing some acidity in the CuO/SiO_2. Both effects were supposed to improve acetol production. To this purpose, and according to the previous characterization section, a series of materials having different CuO particle sizes and, therefore, different acidities, were successfully prepared (see *Section 5.2*). These materials were tested in the catalytic dehydration of glycerol to acetol, and the results are shown in Figure 5.18.

Figure 5.18a reveals the cumulative data for glycerol conversion, yield to the different products, and carbon balance in the dehydration of glycerol for a time on stream (TOS) between 1-8 h. In addition, Figure 5.18b illustrates the cumulative selectivity to acetol and Figures 5.18c and 5.18d show glycerol conversion and selectivity to acetol as a function of TOS for the different CuO/SiO_2 materials herein prepared. As can be seen, the best results were attained with the CuO-PD/SiO_2-AL and CuO-AP/SiO_2-AL, with the nearly total conversion of glycerol (≈100%), yield to liquid products ≈80% (Acetol + PDOs + Acid & Esters + Others), and selectivity to acetol up to 70% in the liquid fraction. Furthermore, every graph shows in what manner the smaller the CuO particle size, the higher activity and selectivity towards the desired acetol, this effect being very significant when comparing CuO-PD/SiO_2-AL (5.8 nm, by N_2O measurements) and CuO-AP/SiO_2-AL (6.3 nm, by N_2O measurements) with CuO-PD/SiO_2-CH (9.5 nm, by N_2O measurements) and, especially with CuO-IW/SiO_2-CH (12.2 nm, by N_2O measurements). Consequently, results suggest that those materials exhibiting higher acidity and preferably prepared by methods affording a higher degree of dispersion for the copper oxide, such as the precipitation-deposition method (PD) and the grafting with APTES (AP), are more capable of attaining better results. Regarding the explanation of the much more subtle catalytic differences between them, it seems that the presence of a considerably larger number of acid sites observed in CuO-AP/SiO_2-AL to CuO-PD/SiO_2-AL (observed by NH_3-TPD measurements) is having a substantial effect on the catalytic activity, which could consist of stronger acetol adsorption (see *Section 4.3.3.4*), resulting in lower selectivities and a more marked catalyst deactivation (Figure 5.18c).

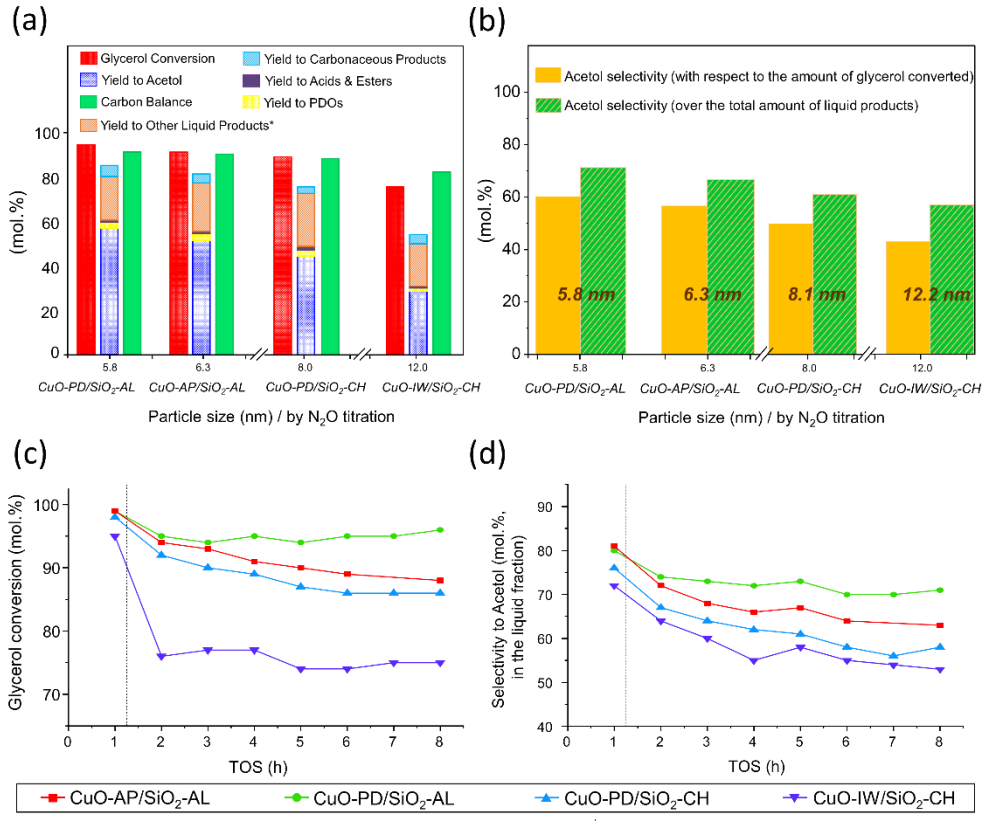

Figure 5.18. Cumulative (a) glycerol conversion, yield to liquids and carbon balance, (b) Acetol selectivities, (c) Glycerol conversion vs time on stream, and (d) Acetol selectivity vs time on stream for the dehydration of glycerol over different CuO supported on SiO_2 catalysts. Reaction conditions: feed = methanol/glycerol (50/50 in weight), flow = 2 mL/h, with 0.5 g catalyst, at 240 ºC, TOS = 8 h. *Other liquid products: acetoin, acetoin methyl ether, 3-methoxybutanol, hydroxyacetone dimethyl acetal, solketal and other unidentified by-products.

5.5.2 Structure-activity relationships for CuO supported on SiO_2 materials

Figure 5.19 depicts (a) the correlation between acidity and the particle size of the CuO nanoparticles and (b) the behaviour of each catalyst in terms of acetol production per Cu site in that period when no catalyst has started to suffer from any significant deactivation (TOS = 1-4h). The tendency mentioned above, consisting of an increase in the acidity if improving the CuO dispersion, is well illustrated in Figure 5.19a. Both particle size

measurements (STEM imaging and N_2O titration) fit reasonably well with exponential curves when representing the acid site density with respect to them. Interestingly, the effect of reducing the CuO particle size on the catalytic activity and, at the same time, increasing the acidity coincides with an improvement of the acetol production rate per mol of Cu present in the catalyst (Figure 5.19b). Furthermore, the acetol production rate enhancement with the amount of Cu exposed (i.e., CuO particle size) adjusts quite well to a linear fit (Figure 5.19b, purple trace). Additionally, Figure 5.19b shows an opposite trend when increasing the number of acid sites per unit area (green trace). However, an asymptotic tendency is observed in this case, probably meaning that excessively high concentrations of acid sites could unpair the specific activity towards producing the desired acetol.

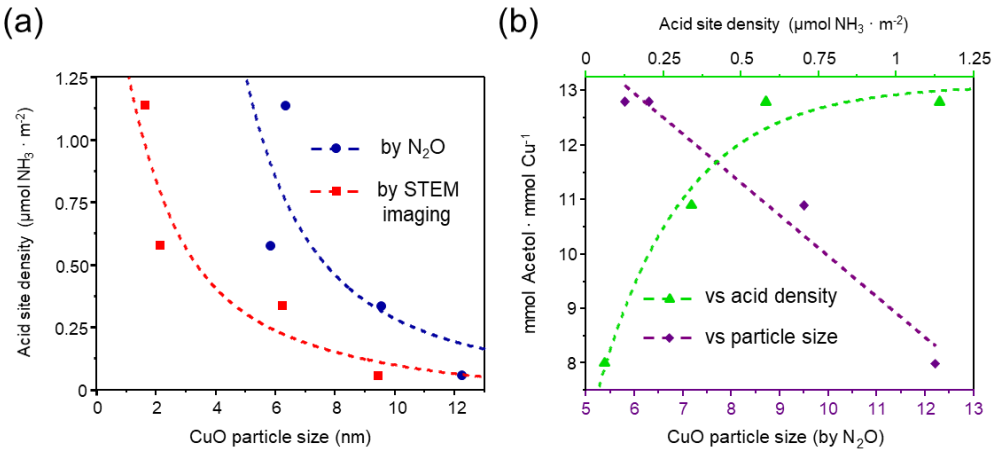

Figure 5.19. (a) Correlation between acid site density and CuO particle size. (b) Specific activities (SA) towards the acetol production calculated based on total amount of Cu (ICP). Reaction conditions: feed = methanol/glycerol (50/50 in weight), flow = 2 ml/h, with 0.5 g catalyst, at 240 ºC, at TOS = 1-4 h.

At this point, it could be possible to attribute the acetol production rate upgrading to three distinct factors: 1) an increase in the amount of Cu exposed, 2) an increment in the number of acid sites per unit area, but also to 3) an intrinsically superior activity of those Cu sites which are present in smaller CuO nanoparticles. To evaluate the third point, a comparison should be made by considering the amount of CuO exposed in every case

(Figure 5.20). When considering the amount of acetol produced by only those Cu atoms that are genuinely accessible to the substrate (calculate by N_2O titration of the reduced catalyst and subsequent re-reduction), it appears to be a maximum located at particles sizes around 10 nm. Accordingly, it seems that those Cu sites present when there are nanoparticles around 10 nm exhibit an equal if not superior intrinsic activity to carry out the glycerol dehydration to acetol than those present in systems with smaller CuO particle sizes. Indeed, the reducibility commented in *Section 5.2* discloses that every system has a reduction temperature below the reaction temperature. Consequently, every system is in with a chance of generating the Cu(I) species, believed to be the crucial ones to carry out this reaction (see *Chapter 4* and ref.[12]).

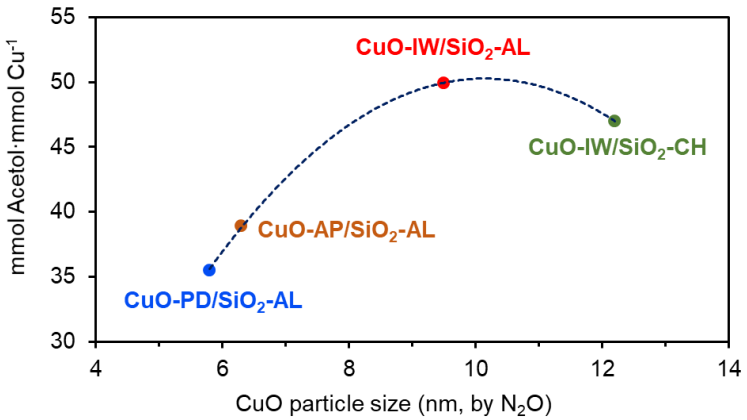

Figure 5.20. Specific activities (SA) towards the acetol production for different CuO supported on SiO_2 catalysts. SA have been calculated correcting the total amount of Cu (ICP) by the % of surface Cu (calculated by N_2O titration). Reaction conditions: feed = methanol/glycerol (50/50 in weight), flow = 2 ml/h, with 0.5 g catalyst, at 240 ºC, at TOS = 1-4 h.

This conclusion relating to the inherent activity of CuO nanoparticles with different sizes points out the other two factors (1 and 2) as the leading causes for the improvement achieved when decreasing the CuO particle size. In that direction, Figure 5.19b (purple trace) provides clear proof concerning an enhancement in the acetol production rate with the amount of copper exposed (i.e., CuO particle size). Agreeing with this finding, copper dispersion has recently been claimed to be a sensitivity descriptor for the activity[5].

Moreover, the preceding chapter has disentangled the need for acidity to allow for the first interaction glycerol – catalyst. Thus, it can be concluded that the two main reasons for this catalytic improvement are the number of active sites, larger for smaller nanoparticles, although not necessarily more active, together with the appearance of acidity generated when decreasing the particle size, as reported in the literature[2,3].

5.5.3 Catalytic activity for CuO supported on alumina materials

This section shows the catalytic results achieved with supported copper oxide-based catalysts on different commercial alumina samples. In this sense, Figure 5.21a illustrates the cumulative data for glycerol conversion, yield to the different products, and carbon balance. For CuO/Al_2O_3-*npw* cumulative data corresponds to times on stream between 1-8 h, whereas for CuO/Al_2O_3-*ac* and CuO/Al_2O_3-*bas*, the reactions were stopped at 6 and 5 h, respectively, due to worse results. On the other hand, Figure 5.21b illustrates the cumulative selectivity to acetol and Figures 5.21c and 5.21d show glycerol conversion and selectivity to acetol with TOS, respectively. As reflected in figure, the best results were attained with CuO/Al_2O_3-*npw*, with a very high glycerol conversion (≈97%) and yield to liquid products ≈91% (Acetol + PDOs + Acid & Esters + Others), and selectivity to acetol up to 60% in the liquid fraction.

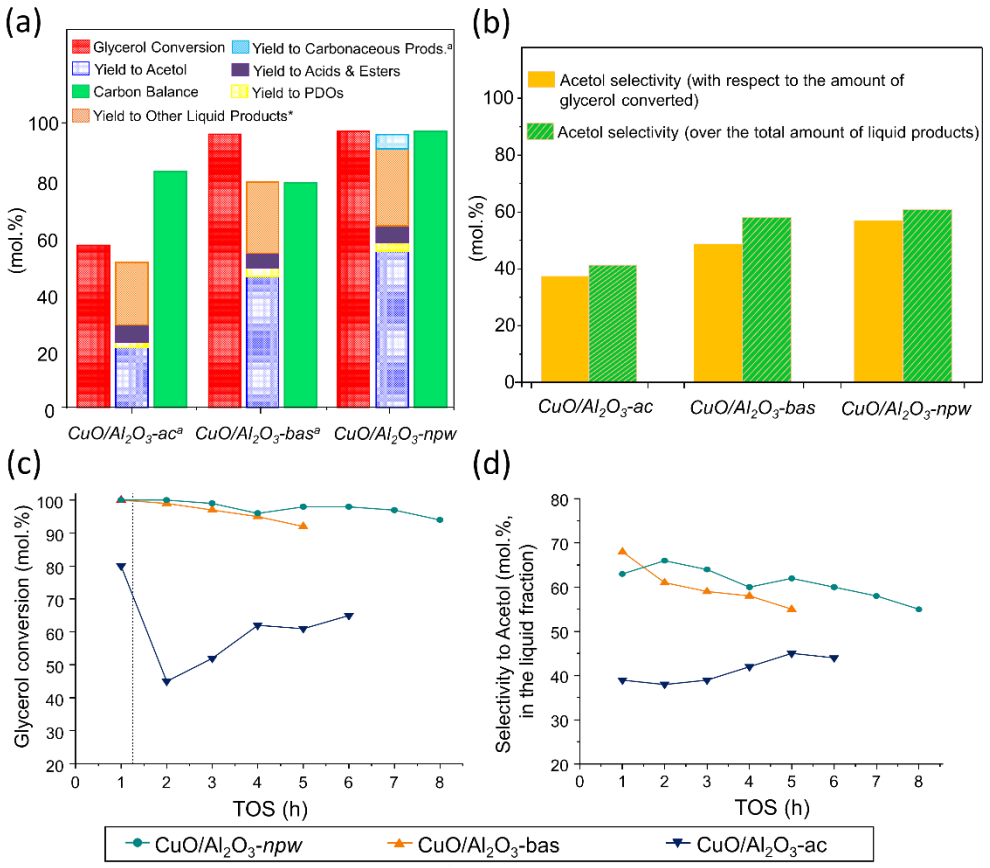

Figure 5.21. Cumulative (a) glycerol conversion, yield to liquids and carbon balance, (b) Acetol selectivities, (c) Glycerol conversion vs time on stream, and (d) Acetol selectivity vs time on stream for the dehydration of glycerol over different CuO supported on Al_2O_3 catalysts. Reaction conditions: feed = methanol/glycerol (50/50 in weight), flow = 2 mL/h, with 0.5 g catalyst, at 240 ºC, TOS = 8 h. [a] Calculations for CuO/Al_2O_3-*ac* and CuO/Al_2O_3-*bas* based only on the liquid fraction and TOS of 6 and 5 h, respectively. *Other liquid products: acetoin, acetoin methyl ether, 3-methoxybutanol, hydroxyacetone dimethyl acetal, solketal and other unidentified by-products.

5.5.4 Structure-activity relationships for CuO supported on Al_2O_3 materials

The most notable differences that can be observed in Figure 5.21 between the catalytic activity for glycerol dehydration of different copper oxide catalysts supported on alumina correspond to *i*) the yield of liquid products, and *ii*) the much lower glycerol conversion observed for CuO/Al_2O_3-*bas*. Expressly, the CuO/Al_2O_3-*npw* produces a higher yield of all those products collected in a liquid state (i.e., acetol, acids and esters, propanediols and others), averaging a 92% yield to liquids over the first 5 hours of reaction. On the contrary, CuO/Al_2O_3-*bas* averages 79% over the same time, and CuO/Al_2O_3-*ac* just 49%.

Interestingly, these catalysts show very similar reducibilities, copper oxide particle sizes and surface areas (see *Section 5.3*). Therefore, it is sensible to explain their dissimilarities in catalytic behavior based on their different acid-base properties. In particular, as NH_3 and CO_2 desorption curves exhibit very similar profiles in the three cases (Figure 5.11), the discussion can focus on the total number of centers. In that direction, that catalyst presenting the lower number of total acid sites and basic sites is the CuO/Al_2O_3-*npw* (see Table 5.5). As occurring for CuO/Al_2O_3-*bas*, introducing more acidity results in a decrease in the yield to every liquid product, but keeping a very high glycerol conversion. On the other hand, the introduction of more acidity combined with more basicity, as is the case for CuO/Al_2O_3-*ac*, results in a decrease in glycerol conversion, which even generates a more pronounced drop in the yield to liquid products.

The reduction in the liquid fraction should be associated with the generation of products resulting from secondary reactions. One possibility could be the formation of heavier by-products that will be either present in the solid fraction, stuck to the catalyst surface, or in the liquid phase but remaining undetected by GC. Another option would be decomposition reactions leading to gas formation. In both cases, as long as the conversion keeps being high, as in the case of CuO/Al_2O_3-*bas*, the catalyst overreacts with our reaction mixture. Thus, when the catalyst has enough acidity to enable the glycerol – catalyst interaction, the introduction of more acid functionalities brings about the formation of undesired by-products.

On the other hand, the obvious lower activity observed for CuO/Al_2O_3-*ac*, which has almost an equivalent acidity to CuO/Al_2O_3-*bas* (200 vs 192 μmol/g), should be associated with the more significant number of basic sites (54 vs 33 μmol/g). Nonetheless, further

studies would be necessary to understand exactly which role might be ascribed to the basic centers.

5.5.5 Catalytic activity for CuO supported on zirconia materials

The current section describes the results obtained for catalysts based on copper oxide supported on zirconium oxide, summarized in Figure 5.22. First, it is necessary to highlight there are no significant differences in the catalytic activity (i.e., glycerol conversion) between tetragonal zirconia and monoclinic zirconia. In this sense, the three catalysts present practically quantitative accumulative conversions of glycerol (TOS=1-8 h, see Figure 5.22a). However, a noticeable deviation between these catalysts is found in the selectivity towards acetol (Figure 5.22b and 5.22d) and, therefore, the yield towards this product. Mainly, this difference can be seen when comparing the catalyst containing only tetragonal zirconia (CuO/*t*-ZrO_2) as support to those containing either pure (CuO/*m*-ZrO_2) or mixed monoclinic phase (CuO/*mxt*-ZrO_2). Both materials containing 100 wt.% monoclinic phase and 60 wt.% monoclinic phase present selectivities greater than 60 mol.% towards the desired product, and since glycerol conversions are essentially quantitative, yields are of the same order. However, in the case of CuO/*t*-ZrO_2, selectivity towards acetol is below 50% as well as its yield, being this a very significant difference between the materials described in this section.

Additionally, another significant difference is the pace at which deactivation takes place in these materials. Thus, even though none of the catalysts significantly loses activity in the operation time studied, a remarkable change is observed in the selectivity calculated taking into account the composition of the liquid fraction. This fact reveals an alteration in the surface physicochemical properties of the catalysts, this change being more noticeable in the case of CuO/*t*-ZrO_2 catalyst, which is possibly related to the presence of a greater number of by-products. Although these by-products do not seem to poison the catalyst significantly in terms of activity, they modify the selectivity to acetol by either inhibiting the centres promoting the acetol pathway or promoting those leading to the formation of other by-products different from our target molecule.

Finally, and in the same line as the two differences mentioned above, the carbon balance for the catalyst based solely on tetragonal zirconium oxide (CuO/*t*-ZrO_2) presents a

significantly lower value than that calculated for the monoclinic phase (CuO/*m*-ZrO_2). If we compare catalyst CuO/*m*-ZrO_2 with catalyst CuO/*t*-ZrO_2, by also considering the carbon present in the solid fraction (measured by EA), we can observe a difference in a carbon balance of ≈95% compared to a carbon balance ≈80%, respectively. This discrepancy shows the more significant presence of undetected by-products in the case of CuO/*t*-ZrO_2 sample, either heavy compounds or gaseous compounds. However, given that the yield to carbonaceous material deposited on the catalyst is practically identical in both cases, around 2 mol%, it is likely that the difference is found in the gas fraction, being the tetragonal zirconium catalyst more prone to produce this type of by-products. However, a detailed analysis of the gas fraction produced in each of these reactions remains as a future task to confirm this hypothesis.

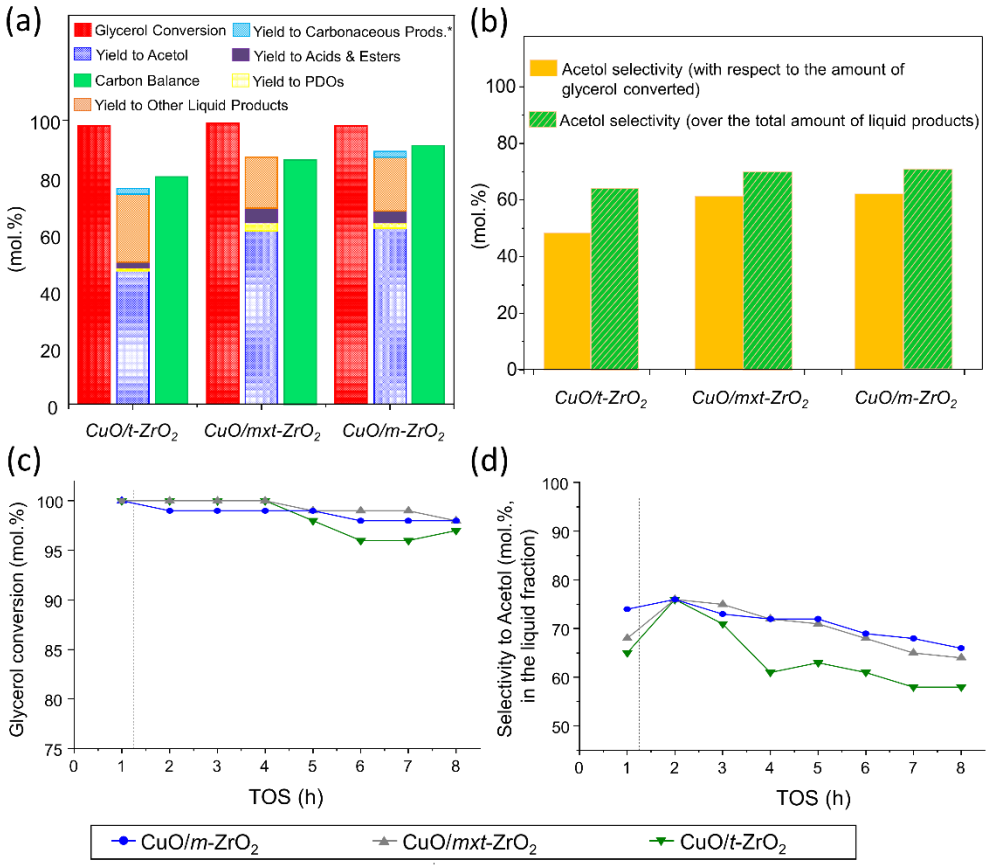

Figure 5.22. Cumulative (a) glycerol conversion, yield to liquids and carbon balance, (b) Acetol selectivities, (c) Glycerol conversion vs time on stream, and (d) Acetol selectivity vs time on stream for the dehydration of glycerol over different CuO supported on ZrO_2 catalysts. Reaction conditions: feed = methanol/glycerol (50/50 in weight), flow = 2 mL/h, with 0.5 g catalyst, at 240 ºC, TOS = 8 h. [a] Calculations for CuO/*mxt*-ZrO_2 based only on the liquid fraction. *Other liquid products: acetoin, acetoin methyl ether, 3-methoxybutanol, hydroxyacetone dimethyl acetal, solketal and other unidentified by-products.

5.5.6 Structure-activity relationships for CuO supported on ZrO_2 materials

Despite the higher reducibility observed for CuO when supported onto tetragonal ZrO_2, with respect to the other ZrO_2 polymorph, every CuO_x species in this system (see Figure 5.17) has a reduction temperature below that employed throughout the catalytic process.

Considering that plenty of hydrogen is produced during the process (see *Chapter 4*, *Section 4.3.3.3*), we can assume that every catalyst would be equally capable of generating the reduced active copper species with only this information. Therefore, a similar justification to what has been used in *Section 5.5.4* for CuO/Al_2O_3 materials can explain the differences observed between CuO/ZrO_2 materials. That is to say, the difference in the acid-base properties should be held accountable for the different catalytic behaviour.

In that direction, Table 5.8 shows yield to liquid products, yield to acetol, and number of acid sites. In this series, due to the different surface areas, acid sites were normalized per area unit. Significantly, the larger the total number of acid sites (per area unit), the lower the yield to liquid products and the yield to the desired acetol. In good agreement with what has been previously reported for CuO/Al_2O_3 materials (see *Section 5.5.4*), it seems that an excess of acid centres starts to impair the selectivity towards liquid products, resulting in the generation of by-products coming from secondary reactions, likely consisting, in this case, in gaseous products. Nonetheless, the role of the basic functionalities in these catalysts could not be totally ruled out, and TPD analysis with CO_2 must be done to complete the discussion.

Table 5.8. Yield to liquid products and yield to acetol compared to total acidity per area unit.

Catalyst	Yield to liquid products (mol.%)[a]	Yield to Acetol (mol.%)[a]	Acid site density (μmol NH_3/m^2)[b]
$CuO/t\text{-}ZrO_2$	73	47	2.53
$CuO/mxt\text{-}ZrO_2$	88	61	1.69
$CuO/m\text{-}ZrO_2$	87	62	1.53

[a] Reaction conditions: feed = methanol/glycerol (50/50 in weight), flow = 2 mL/h, with 0.5 g catalyst, at 240 ºC, average results for TOS = 1-8 h. [b] Measured by NH_3-TPD adsorption pulses until saturation.

Interestingly, it is also true that CuO/ZrO_2 presents an acid-base distribution and a total number of acid sites quite like that presented by CuO/Al_2O_3-*npw* (see *Sections 5.3* and *5.4*).

However, following the previous discussion in *Section 5.5.4*, its higher number of basic sites would be expected to result in worse catalytic behaviour. At this point, it is important to mention that section arrangement in this chapter has not been arbitrarily selected. The difficulties involved in making crossed comparisons rely on the variety of catalyst features changing from one catalyst belonging to one family to the another from a different one, making it challenging to explain and ascribe the differences to one specific factor. For instance, if we wanted to compare between CuO-PD/SiO_2-AL and CuO/*m*-ZrO_2 we should consider the different CuO_x reducibilities, the higher dispersion of the CuO nanoparticles in the former, the different acidity per area unit, and the different basicity per area unit. Not to mention that the nature of the active centres and the interface CuO – support can hardly be compared. In this sense, comparisons involving structure-activity associations have been limited between the materials belonging to one catalyst family (i.e., with an equivalent elemental composition).

5.6 Long term use, further selection, and reusability

At this point, an optimal catalyst has been found in each of the families studied. If we recapitulate the results of the previous sections, the most promising catalysts are CuO-PD/SiO_2-AL, CuO/Al_2O_3-*npw*, and CuO/*m*-ZrO_2. The three materials attaining similar results regarding yield to acetol (≈60%), for operating times between 1 and 8 h. Although, indeed, a too significant deactivation (in terms of glycerol conversion) is not observed for any of them, in the cases CuO/Al_2O_3-*npw* and CuO/ZrO_2-*m*, there seems to be a more significant selectivity loss towards the desired compound over time, with respect to the catalyst CuO-PD/SiO_2-AL. Nonetheless, to further strengthen the final catalyst selection, aiming at maximizing acetol production for the following steps towards the desired organonitrogen chemicals, the three catalysts are compared in Figure 5.23 and forced to work until starting to suffer a more noticeable deactivation.

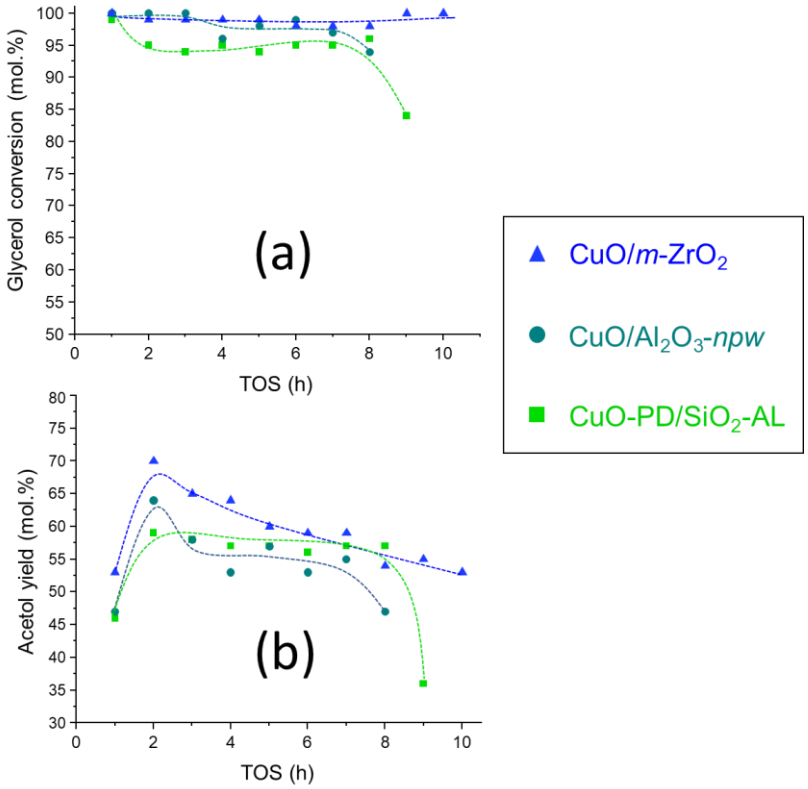

Figure 5.23. (a) Glycerol conversion, and (b) yield to acetol for CuO-based materials onto different supports. Reaction conditions: feed = methanol/glycerol (50/50 in weight), flow = 2 mL/h, with 0.5 g of catalyst at 240 ºC). Note: Dashed traces only serve as visual guidelines.

Regarding conversion (Figure 5.23a), no major deactivation is seen for CuO/*m*-ZrO_2 and CuO/Al_2O_3-*npw* catalysts, although it seems to be slightly starting at TOS = 8 h in the case of the alumina-based material. On the contrary, a critical drop is observed at TOS = 9 h for the CuO-PD/SiO_2-AL catalyst. It must be mentioned that this drop is very likely to be associated with reactor blockages rather than with a true catalyst deactivation. Notoriously, the liquid mass collected at the reactor outlet was significantly lower than what was ordinarily being weighted. Moreover, in several experiments carried out with this catalyst, the reactor was blocked at times in-between 9 and 10 h, being impossible to unseal the system and continue the experiment. Probably, a major disadvantage of this silica-based catalyst is the difficulty that the catalyst particles present to keep together and not disintegrate into finer powder throughout the reaction. Therefore, with respect to the

content of this thesis, we opted to discard this catalyst and continue using CuO/*m*-ZrO_2 and CuO/Al_2O_3-*npw*, since the pellets prepared at the beginning of the experiment were more compact and resistant than any of those that contained silica as support. Notwithstanding, an open research line is still dedicated to improving the CuO-PD/SiO_2-AL catalyst compaction process and thus studying avoiding its disintegration during the catalytic process and its long-term operational possibilities.

Hence, staying with the other two catalysts CuO/*m*-ZrO_2, and CuO/Al_2O_3-*npw*, both show almost quantitative glycerol conversions, although deactivation seems to happen earlier (at TOS ≈7 h) for CuO/Al_2O_3-*npw*. In any case, it is by taking a closer look at the acetol yield profiles depicted in Figure 5.23a when a gradual drop in the yield to acetol can be seen for both materials. As discussed in previous sections, an excess of active sites generating undesired by-products are likely to be the cause of this steady change in the preferred reaction pathways. Nonetheless, in the case of the CuO/Al_2O_3-*npw* catalyst, this decrease in yield to the desired product seems to be more pronounced. The values exhibited during the previous operating times are generally lower than those presented by CuO/*m*-ZrO_2 catalyst. In fact, the difference corresponding to the operating times between 1 and 7 hours regarding the acetol yield is almost 10 points, with the CuO/*m*-ZrO_2 catalyst presenting a cumulative yield of 63% compared to the 56% exhibited by the catalyst CuO/Al_2O_3-*npw* during the same time on stream.

Based on this last comparison, the decision was made to continue with the catalyst CuO/*m*-ZrO_2 the studies, the optimizations, and its use in the production of acetol for the subsequent research for the synthesis of the desired nitrogen heterocycles. However, it is necessary to consider the CuO/*m*-ZrO_2 catalyst suffers a process of change during the reaction that, although it does not affect the activity, that is to say, the glycerol conversion, in the times studied (up to 10 hours), it does cause a progressive decrease in selectivity and therefore in the yield to the product of interest. This drop means going from 70% yield at TOS = 2h to 53% at TOS = 10h. For this reason, it was decided to study the possibility of regenerating the catalyst after 10 hours of use by an *in-situ* calcination process, under air flow, at 550 ºC (4 h). In table 5.9, we see that the regenerated catalyst does not lose metallic content. In addition, the equivalent X-ray diffraction pattern and TPR profile suggest that the regenerated catalyst does not present a significant metallic dispersibility loss either (see

Figure 5.24). But beneficially, the regeneration process allows for cleaning the catalyst surface.

Table 5.9. Effect of use (TOS = 8 h) and regeneration on metal loading, surface area, organic matter deposition and metallic dispersion for CuO/*m*-ZrO_2.

Physicochemical parameter	**Fresh CuO/*m*-ZrO_2**	**Used CuO/*m*-ZrO_2**	**Regenerated* CuO/*m*-ZrO_2**
Cu loading (wt%)[a]	4.8 ± 0.2	n/d	4.6 ± 0.2
BET Area (m^2/g)[b]	45	n/d	42
Organic matter (wt%)[c]	-	10.3	3.3

[a] Calculated by ICP. Random error estimated by applying the *t student* (0.98) criterion to three repeated measurements of a Cu-containing material. [b] From N_2-adsorption isotherms (BET method). [c] Estimated by TGA (after TOS = 10 h). *Washed with 40 mL of MeOH (2 mL/h) in the reactor at 240 ºC, then treated at 550 ºC for 4 h in air flow (3 ºC/min, 50 mL/min).

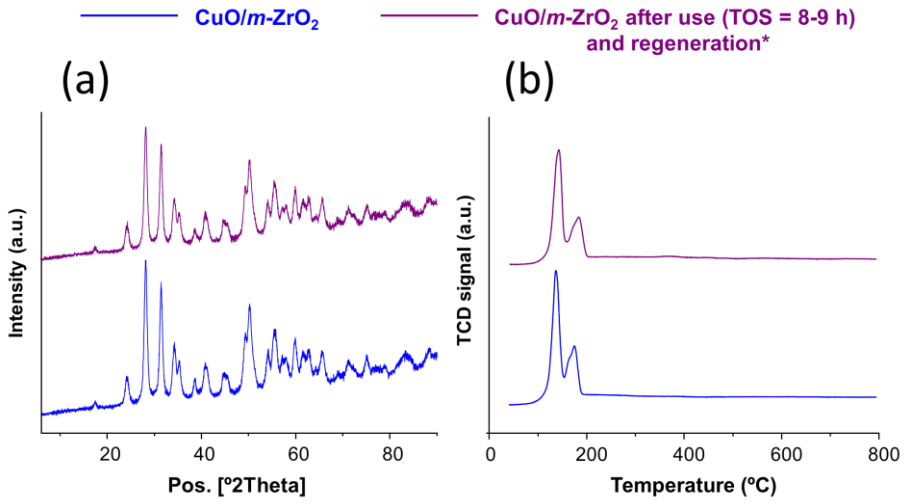

Figure 5.24. (a) XRD patterns and (b)TPR traces for CuO/*m*-ZrO_2 (blue), and CuO/*m*-ZrO_2 used for 9 h and regenerated (purple). *Washed with 40 mL of MeOH (2 mL/h) in the same reactor at the reaction temperature, then treated at 550 ºC during 4 h in air flow (3 ºC/min, 50 mL/min).

As we see in Figure 5.25, the catalyst was successfully used after *in-situ* regeneration in the dehydration of glycerol to acetol for 8 hours on stream, showing an acetol yield essentially analogous to the fresh material in the first hours. This fact is of great importance, not only because it unlocks the possibility of using this catalyst repeatedly for the continuous production of acetol with high productivity, but also because shows that the main cause of the change in catalytic specific activity towards acetol, is caused either by the progressive poisoning of the active centers favoring acetol or due to a physicochemical modification of the catalyst surface. This physicochemical modification could involve a total copper reduction to Cu(0), already proved in *Chapter 4* to be less active than Cu(I), or a generation of new acid-base functionalities so that new centers could be generated during the reaction, leading to the formation of unwanted by-products. In any case, a thermal regeneration treatment is sufficient for the catalyst to recover original properties both at the level of surface cleanliness and the nature of the active sites. Nonetheless, although the regeneration treatment does not seem to affect either the metallic dispersion or other textural properties of the catalyst, such as the surface area (see Table 5.9 and Figure 5.24), the cleaning is not entirely effective (from 10.3 to 3.3 % of carbonaceous matter). In this line, the catalyst deactivation process starts earlier in the catalyst used a second time, compared to the fresh catalyst. Therefore, further optimization of the catalyst regeneration, allowing for a more successful cleaning but remaining harmless to metal dispersion, is required.

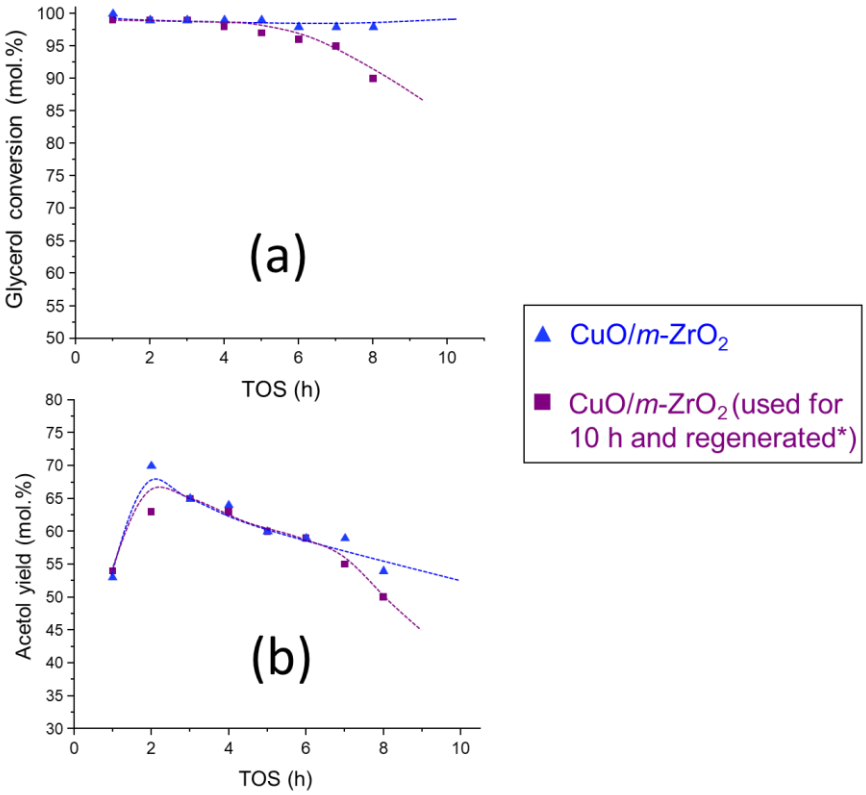

Figure 5.25. (a) Glycerol conversion, and (b) yield to acetol for CuO/m-ZrO_2 onto different supports. Reaction conditions: feed = methanol/glycerol (50/50 in weight), flow = 2 mL/h, with 0.5 g of catalyst at 240 ºC). Note: Dashed traces only serve as visual guidelines. *Washed with 40 mL of MeOH (2 mL/h) in the same reactor at the reaction temperature, then treated at 550 ºC during 4 h in air flow (3 ºC/min, 50 mL/min).

5.7 Insights into the catalyst behaviour: an *in-situ* XPS-FTIR study

With the aim of tackling and disentangling the true nature of the "working catalyst" CuO/*m*-ZrO_2 an *in-situ* study combining XPS and FTIR experiments was carried out.

In *Chapter 4* we worked with 1,2-propanediol as a probe molecule but experiments to demonstrate how the real molecule (glycerol) interacts with the catalyst could mean a

substantial increase in the impact of this research. Therefore, mixtures glycerol/ methanol and glycerol/water were adsorbed on CuO/*m*-ZrO_2, by incipient wetness impregnation. The idea was slowly raising the temperature, following by XPS the evolution of Cu*2p* and Cu *AES*, and by FTIR the reactivity of the organic molecule with three objectives: *i*) ascertaining how Cu gets partially reduced on the presence of glycerol and methanol (both should act as a reducing agent, at some point), *ii*) providing compelling evidence of the true nature of the active species and of whether, when the catalyst generates these active species, the reaction proceeds towards the formation of a molecule containing a C=O, *iii*) comparing the catalyst specific activity in the absence and presence of MeOH.

Figure 5.26 shows the XPS analyses of the catalyst CuO/*m*-ZrO_2 (a) and (b) the same material but impregnated with a 50:50 wt.% glycerol/MeOH mixture. Two different contributions could be identified in the Cu$2p_{3/2}$ signal based on CuO and Cu_2O standards analyses in every spectrum at 932.2-932.6 eV and 933.8-934.1 eV, assigned to Cu(II) and Cu(I/0), respectively.

Interestingly, by heating up the system CuO/*m*-ZrO_2 impregnated with the mixture MeOH/glycerol and comparing it to the catalyst itself CuO/*m*-ZrO_2, XPS analyses lead us to conclude that the reduction degree is higher in the presence of a methanol/glycerol mixture than to what the catalyst could experiment just under the photo reductive conditions. In this sense, Table 5.10 shows the quantification for Cu(I/0) and Cu(II) components. That is again a proof of the reaction mixture reducing the catalyst and of the fact that the active centers should be reduced copper species.

Although the Cu*2p* spectra has been fitted using standards for CuO and Cu_2O, the Cu(I) component may also include a contribution from Cu(0). Nonetheless, when calculating the modified Auger parameter in these samples CuO/*m*-ZrO_2 heated alone and with the glycerol/MeOH mixture, the values are between 1848.0 and 1848.5 eV, thereby reassuring most of that component should correspond to Cu(I), and as in *Chapter 4*, pointing to these species as the active Cu centers to carry out the glycerol dehydration to acetol.

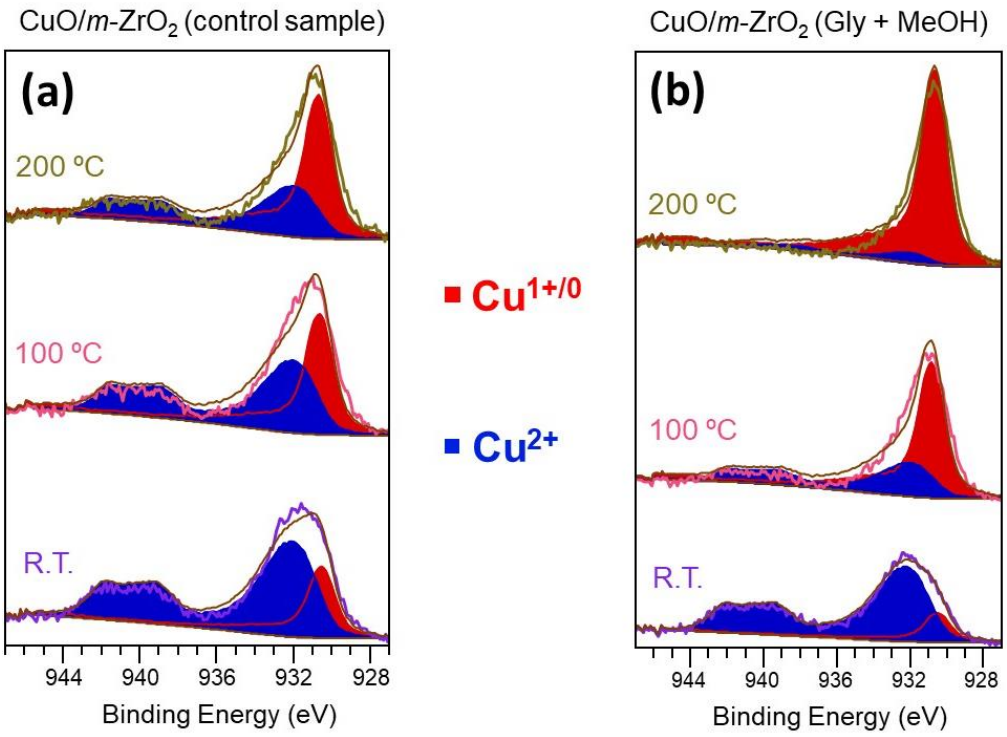

Figure 5.26. (a) Cu$2p_{3/2}$ XPS region studied at different temperatures for (a) CuO/*m*-ZrO_2 and (b) CuO/*m*-ZrO_2 catalyst impregnated with a mixture MeOH/Glycerol (50:50 wt.).

Table 5.10. Qualitative and quantitative data for "*in-situ*" XPS experiments with CuO/*m*-ZrO_2.

Experiment	$Cu2p_{3/2}$ maxima (eV)	Cu $L_3M_{45}M_{45}$ maxima (eV)	α^a (eV)	$Cu^{1+/0}$: Cu^{2+}
Control (R.T.)	933.3	915.9	1849.2	27 : 73
Control (100 ºC)	932.8	915.6	1848.4	45 : 55
Control (200 ºC)	932.8	915.3	1848.1	58 : 42
Gly + MeOH (R.T.)	934.0	915.7	1849.7	16 : 84
Gly + MeOH (100 ºC)	932.7	915.5	1848.2	66 : 34
Gly + MeOH (200 ºC)	932.4	915.6	1848.0	92 : 8

[a] $Cu2p_{3/2}$ XPS (BE) + $L_3M_{45}M_{45}$ CuAES (KE).

Once the presence of this copper (I) species on the system CuO/*m*-ZrO_2 impregnated with the mixture MeOH/glycerol was confirmed, an FTIR study was carried out with an analogous mixture and with a system based on CuO/*m*-ZrO_2 impregnated with a mixture MeOH/H_2O (see *Section 3.3.7.5*). Figure 5.27 shows how the reaction proceeds through the formation of a C=O group, which takes place much more easily when using MeOH as the solvent. In the case of the sample with glycerol and methanol co-adsorbed on CuO/*m*-ZrO_2, by increasing the temperature, the bands corresponding to the carbonyl group (1705 cm^{-1}) and the carbonyl group coordinated to a metal center (1665 cm^{-1}) can already be observed at 60 ºC, being noticeably increased when the temperature rises above this value and being perfectly obvious at 120 ºC. On the contrary, in the sample impregnated with glycerol and water, at temperatures below 140 ºC, any increase at the wavenumbers corresponding to the bands described above for the carbonyl group was detected. Instead, the temperature had to be increased to 140 ºC and especially up to 160 ºC to observe significant changes corresponding to the C=O group formation. Therefore, this study supports and completes those carried out at Chapter 4, pointing out copper (I) as the critical active site to generate the carbonylic group.

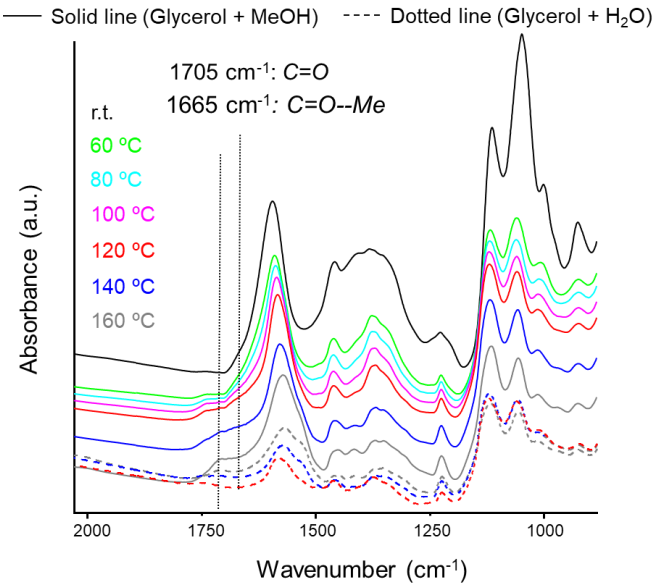

Figure 5.27. FTIR spectra acquired at different temperature steps under static vacuum conditions for samples impregnated with a mixture of 90 wt.% solvent (MeOH or water) and 10 wt.% glycerol.

5.8 Additional improvement on the CuO/*m*-ZrO_2 system

Throughout this chapter and *Chapter 4* we have seen and verified the system capacity to generate the active copper species together with CuO dispersion, already described as a catalytic descriptor for this reaction[5], are two properties that could lead to a better catalytic result. Thus, to further improve the CuO/*m*-ZrO_2 catalyst, it was decided to prepare the compositionally equivalent catalyst by an alternative route, trying to find nanoparticles with dispersion, morphologies, and surface properties other than those provided by the pore volume impregnation method. With this aim, two catalysts were prepared containing ≈3.5% by weight of copper (3.5RV-CuO/*m*-ZrO_2) and ≈5.0% (5.0RV-CuO/*m*-ZrO_2), see Table 5.11. The particles were formed by preparing reverse micelles (RV), that is, aqueous micelles containing the copper nitrate solution developed in an organic medium (hexane). Later, the support was added, and the solid-liquid mixture was well homogenized. Then, the particles were precipitated by chemical reduction with hydrazine and end up mostly placed onto the support. These particles are subsequently oxidized in the process of

removing the surfactant, giving rise to supported copper oxide nanoparticles. The full explanation regarding the chosen method can be found in *Section 3.2.6*. The two catalysts selected to make the comparisons are CuO/*m*-ZrO_2 (with a 5 wt.% Cu, the typical catalyst so far reported) and 3.5CuO/m-ZrO_2 (with a 3.6% Cu, measured by ICP).

Table 5.11. Main physicochemical and textural properties of *m*-ZrO_2-supported CuO materials prepared by reverse micelle methodology.

Catalyst	Cu loading (wt%) [a]	BET area (m^2/g) [b]	Pore volume (cm^3/g) [c]
3.5RVCuO/*m*-ZrO_2	3.6	95	0.22
5.0RVCuO/*m*-ZrO_2	6.4	91	0.28

[a] Calculated by ICP. [b] Calculated from N_2-adsorption isotherms data (BET method).

For these new materials, XRD patterns show what appears to be a significant difference (Figure 5.28) with respect to those obtained for materials prepared by incipient wetness impregnation. At 30.3º, a shoulder can be exclusively seen in both materials prepared by the reverse micelle method. This peak, which does not correspond to the reflection of any crystalline plane of copper (II) oxide, nor to any characteristic peak of monoclinic zirconia, might be associated with the (*2 0 0*) planes of a crystalline copper oxide phase known as paramelaconite, containing copper(I) in its structure, and crystallizing in the tetragonal crystal system (Cu_4O_3, specifically $Cu^{I}_2Cu^{II}_2O_3$). Additionally, lattice space analyses of HR-TEM measurements detected a distance of 0.286 nm which, when compared to the reference pattern of paramelaconite (JCPDS code: 00-003-0879), could be ascribed to the interplanar distance between the *(2 0 0)* crystallographic planes (0.290 nm). However, we must be cautious because no other peaks for paramelaconite were detected in the XRD diffractogram, and XRD peaks from planes (*1 0 1*) of cubic/tetragonal zirconia might also appear in that region (30.0-30.5º, JCPDS code: 01-079-1764). More importantly, paramelaconite was reported in 1986 to be a product of the decomposition of CuO under an electron microscope[13].

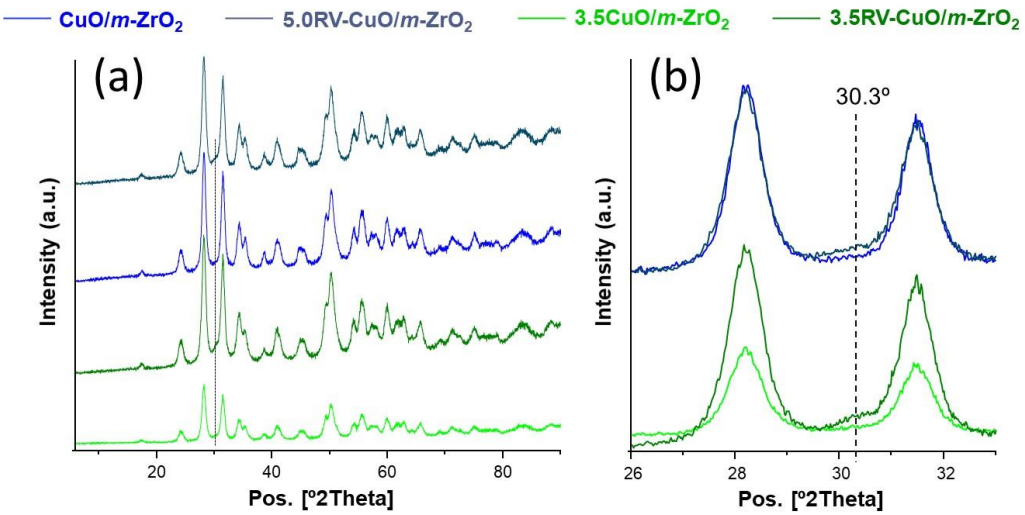

Figure 5.28. (a) XRD patterns of CuO supported on *m*-ZrO_2 materials prepared by different procedures. (b) Inset of Figure 5.28a.

The H_2-TPR traces in Figure 5.29a expose how the catalysts prepared by the reverse micelle methodology have higher reducibility when comparing those materials with the lowest amount of copper, the high temperature peak disappearing with respect to the material prepared by the original procedure. This reducibility variance indicates that the supported copper oxide species have a different nature, either in its particle size, crystalline phase, interaction with the support (unlikely because monoclinic zirconium oxide is present in both cases) or concerning the particle morphology and/or the surface species present on it. The fact that this distinction can only be detected by H_2-TPR at lower copper loadings, probably means that the reverse micelle methodology allows for a higher dispersion of the CuO on the zirconia surface but, from a specific copper loading onwards, the saturation of CuO in the material surface decreases the amount of highly dispersed CuO regardless of the synthesis methodology.

Although H_2-TPR had been previously used as an indirect measure of the metallic dispersion, by HR-TEM very similar particles in size and shape were detected for the four samples (Figure 5.30). Nonetheless, as previously discussed in *Section 5.4*, lattice spacing was required to distinguish between CuO nanoparticles and the support, so that not a representative number of particles could be considered in any of the cases. Sadly, we could

not count in the present thesis on N_2O titration for these materials. Therefore, this similar size and shape detected by HR-TEM can be just taken as a preliminary clue indicating no major differences in copper oxide dispersion, unfortunately pointing out the opposite of H_2-TPR analyses.

Interestingly, comparing the FTIR spectra of CO titration at low temperature for both materials CuO/*m*-ZrO_2 and 5.0RV-CuO/*m*-ZrO_2 (Figure 5.29b) unravels two remarkable facts. First, the reverse micelle methodology results in CuO particles that block the acid centers of the support to a lower extent than those prepared by the classic pore volume impregnation method. These Lewis acid sites characteristics of monoclinic zirconia are reportedly located in the marked area (Figure 5.29, from 2190 – 2145 cm^{-1})[14]. Second, part of the spectra corresponding to reduced Cu(0) particles seems to have a more critical contribution from oxyphilic copper (2100 cm^{-1}), sometimes reported as Cu_2O[15]. Therefore, with respect to the material CuO/*m*-ZrO_2 the reverse micelle methodology seems to result in a material with less acidity and a greater tendency to generate Cu(I) when submitted to a reducing environment.

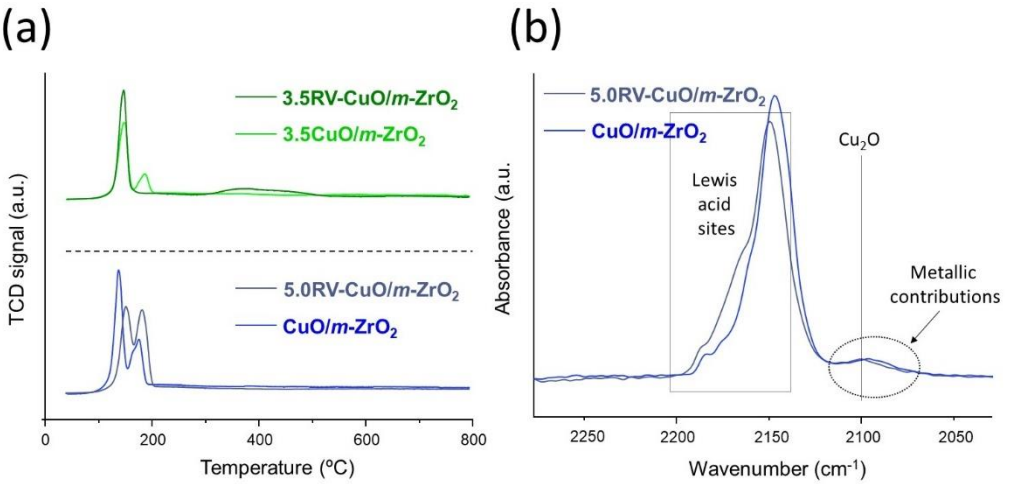

Figure 5.29. (a) TPR traces and (b) FTIR for low temperature CO titration at saturation coverage for CuO supported *m*-ZrO_2 materials prepared by different procedures.

Considering all the characterization data handled together, we can suggest that those copper oxide nanoparticles synthesized by preparing reverse micelles present higher

reducibility and are likely to have a more significant tendency to generate Cu(I) species. These distinctions unravel specific differences in nature. Importantly, these differences seem to involve the higher presence of copper (I), which can be of interest in our catalytic application. Explanation on the origin of these differences might be the formation of an alternative copper oxide phase or the higher dispersion achieved by the reverse micelle procedure. Nonetheless, further characterization will be needed to find the right justification for the changes seen in the physicochemical properties.

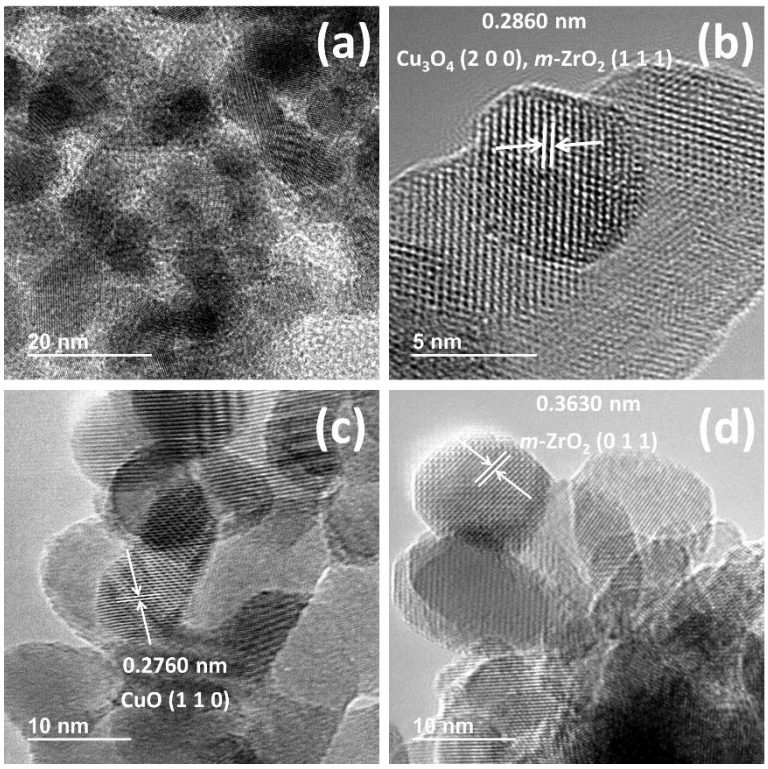

Figure 5.30. HR-TEM micrographs for 3.5RVCuO/*m*-ZrO_2: (a) and (b); and for 5.0RVCuO/*m*-ZrO_2: (c) and (d).

Once we had verified that we had succeeded in synthesizing some copper oxide nanoparticles that are somehow different to those prepared by incipient wetness impregnation, these materials were evaluated in catalysis. In Figure 5.31a, we can see how, when comparing materials with the highest copper percentage, there are no significant differences in glycerol conversion, showing a very similar behaviour. However, when representing the acetol yield evolution over time on stream, the 5.0RV-CuO/*m*-ZrO_2 can keep the yield much steadier. Nonetheless, the amount of copper in 5.0RV-CuO/*m*-ZrO_2 is slightly higher than that usually seen in those batches usually prepared for CuO/*m*-ZrO_2 (see Tables 5.6 and 5.9) so that this result needs to be interpreted with caution. More unequivocally, when we reduce the amount of copper, it is noticeable the material prepared by reverse micelles shows a higher yield towards the desired product (Figure 5.31b). In this case, both materials had exactly the same amount of copper (according to ICP data). This result leads to thinking that this methodology, in theory, can provide some copper oxide nanoparticles different in nature, probably in their dispersion and/or capability to generate copper (I) oxide, which results in a significant improvement in specific catalytic activity. In this way, when this procedure prepares the catalyst, it would be possible to work with smaller amounts of copper and, therefore, with a cheaper catalyst. However, this catalyst remains a line of future research and aspects such as long-term use, and reusability of this catalyst must be studied. For example, it is still necessary to investigate whether the 5 wt.% catalyst prepared by reverse micelles can maintain catalytic activity more than that prepared by pore volume impregnation. On the other hand, it would also be necessary to check if either the reaction or the regeneration process does not give rise to equivalent nanoparticles to those attained with the original method.

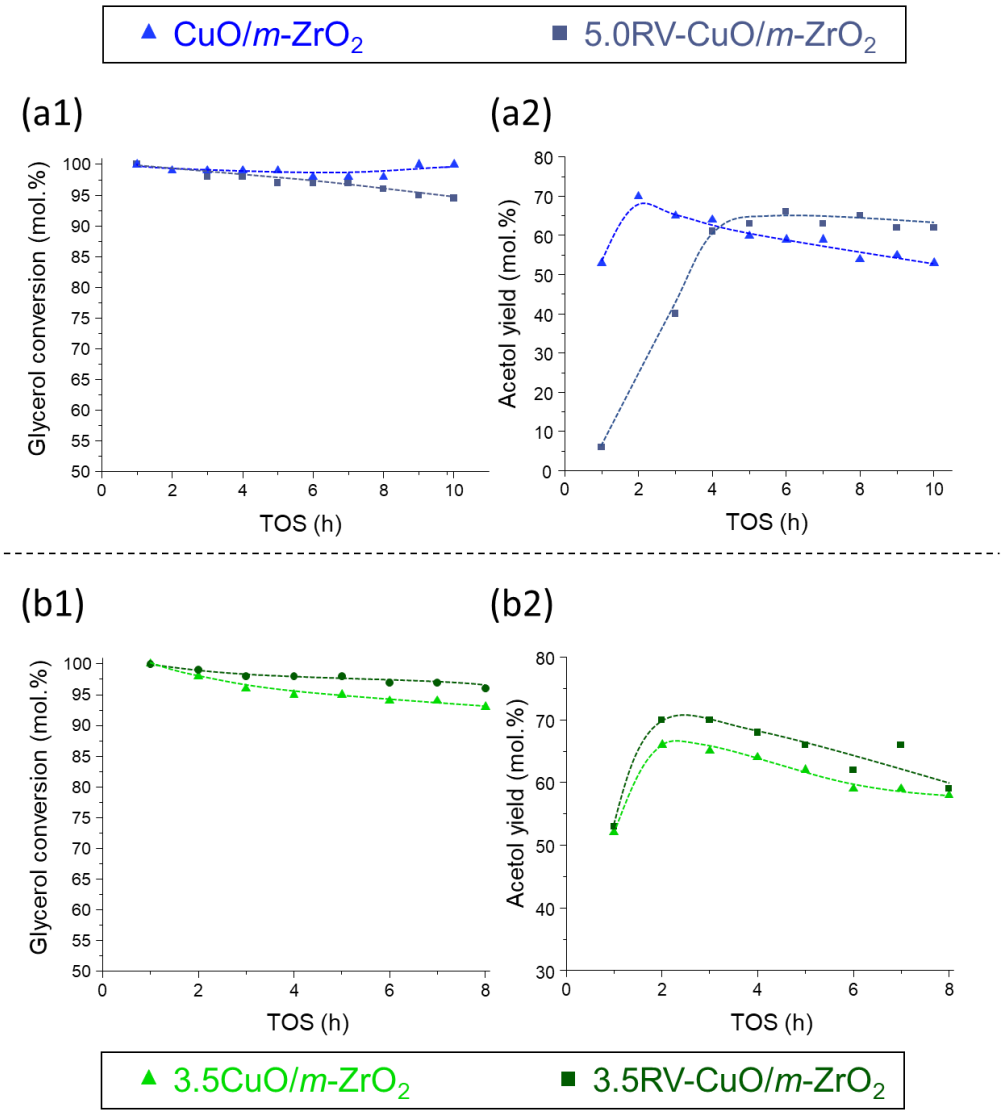

Figure 5.31. (1) Glycerol conversion, and (2) yield to acetol for (a) CuO/*m*-ZrO_2 and 5.0RV-CuO/*m*-ZrO_2 and (b) 3.5RV-CuO/*m*-ZrO_2. Reaction conditions: feed = methanol/glycerol (50/50 in weight), flow = 2 mL/h, with 0.5 g of catalyst at 240 ºC. Note: Dashed traces only serve as visual guidelines.

5.9 Conclusions

In this chapter, different families of materials based on copper oxide supported on different high surface area inorganic supports have been synthesized. A detailed characterization study together with catalytic tests in the glycerol dehydration to acetol has allowed for establishing the following conclusions:

- The series of materials based on copper oxide supported on SiO_2 shows a catalytic behaviour highly dependent on the dispersion degree achieved for the CuO nanoparticles. Higher dispersion (smaller particle sizes) brings with it an increase in the metal active area and higher acidity. These factors are beneficial to increase the yield of the desired product. However, an excess of dispersion results in too high acidity, causing a decrease in the acetol yield. Therefore, there is an optimum for these small particle sizes (2.1 nm measured by STEM, 5.8 nm measured by N_2O chemisorption).

- The family of copper oxide on alumina catalysts having similar CuO particle sizes presents a high dependence on acid-base properties to achieve adequate performance for acetol production. In that sense, the material CuO/Al_2O_3-*npw* seems to expose only the acidity needed to permit glycerol adsorption. However, higher acid site densities and the presence of basic centers result in undesired products, thus impairing yield to liquids, glycerol conversion and, therefore, giving lower acetol yields.

- In the study of CuO/ZrO_2 materials, again, the different acid-base properties that occur depending on the crystalline phase of the zirconia used are fundamental to determine the catalytic activity. In this sense, CuO/*m*-ZrO_2 has lower acid density than CuO/*t*-ZrO_2, leading it to carry out the reaction more selectively and with less formation of certain by-products that seem to contribute to catalyst poisoning. Specifically, this catalyst is the one that, among all the families studied, presents the best productivity for the desired product, and can carry out the process for a longer time, its reuse being more possible from an industrial viewpoint.

- Thanks to the combination of *in-situ* studies by FTIR and XPS spectroscopy applied to the CuO/*m*-ZrO_2 material, it has been possible to corroborate the conclusions established in *Chapter 4* regarding catalyst operation. In this respect, the catalyst generates copper (I) species, which are those fundamentally active for the glycerol acetol dehydration reaction, and the reaction proceeds through an intermediate containing a carbonyl group.

- Finally, it is possible to improve the CuO/*m*-ZrO_2 catalyst by incorporating copper oxide particles synthesized through the formation of reverse micelles. These new copper oxide nanoparticles have a different nature, which includes different reducibility, and an enhanced ability to generate the active species (Cu(I)). Its different nature is likely to be based on the presence of copper oxide in another crystalline phase and/or a better dispersion achieved by this synthetic methodology.

5.10 References

[1] Z. Ma, F. Zaera, Heterogeneous Catalysis by Metals, Wiley, 2006. https://doi.org/10.1002/0470862106.IA084.

[2] Federica Zaccheria, Nicola Scotti, Marcello Marelli, Rinaldo Psaro, Nicoletta Ravasio, Unravelling the properties of supported copper oxide: can the particle size induce acidic behaviour?, Dalt. Trans. 42 (2013) 1319–1328. https://doi.org/10.1039/C2DT32454G.

[3] F. Zaccheria, N.I. Shaikh, N. Scotti, R. Psaro, N. Ravasio, New Concepts in Solid Acid Catalysis: Some Opportunities Offered by Dispersed Copper Oxide, 57 (2014) 1085-1093. https://doi.org/10.1007/s11244-014-0273-9.

[4] S. Sato, M. Akiyama, R. Takahashi, T. Hara, K. Inui, M. Yokota, Vapor-phase reaction of polyols over copper catalysts, Appl. Catal. A Gen. 347 (2008) 186-191. https://doi.org/10.1016/j.apcata.2008.06.013.

[5] R.J. Chimentão, P. Hirunsit, C.S. Torres, M.B. Ordoño, A. Urakawa, J.L.G. Fierro, D. Ruiz, Selective dehydration of glycerol on copper based catalysts, Catal. Today. 367 (2021) 58–70. https://doi.org/10.1016/J.CATTOD.2020.09.031.

[6] C.V. Rode, M.A. Hengne, A.A. Ghalwadkar, R.B. Mane, P.H. Mohite, H.S. Potdar, Process for preparation of hydroxyacetone or propylene glycol, WO2011/138643, 2014.

[7] R.B. Mane, C. V. Rode, Continuous dehydration and hydrogenolysis of glycerol over non-chromium copper catalyst: Laboratory-scale process studies, Org. Process Res. Dev. 16 (2012) 1043-1052. https://doi.org/10.1021/op200383r.

[8] J. Garcés, R. Arrué, N. Novoa, A.F. Peixoto, R.J. Chimentão, Glycerol Valorization

over ZrO2-Supported Copper Nanoparticles Catalysts Prepared by Chemical Reduction Method, Catal. 11 (2021) 1040. https://doi.org/10.3390/CATAL11091040.

[9] W. Hertl, Surface Chemistry of Zirconia Polymorphs, Langmuir. 5 (1989) 96–100. https://pubs.acs.org/sharingguidelines (accessed September 28, 2021).

[10] K.-H. Jacob, E. Knözinger, S. Benier, Adsorption sites on polymorphic zirconia, J. Mater. Chem. 3 (1993) 651–657. https://doi.org/10.1039/JM9930300651.

[11] Y. Zhang, C. Chen, X. Lin, D. Li, X. Chen, Y. Zhan, Q. Zheng, CuO/ZrO2 catalysts for water–gas shift reaction: Nature of catalytically active copper species, Int. J. Hydrogen Energy. 39 (2014) 3746–3754. https://doi.org/10.1016/J.IJHYDENE.2013.12.161.

[12] S. Célerier, S. Morisset, I. Batonneau-Gener, T. Belin, K. Younes, C. Batiot-Dupeyrat, Glycerol dehydration to hydroxyacetone in gas phase over copper supported on magnesium oxide (hydroxide) fluoride catalysts, Appl. Catal. A Gen. 557 (2018) 135-144. https://doi.org/10.1016/j.apcata.2018.03.022.

[13] N.J. Long, A.K. Petford-Long, In-situ electron-beam-induced reduction of CuO: A study of phase transformations in cupric oxide, Ultramicroscopy. 20 (1986) 151–159. https://doi.org/10.1016/0304-3991(86)90181-6.

[14] K.I. Hadjiivanov, G.N. Vayssilov, Characterization of Oxide Surfaces and Zeolites by Carbon Monoxide as an IR Probe Molecule, Adv. Catal. 47 (2002) 307–511.

[15] X. Yang, S. Kattel, K. Xiong, K. Mudiyanselage, S. Rykov, S.D. Senanayake, J.A. Rodriguez, P. Liu, D.J. Stacchiola, J.G. Chen, Direct Epoxidation of Propylene over Stabilized Cu+ Surface Sites on Titanium-Modified Cu2O, Angew. Chemie. 127 (2015) 12114–12119. https://doi.org/10.1002/ANGE.201504538.

Chapter 6
Towards a semicontinuous catalytic process for 2-methylpiperazine synthesis *via* acetol

6.1 Introduction

As thoroughly detailed in *Chapter 1: Introduction*, the piperazine ring finds application as a building block for many high added value drugs[1–3], as well as in CO_2 scavenging systems[4–8]. Nonetheless, mainly due to their severe reaction conditions, large-scale commercial application of their synthetic routes is still complex. Therefore, this thesis intended to design a new catalytic route using glycerol as a carbon source to produce 2-methylpiperazine, *via* its derivative hydroxyacetone (or acetol), under moderate conditions through reductive cyclo-amination with ethylenediamine (see Scheme 1.5, in *Chapter 1: Introduction*). In our case, the use of acetol is proposed to keep the right balance between the high reactivity of the corresponding di-carbonyl compound (i.e., pyruvaldehyde) and the low reactivity of the glycol (i.e., 1,2-propylenglycol).

The process requires redox-type active centers, and, additionally, acid-base centers of moderate strength can at times facilitate the process. The proposed mechanism for the reductive amination of carbonyl compounds is attached below (Scheme 6.1):

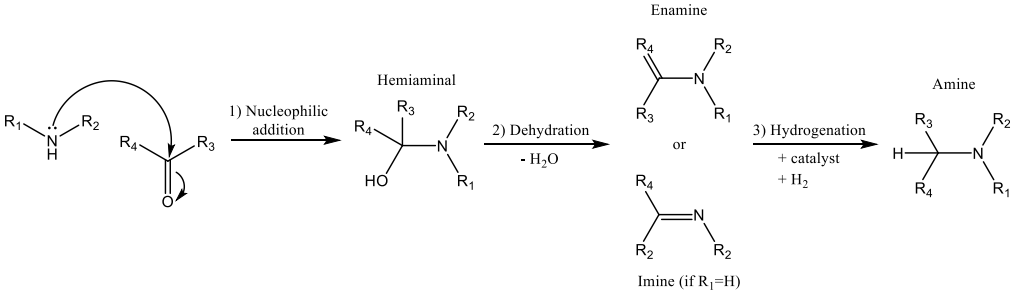

Scheme 6.1. Reductive amination mechanism for carbonyl-type compounds – Adapted from Refs.[9,10].

When the reagents are aldehydes or ketones, the reaction will comprise: i) nucleophilic addition and generation of the hemi-aminal intermediate, ii) dehydration and formation of the intermediate imine or enamine, and iii) imine or enamine reduction to yield the final substituted amine. The dehydration of the enamine or imine is usually the controlling stage of the reaction rate since it would compete with the carbonyl group hydrogenation[11].

The reductive amination of aldehydes and ketones using different boron reducers has been widely studied, with sodium triacetoxyborohydride standing out above the rest for the steric and electronic properties that make it a more moderate reducer than sodium borohydride or sodium cyanoborohydride. Furthermore, the use of $NaBH(OAc)_3$ avoids the formation of toxic by-products generated with the use of cyanoborohydride and is also easily separable from the reaction products [12–15]. However, the *in-situ* generations of this compound from sodium borohydride as well as the use of acetic acid and other additives constitute significant drawbacks that it would be essential to overcome.

On the other hand, over the last decades, different processes have been described that use complexes of Fe, Ir or Pd as catalysts and molecular hydrogen as a reducing agent, these being critical in the synthesis of chiral amines[16–18]. However, in addition to the use of expensive and ineffective catalysts, it can be found that these processes tend to use quite extreme pressure and/or temperature conditions, and on top of that, they present the usual downsides associated with homogeneous catalysis. For this reason, the development of heterogeneous catalysts capable of accomplishing this reaction under moderate conditions with aldehydes, ketones and, even, β-hydroxyketones to generate nitrogen heterocycles is a captivating pathway that had already been explored by some authors, being the most used catalysts mixed metal oxides and modified zeolites with metal functions (Cu, Zn, Ni, Co, Pt, Pd, Ag)[19–22]. In this sense, our group carried out several preliminary studies that, through the screening of a wide variety of catalysts with different supports and Au, Pt or Pd as metals, have shown that systems based on supported Pt or Pd can constitute a sustainable alternative to the procedures already described[9,10,23]. From there on, numerous examples based on the use of noble metals supported on metal oxides as heterogeneous catalysts for reductive aminations have been reported in the literature. For instance, systems such as Pt/TiO_2[24,25], and $Pt\text{-}MoO_x/TiO_2$[26], are very efficient catalysts in reductive amination reactions with ethyl levulinate and levulinic acid, respectively. More recently, Pd supported on magnetite demonstrated to be efficient for the one-pot reductive amination of aldehydes with nitroarenes[27].

In this line, special attention will be paid to the study of supported metal catalysts. Specifically, those composed of Pd nanoparticles supported on various supports by incipient wetness impregnation. These catalysts will be tested to synthesize 2-

methylpiperazine under moderate conditions through reductive cyclo-amination with ethylenediamine and bio-derived acetol. Catalytic activity comparisons together with the exhaustive characterization of Pd-based materials will allow for establishing correlations between catalytic performance and physicochemical properties, thus providing new innovative concepts to the reductive amination process taking place over these Pd-based catalytic systems and allowing for designing a highly efficient system. Ultimately, the best catalyst, will be tested with a real feed containing acetol and coming from the selective glycerol dehydration using the catalysts developed in *Chapter 5*.

6.2 Preparation and characterization of Pd-supported materials

Commercial Al_2O_3 (basic), MgO, TiO_2 and ZrO_2 (60/40 physical blend in weight of monoclinic and tetragonal commercial zirconia materials, both from Chempur) supports were calcined before use at 250 ºC, whereas mixed metal oxides (TiO_2-Al_2O_3, TiO_2-ZrO_2 and ZrO_2-Al_2O_3) were prepared by co-precipitation in ammonia medium of metallic precursors and the precipitate aged at 60 ºC. After filtration, the solid was dried at 100 ºC and calcined at 500 ºC (for more details, see *Section 3.2.2*). The incorporation of Pd was achieved by incipient wetness impregnation, and all the catalytic systems were calcined and thermally reduced under a H_2 flow before their use in catalytic experiments (see *Section 3.2.3*).

The catalysts based on Pd supported on simple metal oxides present quite similar surface areas (≈150 m^2/g) and, in general, average metallic particle sizes ranging between 4 and 8 nm (measured by TEM), only excluding the Pd/MgO sample (surface area >200 m^2/g and average particle size ≥14 nm), as demonstrated by their measured textural and physicochemical properties listed in Table 6.1. Interestingly, the method applied for metallic mixed oxide synthesis permits attaining materials with improved properties, i.e., surface areas ≥250 m^2/g and average Pd particle sizes around 2–3 nm, in contrast with any simple oxide-based materials.

Table 6.1. Main textural and physicochemical properties of Pd-supported materials.

Material	Pd (wt%)[a]	Surface area (m^2/g)[b]		Particle size (nm)	
		Catalyst	Support	TEM[c]	CO[d]
Pd/TiO_2	1.2	120	148	4	8
Pd/Al_2O_3	1.0	135	138	8	4
Pd/ZrO_2	1.1	158	180	5	4
Pd/MgO	1.0	194	226	10	n/d
Pd/TiO_2-Al_2O_3	1.0	318	351	1	3
Pd/TiO_2-ZrO_2	1.1	257	292	4	4
Pd/ZrO_2-Al_2O_3	0.9	215	247	4	2

[a] Pd content and chemical composition measured by ICP. [b] Values calculated from N_2 adsorption isotherms (BET method). [c] Average diameter of Pd nanoparticles calculated from TEM measurements of, at least, 100 particles. [d] Average diameter of Pd nanoparticles evaluated by CO chemisorption, with the stoichiometry considered to be Pd:CO = 1:1.

Figure 6.1a depicts the X-ray diffraction patterns of the various Pd supported on simple oxide materials. The characteristic peaks for γ-alumina were detected in the reduced Pd/Al_2O_3 material, whose width implies a low level of crystallinity. Additionally, this catalyst barely presented a weak peak, characteristic of the Pd^0 species, most likely due to small Pd nanoparticles, which were fairly well dispersed on the support. The characteristic diffraction peaks of the periclase phase of MgO has been shown by the X-ray diffractogram of the reduced Pd/MgO sample, while the diffraction peaks assigned to Pd^0 species cannot be visibly discerned in the Pd/MgO reduced sample. Pd/TiO_2 predominantly showed the anatase phase and a small percentage of brookite. Concerning Pd/ZrO_2, the reduced sample shows certain peaks associated with the tetragonal phase and some others that emerge because of the characteristic reflections of the monoclinic phase. In contrast, it is almost impossible to discern those peaks corresponding to the presence of Pd^0 species.

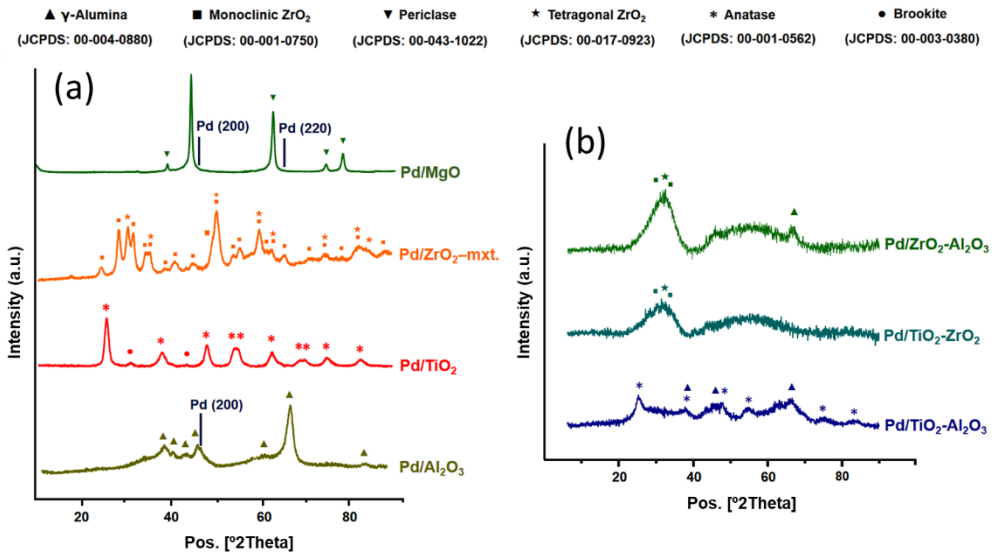

Figure 6.1. X-ray diffraction patterns of Pd supported materials (after reduction): a) Pd/Al_2O_3, Pd/TiO_2, Pd/ZrO_2 and Pd/MgO; b) Pd/TiO_2-Al_2O_3, Pd/TiO_2-ZrO_2 and Pd/ZrO_2-Al_2O_3.

As for the diffractograms obtained for Pd supported on metallic mixed oxide materials after reduction (Figure 6.1b), although some peaks showing very low crystallinity and corresponding to single oxide phases have been identified, the predominant structure in every case is that of an amorphous mixed oxide. In this line, sample homogeneity has been confirmed through EDAX compositional analyses (Figures 6.2-6.4), where an excellent dispersion is seen for both metals participating in each one of the compositions.

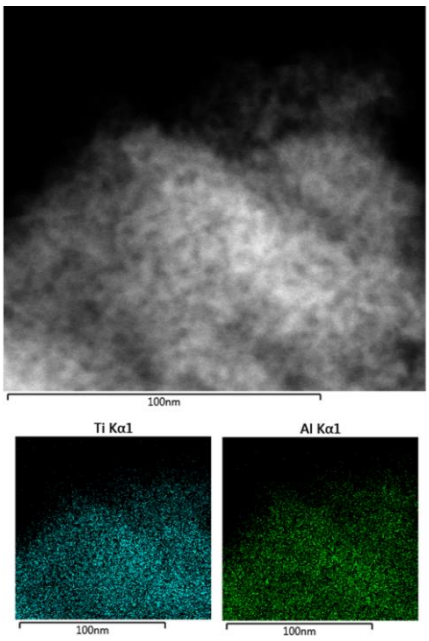

Figure 6.2. EDS mapping of Ti-Al-O_x support.

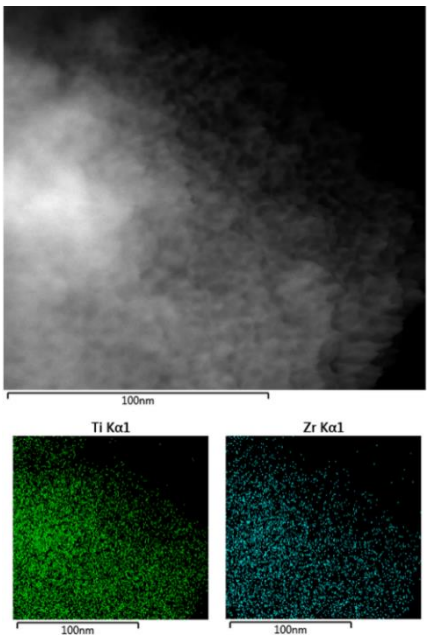

Figure 6.3. EDS mapping of Ti-Zr-O_x support.

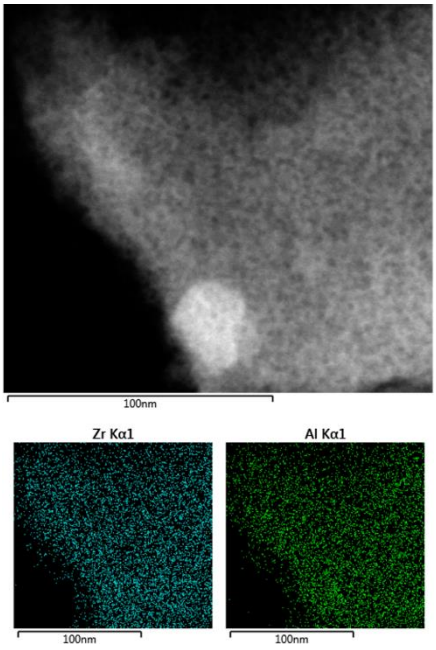

Figure 6.4. EDS mapping of Zr-Al-O_x support.

Furthermore, Pd supported materials were also analyzed employing high-resolution transmission electron microscopy. Images for each of the catalysts studied are shown in Figures 6.5 and 6.6 for single and mixed oxide-based samples, respectively. The occurrence of metallic Pd nanoparticles can be recognized in all of them. Regarding particle size distribution for single oxide-based materials (Figure 6.7), Pd/MgO and Pd/Al_2O_3 show higher average particle sizes, whereas the Pd/ZrO_2 sample presents particle size values around 4.0–6.0 nm. These Pd particle sizes are slightly larger than those observed for Pd/TiO_2–ZrO_2 and Pd/ZrO_2–Al_2O_3 (2.0–4.0 nm, see Figure 6.8), whereas Pd/TiO_2–Al_2O_3 and Pd/TiO_2 samples are the only ones showing a maximum in particle size distribution between 1.0 and 3.0 nm and exhibiting particles with sizes below 1.0 nm (Figure 6.7). HR-TEM measurements of the catalysts after reuses and subsequent regeneration were also done and illustrated in Figures 6.7 and 6.8 (discussed later).

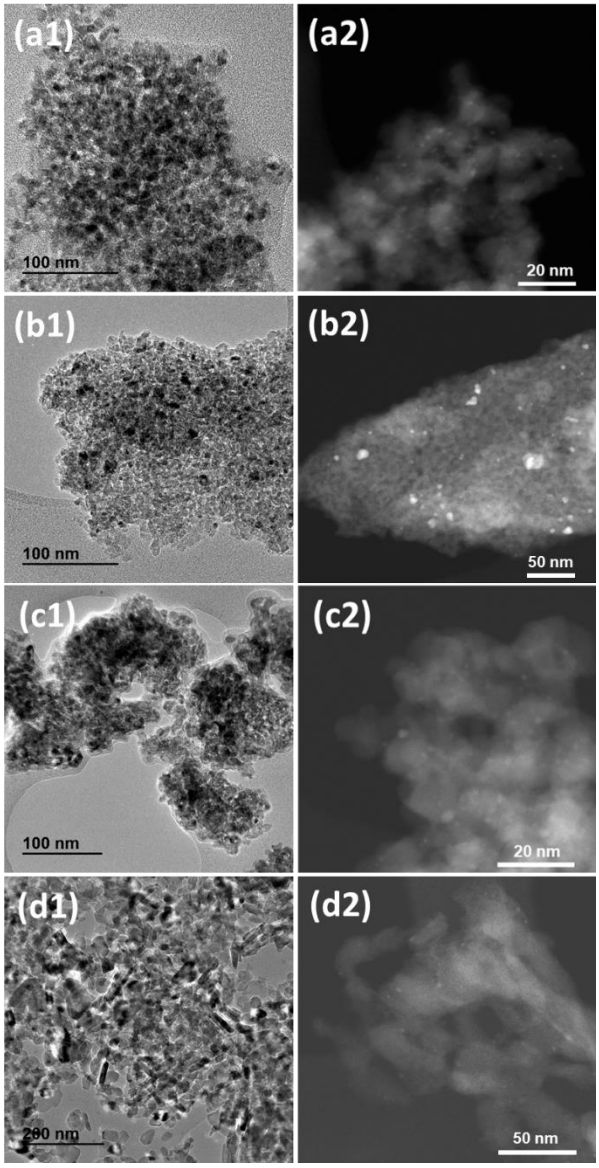

Figure 6.5. (1) HR-TEM and (2) HR-STEM micrographs for a) Pd/TiO_2, b) Pd/Al_2O_3, c) Pd/ZrO_2 and d) Pd/MgO (after reduction).

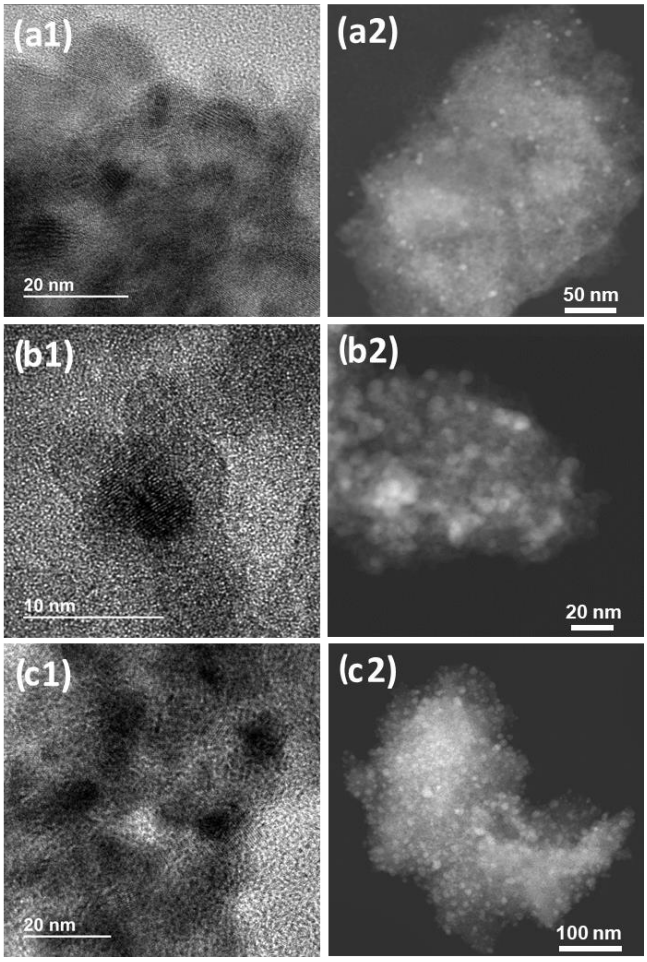

Figure 6.6. (1) HR-TEM and (2) HR-STEM micrographs for a) Pd/TiO_2-Al_2O_3, b) Pd/TiO_2-ZrO_2 and c) Pd/ZrO_2-Al_2O_3 (after reduction).

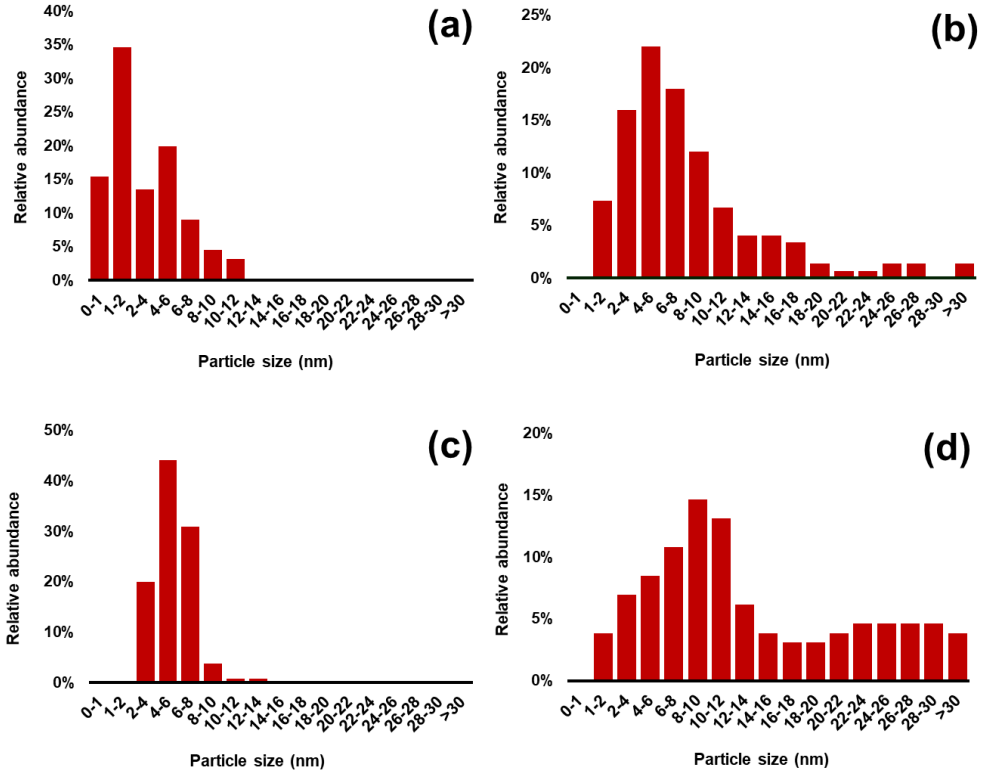

Figure 6.7. Metal particle size distribution of (a) Pd/TiO_2 (b) Pd/Al_2O_3 (c) Pd/ZrO_2, and (d) Pd/MgO reduced catalysts by considering, at least, 100 particles.

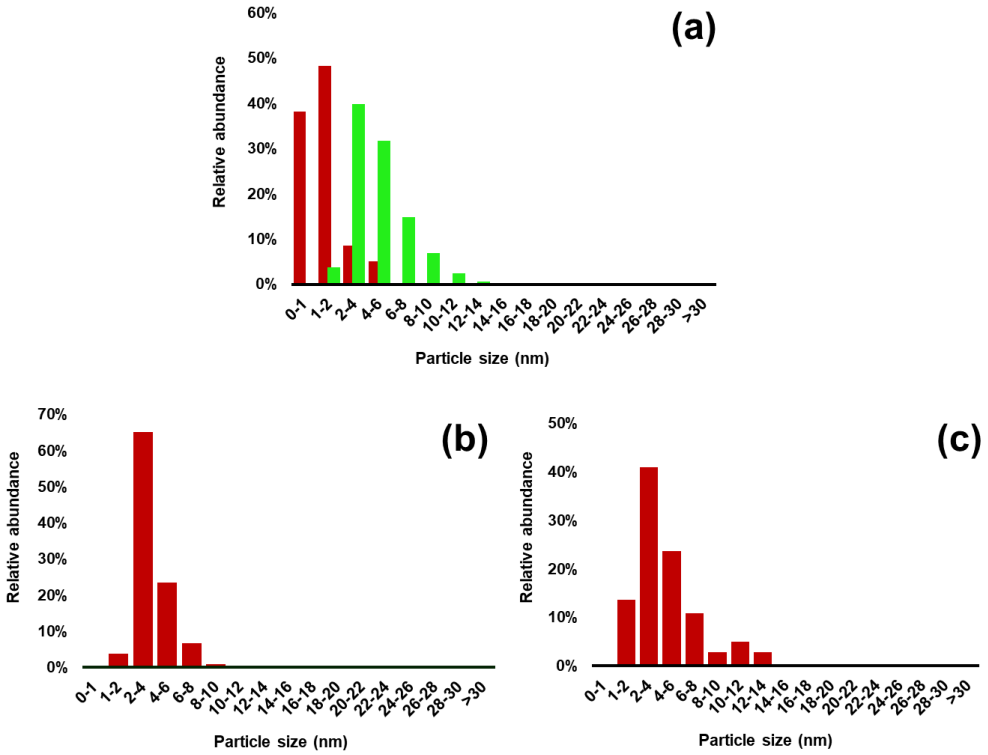

Figure 6.8. Metal particle size distribution of (a) Pd/TiO_2-Al_2O_3, (b) Pd/TiO_2-ZrO_2, and (c) Pd/ZrO_2-Al_2O_3 reduced catalysts. (■): fresh, (■): regenerated after 7 h reaction at 90 ºC and 13 bar of H_2, with 5 wt.% catalyst loading, and using MeOH as solvent. Distributions done by considering, at least, 100 particles.

In addition, to establish structure-activity relationships for the catalysts herein presented, a study of their acidic properties was carried out through ammonia temperature-programmed desorption (NH_3-TPD). Table 6.2 shows the total ammonia adsorbed for each catalyst, except for Pd/MgO, believed to be a non-acidic material and with negligible ammonia adsorption. Although NH_3-TPD desorption profiles should be used to differentiate between strong, moderate, and weak acid centers, in this case, and because of instrument trouble, the experimental procedure used for NH_3 desorption is only based in the TCD signal and, therefore, the resolution of the original spectra is too low as to properly distinguish between acid centers with different strengths. Indeed, as indicated at the bottom

of Figure A9, every profile has been previously smoothed, and the discussion will just involve the total number of acid sites. Nonetheless, important differences were established between the different materials, whose total amount of acid sites can be ordered as follows: Pd/ZrO_2 > Pd/TiO_2–Al_2O_3 > Pd/TiO_2 > Pd/ZrO_2–Al_2O_3 > Pd/TiO_2–ZrO_2 > Pd/Al_2O_3. These differences might have an effect on the catalytic properties of the different materials in the reductive amination reaction, which will be discussed in the next sections.

Table 6.2. Ammonia adsorption on the different catalysts.*

Catalyst	**Pd/Al_2O_3**	**Pd/TiO_2-ZrO_2**	**Pd/TiO_2**	**Pd/ZrO_2-Al_2O_3**	**Pd/TiO_2-Al_2O_3**	**Pd/ZrO_2**
μmol NH_3/g	197	213	241	280	399	460

* NH_3-TPD desorption profiles can be found in *Annex* (Figure A9).

6.3 Preliminary catalytic tests

Initially, a reductive cyclo-amination of acetol with ethylenediamine was conducted by placing the two reactants, the solvent, and a commercial catalyst Pd/Al_2O_3 (1 wt.% Pd) at the same time in a batch reactor under mild reaction conditions (at 90 ºC and P_{H_2} = 13 bar). In this reaction, methanol (MeOH) was initially chosen as solvent with the intention that some adverse effects of water during the intermediate dehydration step could be prevented (see Scheme 6.1). For the purpose of increasing the yield of 2-methylpiperazine, the catalyst loading in the reaction media was varied from 0 to 35 wt.% with respect to the amine. From a 25 wt.% catalyst loading onwards, maximum yields of 2-methylpiperazine were produced (Figure 6.9). However, a “plateau” effect occurs beyond this value, almost certainly due to substrate limitations.

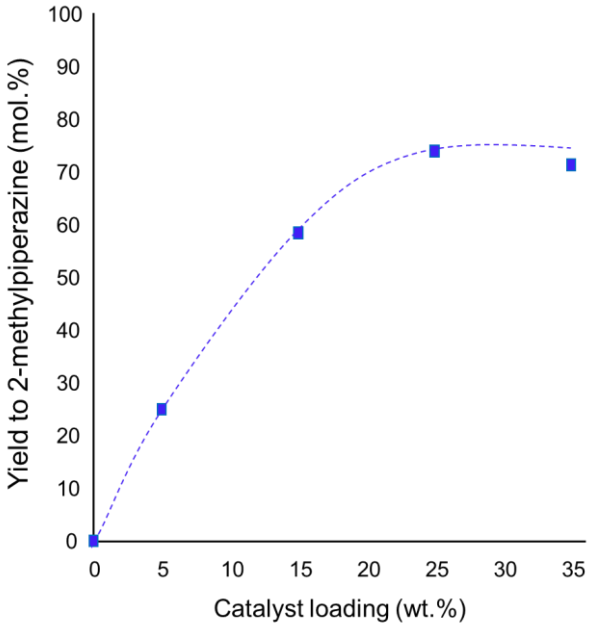

Figure 6.9. Catalyst loading optimization in the reductive cyclo-amination of acetol with ethylenediamine with Pd/Al_2O_3 (1 wt.% Pd, commercial catalyst). Reaction conditions: 0.325 g acetol, 0.227 g ethylenediamine, 1.250 g MeOH, at 13 bar of H_2 and 90 ºC, during 7 h. Note: Dashed trace only serves as visual guideline.

Importantly, slow acetol addition was found to be a critical point to avoid secondary non-desired reactions and by-product formation. Results in Figure 6.10a indicate that acetol slow addition leads to better ethylenediamine conversion values (>95%) when using the Pd/Al_2O_3 commercial catalyst. We can sensibly hypothesize that, with many acetol molecules in the reaction mixture (situation when both reactants are present from the beginning in the initial mixture), an ethylenediamine molecule would preferably react with two acetol molecules by reaction between the carbonyl group of acetol and the terminal amines of the ethylenediamine. Therefore, instead of reacting with the same acetol molecule hydroxyl group towards the cyclic intermediates (see Scheme 6.2), the reaction will involve a second acetol molecule generating linear nitrogen-containing by-products, so that this acetol molecule will not be available to react with another ethylenediamine molecule. Consequently, considering that reactants were added in equimolar quantities (1:1

mol), this intermolecular reaction would lead to lower diamine conversions and lower yields of the desired 2-methylpiperazine. On the contrary, the slow acetol addition to the reaction mixture strongly favors the intramolecular reaction, as illustrated in Scheme 6.2, as ethylenediamine cannot easily find a second acetol molecule. A selectivity comparison at isoconversion (see Figure 6.10b) for both standard and slow acetol addition experiments also confirms that higher amounts of nitrogen-containing by-products (N-by-products) are produced in the case of the reaction started with equimolar amounts of acetol and ethylenediamine (Figure 6.10c). On the contrary, the selectivity shifts towards the mixture comprising 2-methylpiperazine and its precursors (imine molecules) when acetol is added slowly to the reaction medium.

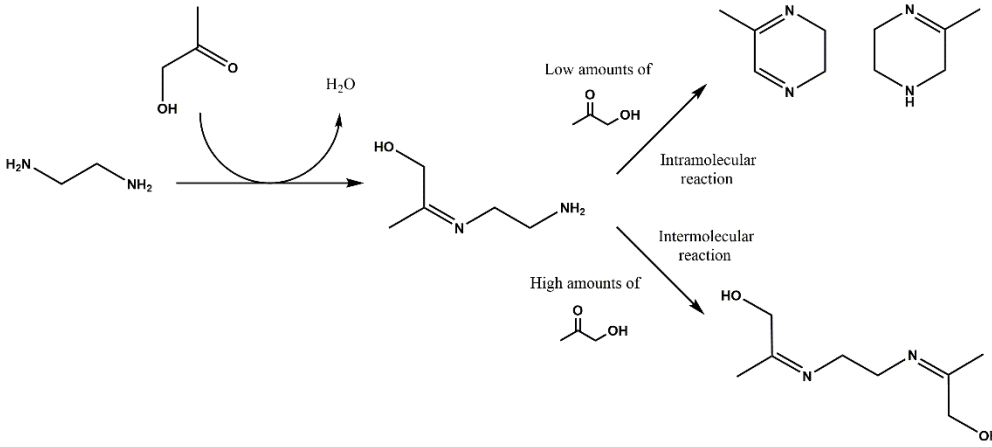

Scheme 6.2. Possible reaction pathways for the reductive cyclo-amination of acetol with ethylenediamine.

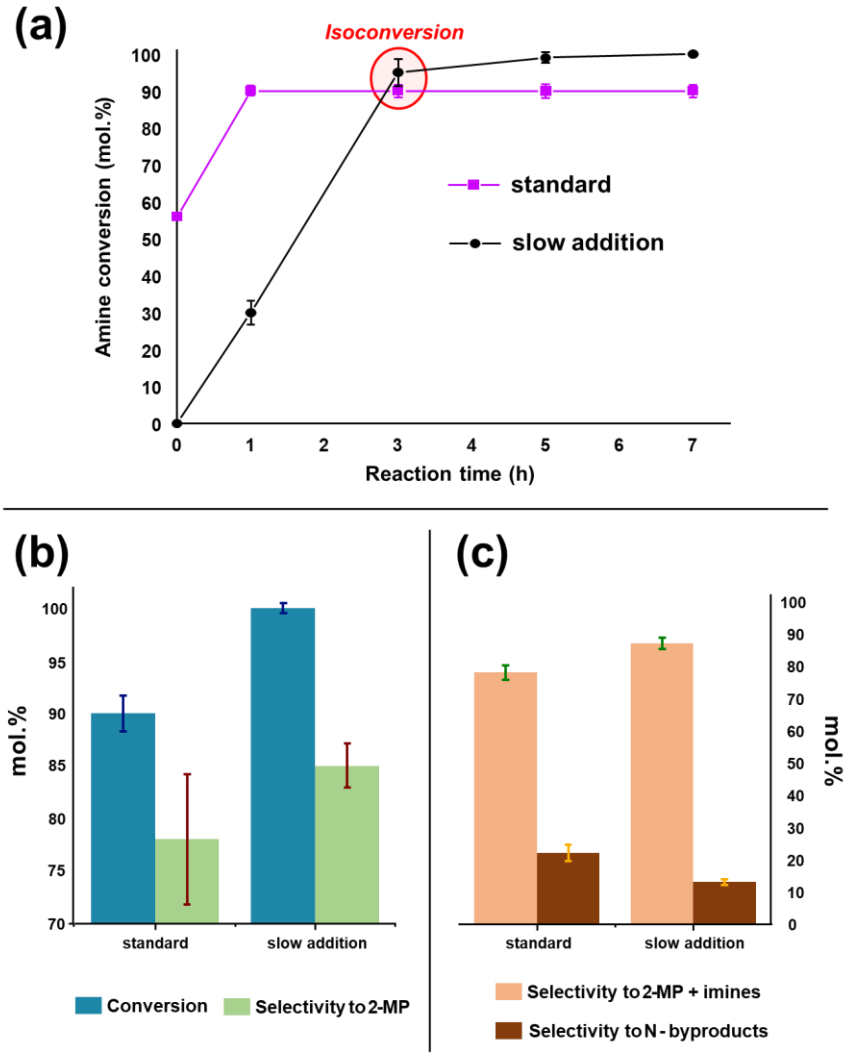

Figure 6.10. Effect of the slow addition of acetol to the reaction media in the reductive cyclo-amination of acetol with ethylenediamine over Pd/Al_2O_3 (1 wt.% Pd, commercial catalyst). (a) Ethylenediamine conversion for standard and slow acetol addition experiments. (b) Conversion and selectivity at 7 h. (c) Selectivity towards the different products compared at the same conversion level (time = 3h, marked in (a)). Reaction conditions: 0.325 g acetol, 0.227 g ethylenediamine, 1.250 g MeOH, 0.056 g of catalyst, at 13 bar of H_2, and 90 ºC.

6.4 Catalytic activity of Pd supported on simple metal oxides.

As soon as the most appropriate reaction system for the reductive cyclo-amination of acetol with ethylenediamine through slow addition of acetol was designed (see previous section), different Pd supported on simple metallic oxides prepared in this study were assayed in order to maximize the yield of the 2-methylpiperazine desired product. The key results are compiled in Table 6.3. Results prove that, regardless of the support (Al_2O_3, ZrO_2, TiO_2 and MgO), Pd metallic species can effectively carry out the reductive amination of acetol. In fact, the differences between these catalysts are almost not significant, even at short reaction times, and more experiments should be carried out to discern between these catalysts.

Table 6.3. Catalytic activity of Pd supported on simple metal oxide materials in the reductive cyclo-amination of acetol with ethylenediamine.

Catalyst	Ethylenediamine conversion (mol. %)		Selectivity to 2-methylpiperazine (mol. %)		Yield to 2-methylpiperazine (mol. %)*	
	1 h	7 h	1 h	7h	1 h	7 h
Pd/Al_2O_3 (commercial)	30	100	77	85	27	79
Pd/Al_2O_3	34	96	88	86	29	83
Pd/TiO_2	38	100	88	83	34	83
Pd/ZrO_2	38	99	80	82	30	79
Pd/MgO	41	94	81	81	33	76

Reaction conditions: 0.325 g acetol, 0.227 g ethylenediamine, 1.250 g MeOH, 0.056 g of catalyst, at 13 bar of H_2, and 90 ºC, during 7 h and with slow addition of acetol (100 µl/h). *Carbon balances for all reactions were higher than 95%.

In order to establish differences between these catalysts, the degree of deposition of organic matter on them and the metallic leaching was evaluated. Importantly, their stability

will be expected to be strongly related to the amount of carbonaceous matter stuck on the catalyst surface. No significant metallic loss was detected for any of the catalysts during the reaction (Table 6.4). Nevertheless, interestingly, the Pd/MgO material, the only one with a pure basic character, shows a higher degree of organic matter deposition during the reaction (Table 6.4), revealing a higher intensity of polymerization reactions occurring at the surface of this catalyst. This fact is in good agreement with what has been reported about side polymerization reactions in acetone and vinyl ketone reaction systems[28,29]. Owing to this finding, Pd/MgO was discarded for further studies.

Table 6.4. Effect of catalyst use on organic matter deposition, and metal loading for Pd supported on simple metal oxides.

Catalyst	Pd (wt.%)[a] [fresh]	Pd (wt.%)[a] [after use]	C/N (wt.%)[b] [after use]
Pd/Al_2O_3	1.0	1.0	0.9/0.3
Pd/TiO_2	1.2	1.1	1.3/0.8
Pd/ZrO_2-mxt	1.1	1.0	1.3/0.3
Pd/MgO	1.0	1.0	5.8/0.7

[a] Pd content measured by ICP.

[b] Results from elemental analyses (EA).

6.5 Catalytic activity of Pd supported on mixed metal oxides.

Because Pd supported on Al_2O_3, TiO_2 and ZrO_2 catalysts produced very promising results in the reductive amination of acetol with ethylenediamine, high surface area mixed oxides TiO_2-Al_2O_3, TiO_2-ZrO_2 and ZrO_2-Al_2O_3 were prepared, and Pd (≈1% in weight) was incorporated onto these materials by incipient wetness impregnation (See Table 6.1). The thus obtained Pd-catalysts were tested in the reductive amination process. Kinetic profiles for Pd-supported on metallic mixed oxide materials are depicted in Figure 6.11 and compared in terms of 2-methylpiperazine yields with those of Pd-supported on simple

oxides. Remarkably, the three Pd-supported mixed oxide catalysts presented higher specific activity than the respective materials based on simple oxides, raising the values for the yield to 2-methylpiperazine at 3 h of reaction from ≈75% in the case of simple oxides to c.a. 85% for mixed oxides (Figure 6.11).

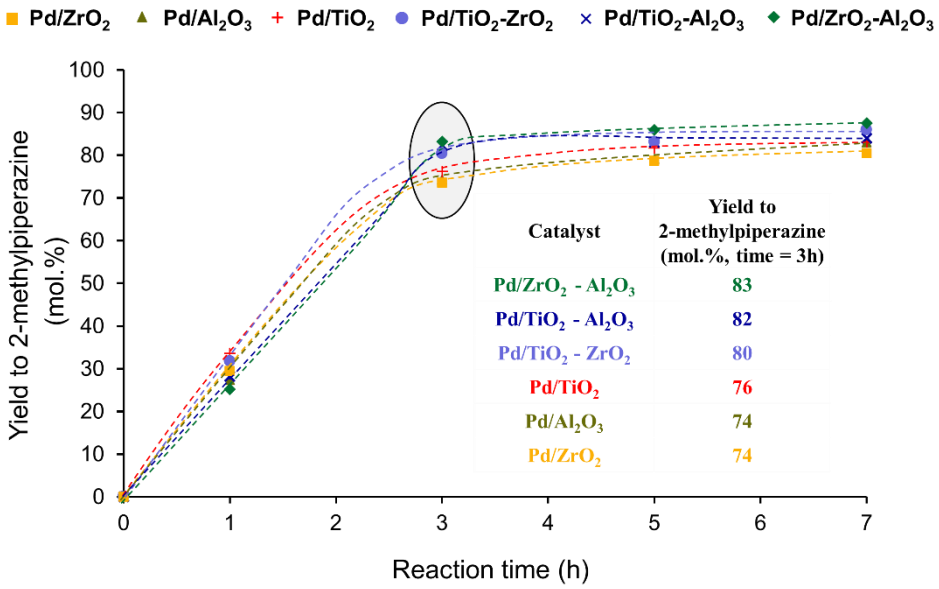

Figure 6.11. Kinetic comparison of Pd supported on simple and mixed metal oxides. Reaction conditions: 0.325 g acetol, 0.227 g ethylenediamine, 1.250 g MeOH, 0.056 g of catalyst, at 90 ºC and 13 bar of H_2, during 7 h and with slow addition of acetol (100 µl/h). Note: Dashed traces only serve as visual guidelines.

As carried out for Pd-supported on simple oxides, measures of the organic matter deposits together with metallic leaching were conducted to see if these materials were also good candidates to keep their catalytic behaviour during several cycles. Results in Table 6.5 show that, again, the catalysts do not lose palladium content significantly during the reaction. On the other hand, the amount of organic matter deposited is higher than in the case of the catalysts based on simple oxides. This fact is likely to be caused by the more significant amounts of active sites combined with the higher acidity found in the mixed oxides-based materials described in this section.

Table 6.5. Effect of reusability and regeneration on organic matter deposition, metal loading and metallic dispersion of Pd supported on mixed metal oxides.

Catalyst	Pd (wt.%)[a] [fresh]	Pd (wt%)[a] [after 1st use]	C/N (wt%)[b] [after 1st use]
Pd/TiO_2-Al_2O_3	1.0	1.0	2.7/1.2
Pd/TiO_2-ZrO_2	1.1	1.1	2.9/1.6
Pd/ZrO_2-Al_2O_3	1.0	0.9	2.5/0.7

[a] Pd content and chemical composition measured by ICP.

[b] Results from elemental analyses (EA).

[c] Average diameter of Pd nanoparticles calculated from TEM measurements of, at least, 100 particles.

Despite these findings, the differences between these materials, as well as with respect to those catalysts based on simple oxides, are not significant enough to draw solid conclusions. Therefore, in the next section, further comparisons under more limiting conditions will be conducted.

6.6 Further comparison, understanding and catalyst selection.

For the purpose of a more accurate differentiation between the three mixed oxide-supported Pd materials (i.e., Pd/TiO_2-Al_2O_3, Pd/TiO_2-ZrO_2, Pd/ZrO_2-Al_2O_3) and the other three simple oxides suffering from less carbonaceous deposition (i.e., Pd/TiO_2, Pd/Al_2O_3 and Pd/ZrO_2), shorter time (3 h) reactions were carried out for each one of the materials by using a significantly reduced amount of catalyst (0.011 g; 5wt% with respect to the amine). By doing this, the differences previously observed (Figure 6.11) are supposed to appear now much clearer. Additionally, Table 6.6 shows how the "specific activity of the catalyst" (i.e., yield to 2-methylpiperazine, see *Section 3.5.2*) has always been kept far below 80%.

Data of Table 6.6 indicate that Pd/TiO_2-Al_2O_3 was, in fact, the material inherently most active (Yield to 2-methylpiperazine = 57%, TON = 2028 at 3 h of reaction), followed by Pd/ZrO_2-Al_2O_3 (Yield to 2-methylpiperazine = 49%, TON = 1937). In addition to these experiments, the acid properties of the different Pd-supported materials studied herein were ascertained by adsorption-desorption experiments with ammonia (NH_3-TPD measurements, see Table 6.2). As a result, a correlation between the specific catalytic activity (yield to 2-methylpiperazine) and the total Lewis acidity (examined by NH_3-TPD) of the Pd-supported materials was established and depicted in Figure 6.12, results identifying Pd/ZrO_2-Al_2O_3 and Pd/TiO_2-Al_2O_3 as the two materials with the highest 2-methylpiperazine production values.

Table 6.6. Yield to 2-methylpiperazine and TON in the reductive cyclo-amination of acetol with ethylenediamine at shorter reaction times and with lower catalyst loadings.

Catalyst	Yield to 2-methylpiperazine (mol.%)	TON
Pd/Al_2O_3	23	818
Pd/TiO_2-ZrO_2	26	841
Pd/ZrO_2	29	938
Pd/TiO_2	44	1304
Pd/ZrO_2-Al_2O_3	49	1937
Pd/TiO_2-Al_2O_3	57	2028

Reaction conditions: 0.325 g acetol, 0.227 g ethylenediamine, 1.250 g MeOH, 0.011 g of catalyst at 90ºC and 13 bar of H_2, during 3 h and with slow addition of acetol (100 µl/h). [a] TON = mol 2-methylpiperazine/mol Pd.

Nevertheless, the explanation for this tendency concerning the total number of Lewis acid sites is not that simple, and, on the contrary, the acidity seems not to be enough to entirely understand the reactivity in this series of materials. A detailed analysis of the product distribution for the different materials unveiled those high concentrations of acid

sites shift the selectivity towards the appearance of non-desired nitrogen-containing by-products (see Table 6.7). However, why low concentrations of acid sites are detrimental for achieving high yields to 2-methylpiperazine is not apparent. Acid sites are often described in the literature to be a key feature to foster the formation of the imine intermediate[30]. However, this generation of the imine intermediates seems to happen regardless of the support used at both ends of the graph (Figure 6.12), which also occurs without catalyst, and even in the absence of hydrogen (see Table 6.7). On the other hand, no substantial amounts of Nitrogen-containing by-products (N-by-products different from imines) are observed for any material apart from Pd/ZrO_2 (see Table 6.7).

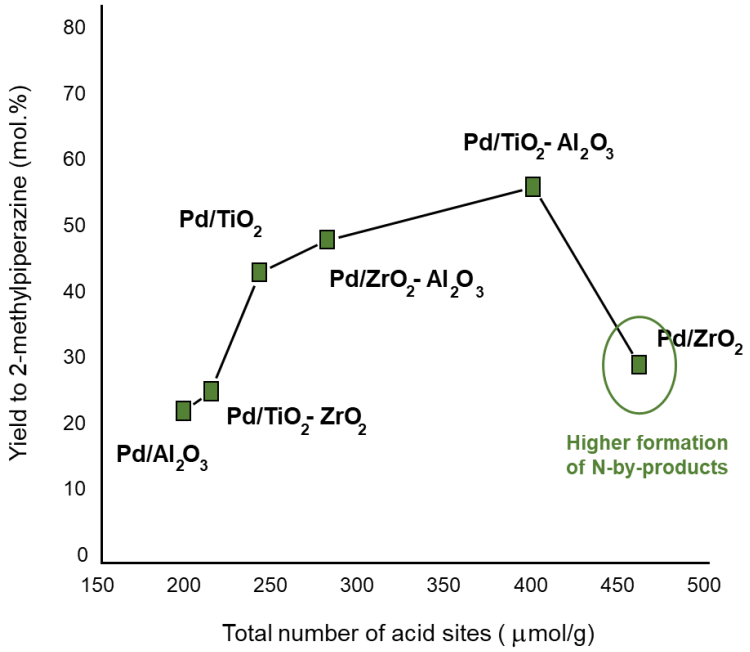

Figure 6.12. Yield to 2-methylpiperazine vs total number of Lewis acid sites for Pd-supported materials in the reductive cyclo-amination of acetol with ethylenediamine. Reaction conditions: 0.325 g acetol, 0.227 g ethylenediamine, 1.250 g MeOH, 0.011 g of catalyst, at 90 ºC and 13 bar of H_2, during 3 h and with slow addition of acetol (100 µl/h).

Table 6.7. Catalytic data for Pd supported catalysts for tests with 5wt.% catalyst loading.

Catalyst	Amine Conversion[a] (mol.%)	Amine Conversion[b] (mol.%)	Selectivity to N-by-products[a] (mol.%)	Selectivity to Imines[a] (mol.%)	Yield to 2-methylpiperazine (mol.%)
Pd/Al_2O_3	85	90	24	47	23
Pd/TiO_2-ZrO_2	86	n/d	24	41	26
Pd/TiO_2	89	n/d	24	25	44
Pd/ZrO_2-Al_2O_3	91	n/d	19	20	49
Pd/TiO_2-Al_2O_3	92	93	17	14	57
Pd/ZrO_2	91	95	40	22	30
Thermal reaction	n/d	94	n/d	n/d	n/d

Reaction conditions: 0.325 g acetol, 0.227 g ethylenediamine, 1.250 g MeOH, 0.011 g of catalyst at 90 ºC, during 3 h and with slow addition of acetol (100 µl/h). [a]: 13 bar of H_2, [b]: 13 bar of N_2.

Therefore, and taking into account that, according to Table 6.6, difference in imine hydrogenation primarily defines the variations between catalysts, attention must be fixed on hydrogen activation and C=N bond activation. Consequently, particle morphology analysis, together with an assessment of each of the catalysts to activate H_2, have been conducted to explain the catalytic differences convincingly. Therefore, IR spectroscopy of CO adsorption and H_2/D_2 isotopic exchange experiments have been carried out to characterize the surface metal sites (i.e., crystal facets, uncoordinated sites, and average particle morphology) and the H_2 activation on the studied catalysts, respectively. In this regard, the latest literature on hydrogenation reactions catalyzed by supported metal nanoparticles has stressed the role of specific metal nanoparticle features (i.e., facets, terraces, defects) on the preferential activation of specific functional groups[24,31,32]. Particularly, uncoordinated surface sites in Pt[24] and Pd[31] nanoparticles have been

proposed as chemo-selective for the hydrogenation of the imine (C=N) group. In the same line, in our study, by performing IR spectroscopy of CO adsorption studies, unsaturated sites characterized by an IR band of the Pd-CO interaction at 2042 cm^{-1} have been predominately observed in the Pd/TiO_2-Al_2O_3 sample (Figure 6.13, blue line) and in minor extent in the Pd/ZrO_2-Al_2O_3 sample (Fig. 6.13, green line). In addition, (111) and (100) facets (IR bands at 2092 and 2085 cm^{-1}) together with bridge CO and 3-fold CO configuration on Pd terraces (IR bands at 1988 and 1925 cm^{-1}, respectively) have also been detected, but being more dominant in the Pd/TiO_2 and Pd/Al_2O_3 samples (Figure 6.13, red and dark yellow lines, respectively)[33–36]. Thus, according to the IR-CO results and its correlation with the catalytic data of Table 6.5, we can assume that it is likely that uncoordinated Pd sites (as in the Pd/TiO_2-Al_2O_3 sample) favor imine hydrogenation. Moreover, these sites are more abundant at smaller particle sizes, as is the case of the Pd supported on mixed oxides-based catalysts. On the other hand, H_2 activation does not seem to be a determining factor for catalyst activity since, based on the H_2/D_2 isotopic exchange experiments (Table 6.8 and Figure 6.14), similar and high enough H_2 activation capabilities were measured over all samples.

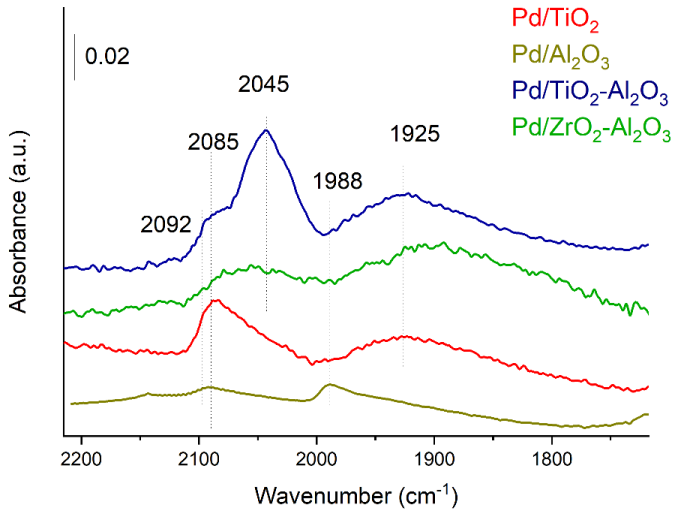

Figure 6.13. IR spectra of CO adsorption at 25 ºC and saturation coverage (i.e., 8.5 mbar CO) on Pd supported catalysts (after reduction).

Table 6.8. HD/H_2 mass signal ratio during the H_2/D_2 experiments over Pd-supported catalysts at different temperatures.

Catalyst	**HD (T) / H_2-bypass**			
	25 ºC	**60 ºC**	**90 ºC**	**120 ºC**
Pd/Al_2O_3	0.40	0.48	0.51	0.54
Pd/TiO_2-Al_2O_3	0.21	0.32	0.38	0.43
Pd/ZrO_2-Al_2O_3	0.26	0.39	0.45	0.50

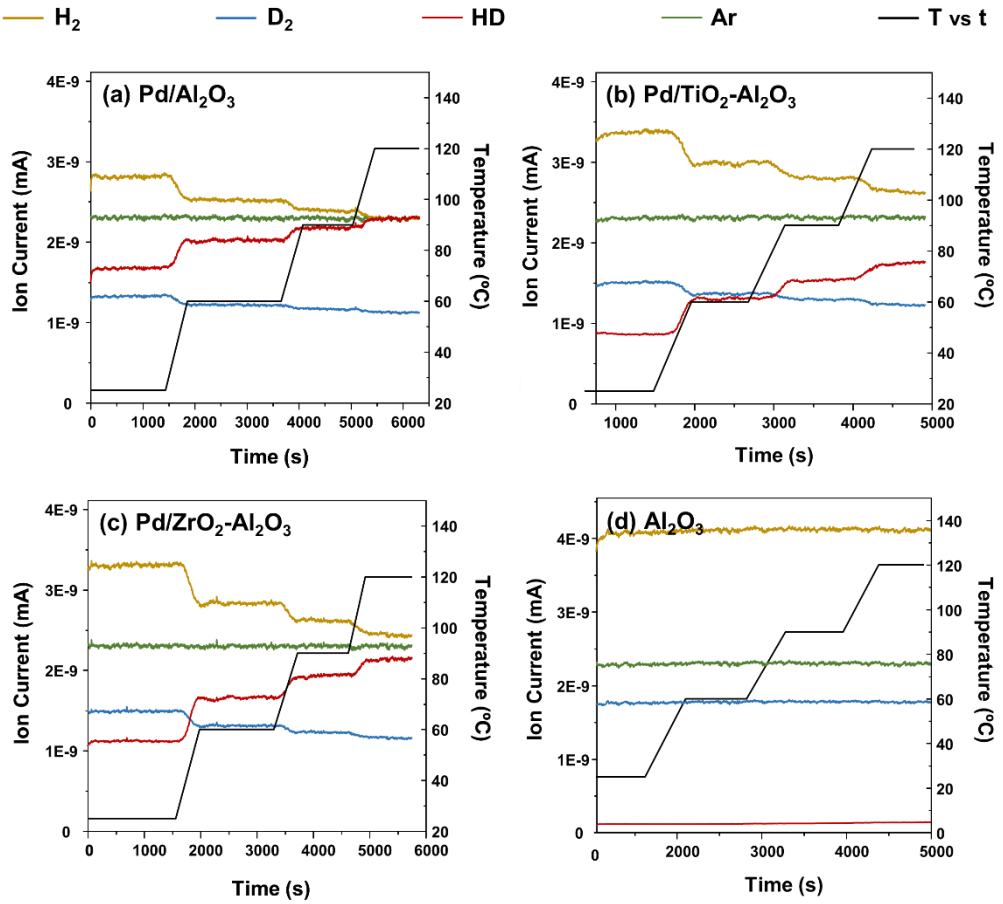

Figure 6.14. Evolution of HD (m/z=3), H_2 (m/z=2) and D_2 (m/z=4) in the isotopic exchange H/D over (a) Pd/Al_2O_3, (b) Pd/TiO_2-Al_2O_3, (c) Pd/ZrO_2-Al_2O_3, and (d) Al_2O_3 (bare support, reference sample). Note: Black line corresponds to the temperature profile during measurement.

After these experiments, the enhanced catalytic performance of Pd/TiO_2-Al_2O_3 and Pd/ZrO_2-Al_2O_3 could be justified. At this stage, granting that Pd/TiO_2-Al_2O_3 could already be selected as the best catalyst on account of its higher TON (see Table 6.5), an additional justification for its selection can be stated: the inexpensive price of the Ti precursor in comparison with the Zr precursor used in catalyst preparation.

6.7 Reusability of *Pd/TiO_2-Al_2O_3* catalyst, its use in water presence and extension to other reactants

Aiming at increasing catalytic applicability in 2-methylpiperazine synthesis from acetol and considering the outstanding performance of Pd/TiO_2-Al_2O_3 catalyst, the possibility of achieving high yields to 2-methylpiperazine with low catalyst loadings (5 wt.% with respect to the amine) was investigated, and the reusability of the catalyst when working under these convenient reaction conditions also tested. Figure 6.15 shows that 2-methylpiperazine yields close to 80% with Pd/TiO_2-Al_2O_3 are attainable at 7 h of reaction, even when working with low catalyst loadings. Still, an inevitable loss of activity over the subsequent reuses is observed. This finding was anticipated since the organic matter deposition on the catalytic surface is considerable, as the elemental analysis studies revealed (see Table 6.9). Nonetheless, it is possible to cleanse the catalytic surface and recover nearly the catalytic activity after a regeneration process (Figure 6.15 and Table 6.9). Notably, after use and regeneration, the average Pd particle size of the catalyst slightly increases, particle size distributions for the regenerated samples moving towards higher values, and particles with sizes below the nanometer practically disappearing (see *Section 6.2*, Figure 6.8a). This particle growth may be the cause of the moderate-to-low specific activity loss observed.

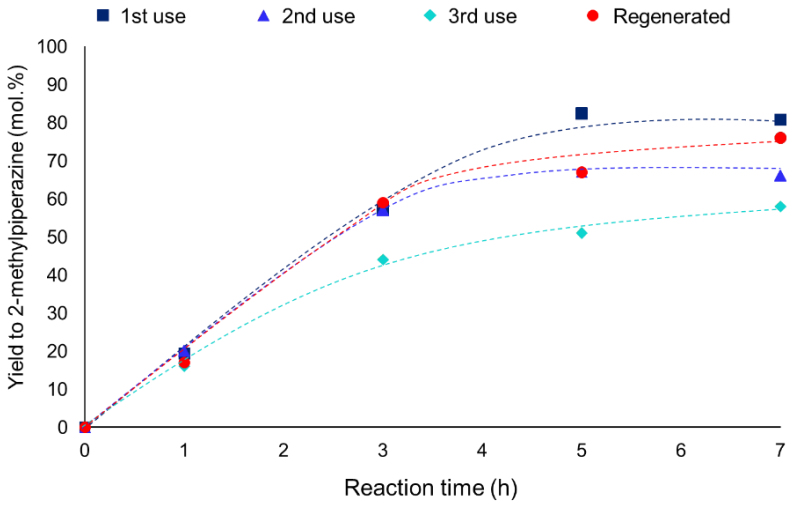

Figure 6.15. Yield to 2-methylpiperazine in the reductive cyclo-amination of acetol with ethylenediamine with Pd/TiO_2-Al_2O_3 over three consecutive catalytic cycles and the regenerated catalyst. Reaction conditions: 0.325 g acetol, 0.227 g ethylenediamine, 1.250 g MeOH, 0.011 g of catalyst, at 90 ºC and 13 bar of H_2, during 7 h and with slow addition of acetol (100 µl/h). Note: Dashed traces only serve as visual guidelines.

Table 6.9. Results of elemental analysis (EA) of Pd/TiO_2-Al_2O_3 after reaction under optimum conditions and after regeneration.

Solvent	**C/N (wt%)[a] [after 1st use]**	**C/N (wt%)[b] [after regeneration]**
H_2O	5.1/2.5	0.1/0.0
MeOH	3.1/1.3	0.4/0.0

Reaction conditions: 0.325 g acetol, 0.227 g ethylenediamine, 0.011 g of Pd/TiO_2-Al_2O_3 at 90 ºC and 13 bar of H_2, during 7 h and with slow addition of acetol (100 µl/h).

Finally, the feasibility of using this catalyst in aqueous systems and other reductive amination reactions with different carbonyl compounds derived from biomass feedstocks could be appealing from an industrial viewpoint. For instance, glyoxal (1,2-ethanediol) could be an attractive candidate as the starting substrate. This extremely reactive

dialdehyde suggests many alternatives for reductive amination processes, either with amines[37] or amino acids[38], as a source of amino groups, and it can be manufactured from either biomass[39] or ethylene glycol oxidation[40,41]. Therefore, there are numerous synthetic opportunities for glyoxal and amines in an aqueous medium, and they would include, among others, compounds of interest such as N,N'-diisopropyl-ethylenediamine or N,N′-acetic acid-ethylenediamine (EDTA), with problematic synthesis involving either several reaction steps or the use of traditional reductive agents.

In our instance, catalytic experiments were carried out using glyoxal and tert-butylamine (as N source), by connecting imination and hydrogenation reactions in a single step, with commercial Pd/Al_2O_3 and Pd/TiO_2-Al_2O_3 as catalysts. Additionally, since most of the already reported reductive aminations concerning glyoxal use water as solvent, a test was done with acetol and ethylenediamine to find out to what extent water instead of MeOH would be detrimental for catalytic performance. Results are summarized in Figure 6.16.

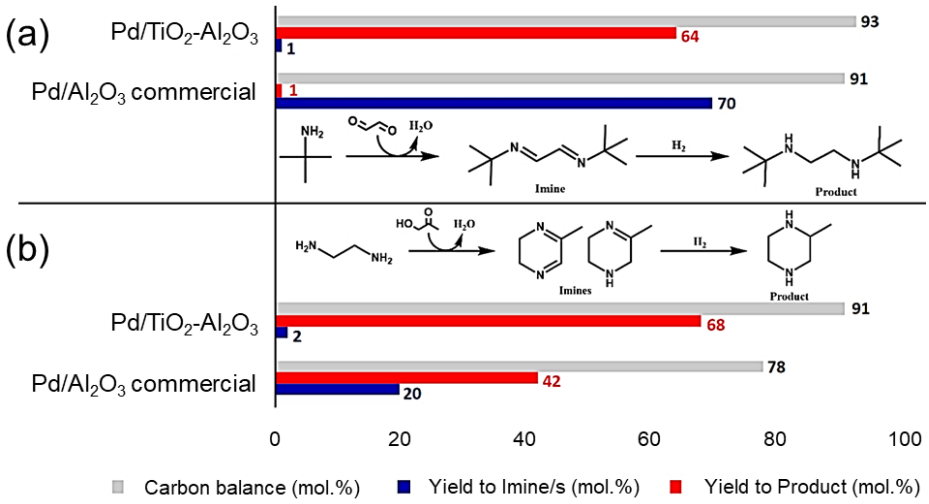

Figure 6.16. Reductive amination with (a) glyoxal and tert-butylamine and (b) acetol and ethylenediamine over 1%wt.Pd/Al_2O_3 (commercial catalyst) and 1%wt.Pd/TiO_2-Al_2O_3 material. Reaction conditions: (a): 0.550 g tert-butylamine, 0.430 ml glyoxal, 0.500 g H_2O (40% ac., slow addition = 140 µl//h), 0.135 g of catalyst, at 90 ºC and 15 bar of H_2, during 4 h. (b) 0.325 g acetol, 0.227 g ethylenediamine, 1.250 g H_2O, 13 bar H_2, 0.011 g of catalyst at 90 ºC, during 7 h and with slow addition of acetol (100 µl/h).

Figure 6.16. clearly shows how our catalyst works better in water than the commercial Pd/Al_2O_3 in the 2-methylpiperazine synthesis and, mainly, in the reductive amination with glyoxal and tert-butylamine. Thus, 64% yield of the desired N-compound synthesized from glyoxal was attained with the Pd/TiO_2-Al_2O_3 catalyst, whilst meager amounts of the product were detected with the Pd-based commercial catalyst. Besides, 68% yield to 2-methylpiperazine was attained using the Pd-supported mixed oxide catalyst instead of the 42% yield reached with Pd/Al_2O_3. These pieces of evidence further confirm the exceptional capability of Pd/TiO_2-Al_2O_3 to hydrogenate the C=N functionality. It is also noted that carbon balances in water decrease when compared to those reactions carried out in MeOH (>95% in both cases). This fact is also backed by elemental analyses (see Table 6.8), which will likely lead to a more critical deactivation. Nonetheless, the much better result obtained for the glyoxal reaction with Pd/TiO_2-Al_2O_3 made us think that it would be possible to use this catalyst to carry out this sort of reaction with high yields of the desired nitrogen-compound mild reaction conditions, viable at an industrial scale.

6.8 Consecutive two-step process to produce 2-methylpiperazine from glycerol

Once we had achieved a suitable catalyst both to produce acetol via selective glycerol dehydration and for its subsequent conversion into 2-methylpiperazine by condensation and cyclization with ethylenediamine and ulterior hydrogenation, the next step was to be able to couple both processes. Thus, the acetol produced in the first catalytic step (glycerol dehydration) of the process will be used as feed together with ethylenediamine for the second catalytic step (reductive amination) to attain the 2-methylpiperazine finally.

Bearing that objective in mind, a fraction corresponding to operational times between 1 and 4 hours, working with copper oxide supported on monoclinic zirconium oxide as catalyst (CuO/*m*-ZrO_2, see *Chapter 4*), was collected at the outlet of the continuous reactor used to produce acetol from glycerol. This reaction mixture, with a density of ≈0.95 g/mL, contained an acetol percentage around 25 wt.% by weight together with other by-products characteristic of this reaction, such as methyl lactate, methyl glycolate, 1,2-propanediol, acetic acid or acetoin, among others. This reaction mixture collected at the continuous

reactor output for the selective dehydration of glycerol was added in a controlled way in the second batch reactor, just as pure acetol was previously introduced. The reactor was previously filled with a mixture ethylenediamine:MeOH (50:50 by weight). Total volume and addition rate were calculated so that addition was finished and the mixture equimolar after 3 hours of reaction.

Figure 6.17 shows the complete reaction kinetics of the Pd/TiO_2-Al_2O_3 catalyst when the reactor is fed with this real mixture (a) and compared to that obtained with pure acetol (b). It becomes evident that the catalyst loses hydrogenating capacity since the proportion of imines detected with respect to the desired product is more significant than in the case of the catalyst working with pure acetol. Moreover, it is also very likely that the presence of oxygenated products, especially those containing carbonyl groups, makes the imine react towards the formation of other non-desired nitrogen by-products. However, the yield obtained from 2 methyl piperazine is close to 20% under these reaction conditions, thus the overall process is very promising.

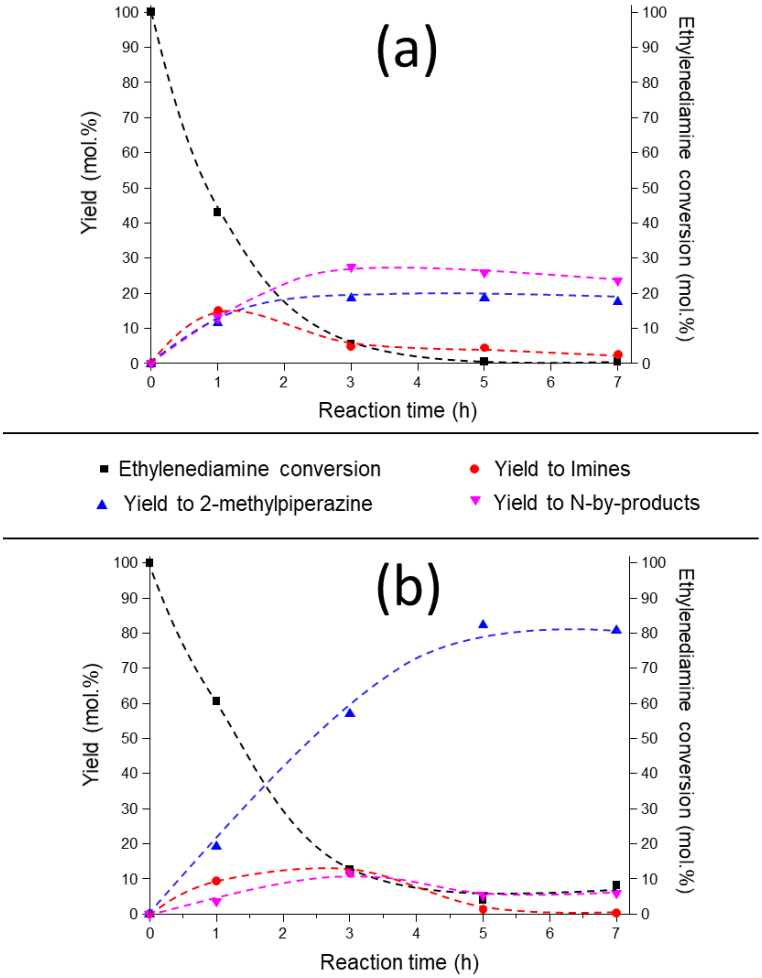

Figure 6.17. Comparison of the catalytic performance of Pd/TiO_2-Al_2O_3 with reactant and product evolution when (a) reactor fed with a stream containing acetol (≈25 wt.%) (b) reactor fed with pure acetol. Reaction conditions: (a) 0.325 g acetol, 0.227 g ethylenediamine, 1.250 g MeOH, 0.011 g of catalyst, at 90 ºC and 13 bar of H_2, during 7 h and with slow addition of acetol (100 µl/h). (b) (a) 1.579 g acetol-containing mixture, 0.227 g ethylenediamine, 0.227 g MeOH, 0.011 g of catalyst, at 90 ºC and 13 bar of H_2, during 7 h and with slow addition of acetol (554 µl/h). Note: Dashed traces only serve as visual guidelines.

After obtaining these results and, even though the room for improvement is evident and necessary, especially concerning the first step selectivity, the development potential of this

semi-continuous process in two stages can be acknowledged. In this process, acetol would be continuously synthesized from glycerol and added to a batch reactor containing ethylenediamine. The overall process might be successfully carried out, reaching overall yields that at this moment are around 20%, but could be further improved by optimizing the overall process conditions. Figure 6.18 illustrates a schematic idea of the concept designed up to this stage of the present thesis.

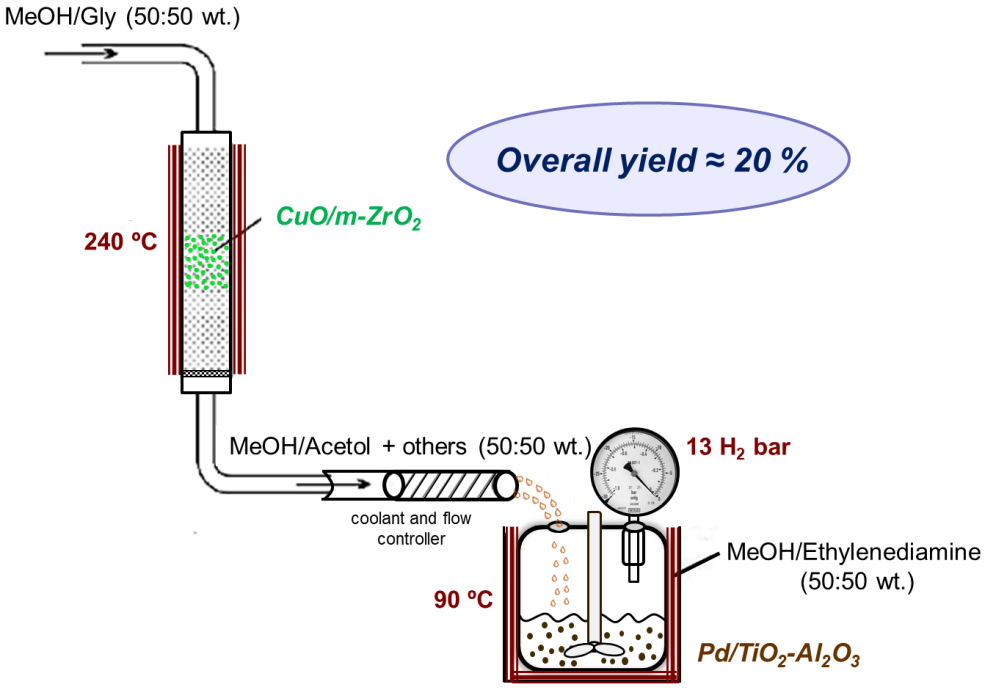

Figure 6.18. Schematic representation of a proposed consecutive semicontinuous two step-process to produce 2-methylpiperazine through glycerol valorization.

6.9 Conclusions

This chapter evaluated different catalysts based on palladium nanoparticles supported on different inorganic oxide supports with high surface areas. Again, the combination of catalytic studies and advanced characterization techniques has led to the development of a highly efficient catalyst for the synthesis of 2-methylpiperazine from bio-derived acetol and

ethylenediamine, making significant contributions to the understanding of the reaction and the catalyst-reactant interactions. In particular, the main conclusions are:

- Preliminary tests carried out with a commercial Pd/Al_2O_3 catalyst showed that preparing 2-methylpiperazine using ethylenediamine and acetol as starting reagents is feasible. Nevertheless, the design of the reaction system is critical, being key a slow acetol addition to the reaction media to achieve higher amine conversions and, therefore, higher yields to the desired product.

- A series of materials based on Pd nanoparticles supported onto simple and mixed metal oxides were prepared, characterized, and successfully applied in the reaction to produce 2-methylpiperazine from acetol and ethylenediamine. Comparable yields to those of the commercial catalyst were achieved under optimized conditions.

- The catalytic tests carried out forcing even more the operating conditions of the catalyst showed that especially the Pd/TiO_2-Al_2O_3 catalyst has high specific activity towards the formation of 2-methylpiperazine, being able to carry out the reaction at shorter reaction times or with lower catalyst loadings.

- Correlating characterization results for the materials and their catalytic behavior using lower catalyst loadings has allowed concluding an excess of acid centers is detrimental to the accomplishment of the reaction, directing the selectivity towards the formation of non-desired nitrogen by-products. On the other hand, the presence of unsaturated metal centers is critical to activate the carbon-nitrogen double bond and thus proceed to the hydrogenation of the intermediate imines. This imine hydrogenation constitutes, apparently, the limiting step of the reaction.

- Pd/TiO_2-Al_2O_3 has proven to be an efficient catalyst capable of carrying out the reaction with low catalyst loadings and reusable, experiencing only a slight deactivation after the regeneration process. Additionally, the catalyst usage can be extended to other starting substrates and even working in an aqueous medium.

However, in this case, the deposition of organic material on the catalyst is more evident.

- Finally, Pd/TiO_2-Al_2O_3 has been successfully used in the reductive amination of acetol with ethylenediamine using a stream derived from the selective dehydration reactor of glycerol, working with the CuO/*m*-ZrO_2 catalyst. In this way, and although the yields attained are moderate, it has been possible to complete a glycerol valorization process to produce the desired N-heterocycle 2-methylpiperazine.

6.10 References

[1] R.D. Taylor, M. MacCoss, A.D.G. Lawson, Rings in Drugs, J. Med. Chem. 57 (2014) 5845–5859. https://doi.org/10.1021/JM4017625.

[2] E. Vitaku, D.T. Smith, J.T. Njardarson, Analysis of the Structural Diversity, Substitution Patterns, and Frequency of Nitrogen Heterocycles among U.S. FDA Approved Pharmaceuticals, J. Med. Chem. 57 (2014) 10257–10274. https://doi.org/10.1021/JM501100B.

[3] K.E. Gettys, Z. Ye, M. Dai, Recent Advances in Piperazine Synthesis, Synthesis (Stuttg). 49 (2017) 2589–2604. https://doi.org/10.1055/S-0036-1589491.

[4] D.W. Keith, Why Capture CO2 from the Atmosphere?, Science. 325 (2009) 1654–1655. https://doi.org/10.1126/SCIENCE.1175680.

[5] S.A. Freeman, R. Dugas, D.H. Van Wagener, T. Nguyen, G.T. Rochelle, Carbon dioxide capture with concentrated, aqueous piperazine, Int. J. Greenh. Gas Control. 4 (2010) 119–124. https://doi.org/10.1016/J.IJGGC.2009.10.008.

[6] G. Rochelle, E. Chen, S. Freeman, D. Van Wagener, Q. Xu, A. Voice, Aqueous piperazine as the new standard for CO2 capture technology, Chem. Eng. J. 171 (2011) 725–733. https://doi.org/10.1016/J.CEJ.2011.02.011.

[7] F. Closmann, T. Nguyen, G.T. Rochelle, MDEA/Piperazine as a solvent for CO2 capture, Energy Procedia. 1 (2009) 1351–1357. https://doi.org/10.1016/J.EGYPRO.2009.01.177.

[8] L. Li, A.K. Voice, H. Li, O. Namjoshi, T. Nguyen, Y. Du, G.T. Rochelle, Amine blends using concentrated piperazine, Energy Procedia. 37 (2013) 353–369. https://doi.org/10.1016/J.EGYPRO.2013.05.121.

[9] M.E. Domine, M.C. Hernández-Soto, M.T. Navarro, Y. Pérez, Pt and Pd nanoparticles supported on structured materials as catalysts for the selective reductive amination of carbonyl compounds, Catal. Today. 172 (2011) 13–20. https://doi.org/10.1016/J.CATTOD.2011.05.013.

[10] M.E. Domine, M.C. Hernández-Soto, Y. Pérez, Development of metal nanoparticles

supported materials as efficient catalysts for reductive amination reactions using high-throughput experimentation, Catal. Today. 159 (2011) 2–11. https://doi.org/10.1016/J.CATTOD.2010.08.011.

[11] R. Sheldon, H. Van Bekkum, Fine chemicals through heterogeneous catalysis, 1st ed., Wiley, New York, 2008.

[12] E.W. Baxter, A.B. Reitz, Reductive Aminations of Carbonyl Compounds with Borohydride and Borane Reducing Agents, Org. React. 59 (2002) 1–714. https://doi.org/10.1002/0471264180.OR059.01.

[13] A. Pelter, R. M. Rosser, S. Mills, Reductive aminations of ketones and aldehydes using borane–pyridine, J. Chem. Soc. Perkin Trans. 1 (1984) 717–720. https://doi.org/10.1039/P19840000717.

[14] A.F.Abdel-Magid, S.J. Mehrman, A Review on the Use of Sodium Triacetoxyborohydride in the Reductive Amination of Ketones and Aldehydes, Org. Process Res. Dev. 10 (2006) 971–1031. https://doi.org/10.1021/OP0601013.

[15] A.F. Abdel-Magid, K.G. Carson, B.D. Harris, C.A. Maryanoff, R.D. Shah, Reductive Amination of Aldehydes and Ketones with Sodium Triacetoxyborohydride. Studies on Direct and Indirect Reductive Amination Procedures1, J. Org. Chem. 61 (1996) 3849–3862. https://doi.org/10.1021/JO960057X.

[16] L. Rubio-Pérez, F.J. Pérez-Flores, P. Sharma, L. Velasco, A. Cabrera, Stable Preformed Chiral Palladium Catalysts for the One-Pot Asymmetric Reductive Amination of Ketones, Org. Lett. 11 (2008) 265–268. https://doi.org/10.1021/OL802336M.

[17] D. Imao, S. Fujihara, T. Yamamoto, T. Ohta, Y. Ito, Effective reductive amination of carbonyl compounds with hydrogen catalyzed by iridium complex in organic solvent and in ionic liquid, Tetrahedron. 61 (2005) 6988–6992. https://doi.org/10.1016/J.TET.2005.05.024.

[18] S. Enthaler, Synthesis of Secondary Amines by Iron-Catalyzed Reductive Amination, ChemCatChem. 2 (2010) 1411–1415. https://doi.org/10.1002/CCTC.201000180.

[19] N.R. Candeias, C.A.M. Afonso, Preparation of non-fused heterocycles in zeolites and mesoporous materials, J. Mol. Catal. A Chem. 242 (2005) 195–217. https://doi.org/10.1016/J.MOLCATA.2005.07.042.

[20] S. Shimizu., T. Niwa, T. Shoji, No Title, 02011577, 1988.

[21] U. Dingerdissen, W. Hoelderich, Preparation of amines by reductive amination using zeolite catalyst, US Patent 5,290,932, 1994.

[22] A.L. Nuzhdin, M. V Bukhtiyarova, G.A. Bukhtiyarova, Cu-Al mixed oxide derived from layered double hydroxide as an efficient catalyst for continuous-flow reductive amination of aromatic aldehydes, J. Chem. Technol. Biotechnol. 95 (2020) 3292–3299. https://doi.org/10.1002/JCTB.6508.

[23] A. Corma, T. Ródenas, M.J. Sabater, A Bifunctional Pd/MgO Solid Catalyst for the One-Pot Selective N-Monoalkylation of Amines with Alcohols, Chem. – A Eur. J. 16 (2010) 254–260. https://doi.org/10.1002/CHEM.200901501.

[24] J.D. Vidal, M.J. Climent, P. Concepcion, A. Corma, S. Iborra, M.J. Sabater, Chemicals from Biomass: Chemoselective Reductive Amination of Ethyl Levulinate with Amines, ACS Catal. 5 (2015) 5812–5821. https://doi.org/10.1021/ACSCATAL.5B01113.

[25] J.D. Vidal, M.J. Climent, A. Corma, D.P. Concepcion, S. Iborra, One-Pot Selective Catalytic Synthesis of Pyrrolidone Derivatives from Ethyl Levulinate and Nitro Compounds, ChemSusChem. 10 (2017) 119–128. https://doi.org/10.1002/CSSC.201601333.

[26] A.S. Touchy, S.M.A.H. Siddiki, K. Kon, K. Shimizu, Heterogeneous Pt Catalysts for Reductive Amination of Levulinic Acid to Pyrrolidones, ACS Catal. 4 (2014) 3045–3050. https://doi.org/10.1021/CS500757K.

[27] S. Wei, Z. Dong, Z. Ma, J. Sun, J. Ma, Palladium supported on magnetic nanoparticles as recoverable catalyst for one-pot reductive amination of aldehydes with nitroarenes under ambient conditions, Catal. Commun. 30 (2013) 40–44. https://doi.org/10.1016/J.CATCOM.2012.10.024.

[28] W. Ueda, T. Yokoyama, Y. Moro-Oka, T. Ikawa, Catalytic synthesis of vinyl ketones over metal oxide catalysts using methanol as the vinylating agent, J. Chem. Soc. Chem. Commun. 1 (1984) 39–40. https://pubs.rsc.org/en/content/articlepdf/1984/c3/c39840000039.

[29] N.E. Fouad, P. Thomasson, H. Knözinger, IR study of adsorption and reaction of methylbutynol on the surface of pure and modified MgO catalysts: probing the catalyst surface basicity, Appl. Catal. A Gen. 194–195 (2000) 213–225. https://doi.org/10.1016/S0926-860X(99)00369-5.

[30] G. Liang, A. Wang, L. Li, G. Xu, N. Yan, T. Zhang, Production of Primary Amines by Reductive Amination of Biomass-Derived Aldehydes/Ketones, Angew. Chemie. 129 (2017) 3096–3100. https://doi.org/10.1002/ANGE.201610964.

[31] A. García-Ortiz, J.D. Vidal, M.J. Climent, P. Concepción, A. Corma, S. Iborra, Chemicals from Biomass: Selective Synthesis of N-Substituted Furfuryl Amines by the One-Pot Direct Reductive Amination of Furanic Aldehydes, ACS Sustain. Chem. Eng. 7 (2019) 6243–6250. https://doi.org/10.1021/ACSSUSCHEMENG.8B06631.

[32] J. Mazarío, M. Parreño Romero, P. Concepción, M. Chávez-Sifontes, R.A. Spanevello, M.B. Comba, A.G. Suárez, M.E. Domine, Tuning zirconia-supported metal catalysts for selective one-step hydrogenation of levoglucosenone, Green Chem. 21 (2019) 4769–4785. https://doi.org/10.1039/c9gc01857c.

[33] H. Borchert, B. Jürgens, V. Zielasek, G. Rupprechter, S. Giorgio, C.R. Henry, M. Bäumer, Pd nanoparticles with highly defined structure on MgO as model catalysts: An FTIR study of the interaction with CO, O2, and H2 under ambient conditions, J. Catal. 247 (2007) 145–154. https://doi.org/10.1016/J.JCAT.2007.02.002.

[34] D. Tessier, A. Rakai, F. Bozon-Verduraz, Spectroscopic study of the interaction of carbon monoxide with cationic and metallic palladium in palladium–alumina catalysts, J. Chem. Soc. Faraday Trans. 88 (1992) 741–749. https://doi.org/10.1039/FT9928800741.

[35] S. Bertarione, D. Scarano, A. Zecchina, V. Johánek, J. Hoffmann, S. Schauermann, M. M. Frank, J. Libuda, G. Rupprechter, H.J. Freund, Surface Reactivity of Pd Nanoparticles Supported on Polycrystalline Substrates As Compared to Thin Film Model Catalysts: Infrared Study of CO Adsorption, J. Phys. Chem. B. 108 (2004) 3603–3613. https://doi.org/10.1021/JP036718T.

[36] D. Ferri, C. Mondelli, F. Krumeich, A. Baiker, Discrimination of Active Palladium

Sites in Catalytic Liquid-Phase Oxidation of Benzyl Alcohol, J. Phys. Chem. B. 110 (2006) 22982–22986. https://doi.org/10.1021/JP065779Z.

[37] H. Mueller, W. Mesch, US Pat. 4792631A, 1987.

[38] D.A. Bassett, E.L.M. Cowton, 0820430B1, 1996.

[39] K.H. Oehr, J. Mckinley, No Title, in: A.V. Bridgwater (Ed.), Adv. Thermochem. Biomass Convers., 1st ed., Springer, Dordrecht, 1993, 1452–1455.

[40] J.B. Trecek, G.L. Wiesner, Vapor phase oxidation process for glyoxal, US Pat. 4258216A, 1979.

[41] Y. Toyoda, K. Wakimura, T. Hase, N. Arashiba, Preparation process for glyoxal, US Pat. 4555583A, 1983.

Chapter 7
Towards a continuous catalytic process to 2-methylpyrazine *via* acetol

7.1 Introduction

The other targeted organonitrogen chemical that was intended to be reached through the development of this thesis was 2-methylpyrazine. Pyrazine-type compounds are widely used in flavor and aroma industries[1] and present in several drugs[2,3], as explained in greater detail in *Chapter 1: Introduction*.

Routes to produce pyrazines from glycerol and propylene glycol are diverse, and reaction schemes can be rather complex and challenging in terms of selectivity. Moreover, amine condensation and dehydrocyclization of glycerol requires very drastic reaction conditions[4–9]. In this sense, what has been pursued during the present chapter is simplifying and directing the process through preparing the 2-methylpyrazine in a fix-bed reactor starting from hydroxyacetone (or acetol) and ethylenediamine. Thereafter, the possibility of combining this last process with the first step glycerol dehydration reaction would be explored (see Scheme 7.1).

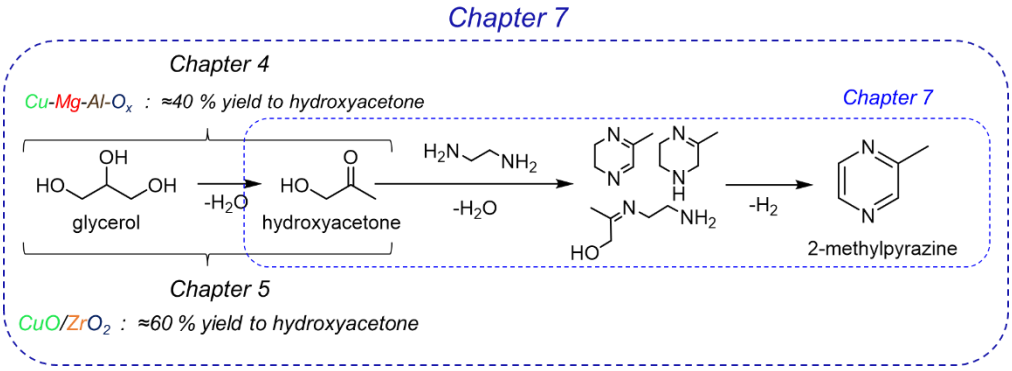

Scheme 7.1. Proposed route for the synthesis of 2-methylpyrazine from glycerol.

Theoretically, our strategy would be able to skip many of the undesired secondary reactions and avoid the use of extremely harsh reaction conditions. Consequently, the selectivity towards the desired product would be increased.

On the other hand, and always bearing in mind the need for sustainable catalysts and processes, several requirements have been self-imposed in the development and search for suitable catalysts to produce 2-methylpyrazine from acetol and ethylenediamine. In this

sense, and to set this work apart from others in the literature, it has been worked with catalysts having low copper loading, avoiding the use of chromium, which is present in the vast majority of the catalysts described to date for the production of 2-methylpyrazine from glycerol or propylene glycols, and also evading catalyst activation with hydrogen.

Therefore, and always taking into account that, as in the synthesis of 2-methylpiperazine, the objective was developing a valorization process in which glycerol would be the ultimate carbon source to produce 2-methylpyrazine, analogous catalysts to those described in *Chapter 5* of the present doctoral thesis (CuO-supported materials for glycerol dehydration) were used in this section. These catalysts based on inorganic supports with a high surface area and containing acid-base centers will allow interaction with the reactant species. At the same time, they have copper oxide moieties capable of generating and acting as a dehydrogenating functionality. Consequently, they are promising candidates, first, to carry out the reaction of production of 2-methylpyrazine from acetol and ethylenediamine, but also to be able to establish a final one-pot process with glycerol and ethylenediamine to yield the desired 2-methyl pyrazine.

For this reason and given that the catalysts used in this chapter will be basically those described in *Chapter 5*, only the most fundamental characterization data will be presented before the catalytic results obtained for each of the materials, referring the reader to *Chapter 5* to find additional information. However, throughout the discussion of the catalytic properties and whenever required, the necessary characterization data will be provided to facilitate the reader's understanding of the relevant catalytic properties and of those structure-activity correlations critical for the reaction success.

7.2 First catalytic screening with supported CuO materials

In the first place, some preliminary catalytic tests were performed to approach the reaction and determine the optimum operating conditions[10]. In order to investigate these parameters, a commercial $2CuO{\cdot}Cr_2O_3$ material, described among the family of chromite catalysts efficient for the synthesis of pyrazine from glycerol and 1,2-propylendiamine[11], was used to assess the influence of both the reaction temperature and the solvent. In these experiments, the catalyst was not reduced before reaction.

These preliminary results will not be discussed in deep here, and the reader is referred to the corresponding MSc thesis carried out in our research group and experimentally supervised by the PhD candidate for more detail[10]. In brief, experiments were carried out from 250 to 400 ºC, using water as solvent (see Figure 7.1). The highest ethylenediamine conversions were achieved at 350 ºC and 400 ºC, whereas conversion values were lower below 350 ºC, and a more extended induction period was required for the catalyst to start displaying high activity. Between 350 and 400 ºC, although conversions and selectivities to 2-methylpyrazine in the liquid fraction were similar, the former temperature gave the best results in terms of yield to liquids and carbon balance. Therefore, 350 ºC was selected as the working temperature. Regarding the solvent, MeOH (preferred solvent for glycerol dehydration) and water were compared at 350 °C. Ethylenediamine conversion values were close to 100% in both cases, but methanol meant lower pyrazine selectivities. Consequently, and considering the overall sustainability of the future process, water was eventually selected.

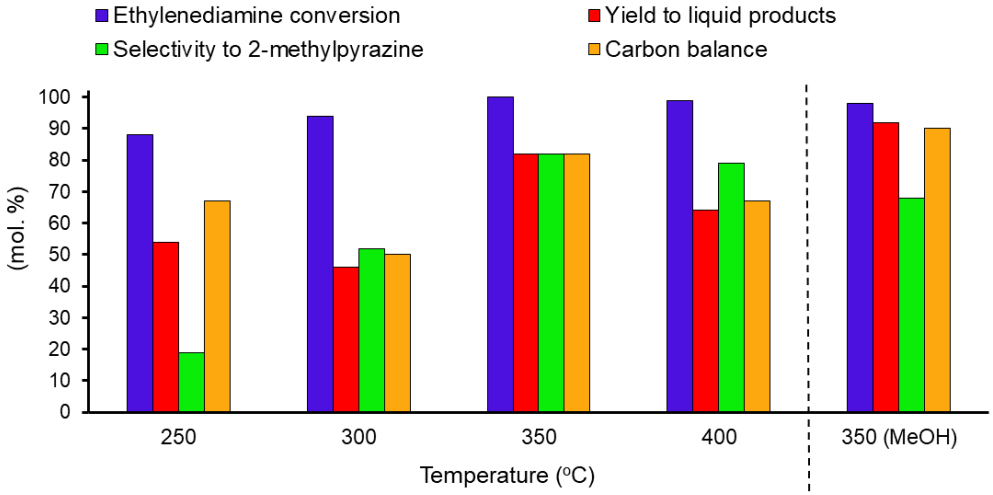

Figure 7.1. Preliminary catalytic tests for 2-methylpyrazine synthesis over $2CuO{\cdot}Cr_2O_3$ catalyst[10]. Average results for TOS = 0.5 – 4.5 h. Reaction conditions: 350 ºC, solvent: H_2O, reagents/solvent-ratio: 0.4/0.6 (in wt.), diamine flow: 1.00 ml/h; acetol flow: 1.24 ml/h, 0.5 g of catalyst, particle size: 0.4-0.6 mm.

7.2.1 Catalytic results for CuO-based catalysts

Keeping in mind the possibility of achieving a one-pot process to produce 2-methylpyrazine from glycerol (see Scheme 7.1), a series of materials based on copper oxide supported onto different metallic oxides and prepared by the incipient wetness impregnation method were tested in the condensation and dehydrogenation reaction between acetol and ethylenediamine. Importantly, these materials had already been used in the glycerol dehydration reaction to acetol. In fact, the only notable difference is that the support used in the preparation of CuO/*mxt*-ZrO_2 corresponds to a synthesized material (as defined in *Section 3.2.7*), instead of the mixture of commercial phases previously described (see *Chapter 5*). This change was prompted by a shortage of commercial *t*-ZrO_2.

Table 7.1 shows the main physicochemical properties of the materials used in these first catalytic tests. The materials show similar ICP results for Cu content (≈5.0 wt.%), surface areas between 100 and 200 m^2/g, and, as they all were prepared by incipient wetness impregnation, they are expected to have comparable CuO particle sizes. Additionally, Figure 7.2 shows the information obtained by XRD analysis for the different CuO/MO_x. Except for the amorphous silica, XRD patterns clearly show the presence of a set of peaks associated with each one of the metal oxides employed as supports. In addition, none of the diffractograms presented apart from the one for CuO-IW/SiO_2-CH shows peaks corresponding to a crystalline phase of CuO. The absence of these peaks reveals a reasonable dispersion degree on the surface of the MO_x of the supported CuO, only seen in the material CuO-IW/SiO_2-CH due to the poor crystallinity of the support.

Table 7.1. Main textural and physicochemical properties of different CuO-based materials.

Catalyst	Cu content (wt.%)[a]	Surface area (m^2/g)[b]	Pore volume (cm^3/g)[b]
CuO/MgO	5.0	172	0.82
CuO-IW/SiO_2-CH	5.0	211	0.82
CuO/Al_2O_3-*ac*	4.2	125	0.24
CuO/*mxt*-ZrO_2	5.6	125	0.25

[a] Calculated by ICP. [b] Calculated from N_2-adsorption isotherms data (BET method).

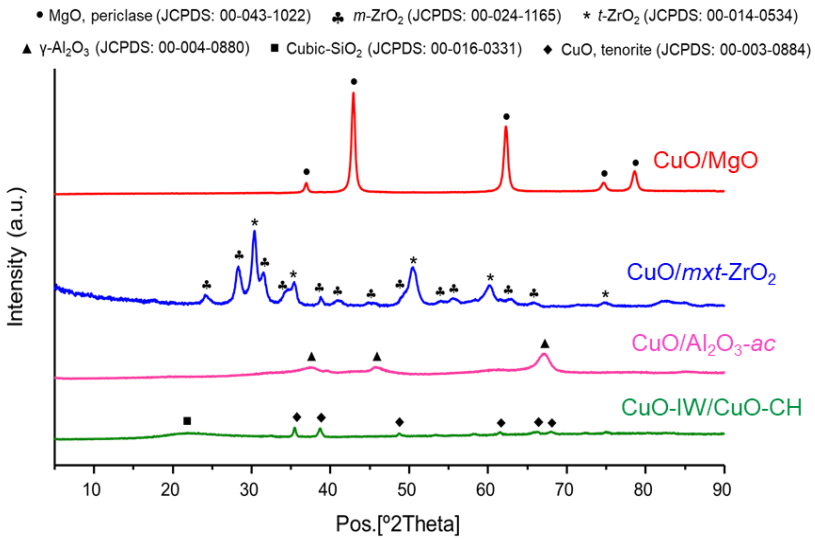

Figure 7.2. XRD patterns of supported CuO materials.

As shown in Figure 7.3a, the average results of these first catalytic tests for 4.5 h of time on stream were auspicious for materials CuO/*mxt*-ZrO_2 and CuO/Al_2O_3-*ac*. For these two catalysts and CuO/MgO, ethylenediamine is completely converted during the process. Although the yield to liquids (values from 30 to 71%) and, therefore, the carbon balance (values from 32 to 83%) is relatively low in the four cases, Cu/*mxt*-ZrO_2 and Cu/Al_2O_3-*ac* provided the best results with ≈70% yield to liquids and ≈60% selectivity to 2-methyl-pyrazine in that liquid fraction. Moreover, both catalysts were able to maintain the yield to 2-methylpyrazine around 40% for the total duration of the experiment (TOS = 4.5 h, Figure 7.3b). These findings were very encouraging for the development of the overall process since, if we remember, these same materials are the ones that had shown the best results in the selective dehydration of glycerol to acetol (see *Chapter 5*).

Furthermore, to rule out metallic leaching, the used catalysts were calcined at 550 ºC to eliminate the organic matter deposits and then analyzed by ICP, comparing them with the fresh materials (Table 7.2). The materials studied have been the most promising to carry out the reaction (i.e., CuO/Al_2O_3-*ac* and CuO/*mxt*-ZrO_2). Additionally, the stability of the CuO/SiO_2 catalyst was also studied since, due to the technologies established in *Chapter 5*, a more sophisticated design of this catalyst could be proposed. However, it was found that

metallic leaching is quite significant on that support. On the contrary, there seems to be no leaching in the catalysts CuO/Al_2O_3-*ac* and CuO/*mxt*-ZrO_2. The increase in the metallic loading observed in the CuO/Al_2O_3-*ac* catalyst after reaction can be attributed to a minor experimental error since there is no significant aluminum leaching during the reaction.

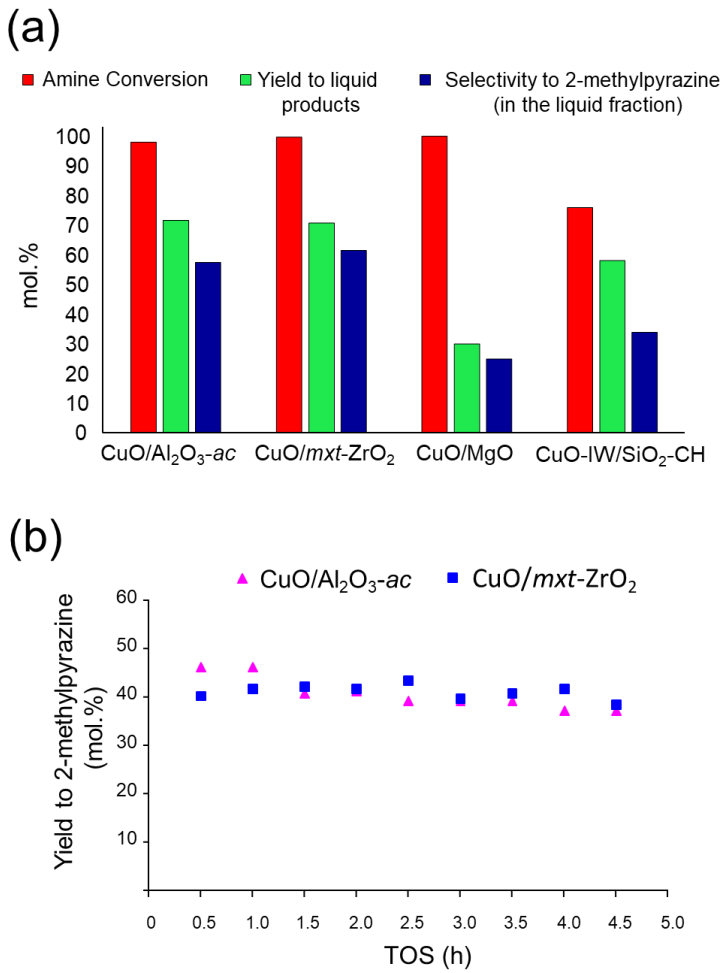

Figure 7.3. (a) Average results for 4.5 h on stream achieved with supported CuO materials in the 2-methylpyrazine synthesis from acetol an ethylenediamine. (b) Yield to 2-methylpyrazine vs TOS for CuO/Al_2O_3-*ac* and CuO/*mxt*-ZrO_2. Reaction conditions: 350 ºC, solvent: H_2O, reagents/solvent-ratio: 0.4/0.6 (in wt.), diamine flow: 1.00 ml/h; acetol flow: 1.24 ml/h, 0.5 g of catalyst, particle size: 0.4-0.6 mm.

Table 7.2. Effect of use (TOS = 4.5 h) and on metal loading (measured by ICP) for CuO-based materials.

Catalyst	Cu wt.% (fresh catalyst)	Cu wt.% (used catalyst)	M* wt.% (fresh catalyst)	M* wt.% (used catalyst)
CuO-IW/SiO_2-CH	5.0 ± 0.2	3.8 ± 0.2	n/d	n/d
CuO/Al_2O_3	4.2 ± 0.2	5.6 ± 0.3	53.2 ± 1.1	54.7 ± 1.1
CuO/*mxt*-ZrO_2	5.6 ± 0.3	5.5 ± 0.3	n/d	n/d

* M = metal of the support (Si, Al or Zr). Note: Random error estimated by applying the *t* student (0.98) criterion to three repeated measurements of a material containing similar amounts of the analyzed metals.

7.2.2 Structure activity relationships for CuO-based catalysts

These first catalytic tests, together with the acid-base characterization of these catalysts, allowed us to establish the first structure-activity relationships, already highlighting the influence of acidity and basicity in the reaction. Interestingly, for the reaction between glycerol/propylene glycols and diamines to yield pyrazines, literature speaks about a hardly understood balance between acid and basic centers necessary to carry out the reaction satisfactorily, whereas little attention is paid to the dehydrogenative metallic function of the catalyst[6,11–13]. Authors attributed the intermolecular cyclization of diamines, the glycerol dehydration to hydroxyacetone and the amine activation to the acidic character. On the other hand, they have associated glycerol dehydrogenation to dihydroxypropanal or dihydroxyacetone with basic sites and, therefore, dehydrocyclization activity involving the oxygenated and the nitrogenated molecule with samples containing both basic and weak acidic sites.

In that sense, Figure 7.4 shows the assessment of acid and base sites present in CuO-supported materials by NH_3-TPD and CO_2-TPD, respectively. Interestingly, the distribution of acidic and basic strengths is essentially the same in all the studied materials except in the case of CuO/MgO (as expected). CuO/MgO shows some more robust acid sites as well as stronger basic sites than the rest. Nonetheless, although CuO/MgO basicity is the highest

both in number and in strength, its acidity is negligible compared to that exhibited by CuO/*mxt*-ZrO_2 and CuO/Al_2O_3-*ac*. Therefore, the discussion can be elaborated only based on the total number of acid centers, the total number of basic centers, and the total number of active sites found for each catalyst, as the numbers reflect the trends very reasonably. These data are compiled in Table 7.3.

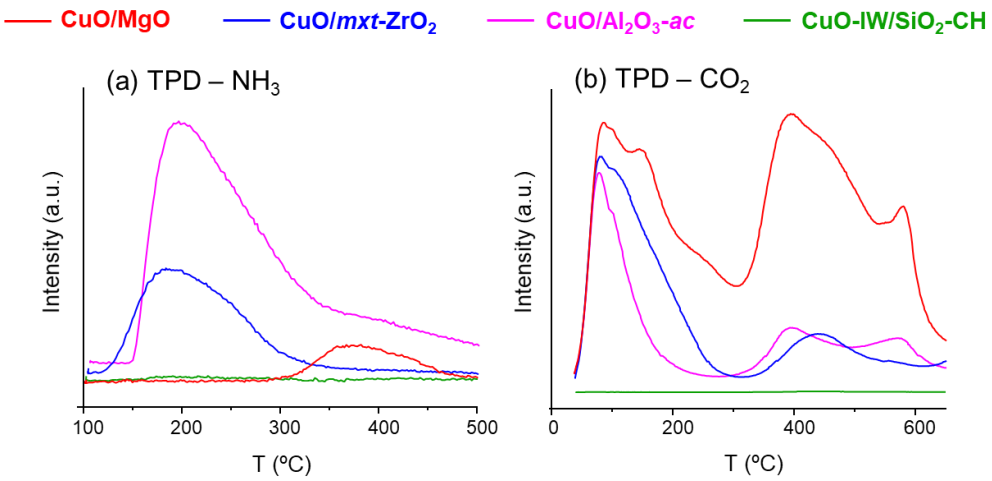

Figure 7.4. (a) NH_3-TPD and (b) CO_2-TPD profiles of CuO/Al_2O_3 materials. Note: non-calibrated mass-spectrometer (MS); qualitative information about strength distribution.

Table 7.3. Acid-base site analyses for different CuO-based materials.

Catalyst	Acid sites (µmol NH_3/g)[a]	Basic sites (µmol CO_2/g)[b]	Acid+base sites (µmol/g)
CuO/MgO	18	111	129
CuO-IW/SiO_2-CH	17	4	21
CuO/Al_2O_3-*ac*	200	54	254
CuO/*mxt*-ZrO_2	222	74	296

[a] Measured by NH_3 adsorption pulses until saturation.

[b] Measured by CO_2 adsorption pulses until saturation.

With these acid-base characterization data and calculating the selectivity considering only the liquid fraction, exciting conclusions can be drawn. In this sense, Figure 7.4 illustrates the selectivity towards the different products as a function of the acid-base properties normalized per area unit. In Figure 7.5a, it can be seen how those more acidic materials give higher selectivities to the desired alkyl pyrazines, whereas Figure 7.5b shows how the material having the largest proportion of basic centers with respect to acid sites drives the reaction towards the formation of unwanted nitrogen by-products. Most of these nitrogen by-products, due to their high molecular weight and aromaticity are expected to be precursors for solid organic matter ending up stuck on the catalyst surface. Last, Figure 7.5c exposes that the material not presenting almost any type of acid-base center (i.e., CuO-IW/SiO_2-CH) is, as expected, inactive, and only the thermal reaction between the acetol and the diamine takes place.

Thus, acid sites seem to benefit dehydrogenation activity to yield the desired pyrazines from the imine intermediates. On the other hand, basic sites seem to direct the reaction towards the formation of N-containing by-products. For materials with lower concentrations of active sites, the reaction lacks an effective driving force and does not progress beyond the imine formation. Scheme 7.2 illustrates the reaction pathway explained in this last paragraph.

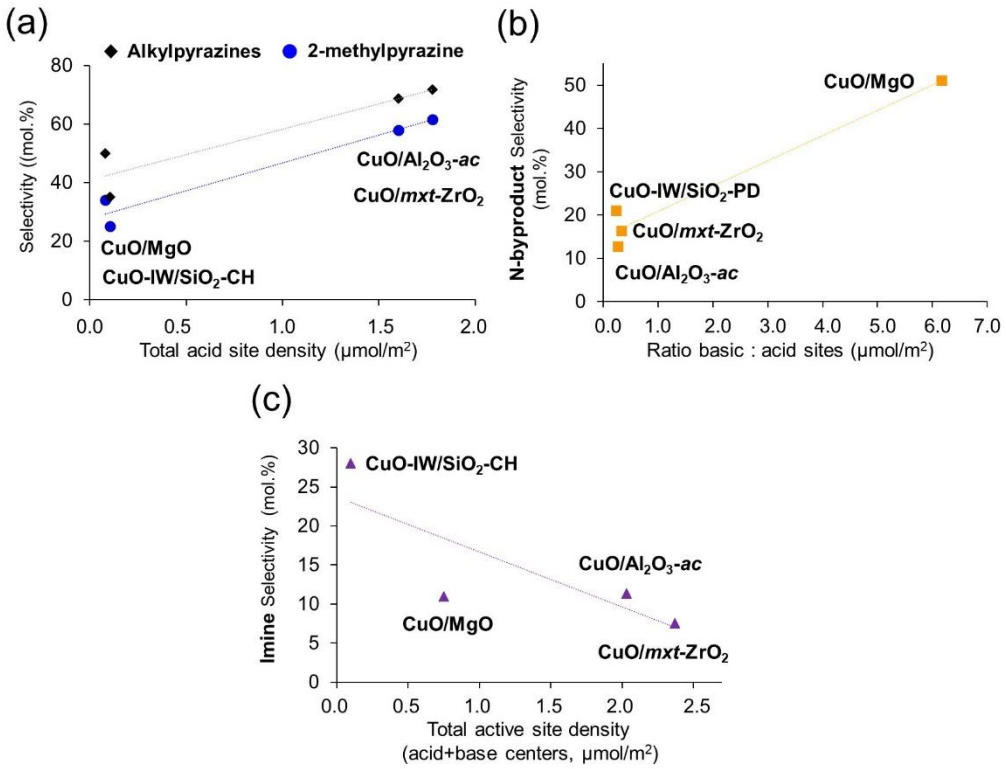

Figure 7.5. Liquid fraction selectivities to (a) alkyl pyrazines and 2-methylpyrazine vs total acid site density, (b) Nitrogen by-products vs basic : acidic site ratio, (c) Imines vs total density of active acid and base sites. Reaction conditions: 350 ºC, solvent: H_2O, reagents/solvent-ratio: 0.4/0.6 (in wt.), ethylenediamine flow: 1.00 ml/h; acetol flow: 1.24 ml/h, 0.5 g of catalyst, particle size: 0.4-0.6 mm.

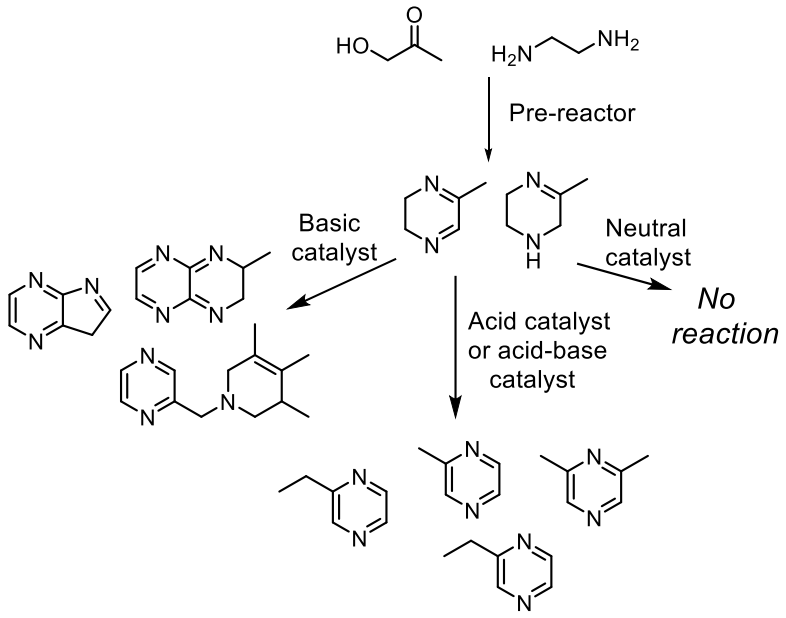

Scheme 7.2. Proposed reaction pathways for the formation of 2-methylpyrazine and alkyl-pyrazines.

However, although acid-base centers are believed to be critical for the cyclization-dehydrogenation reaction between glycerol and ethylenediamine when using previously reduced catalysts, it is necessary to emphasize that, in our reaction system, without hydrogen activation, the efficiency of the catalytic system at generating the active species, together with their characteristics, will also be important. Still, it is also true that the reducibility of these materials, detailed in *Chapter 5*, is high enough so that at the reaction temperature (350 ºC), with a reasonable generation of hydrogen, the metallic copper species responsible for dehydrogenation can be created. Additionally, and since we are comparing catalysts prepared by incipient wetness impregnation, we can also see in *Chapter 5* how this methodology results in CuO particle sizes between 5 and 10 nm in all cases, with broad size distributions. Therefore, significant differences in these catalyst active areas (i.e., in the dehydrogenative area) are not expected. That is why the structure-activity relationships have been simplified to catalyst acidity and basicity in this part of the work. However,

implementing studies to *in-situ* observe the reducibility as well as a more exact determination of the copper active area (by N_2O chemisorption) remain as future tasks.

7.3 Catalyst selection

7.3.1 Catalytic tests for CuO/ZrO_2 system

As recently depicted (see Figure 7.5), acid-base functionalities seem to exert a substantial effect on catalytic performance. Therefore, and considering the different acid-base properties that can be displayed by the different zirconia crystalline phases (see *Chapter 5*), it was decided, as in the study of the selective dehydration of glycerol acetol, to test the different polymorphs of zirconia as copper oxide supports in catalysis. Figure 7.6a shows how, on this occasion, the trend is the opposite of that observed in *Chapter 5*. Although amine conversions are nearly quantitative in the three cases, the two materials with CuO supported total or partially onto tetragonal zirconia (CuO/*mxt*-ZrO_2 and CuO/*t*-ZrO_2) give better yields to 2-methylpyrazine, and to the alkyl-pyrazines in general (i.e., 44% for CuO/*t*-ZrO_2 and 48% for CuO/*t*-ZrO_2 vs 35% for CuO/*m*-ZrO_2). Moreover, they remain stable for longer (see Figure 7.6b), achieving the same catalyst specific activity throughout the process (TOS = 4.5 h), in good agreement with the lower yield to liquid nitrogen containing by-products and solid products (22% for CuO/*t*-ZrO_2 vs 27% for CuO/*m*-ZrO_2).

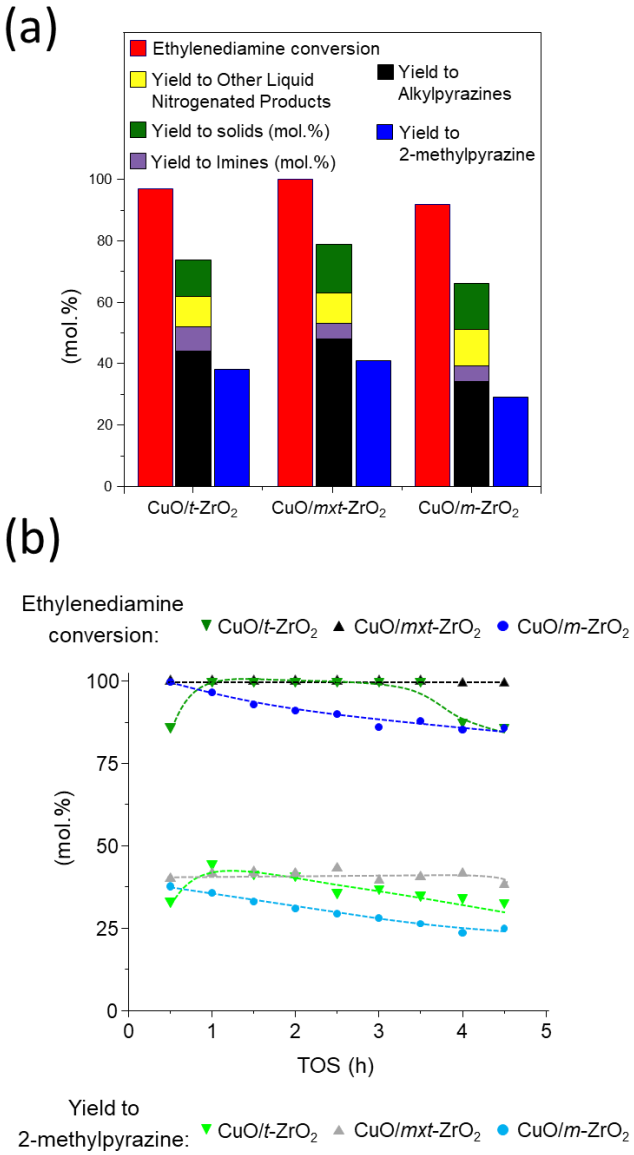

Figure 7.6. (a) Average results for 4.5 h on stream achieved over different CuO supported on ZrO_2 catalysts in the 2-methylpyrazine synthesis from acetol and ethylenediamine. (b) Diamine conversion and yield to 2-methylpyrazine vs TOS for CuO supported on ZrO_2 catalysts. Reaction conditions: 350 ºC, solvent: H_2O, reagents/solvent-ratio: 0.4/0.6 (in wt.), diamine flow: 1.00 ml/h; acetol flow: 1.24 ml/h, 0.5 g of catalyst, particle size: 0.4-0.6 mm. Note: Dashed lines serve only as visual guidelines.

7.3.2 Catalytic tests for CuO/Al_2O_3 system

In the same way that in the case of the copper oxide supported on the zirconia system, different types of alumina were also studied as supports for the CuO nanoparticles. Specifically, those materials developed throughout *Chapter 5*; CuO/Al_2O_3-*ac*, CuO/Al_2O_3-*bas*, and CuO/Al_2O_3-*npw*. Let us remember that these materials differ fundamentally from each other in their acid-base characteristics, which, from a catalyst optimization viewpoint, has all the earmarks of being useful for our reaction. On the other hand, they show equivalent reducibility and similar particle sizes. Interestingly, as occurred in the dehydration reaction of glycerol acetol, there are significant differences in the catalytic behavior of these materials.

Despite ethylenediamine conversions are essentially quantitative in all cases, in particular, the CuO/Al_2O_3-*npw* can achieve higher yields to the desired pyrazines, with a 2-methylpyrazine yield around 50% and a total yield to alkyl pyrazines of about 60% (see Figure 7.7a). CuO/Al_2O_3-*ac* was unable to surpass 40 and 50 % yields to 2-methylpyrazine and alkyl pyrazines, respectively, and CuO/Al_2O_3-*bas* barely reaches a 40% yield for the entire set of alkylpyrazines. On the negative side, although no significant loss of activity is observed, the low carbon balances achieved in these cases (see Figure 7.7a, comparing conversion and yield to the different products) are expected to have a significant impact when working at longer times on stream.

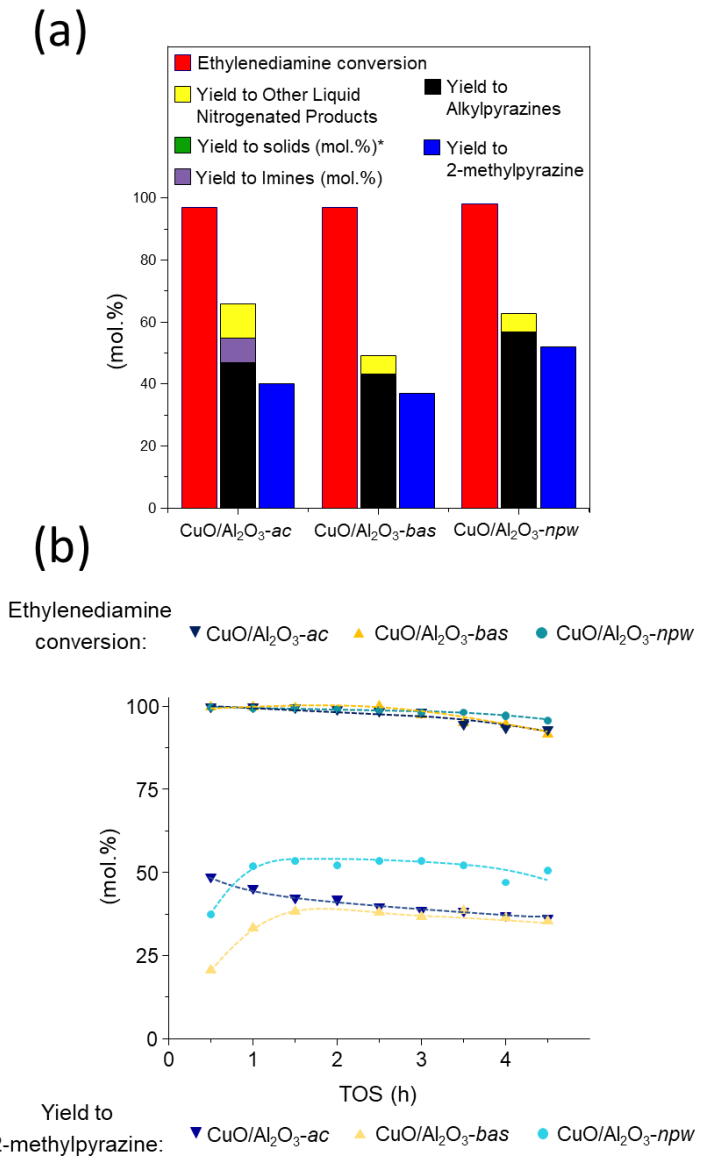

Figure 7.7. (a) Average results for 4.5 h on stream achieved over different CuO supported on Al_2O_3 catalysts in the 2-methylpyrazine synthesis from acetol and ethylenediamine. (b) Diamine conversion and yield to 2-methylpyrazine vs TOS for CuO supported on Al_2O_3 catalysts. Reaction conditions: 350 ºC, solvent: H_2O, reagents/solvent-ratio: 0.4/0.6 (in wt.), Diamine flow: 1.00 ml/h; acetol flow: 1.24 ml/h, 0.5 g of catalyst, particle size: 0.4-0.6 mm. Note: Dashed lines serve only as visual guidelines.

7.3.3 Longer term study for CuO/Al_2O_3-*npw*

For the best catalyst (i.e., CuO/Al_2O_3-*npw*) found up to this point, an experiment was carried out at longer reaction times to verify catalyst stability. Nonetheless, given the results attained in the stability studies for the best catalysts seen in *Chapter 5* (i.e., CuO/*m*-ZrO_2 and CuO/Al_2O_3-*npw*) for the selective dehydration of glycerol acetol, time on stream was not extended beyond 8 hours of reaction.

In Figure 7.8, it can be observed that, despite a small distortion in the data at longer times due to a partial blocking and subsequent unblocking of the reactor, the catalyst maintains good stability, and did not start suffering from a significant deactivation yet. Quantitative conversions to ethylenediamine are observed at the beginning of the experiment, with just a small decay at longer times. On the other hand, it seems that the yield to the desired alkyl pyrazine products follows the same trend. This beginning of the deactivation process can also be observed in the appearance of imine-type reaction intermediates, starting to be detected significantly (yield ≈2%) at six and a half hours of reaction. However, for the reaction times studied, it can be considered that the catalyst does not undergo major deactivation. Importantly, these times correspond to those in which the catalysts developed in *Chapter 5*, to achieve the selective dehydration of glycerol to acetol, present their period of maximum activity. Therefore, it can be accepted that this catalyst CuO/Al_2O_3-*npw* is promising for conducting experiments by coupling both stages; the selective dehydration of glycerol to acetol and its subsequent dehydrocyclization with ethylenediamine.

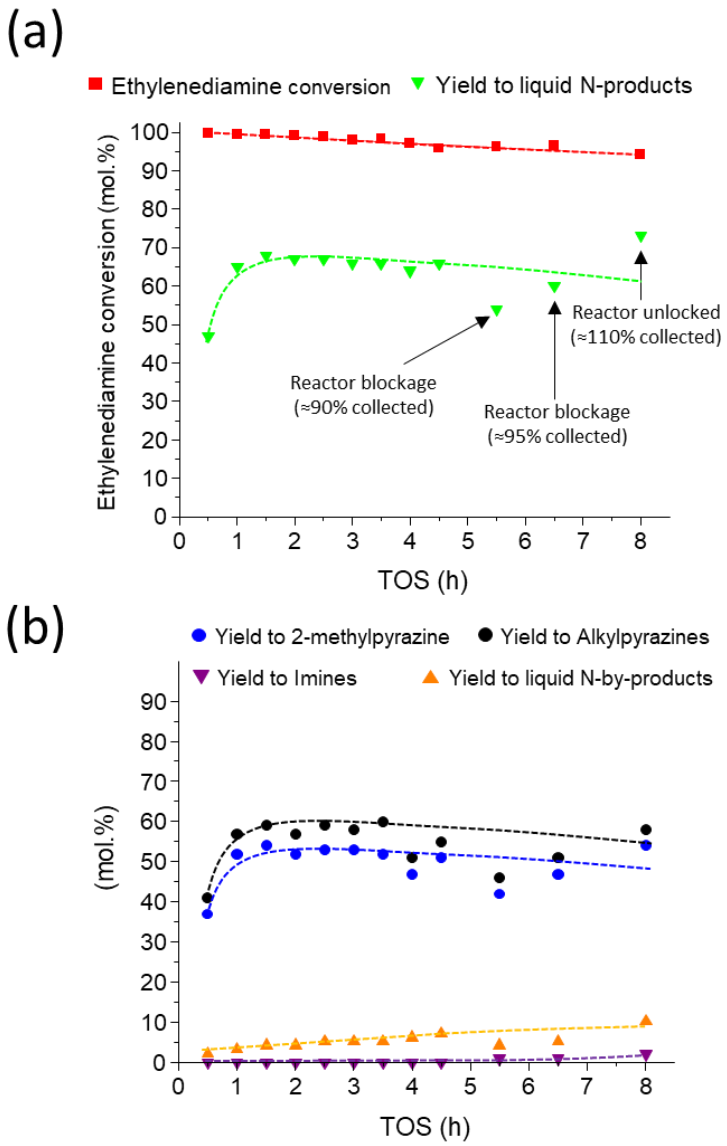

Figure 7.8. (a) Ethylenediamine conversion and yield to 2-methylpyrazine vs TOS, and (b) Yield to the different liquid products vs TOS, for CuO/Al_2O_3-*npw* catalyst. Reaction conditions: 350 ºC, solvent: H_2O, reagents/solvent-ratio: 0.4/0.6 (in wt.), Diamine flow: 1.00 ml/h; acetol flow: 1.24 ml/h, 0.5 g of catalyst, particle size: 0.4-0.6 mm. Note: Dashed lines serve only as visual guidelines.

7.3.4 Overall structure-activity relationships

Once we have introduced more catalysts to study in this reaction system, unravelling structure-activity relationships becomes more complicated. Nonetheless, at the same time, the structure-activity relationships that could be found will likely be more solid.

In this sense, if we represent the yield to both alkyl pyrazines and 2-methylpyrazine as a function of the ratio between acidic and basic centers (Figure 7.9a), the predominantly basic catalysts present lower yields to these products of interest and lower yield to liquid nitrogenated products (Figure 7.9b), which is in good agreement with what was previously found in this chapter. Besides that role of the basicity, high ratios of acidic sites to basic sites also cause a decrease in the yield to the desired pyrazines, although less marked than when the catalyst has an excess of basic centers, and also a decrease in the yield to liquid products. Apparently, there is an optimum ratio at which CuO/*mxt*-ZrO_2 and CuO/Al_2O_3-*npw* are placed (see Figure 7.9b). However, CuO/Al_2O_3-*npw* catalyst seems to exceed the general trend positively.

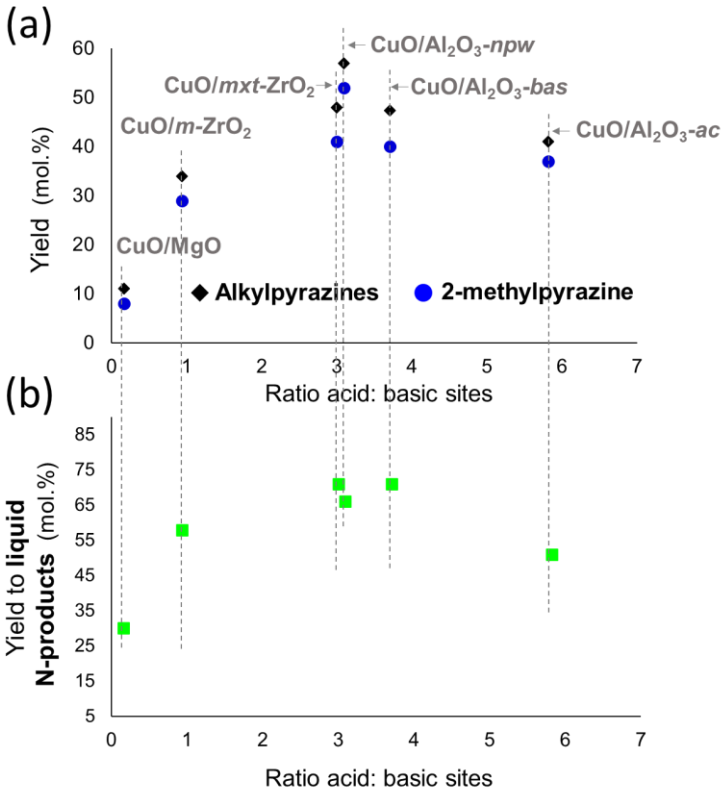

Figure 7.9. Yields to (a) alkyl pyrazines and 2-methylpyrazine and, (b) liquid nitrogenated products vs acid : base sites ratio on the catalysts. Reaction conditions: 350 ºC, solvent: H_2O, reagents/solvent-ratio: 0.4/0.6 (in wt.), diamine flow: 1.00 ml/h; acetol flow: 1.24 ml/h, 0.5 g of catalyst, particle size: 0.4-0.6 mm.

At this point, we can draw some conclusions and raise a few uncertainties to be solved in the future. It seems obvious that basic centers provoke the transformation of the imine intermediates into unwanted nitrogen by-products, fundamentally heavy nitrogen by-products, which will most likely constitute coke precursors. On the other hand, the acid centers seem to play a fundamental role in imine hydrogenation. However, it is unclear if this role of the acid centers in hydrogenation also requires the vicinity of basic centers, as suggested in the literature for the reaction between glycerol and ethylenediamine. Another possibility could involve the dehydrogenation only depending on acid centers, but an excess

of them would also start to result in unwanted nitrogen by-products, likely solids, probably due to imine conversions different from their dehydrogenation to pyrazines. The out-layer point seen for CuO/Al_2O_3-*npw* 7.9a could in fact be explained by these two points, since both acidity and basicity are lower than in the case of CuO/*mxt*-ZrO_2. Additionally, further studies to carefully examine the particle morphology as well as the significance of the substantial fraction of nanoparticles showing very low particle sizes (≤ 2nm, see Figure 5.9, in *Chapter 5*) seen in this material could provide alternative explanations for this outstanding catalytic result encountered for the CuO/Al_2O_3-*npw* material.

7.4 Additional improvement on the CuO/Al_2O_3-*npw* catalyst

In *Chapter 5*, the specific catalytic activity of CuO/*m*-ZrO_2 in the selective dehydration of glycerol to acetol could be enhanced by incorporating the CuO nanoparticles by the reverse micelle alternative method. Thus, it was considered that a significant improvement could also be achieved for the dehydrocyclization of acetol with ethylenediamine following the same strategy. Therefore, an analogous catalyst was prepared with the same composition of the best catalyst CuO/Al_2O_3-*npw*, but the CuO nanoparticles, instead of being incorporated by incipient wetness impregnation, were deposited through the reverse micelle methodology described in *Section 3.2.6*.

7.4.1 Preparation and characterization of RV-CuO/Al_2O_3-*npw*

Catalyst RV-CuO/Al_2O_3-*npw* was prepared by the reverse micelle methodology described in *Section 3.2.6* to attain a catalyst whose compositional and textural property, as shown in Table 7.4, were analogous to those of the reference catalyst. In Figure 7.10a, we can also observe that the X-ray diffractograms are essentially equivalent for both samples, which in principle indicates a reasonable degree of dispersion of the nanoparticles in both cases, with no major changes. Nevertheless, with the current information we cannot discern whether the incorporation method based on the formation of micelles in reversed phase was able to obtain different results in terms of CuO particle size. Even more when the TPR profiles (Figure 7.10b) show very similar reduction temperatures in both samples (193 and 204 ºC for RV-CuO/Al_2O_3-*npw* and CuO/Al_2O_3-*npw*, respectively).

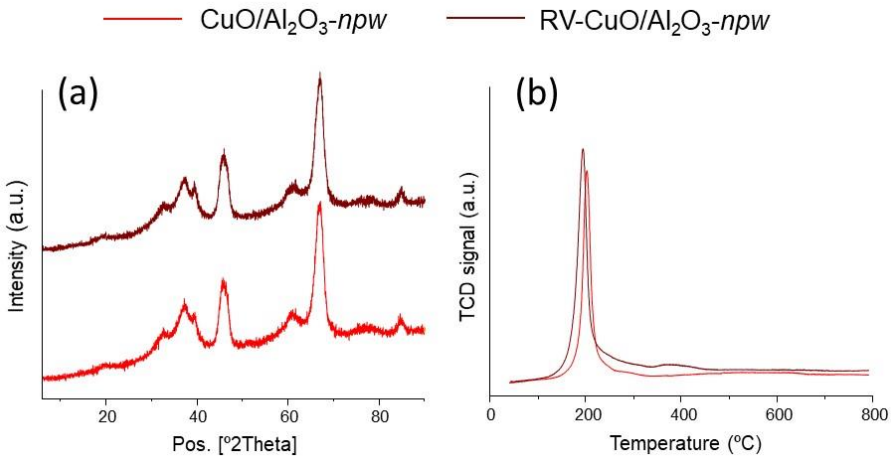

Figure 7.10. a) XRD patterns and (b) TPR profiles for Al_2O_3-*npw*-supported CuO materials prepared by incipient wetness impregnation (CuO/Al_2O_3-*npw*) and reverse micelle methodology (RV-CuO/Al_2O_3-*npw*).

Table 7.4. Main physicochemical and textural properties of Al_2O_3-*npw*-supported CuO materials prepared by incipient wetness impregnation (CuO/Al_2O_3-*npw*) and reverse micelle methodology (RV-CuO/Al_2O_3-*npw*).

Catalyst	Cu loading (wt%) [a]	Surface area (m^2/g) [b]	Pore volume (cm^3/g)[b]
CuO/Al_2O_3-*npw*	5.6	128	0.45
RV-CuO/Al_2O_3-*npw*	5.2	164	0.48

[a] Calculated by ICP. [b] Calculated from N_2-adsorption isotherms data (BET method).

7.4.2 Catalytic tests

Remarkably, and as it happened in *Chapter 5* for the selective glycerol dehydration to acetol with the catalyst RV-CuO/*m*-ZrO_2, the yields obtained for the 2-methylpyrazine and the overall to alkyl pyrazines are substantially higher with the new catalyst RV-CuO/Al_2O_3-*npw* (see Figure 7.11b), averaging 56 and 60% yields in the case of RV-CuO/Al_2O_3-*npw* vs 50 and 55% for CuO/Al_2O_3-*npw*. The reason behind this improvement can be found in the fact that both catalysts CuO/Al_2O_3-*npw* and RV-CuO/Al_2O_3-*npw* achieve nearly the same

selectivity to 2-methylpyrazine (81 vs 82 % in the liquid fraction), but the yield to liquid products (Figure 7.11a) is significantly higher in the case of RV-CuO/Al_2O_3-*npw* (70 vs 65 %), this resulting in the above-mentioned superior yield to the desired products.

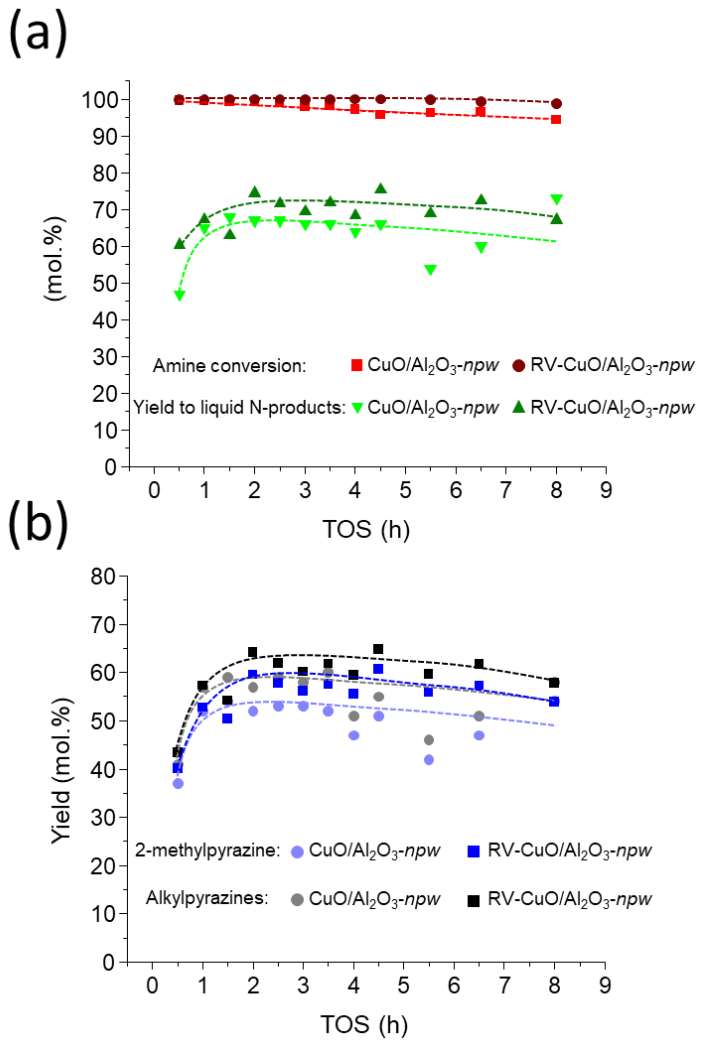

Figure 7.11. Comparison between CuO/Al_2O_3-*npw* and RV-CuO/Al_2O_3-*npw*. (a) Ethylenediamine conversion and yield to 2-methylpyrazine vs TOS, and (b) Yield to the different liquid products vs TOS. Reaction conditions: 350 ºC, solvent: H_2O, reagents/solvent-ratio: 0.4/0.6 (in wt.), diamine flow: 1.00 ml/h; acetol flow: 1.24 ml/h, 0.5 g of catalyst, particle size: 0.4-0.6 mm. Note: Dashed lines serve only as visual guidelines.

Even more significantly, the stability of the new catalyst RV-CuO/Al_2O_3-*npw* is more promising than that of the catalyst prepared by impregnation at pore volume CuO/Al_2O_3-*npw*. This fact becomes more evident in Figure 7.12, where the evolution of the yield to liquid nitrogen by-products and the imine intermediates are represented as a function of TOS. It can be observed how, for catalyst CuO/Al_2O_3-*npw*, the imines are detected when the operation time reaches six and a half hours, not being identified in the catalyst prepared by deposition of the CuO nanoparticles by means of micelles in reversed phase.

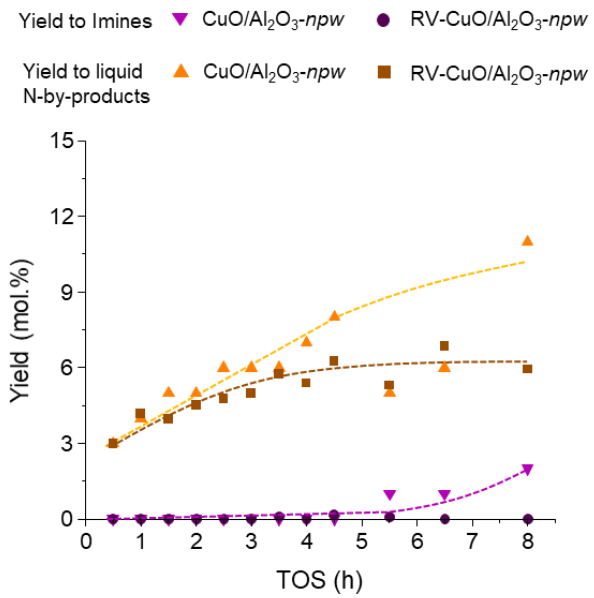

Figure 7.12. Comparison between CuO/Al_2O_3-*npw* and RV-CuO/Al_2O_3-*npw* in terms of yield to nitrogen by-products and imine intermediates vs TOS. Reaction conditions: 350 ºC, solvent: H_2O, reagents/solvent-ratio: 0.4/0.6 (in wt.), diamine flow: 1.00 ml/h; acetol flow: 1.24 ml/h, 0.5 g of catalyst, particle size: 0.4-0.6 mm. Note: Dashed lines serve only as visual guidelines.

7.5 Two-step one-pot process from glycerol to 2-methylpyrazine

In this last section, we have tried to accomplish the objective of using glycerol as a carbon source directly to produce 2-methyl pyrazine and/or alkyl pyrazines through its

selective dehydration to acetol and subsequent dehydrocyclization with ethylenediamine. Since, in this case, both processes have been optimized in a continuous flow reactor, it was possible to propose an alternative reaction system such as that described in *Chapter 3: Experimental Procedure*, in which both processes would be carried out consecutively. In its most straightforward manner, a one-pot two-step process working with two different catalytic beds, each possessing its catalyst and its working temperature.

After the studies carried out independently for both steps, the selective dehydration of glycerol to acetol and the dehydrocyclization of acetol with ethylenediamine to reach the desired pyrazines, several combinations of catalysts may be promising to carry out the process in two consecutive catalytic beds, as designed and explained in *Section 3.4.3.1*. Both RV-CuO/*m*-ZrO_2 and CuO/*m*-ZrO_2 are promising alternatives for generating hydroxyacetone from glycerol in the first fix catalytic bed, working at 240 ºC. At the same time, RV-CuO/Al_2O_3-*npw* and CuO/Al_2O_3-*npw* can be both used in the dehydrocyclization bed.

7.5.1. Catalyst selection based on solvent compatibility

However, we must bear in mind that the solvents used in one stage and the other are different, and therefore it would be necessary to check the compatibility of the catalyst used in the second step with methanol and the catalyst used in the first step with water.

In order to simplify the study and go towards a more sustainable process, it was decided that the overall process would be carried out using only water as a solvent. In addition, we know that MeOH generates hydrogen at 240 ºC in the first catalytic bed and is also capable of producing hydrogen even to a greater extent in the second one (at 350 ºC), which would constitute another disadvantage for the dehydrogenation reaction.

For this reason, it was decided to check the compatibility of the catalyst CuO/*m*-ZrO_2 system (achieving yields to acetol close to 60%) with water by carrying out experiments in which different amounts of water replaced MeOH as the solvent, working from 0 to 100 wt.% of water in the solvent fraction. These studies were carried out in parallel (a final degree project experimentally supervised by the PhD candidate)[14]. Although these results will not be discussed in detail here, the main average results are summarized in Table 7.5

for TOS = 1-4 h. As can be seen, even small amounts of water significantly worsened both the catalytic activity and the acetol yield for CuO/*m*-ZrO_2 catalyst. Although the mixture 50:50 MeOH/H_2O apparently shows similar results than those observed for absolute MeOH at short times, it does not manage to resist the comparison with pure MeOH at longer times on stream (values in parenthesis).

Table 7.5. Results for selective glycerol dehydration to acetol reactions using different MeOH/water concentrations with CuO/*m*-ZrO_2 catalyst[14].

Solvent (MeOH:water, vol. ratio)	**Glycerol conversion (mol.%)**	**Yield to Liquid Products (mol.%)**	**Acetol Selectivity (mol.%)***	**Yield to Acetol (mol.%)**
100:0	99 (98)[a]	90 (87)[a]	74 (71)[a]	66 (62)[a]
80:20	95	92	66	60
50:50	95 (88)[a]	94 (89)[a]	69 (66)[a]	65 (59)[a]
20:80	88	83	70	58
0:100	89	81	71	58

Reaction conditions: feed = solvent/glycerol (50/50 in weight), flow = 2 mL/h, with 0.5 g CuO/*m*-ZrO_2 catalyst, at 240 ºC, TOS = 1-4 h ([a]: TOS = 1-8 h). *Calculated over the total amount of products in the liquid fraction.

Although we already knew that methanol is likely to perform a catalyst pre-activation and facilitate the generation of the active Cu(I) species, we were interested in further investigating this substantial decay when using water. Thus, an *in-situ* FTIR study was carried out. First the catalyst surface of CuO/*m*-ZrO_2 was saturated with water, on the one hand, and with methanol, on the other hand, and subsequently, 1,2-propanediol was absorbed, thus simulating glycerol behaviour. Interestingly, Figure 7.13a shows that, when using MeOH, it was much easier for 1,2-propanediol to displace it from the surface (0.3 mbar of diol were enough), whereas for water, much higher pressures (up to 2.5 mbar) of 1,2-propanediol were required to begin to see the IR bands characteristic of the diol (Figure

7.13b). Therefore, the water molecule exerts a competitive adsorption on the catalytic surface which causes a significant decrease in the catalytic activity of the first step. Having understood this fact, it was decided to use catalyst CuO/Al_2O_3-*npw* in the first reaction step since the compatibility of alumina with water in this reaction had already been studied in the literature. In fact, some of the best catalysts reported to date in the selective glycerol dehydration to acetol reaction were reported to be Cu-Al_2O_3 systems[15–17]. Figure 7.14 shows how the catalyst CuO/Al_2O_3-*npw* achieves higher yields to acetol when introducing water in the feed.

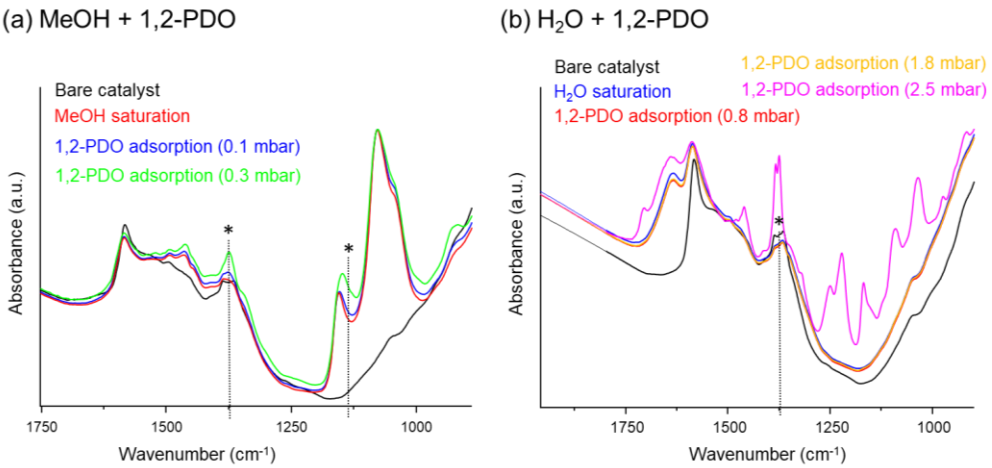

Figure 7.13. FTIR spectra for CuO/*m*-ZrO_2 sample exposed to calibrated (a) MeOH, (b) water volumes until saturation. Then, calibrated volumes of 1,2-propanediol (1,2-PDO, in vapor phase) were introduced, and IR spectra were acquired after each dosage, at specified pressures. * IR bands characteristic of the diol.

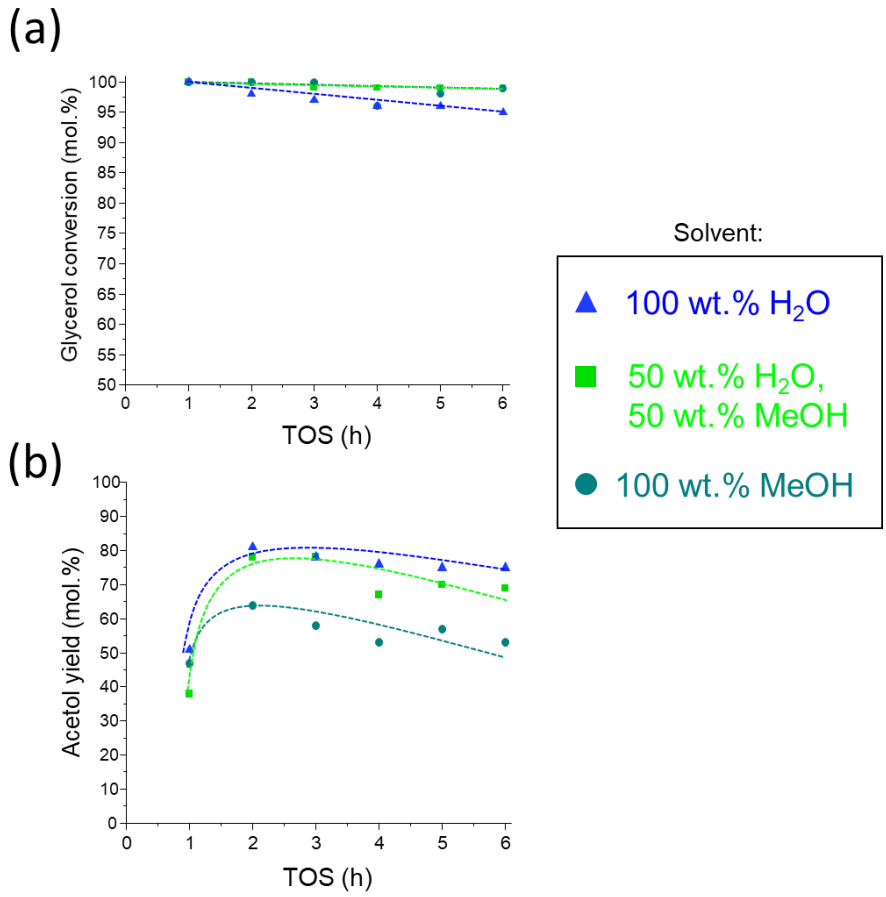

Figure 7.14. (a) Glycerol conversion, and (b) yield to acetol for CuO/Al_2O_3-*npw* and 5.0RV-CuO/Al_2O_3-*npw*. Reaction conditions: feed = methanol/glycerol (50/50 in weight), flow = 2 mL/h, with 0.5 g of catalyst at 240 °C. Note: Dashed lines serve only as visual guidelines.

7.5.2. Catalytic test in the multibed reactor

Once the multi-bed system was designed and its working conditions carefully selected to assure as smoothly operation as possible, a catalytic test was carried out using CuO/Al_2O_3-*npw* in the first step, at 240 ºC, and CuO/Al_2O_3-*npw*, at 350 ºC, in the second. The experiment was carried out for 3 hours.

Figure 7.15 shows the reaction descriptors usually considered, that is, conversions of both glycerol and ethylenediamine, yield to desired products (i.e., 2-methylpyrazine and alkyl pyrazines), yield to imines, and yield to other liquid nitrogen by-products.

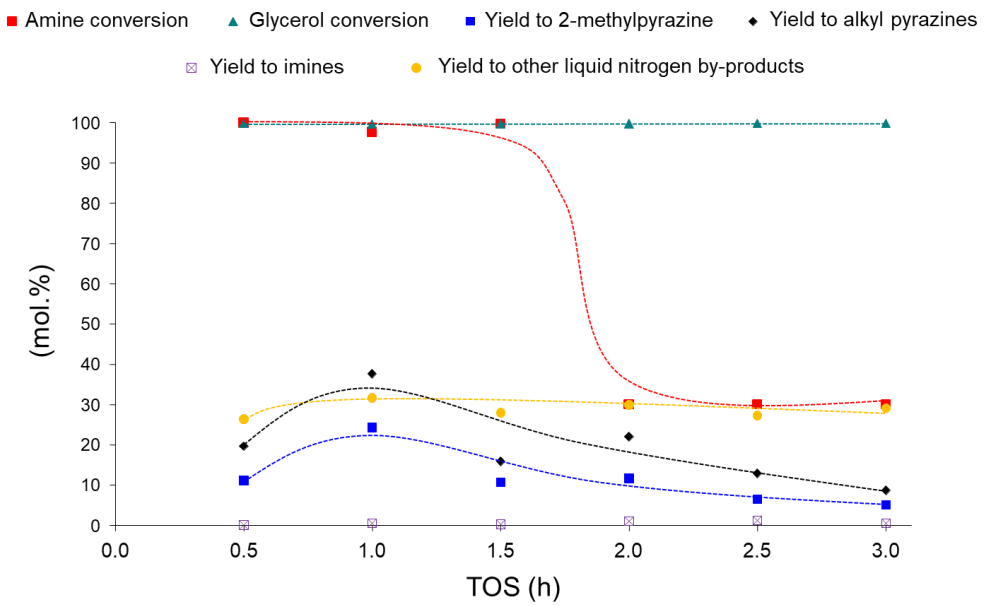

Figure 7.15. Conversions of both reagents, ethylenediamine and glycerol, and yields of ethylenediamine to imines, alkyl pyrazines, 2-methylpyrazine and liquid nitrogen by-products for the multi-bed system. Reaction conditions for the first catalytic bed: 240 ºC, solvent: H_2O, glycerol/solvent-ratio: 0.5/0.5 (in wt.), flow: 1.8 ml/h, 0.45 g of CuO/Al_2O_3-*npw* catalyst, particle size; 0.4-0.6 mm. Reaction conditions for the second catalytic bed: 350 ºC, solvent: H_2O, diamine/solvent-ratio: 0.4/0.6 (in wt.), flow: 1.0 ml/h., 0.5 g of CuO/Al_2O_3-*npw* catalyst, particle size: 0.4-0.6 mm. Note: Dashed lines serve only as visual guidelines.

From these results, we can see how, during the first hour, the system achieves ≈40% yield to alkyl pyrazines and ≈30% yield to 2-methylpyrazine. Nonetheless, as the reaction progresses, a very important decay in the catalyst activity is seen in the amine conversion. The mixture from the first catalytic bed seems to cause significant damage to the second catalyst. Apparently, it is not a matter of impairing dehydrogenation and preventing imines from transforming into pyrazines, but of the appearance of certain oxygenated and nitrogen

by-products that are even inhibiting ethylenediamine to react with hydroxyacetone. On the other hand, as the reaction between ethylenediamine and acetol has been proved to be thermal, this equilibrium established between amine, imines and other nitrogen by-products seems to be stopped and the catalyst totally deactivated. In addition, very considerable carbonaceous deposits are likely to be forming and creating significant damage to the system operation. In this sense, heavy products are formed, both oxygenated as nitrogenated, some of them coke precursors, which prevent the second reaction to take place under the appropriate conditions to obtain the desired final product.

In order to achieve the best performance of the multi-bed reactor, the steps must be individually optimized further. The catalyst used in the first bed should probably be improved to maximize the formation of acetol and avoid the appearance of by-products. In other words, acetol selectivity should be ameliorated as much as possible. As in the reductive amination, oxygenate by-products can drastically affect the second step's results by scavenging the amine or forming coke in the second reactor. In addition, the research group aims to investigate other materials based on the CuO/Al_2O_3-*npw* and CuO/ZrO_2 (different zirconia phases) systems for the second step, where other metallic species capable of improving the dehydrogenating capacity of the systems are being incorporated.

On the other hand, it is necessary to mention that the designed reaction system can also be improved. For example, the intermediate mixing zone between the stream from the first reactor and the ethylenediamine solution feed is not, in this case, at room temperature as with the first pre-reactor designed in the acetol dehydrocyclization with ethylenediamine. Due to the proximity of two catalytic beds working at high temperatures, the temperature is considerably higher, which can favour the formation of unwanted nitrogen by-products from the imine intermediates.

7.6 Conclusions

In this chapter, different catalysts based on CuO supported on other high-area inorganic oxides were applied as catalysts in the dehydrocyclization of acetol with ethylenediamine. The catalytic tests allowed for selecting an efficient catalyst for the reaction. On the other

hand, the characterization studies carried out in other chapters of this thesis prompted the establishment of interesting structure-activity relationships. The following relevant conclusions can be highlighted:

- It has been possible to verify that, when working with 40% aqueous solutions of ethylenediamine and acetol the reaction system designed with a pre-reactor for the formation of the imines and a subsequent catalytic bed at 350 ºC for their dehydrogenation can achieve acceptable yields to alkyl pyrazines (≈40%). However, the presence of a mainly acidic catalyst is necessary to dehydrogenate the imine intermediates. In this sense, supports such as ZrO_2 and Al_2O_3 proved to be the most suitable and stable to carry out the reaction.

- The selection of a CuO/Al_2O_3-*npw* catalyst with a lower number of acidic and basic centers with respect to other CuO/Al_2O_3 compositionally analogous catalysts allows for increasing the yield to 2-methylpyrazine and alkyl pyrazines until values close to 50 and 60%, respectively. Moreover, this catalyst can operate efficiently for up to 8 hours on stream. However, the low carbon balances attained together with the general trend shown by the catalysts described in this section, including catalyst CuO/Al_2O_3-*npw*, show that there is still room for improvement in terms of catalytic stability. Further optimization of catalyst to avoid the formation of solid or gaseous products seems necessary to assure a successful application of the process.

- The influence of the acid-base centers in the reaction has been shown. Basic sites contribute to the formation of heavy nitrogen by-products, and acidic ones participate in the dehydrogenation of the imine intermediates. Nevertheless, it has not been possible to rigorously determine whether dehydrogenation is favoured by a specific ratio of acid and basic centres, this being apparently more favourable to acid centres, or only occurring by the presence of acid sites. In addition, an excess of acid sites also seems to contribute to the formation of undesired nitrogen by-products.

- The incorporation of the CuO nanoparticles in the support Al_2O_3-*npw* using the precipitation-deposition method through the formation of micelles in reversed-phase seems to significantly increase the specific activity of the catalyst. In fact, both the yield to 2-methylpyrazine and the yield to alkyl pyrazines increased by around 5 points with respect to the catalyst prepared by wetness impregnation. However, everything seems to indicate that additional studies to determine the dispersion and morphology of the nanoparticles obtained through this new methodology will be necessary to understand this catalytic improvement.

- The first proof of concept was carried out in the multi-bed reactor, demonstrating that the use of the same CuO/Al_2O_3-*npw* catalyst in both step 1 (glycerol dehydration) and in step 2 (dehydrocyclization), using water as solvent, can give alkyl pyrazine yields up to 40% using glycerol and ethylenediamine directly as starting reagents. The results are very promising and let the door open for future developments. However, the process suffers from a strong decay over time due to several factors related to the optimization of the first step, the second step, and the reaction system that should be further studied in the future.

7.7 References

[1] H.D. Belitz, P. Grosch, Werner, Schieberle, Food Chemistry., 4th ed., Springer, 2009.

[2] S.L. Lewis, S.R. Dirksen, M.M. Heitkemper, L. Bucher, Medical-surgical nursing : assessment and management of clinical problems., 9th ed., St. Louis, MO, 2014.

[3] M.R. Hellberg, A. Rusinko, H.Y. Decornez, Aminopyrazine analogs for treating glaucoma and other rho kinase-mediated diseases and conditions, 200633709A, 2005.

[4] X. Li, C.H. Xu, C.Q. Liu, Y. Chen, J.Y. Liu, Synthesis of pyrazinyl compounds from glycerol and 1,2-propanediamine over Cu-TiO2 catalysts supported on γ-Al2O3, Chinese Chem. Lett. 24 (2013) 751-754. https://doi.org/10.1016/j.cclet.2013.04.010.

[5] R. Sarkari, C. Anjaneyulu, V. Krishna, R. Kishore, M. Sudhakar, A. Venugopal, Vapor phase synthesis of methylpyrazine using aqueous glycerol and ethylenediamine over ZnCr2O4 catalyst: Elucidation of reaction mechanism, Catal. Commun. 12 (2011) 1067-1070. https://doi.org/10.1016/j.catcom.2011.03.021.

[6] V. Akula, R. Sarkari, A. Chatla, K. Vankudoth, K.K. Mandari, Synthesize 2-methylpyrazine using aqueous glycerol and ethylenediamine over zinc oxide-zinc chromite catalysts: Structure-activity relationship, Appl. Catal. A Gen. 441 (2012) 108-

118. https://doi.org/10.1016/j.apcata.2012.07.012.

[7] A. Venugopal, R. Sarkari, C. Anjaneyulu, V. Krishna, M.K. Kumar, N. Narender, A.H. Padmasri, Influence of acid-base sites on ZnO-ZnCr2O4 catalyst during dehydrocyclization of aqueous glycerol and ethylenediamine for the synthesis of 2-methylpyrazine: Kinetic and mechanism studies, Appl. Catal. A Gen. 469 (2014) 398-409. https://doi.org/10.1016/j.apcata.2013.10.023.

[8] R. Sarkari, V. Krishna, M. Sudhakar, T.V. Rao, H. Padmasri, D. Srinivas, A. Venugopal, The Effects of Thermal Treatment of ZnO-ZnCr 2 O 4 Catalyst on the Particle Size and Product Selectivity in Dehydrocyclization of Crude Glycerol and Ethylenediamine 1, Kinet. Catal. 57 (2016) 607–614. https://doi.org/10.1134/S0023158416050177.

[9] Jindou Hou, Wen. Luo, Shizhong Luo, Chao Lin, Ping Liu, Xuemei Liao, FangLi Jing, Xiaopeng Li, Facile synthesis of CuMAl (M = Cr, Mn, Zn, and Co) with highly dispersed Cu and tailorable surface acidity for efficient 2-methylpyrazine synthesis, RSC Adv. 7 (2017) 48662–48669. https://doi.org/10.1039/C7RA08349A.

[10] L. De Lange, Trabajo fin de máster en ingeniería industrial: The designing of a novel continuous flow catalytic process for the direct synthesis of pyrazines from glycerol, Universidad Politécnica de Valencia, 2018.

[11] V. Krishna, S.N. Kumar, S. Reema, A.H. Padmasri, K.V.R. Chary, A. Venugopal, Bio-glycerol utilization: Synthesis of 2,6-dimethylpyrazine over MxOy–MCr2O4 (M = Mg, Fe, Co, Ni, Cu and Zn) catalysts, Appl. Catal. A Gen. 488 (2014) 275–284. https://doi.org/10.1016/J.APCATA.2014.09.019.

[12] R. Sarkari, V. Krishna, C. Anjaneyulu, V. Kumar, S. Sankar, G. Naresh, A. Venugopal, A Sustainable Process for the Synthesis of Alkylpyrazines by Dehydrocyclization of Crude Glycerol and Ethylenediamine over Metal Chromite Catalysts, Catal. Clean Energy Environ. Sustain. Biomass Convers. Green Chem. 1 (2021) 721–737. https://doi.org/10.1007/978-3-030-65017-9_22.

[13] X. Li, C. Xu, C. Liu, N. Zhang, J. You, Q. Wu, Reaction pathway in vapor-phase synthesis of pyrazinyl compounds from glycerol and 1,2-propanediamine over ZnO-based catalysts, J. Mol. Catal. A Chem. 371 (2013) 104–110. https://doi.org/10.1016/J.MOLCATA.2013.01.032.

[14] P. Villasante Iturria, Desarrollo y optimización de un proceso catalítico en continuo para la síntesis de pirazinas a partir de glicerol, Universidad de Valencia, 2021.

[15] S. Sato, M. Akiyama, R. Takahashi, T. Hara, K. Inui, M. Yokota, Vapor-phase reaction of polyols over copper catalysts, Appl. Catal. A Gen. 347 (2008) 186-191. https://doi.org/10.1016/j.apcata.2008.06.013.

[16] C.V. Rode, M.A. Hengne, A.A. Ghalwadkar, R.B. Mane, P.H. Mohite, H.S. Potdar, Process for preparation of hydroxyacetone or propylene glycol, WO2011/138643, 2014.

[17] R.B. Mane, C. V. Rode, Continuous dehydration and hydrogenolysis of glycerol over non-chromium copper catalyst: Laboratory-scale process studies, Org. Process Res. Dev. 16 (2012) 1043-1052. https://doi.org/10.1021/op200383r.

Chapter 8
General Conclusions

Motivated by a spirit of genuine concern about the constantly rising carbon emissions across the world's wealthiest nations, the subsequent global climate change and the shortage of fossil feedstocks, the present thesis sought to respond to the growing demand for chemicals from raw materials alternative to fossil sources. Specifically, the production of organonitrogen chemicals has been a critical scientific target over the last decade, significantly growing during the development of this thesis.

Thus, this doctoral thesis has tried to develop different catalytic routes for producing nitrogen heterocycles of industrial interest from glycerol, using the selective dehydration product of this molecule, hydroxyacetone (acetol), as an intermediate compound to ensure, at least, a partial success of the synthetic strategies here presented.

Materials based on Cu-Mg-Al mixed oxides derived from hydrotalcites show hydroxyacetone yields of approximately 40%, when applied as catalysts in the selective dehydration of glycerol. Moreover, it is possible to increase its performance up to 45% with the introduction of other metals (Ga, Fe, Ni). In addition, throughout that chapter, there has been significant progress regarding understanding the catalytic process over this family of materials. Aspects such as the importance of the Cu(I) centers to carry out the first step in the glycerol dehydration to selectively produce acetol or the need to have a reasonable number of acid centers to absorb considerable amounts of glycerol have been successfully unraveled. Nonetheless, the need to use diluted glycerol feeds, their deactivation by organic matter deposition, and likely, the generated water, were found issues to be solved for applying these materials in this reaction.

In *Chapter 5*, it has been proved that catalytic systems based in the compositions CuO/SiO_2, CuO/Al_2O_3 and CuO/ZrO_2 can attain promising results in the selective dehydration of glycerol to acetol when the support and the CuO nanoparticles incorporation method are chosen correctly. Remarkably, the materials CuO-PD/SiO_2-AL, CuO/Al_2O_3-*npw* and CuO/*m*- ZrO_2, working with much more concentrated streams than in the previous chapter (50% by weight of glycerol), can reach yields of about 60% to acetol. Concretely, the catalyst CuO/*m*-ZrO_2 could be used during longer reaction times (TOS $\geq$10 h), suffering some catalytic deactivation beyond that time solved by a thermal regeneration process, allowing for recovering the initial catalytic activity. Furthermore, the correlation of these

studies with several characterization techniques allowed us to establish as descriptors of the specific activity of the catalyst the high dispersion of copper oxide nanoparticles, and the adequate catalyst acidity, being necessary an acidity sufficient to absorb the glycerol molecule but not excessive so as not to lead to the formation of undesired secondary by-products. Additionally, the catalyst CuO/*m*-ZrO_2 was improved by incorporating the CuO nanoparticles by precipitation-deposition from micelles in reversed phase. As a result, this catalyst 5.0RV-CuO/*m*-ZrO_2 achieved enhanced catalytic results, reaching nearly 65% yield to acetol and being able to be used through 10 hours in reaction when containing just 3.6 wt.% of copper.

Once we had a series of materials capable of selectively dehydrating glycerol to acetol with high yields and productivity, the spotlight was placed on the production of nitrogen heterocycles from this molecule, with greater reactivity than glycerol. With that purpose, a series of catalysts based on Pd nanoparticles on simple metal oxides and mixed metal oxides were prepared to produce 2-methylpiperazine from acetol and ethylenediamine in a batch reactor. Notably, a synthesized catalyst Pd/TiO_2-Al_2O_3 can carry out the reaction efficiently (80% yield) with low catalyst loads and with the possibility of being reused. In fact, this catalyst has a high number of unsaturated palladium metal centers capable of activating the carbon-nitrogen double bond and an adequate number of acid sites, not excessively high so that they could lead to the production of unwanted nitrogen by-products. In addition, this catalyst could also be used with a stream derived from the dehydration reactor and complete the production process of 2-methylpiperazine, having used glycerol as starting reagent with moderate but promising yields to the desired 2-methylpiperazine.

Regarding the synthesis of 2-methylpyrazine, the catalysts prepared and characterized in *Chapter 5* for glycerol dehydration have also proven to be efficient for the dehydrocyclization of acetol with ethylenediamine (*Chapter 7*). Mainly catalysts based on copper oxide supported on zirconia and alumina are the most promising, attaining yields above 40% to alkyl pyrazines. It was possible to select the catalyst CuO/Al_2O_3-*npw* for this reaction yielding ≈50% to the desired 2-methylpyrazine and ≈55% to the total alkyl-pyrazines. Furthermore, incorporating the CuO nanoparticles by the precipitation-deposition method using reverse phase micelles can significantly boost the catalytic (redox and acid/base) properties and its behaviour in the dehydrocyclization process, achieving yields close to 60% to the desired alkyl-pyrazines and allowing its use under reaction

conditions for several hours (TOS >8 h). From the first catalytic screening, exciting conclusions could be drawn regarding the role of acid centers and the acid/base sites ratio, which is very important to achieve the proper balance between acidic and basic centers to maximize both liquid yield and yield to alkyl pyrazines. Thus, promising yields to the desired pyrazines (40%) are attained at short operating times in the process. However, a strong catalyst deactivation leads us to think that improvements are necessary both in the development and optimization of the separate stages as well as in the multi-bed system coupling them.

In summary, although the task faced was stark, several heterogeneous catalysts, reaction systems and reaction conditions could be tested, optimized, developed, and selected to yield nitrogen heterocycles from glycerol. Notably, remarkable results were achieved for producing the intermediate hydroxyacetone (acetol) from glycerol, also establishing new catalytic routes for the N-heterocycles synthesis from acetol which, to the best of our knowledge, had not previously proposed in the literature. Nonetheless, although this thesis research also attained encouraging results, further progress needs to be made to optimize the N-heterocycles production by using glycerol directly as starting raw material.

Chapter 9
List of Figures, Schemes and Tables

Chapter 10
Annex

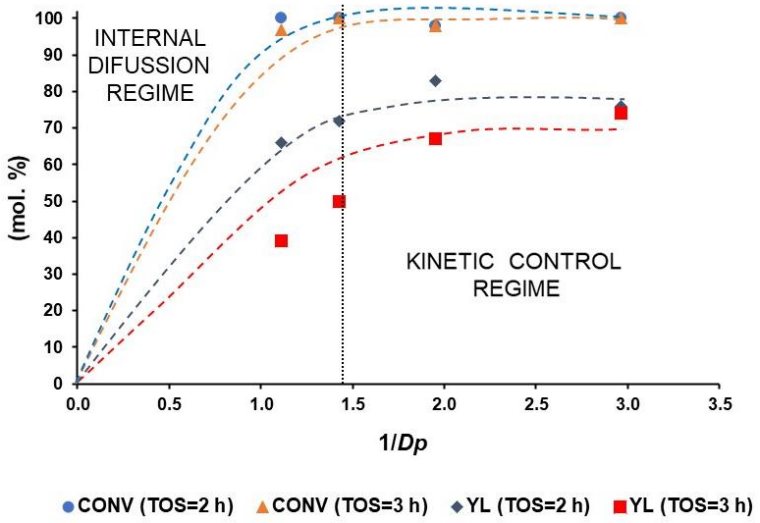

Figure A1. Internal diffusion study with 5.0%Cu-HT-4 catalyst. Reaction conditions: Temperature = 240 ºC, feed: methanol/glycerol (90/10 wt.), catalyst: 0.5 g, 5.0%Cu-HT-4, flow = 2 mL/h. CONV: glycerol conversion, YL: yield to liquid products.

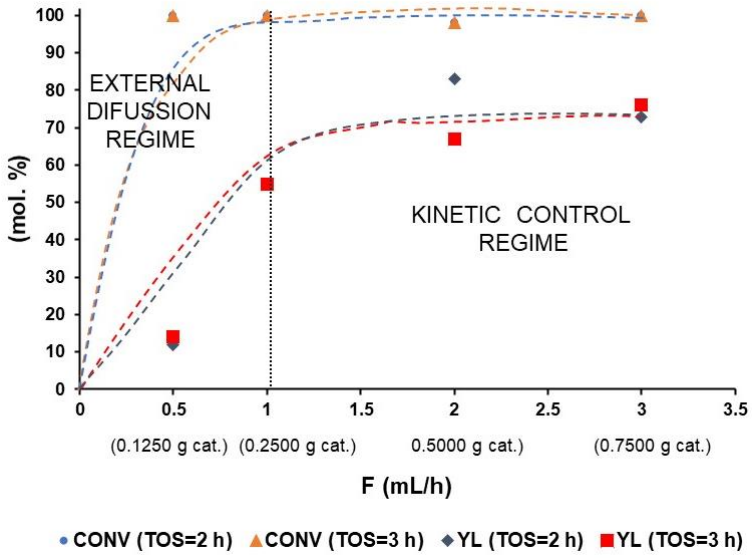

Figure A2. External diffusion study with 5.0%Cu-HT-4 catalyst. Reaction conditions: Temperature = 240 ºC, feed: methanol/glycerol (90/10 wt.), catalyst: 0.5 g, 5.0%Cu-HT-4, particle size = 0.425-0.600 mm. CONV: glycerol conversion, YL: yield to liquid products.

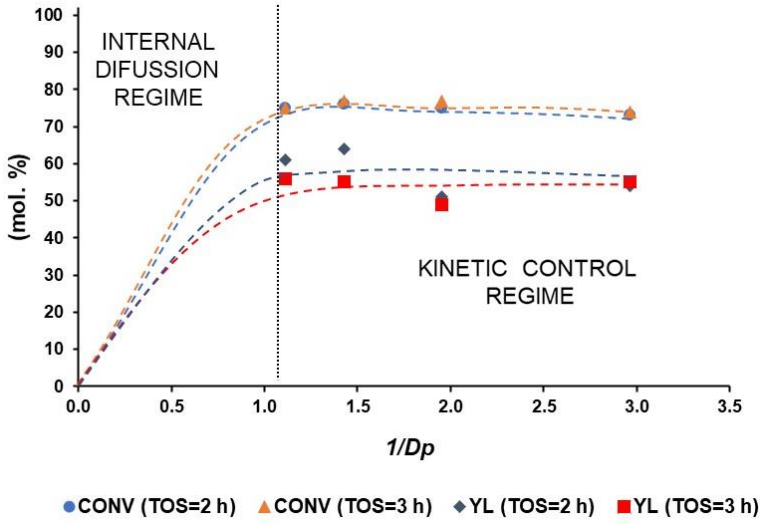

Figure A3. Internal diffusion study with CuO-IW/SiO_2-CH catalyst. Reaction conditions: Temperature = 240 ºC, feed: methanol/glycerol (90/10 wt.), catalyst: 0.5 g, 5.0%Cu-HT-4, flow = 2 mL/h. CONV: glycerol conversion, YL: yield to liquid products.

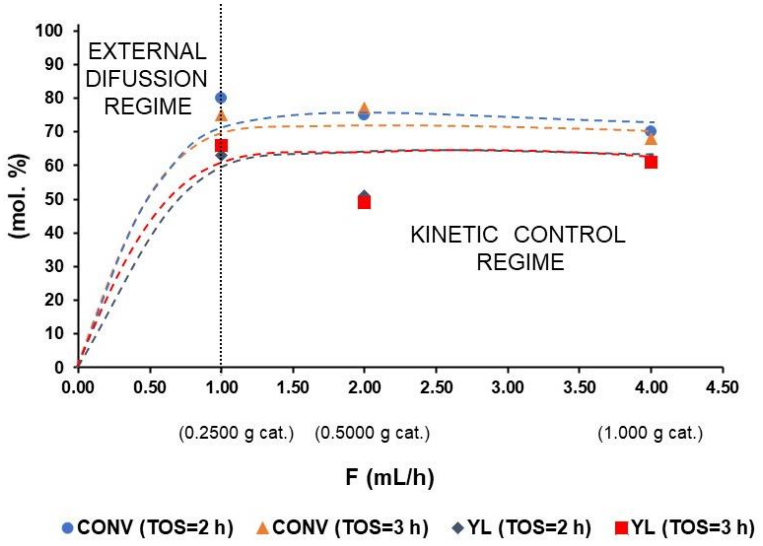

Figure A4. External diffusion study with CuO-IW/SiO_2-CH catalyst. Reaction conditions: Temperature = 240 ºC, feed: methanol/glycerol (90/10 wt.), catalyst: 0.5 g, 5.0%Cu-HT-4, flow = 2 mL/h. particle size = 0.425-0.600 mm. CONV: glycerol conversion, YL: yield to liquid products.

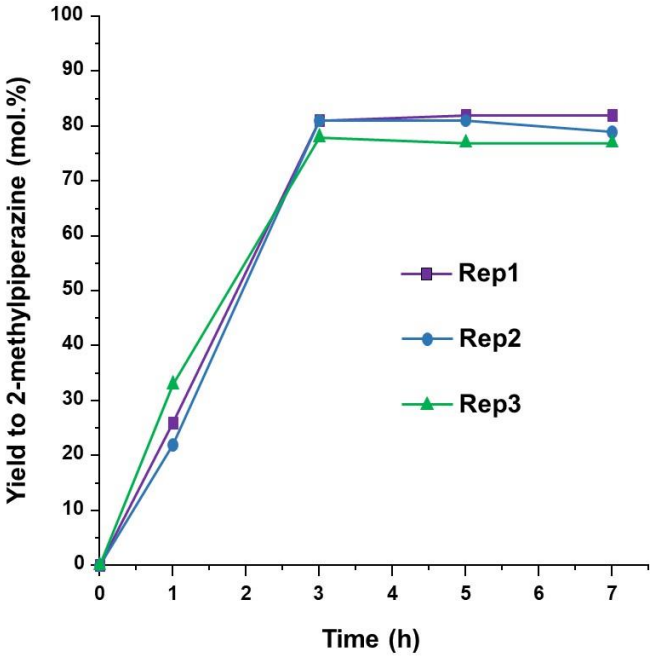

Figure A5. Reproducibility test with commercial Pd/Al_2O_3. Reaction conditions: 0.325 g acetol, 0.227 g ethylenediamine, 1.250 g MeOH, 0.056 g of catalyst, at 13 bar of H_2, and 90 ºC, during 7 h and with slow addition of acetol (100 µl/h).

Table A1. Sampling test for the reductive amination of acetol with ethylenediamine.

Reaction time (h)	Yield to 2-methylpiperazine (mol.%)		
	A	B	C
3	57	54	57 ± 2
7	77	78	78 ± 4

A: One reaction with 4 sample collections
B: Two independent reactions (just one sample collection for each one at the end)
C: Average results (4 different repetitions per every reaction time, including those in this table) with standard deviation.
Reaction conditions: 0.325 g acetol, 0.227 g ethylenediamine, 1.250 g MeOH, 0.011 g of Pd/TiO_2-Al_2O_3 at 13 bar of H_2, and 90 ºC, during 7 h and with slow addition of acetol (100 µl/h).

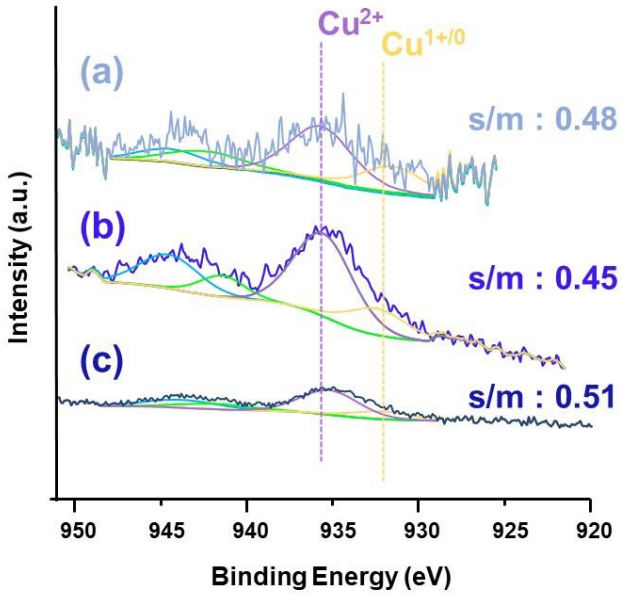

Figure A6. Cu2$p_{3/2}$ XPS peak of a) 5.0%Cu-HT-4 (Mg anode, 1 scan), b) 5.0%Cu-HT4 (Mg anode, 25 scans), c) 5.0%Cu-HT-4 (Al anode after overall acquisition, 25 scans).

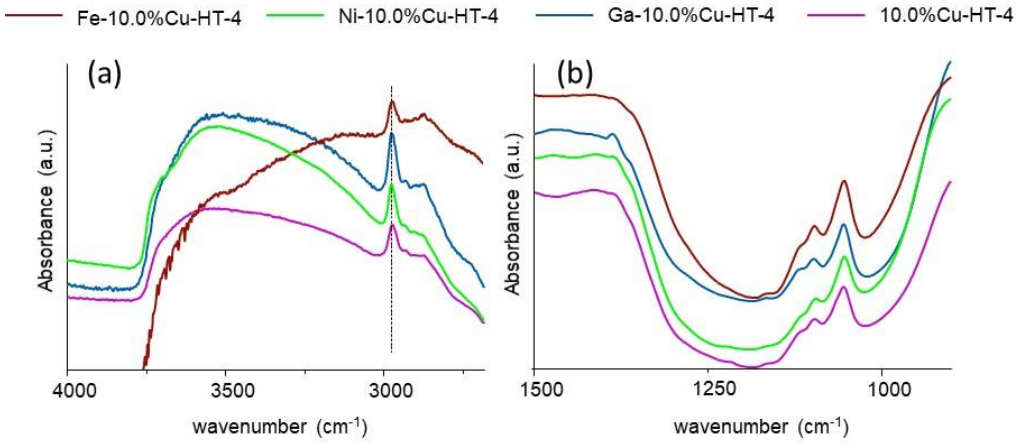

Figure A7. IR spectra of CO adsorption at 25 ºC and saturation coverage for M-Cu-Mg-Al mixed oxides.

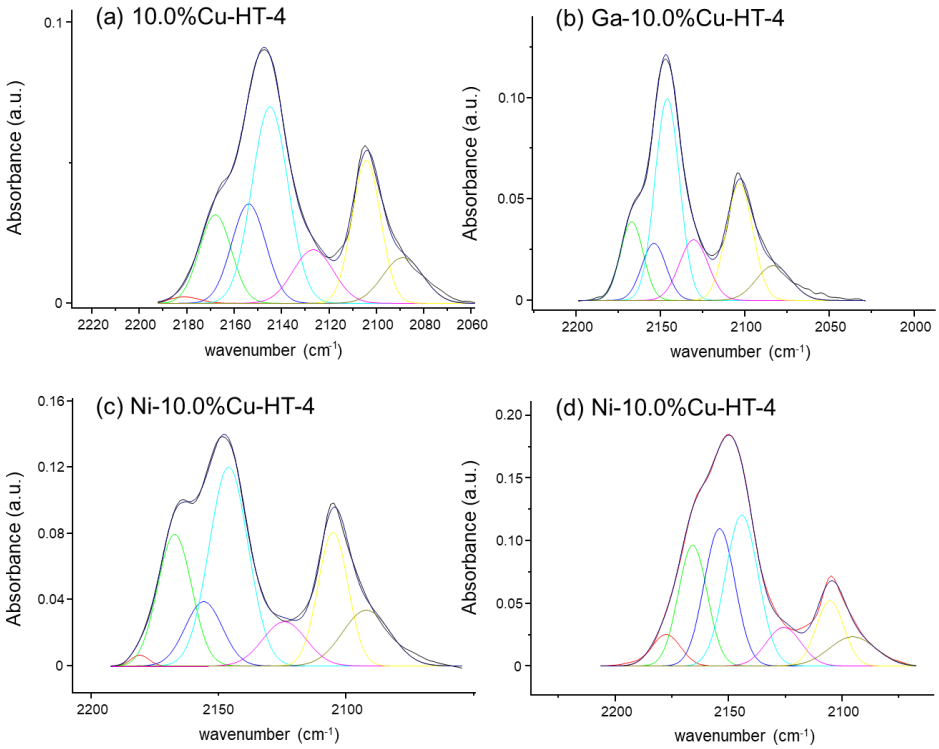

Figure A8. IR spectra deconvolution for CO low temperature adsorption at saturation coverage on several M-10.0%Cu-HT-4 samples after a pre-treatment with 0.1 mbar of MeOH (240 ºC, 30 minutes).

Table A2. Surface area, pore volume extracted from N_2-adsorption isotherms for commercial SiO_2 supports used in this work and acid characterization by Pyridine- FTIR.

Support	Commercial supplier	BET area (m^2/g)[a]	Pore volume (cm^3/g)	Acid sites (µmol PYR/g)[a]
SiO_2-CH	Chempur	224	0.90	3
SiO_2-AL	Sigma-Aldrich	343	0.89	3

[b] Calculated from N_2-adsorption isotherms data (BET method).

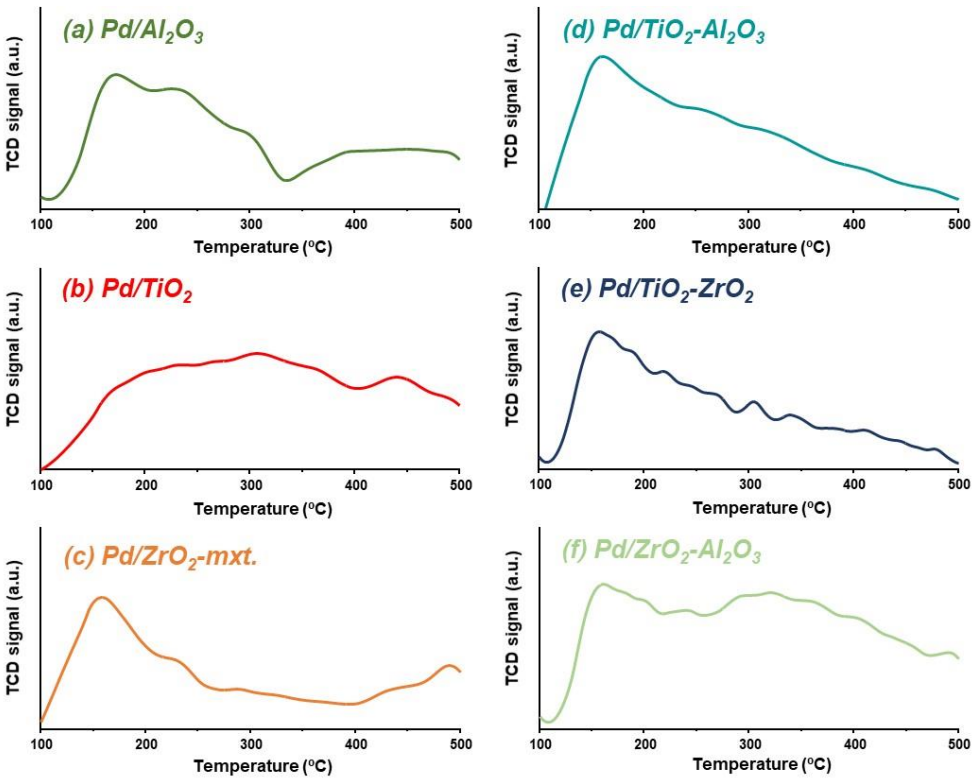

Figure A9. Smoothed NH_3-TPD profiles of Pd-based materials.